

AN INVESTIGATION OF THE MOVEMENT OF PARTICLES  
IN  
FLUIDIZED BEDS

by

JERRY LEE RATHBUN

B. S., Kansas State University, 1962

---

A MASTER'S THESIS

866

submitted in partial fulfillment of the

requirements for the degree

MASTER OF SCIENCE

Department of Nuclear Engineering

KANSAS STATE UNIVERSITY  
Manhattan, Kansas

1965

Approved by:

*P. C. Bailei*

---

Major Professor

2668  
T4  
1965  
R234

C.2  
Document

TABLE OF CONTENTS

1.0	INTRODUCTION-----	1
1.1	Background-----	1
1.1.1	Advantages-----	2
1.1.2	Disadvantages-----	3
1.2	Application to Nuclear Reactors-----	3
1.3	Purpose-----	4
1.4	Scope-----	5
2.0	EXPERIMENTAL-----	6
2.1	Experimental Apparatus-----	6
2.1.1	The Column and its Accessories-----	6
2.1.2	The Gamma-Ray Detection Equipment-----	11
2.1.3	The Measuring and Recording Equipment-----	14
2.2	Materials-----	19
2.3	Calibrations-----	21
2.3.1	Half-life Determination-----	21
2.3.2	Calibration of the Orifice Meter-----	23
2.3.3	Radial Effects-----	23
2.3.4	Gap Width and Shield Thickness-----	27
2.3.5	Calibration of the Electronic System-----	27
2.3.6	Time Constants of the Ratemeters-----	39
2.3.7	Pressure Drop Data-----	42
2.4	Procedure-----	45
3.0	ANALYSIS OF SINGLE PARTICLE EXPERIMENTS-----	48
3.1	Experiment Arrangement-----	48
3.2	Quantities Extracted From Data-----	48
3.3	Determination of Fundamental Quantities From Experimental Data-----	49
4.0	DATA ANALYSIS-----	52
4.1	General Consideration-----	52
4.2	Statistical Analysis of Data-----	55
4.3	Analysis of the Residence Times Distribution-----	60
4.4	Analysis of the Particle Traffic-----	102
4.5	Analysis of the Reflectivity Data-----	102
4.6	Analysis of the Particle Concentrations-----	114
4.6.1	Theoretical Development-----	114
4.6.2	Analysis of Experimental Results-----	126
5.0	DISCUSSION OF RESULTS-----	144
5.1	Residence Times-----	144
5.2	Particle Traffic-----	145
5.3	Reflectivity-----	146
5.4	Particle Concentrations-----	146

6.0	CONCLUSIONS-----	153
7.0	ACKNOWLEDGMENT-----	156
8.0	LITERATURE CITED-----	157
9.0	APPENDICES-----	158
	APPENDIX A: Description and Explanation of the IBM 1620 Computer FORTRAN Program No. 1 for Correcting the Time Increment Data-----	159
	APPENDIX B: Description and Explanation of the IBM 1620 Computer FORTRAN Program No. 2 for Computing the Average Number of Times a Particle Passed a Detector Level per Unit Time-----	170
	APPENDIX C: Description and Explanation of the IBM 1620 Computer FORTRAN Program No. 3 for Performing the Fluidization Statistical Analysis-----	176
	APPENDIX D: Description and Explanation of the IBM 1620 Computer FORTRAN Program No. 4 for Determining the Concentration of Tagged Particles from Individual Particle Data-----	193
	APPENDIX E: Description and Explanation of the IBM 1620 Computer FORTRAN Program No. 5 for Calculating the Average Residence Times as a Function of the Number of Data Values----	200
	APPENDIX F: Description and Explanation of the IBM 1620 Computer FORTRAN Program No. 7 for Computing the Average Time, the Most Probable Time, the Variance, and the Gamma Distribution Parameters $p$ and $\nu$ of the Residence Times Data-----	208
	APPENDIX G: Description and Explanation of the IBM 1620 Computer FORTRAN Program No. 9 for Calculating the T Statistic for Given Gamma Distribution Parameters $p$ and $\nu$ -----	216
	APPENDIX H: Discussion of the Gaussian Quadrature Approximation of the Gamma Distribution-----	222

## NOMENCLATURE

<u>Symbol</u>	<u>Use In Text</u>
$\Delta Z$	Distance between the two detector levels, in.
$Z_1$	Vertical position of the lower detector level, in.
$Z_2$	Vertical position of the upper detector level, in.
R	Ratio of experimental time to true time
$\Delta P$	Pressure drop across the fluidized bed, in. Hg.
$t(Z_i, Z_j)$	Residence time, sec.
$r(Z_i)$	Particle traffic, no. sec <sup>-1</sup> .
$Pr(Z_i, Z_j; Z_i)$	Reflectivity
$Pr(Z_i, Z_j; Z_j)$	Transmissivity
$I(Z_i, Z_j, t)$	Experimental particle concentration, no. in <sup>-2</sup> . sec <sup>-1</sup> .
m	Number of times a particle passes $Z_i$ before reaching $Z_j$ .
i, j	Detector level indices
$\Delta t$	Time increment, sec.
t	Time, sec.
B	Water flow rate through fluidized bed, gal. min <sup>-1</sup> or ft. sec <sup>-1</sup> .
k	Water flow rate index
f(t)	Frequency function of residence times

$f(P_r)$	Frequency function of reflectivities
$I(t)$	Frequency function of particle concentrations
$T$	T Statistic, sec.
$p$	Gamma distribution parameter
$\nu$	Gamma distribution parameter, sec.
$\Gamma(p)$	Gamma function
$\bar{t}$	Average residence time, sec.
$\sigma^2$	Variance of residence times, sec <sup>2</sup> .
$S^2$	Unbiased estimate of variance, sec <sup>2</sup> .
$n$	Number of data values
$t_p$	Most probable residence time, sec.
$\bar{v}$	Average speed of particles, in. sec <sup>-1</sup> .
$v(t_p)$	Speed of particles corresponding to the most probable residence time, in.sec <sup>-1</sup> .
$v(\bar{t})$	Speed of particles corresponding to the average residence time. in.sec <sup>-1</sup> .
$\beta$	Reflection coefficient, in <sup>-1</sup> .
$C$	Theoretical particle concentration, no. in <sup>-3</sup> .sec <sup>-1</sup> .
$E_z$	Dispersion coefficient, in <sup>2</sup> . sec <sup>-1</sup> .
$Q$	Source of particles, no. in <sup>-2</sup> . sec <sup>-1</sup> .
$L$	Height of fluidized bed, in.
$W$	Total time span used to obtain particle concentration data, sec.
JMAX	Number of data values in a data set.

$\tau$	$t E_z L^{-2}$
$x$	$Z/L$
$a(k)$	Christoffel numbers
$x(k)$	Zeros of the Legendre polynomial of given degree

## 1.0 INTRODUCTION

### 1.1 Background

The term "fluidized bed", as it is now used, relates to a technique initiated more than twenty years ago to find a better catalytic-cracking process than the fixed bed method (14).

A fluidized bed is a collection of solid particles which circulate in an enclosed region as the result of the upward flow of fluid, either liquid or gas, past the particles. A fluidized state occurs over a finite range of fluid velocities. At zero fluid velocity, all of the particles are in a static state resting on the bottom of the containment vessel. As the fluid velocity is increased, there is a certain rate of fluid flow at which the bed will be expanded to such a point that the particles will begin to move. The static bed is characterized by a pressure drop across the bed that increases with increased fluid velocity. When a fluid velocity is reached that causes particle movement, only a slight change in the pressure drop occurs across the bed as the fluid velocity is increased. Further increases in the velocity cause the volume of the bed to increase.

At high fluid velocities, a bed fluidized with gas usually remains largely in a compact state. A bed fluidized with a liquid expands steadily with increasing fluid velocity until a state of complete particle isolation is reached. Maximum expanded bed heights for gases rarely exceed twice the static bed height.

At low fluid velocities slightly above those for minimum fluidization, the whole bed is macroscopically homogeneous. This state is sometimes referred to as the state of incipient fluidization. In describing the physical appearance of the bed, this form of flow has been referred to as particulate fluidization.

At higher fluid velocities, a second phase, commonly known as the boiling bed state, often occurs. Bubble formation and slugging take place in the fluidized solids. The physical appearance of the bed is then referred to as aggregative fluidization.

Whether particulate or aggregative fluidization occurs at high fluid velocities relative to the minimum fluidization velocity depends upon the particle size and the ratio of solid to fluid density (7). In general, the particulate form occurs in liquid fluidized systems, and aggregative fluidization occurs in gas fluidized systems.

Particle mobility is the primary difference between a fluidized bed and a fixed bed. Many of the advantages and disadvantages of the fluidized bed technique have been enumerated in the literature (7, 9, 10, 14).

#### 1.1.1 Advantages

The following items are some of the major advantages of applications of the fluidized bed technique.

1. Turbulence within the fluidized system agitates and diffuses any cold or hot spots, providing an approach to isothermal operating conditions.
2. Turbulence provides a more uniform solids distribution.
3. A fluidized bed's ability to handle solids as if they were a liquid enables continuous operations, such as addition and withdrawal of solids from the bed, to occur.
4. High volumetric heat transfer rates can be conveniently accomplished due to the large surface area available for heat transfer.
5. High heat transfer coefficients from the bed to the walls of the containing vessel are possible due to the presence of the fluidized solids.

6. At the same fluid flow rate, smaller pressure drops usually occur in a fluidized bed with no restraints than in a packed bed.

### 1.1.2 Disadvantages

The following items are some of the disadvantages of fluidized beds.

1. Only solids which flow freely and do not tend to agglomerate may be used.
2. For certain processes a temperature gradient may be desirable, and this cannot be accomplished utilizing the fluidized bed technique unless staging, partitions, or internal heat exchangers are incorporated.
3. Erosion of the containing vessel and internal solids may occur.
4. Bubble formations rising through fluidized solids may reduce the available contact surfaces, reducing the efficiency of the process.

## 1.2 Application to Nuclear Reactors

Fluidized bed techniques have been applied with considerable success to many processes where heat removal and temperature control are required. These factors are important in a nuclear reactor, and several proposals of the application of fluidized bed techniques to nuclear reactors have been submitted (8, 9, 10, 14). Advantages of a fluidized bed nuclear reactor design include uniform temperature distribution, uniform burnup independent of power distribution, ease of fission product removal, ease of fuel fabrication and reprocessing, and low fuel holdup (7, 10, 14).

Neutron moderation and heat removal could be accomplished by the fluid in a liquid fluidized bed nuclear reactor. Heat removal would be limited by the fluid velocity required to maintain fluidization under this arrangement.

Ordinary control rods could be inserted directly into the fissionable fluidized solids, or the control could be self-regulating. For self-regulation the bed could be designed so that the critical mass would be independent of reasonable fluctuations in the bed height, but a scram could be accomplished by shutting off the fluid flow (10). Proposals for fluidized bed nuclear reactors should meet the following requirements (9):

1. The fluid must have enough velocity to support the bed.
2. Heat must be removed.
3. A knowledge of the expansions and contractions of the bed and concentrations of the solids is necessary.
4. Pressure drops across the bed will have to be considered.
5. Erosion due to particle mobility must be considered.

### 1.3 Purpose

Although fluidized bed techniques have been applied with great success in many industrial processes, little knowledge has been gathered of the actual movement of particles in fluidized beds. Before it is possible to obtain a basic understanding of heat and mass transfer within a fluidized bed reactor, it will be necessary to have a fundamental understanding of the motion of the particles in the fluidized bed. Knowledge of the degree of backmixing and relative velocities of the particles and fluid, along with other characteristics of the fluidized bed, are fundamental requirements to an understanding of the mechanisms of heat and mass transfer.

The literature reveals hundreds of articles pertaining to fluidized beds, but only Gordon (4) and Wilde (13) have provided information on the statistical behavior of individual particles within the bed. It would seem appropriate

that experimental research work be carried out to further study individual particle mobility. Thus, it has been the purpose of this thesis to study experimentally the movement of individual particles in a fluidized bed.

The solids and fluid used in the study were stainless steel ball bearings and water.

#### 1.4 Scope

Water velocities ranging from minimum fluidization velocity to the velocity required to expand the fluidized bed to twice its static height were used. One ball bearing size and one static bed height of ball bearings were utilized in the experimental study. Particle concentrations and mean vertical speeds were obtained. The development and construction of the experimental apparatus, the method of obtaining the experimental data, and a statistical analysis approach of evaluating the experimental data are included in this thesis. Tracing the movement of a radioactive ball bearing in the fluidized bed was used as the method of studying individual particle mobility.

## 2.0 EXPERIMENTATION

### 2.1 Experimental Apparatus

A photograph of the experimental apparatus is shown in Fig. 1, and a schematic diagram is presented in Fig. 2.

The apparatus may be divided into the following categories: (1) the column and its accessories, (2) the gamma ray detection equipment, and (3) the measuring and recording equipment.

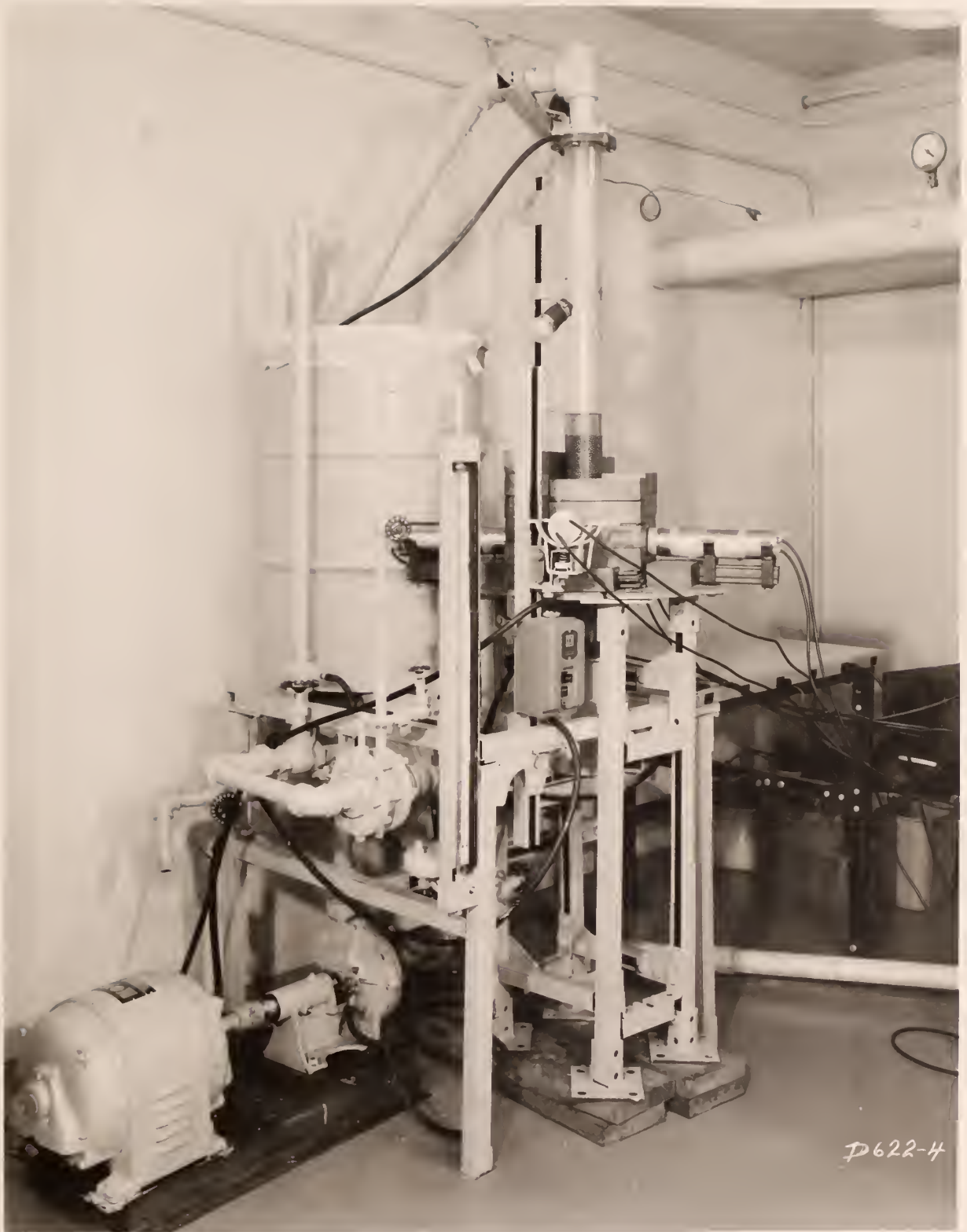
#### 2.1.1 The Column and Its Accessories

A 48-inch-high, 3.0-inch-inside diameter, and 3.5-inch-outside diameter cast acrylic resin tube was used as the fluidizing column. It was fitted with a flange on each end. Figure 3 provides a close-up view of the column and bed of solids. The outlet of the column was fitted with a wire screen to prevent any of the fluidized solids from accidentally escaping the column. The two flanges were fitted with pressure taps for measuring the pressure drop over the bed of solids. The lower flange was bolted to the distributor assembly.

The distributor assembly, shown in Fig. 4, consisted of a calming section of 3/8-inch ceramic balls, housed in a container eight inches high and three inches in diameter. A brass sieve separated the calming section from the fluidized particles. The holes in the brass plate were 3/32-inch diameter, and the ratio of hole area to total area of the sieve was 0.343.

As shown in Fig. 2, a 30-inch mercury manometer was used to measure the pressure difference over the orifice meter.

The water flow through the fluidized bed was provided by a closed system. A 55-gallon drum coated with chromate primer to prevent corrosion served as the water reservoir.



D622-4

Figure 1. The Column and its Accessories.

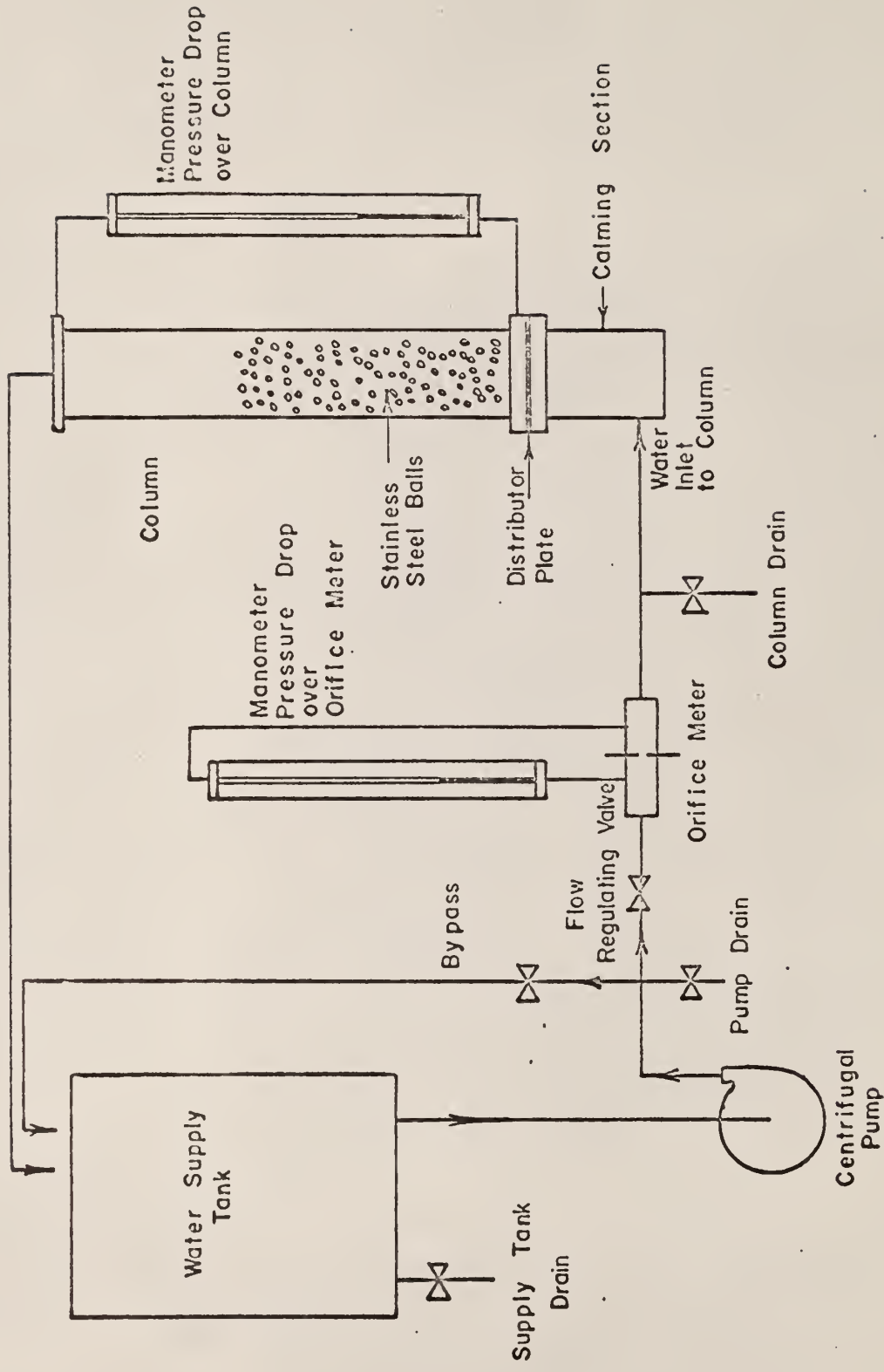


Figure 2. Schematic Diagram of the Column and its Accessories.

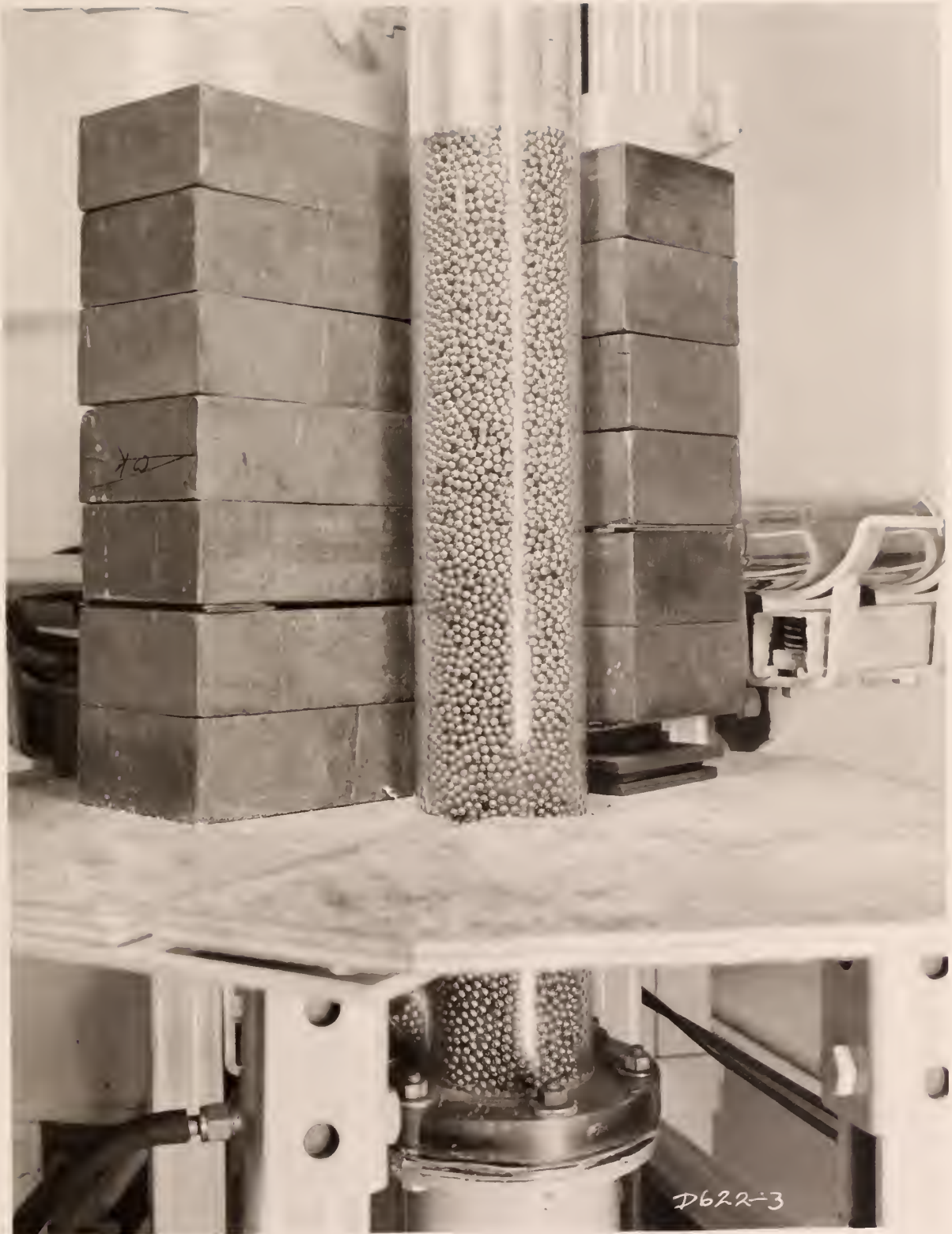


Figure 3. Solids Within the Fluidizing Column.

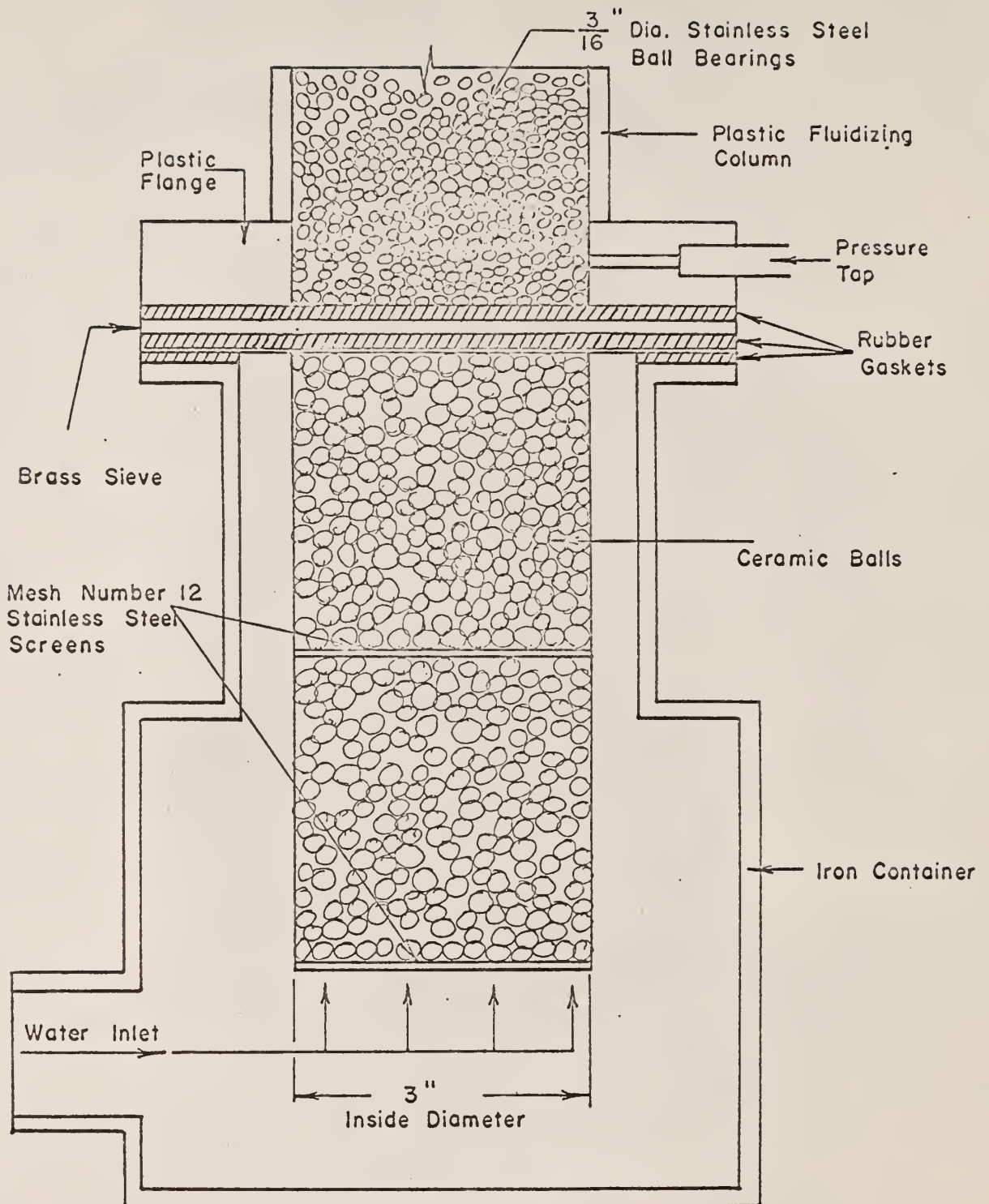


Figure 4. Distributor Assembly.

A Type S.C., U.S. Motor, rated at 5 horsepower, 220 volts, three-phase, 60 cycles, and 1800 revolutions per minute, powered the pump. The pump was a centrifugal type, with a 2.5-inch inlet and a 2.0-inch outlet. It was built by Fairbanks-Morse.

The structure used to support the column and its accessories was constructed from Unistrut.

The water piping system was constructed of standard schedule 40  $1\frac{1}{2}$ -inch diameter galvanized pipe.

### 2.1.2 The Gamma-Ray Detection Equipment

Four scintillation probes were used to detect the radioactive stainless steel ball in the fluidized bed. Two probes were used at each of two horizontal planes. The horizontal planes were constructed in the following manner: Lead bricks of 2x4x8-inch size were stacked around the column, with 1/8-inch lead shims placed between the layers of bricks at each of the two horizontal planes studied. The increased output from the scintillation probes behind each slit provided a means of detecting the movement of the particle each time the radioisotope passed one of the horizontal window slits in the shielding.

Figure 5 is a photograph of the scintillation probes positioned behind the lead shielding. Part of the lead bricks are removed from the top of the shield.

Figure 6 illustrates the vertical position of each scintillation detector level and the distance between the two detector levels,  $\Delta Z$ .

The four scintillation probes used were B.J. Electronics of Borg-Warner Corporation, Type 7D4 Sodium Iodide (Thallium) crystal, Model DP3, serial number B-168, and NE numbers 287, 288, 314, and 353.

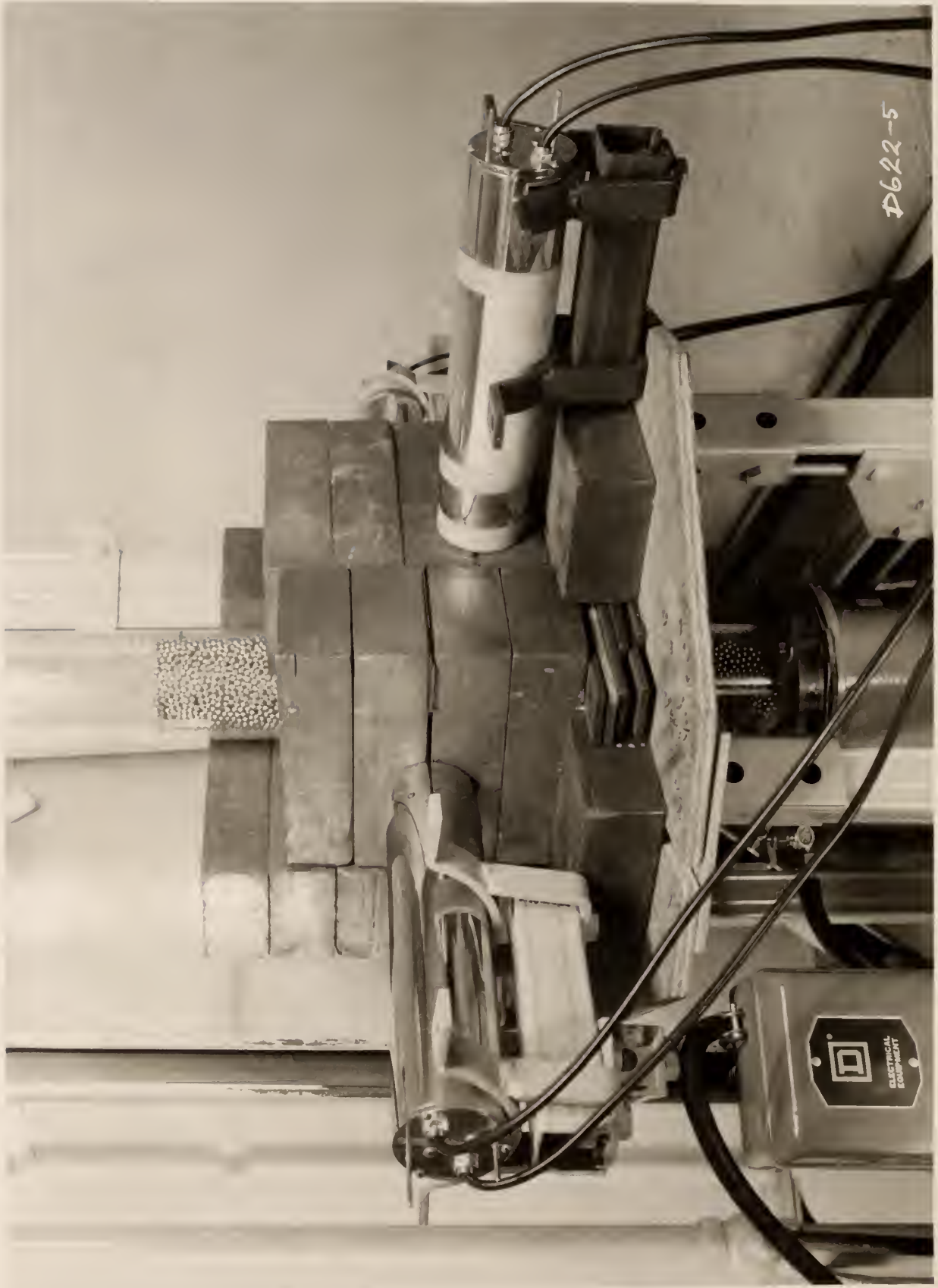


Figure 5. Scintillation Probes and Shielding.

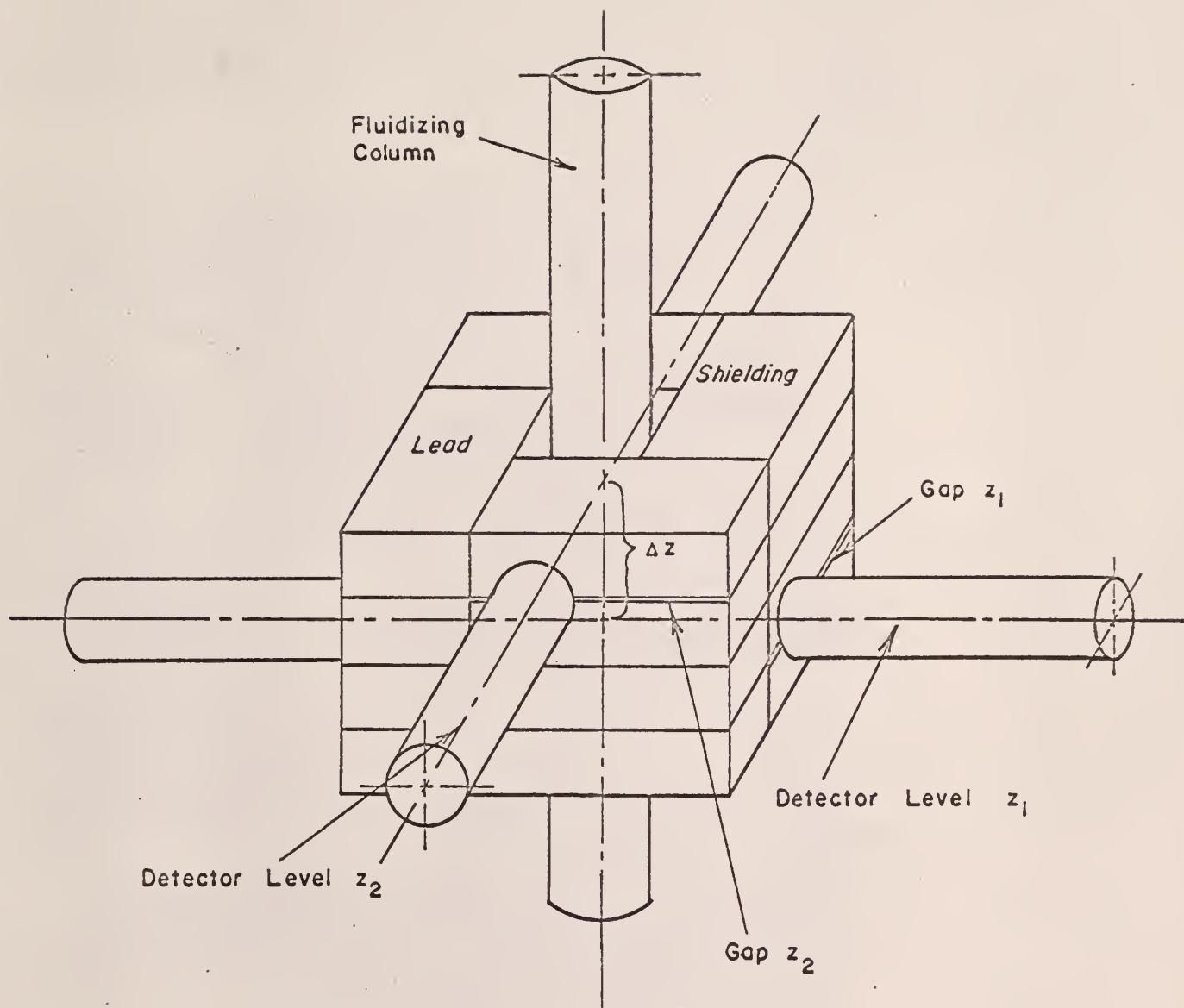


Figure 6. Schematic of Scintillation Probes and Shielding.

### 2.1.3 The Measuring and Recording Equipment

Figure 7 is a schematic diagram of the detection and recording equipment.

High voltage power supplies. The photomultipliers of the two scintillation probes at each of the two detector levels were supplied with high voltage from B.J. Electronics, Borg-Warner Corporation, Model DVI, Detectolab, NE 262 and NE 275 variable high voltage power supplies. NE 275, operated at about 1050 volts, supplied high voltage to the upper detector level, and NE 262, operated at about 1100 volts, supplied high voltage to the lower detector level. The two power supplies are located at the top of the instrument rack in Fig. 8.

Ratemeters. The output from each detector level was fed to a ratemeter, as shown in Fig. 7. The two ratemeters are shown side-by-side directly below the high voltage power supplies in Fig. 8. The ratemeters used were built similar to the Baird-Atomic, Inc., Model 432 A, Research Ratemeter. NE 901, the left-hand ratemeter in Fig. 8, was used for the lower detector level, and NE 902 was used for the upper detector level. The time constants were determined experimentally by a step input to each ratemeter.

When the d-c output of the integrator circuit in a ratemeter exceeded a given value, firing of a neon bulb caused the current to flow in the final stage of the ratemeter. Two outputs were provided from each ratemeter. One output from each ratemeter was sent to a two-channel high-speed recorder, and the other output from each ratemeter served as the input to a Time Interval Meter.

Two-channel recorder. The counting rate at each detector level was monitored by one channel of a dual channel recorder. The recorder, pictured on the stool in Fig. 8, was an Offner Type RS Dynograph, NE 733. The output from the lower detector level ratemeter was the input to the left-hand channel of the

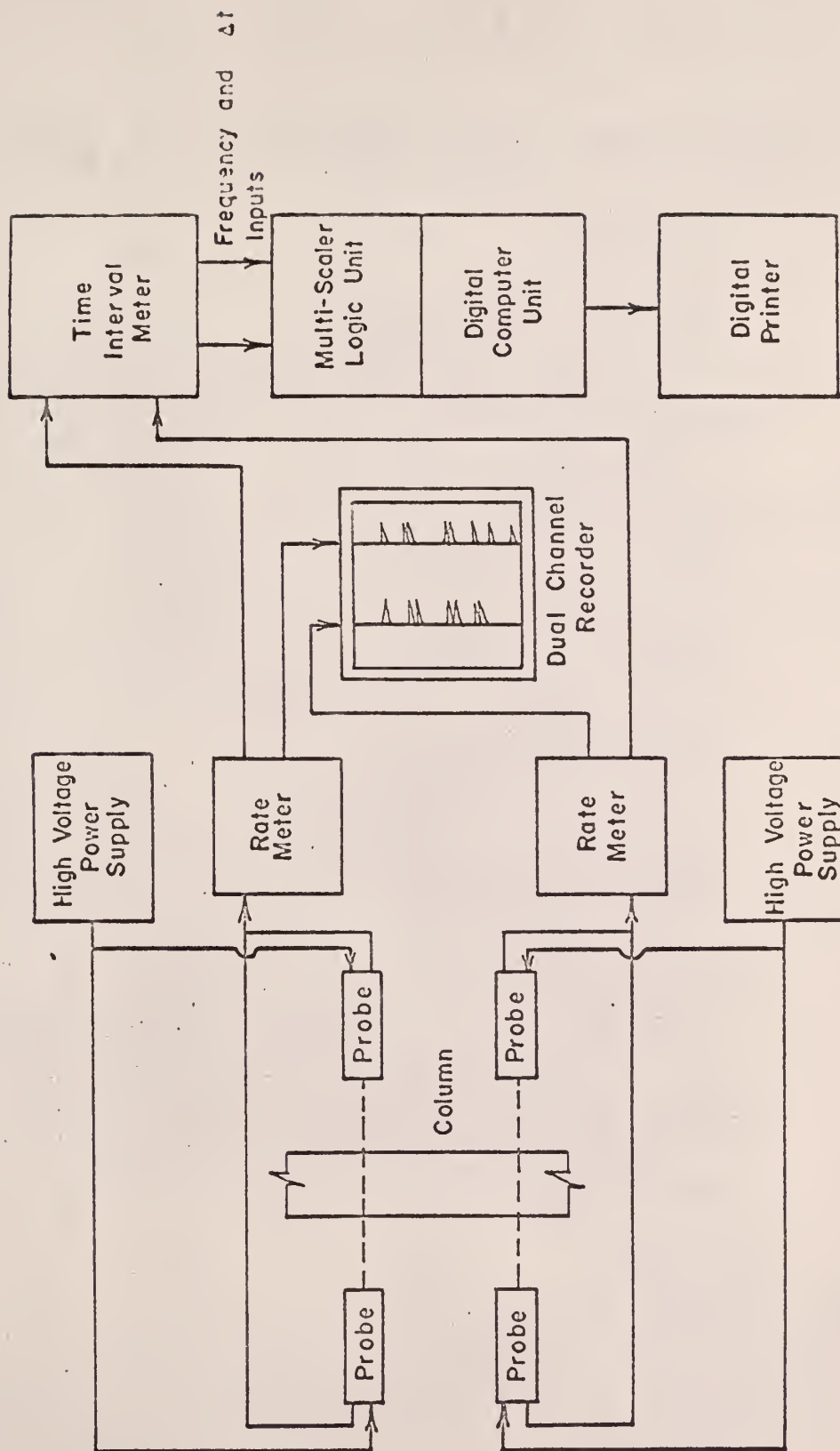


Figure 7. Schematic Diagram of the Detection and Recording Equipment.

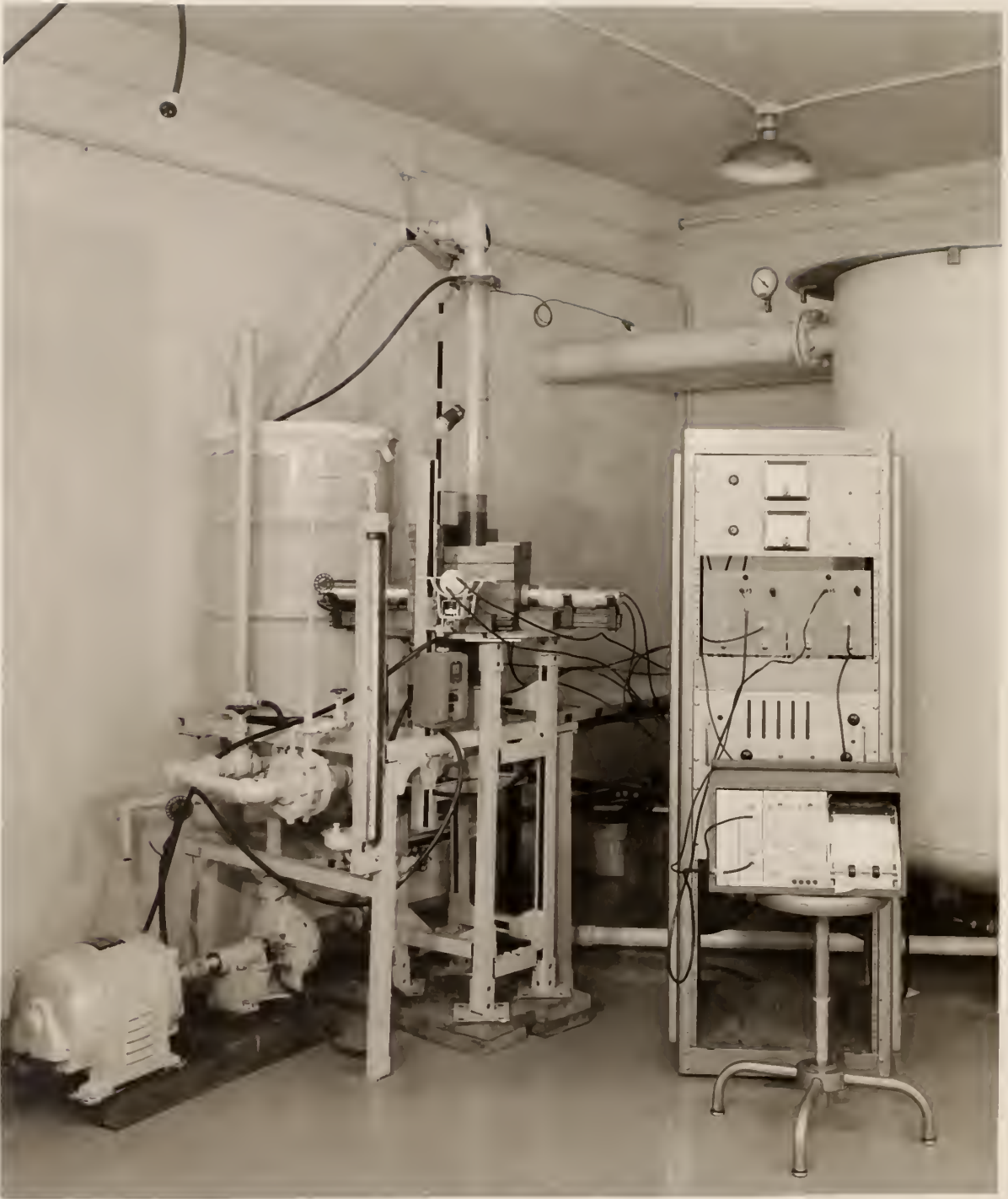
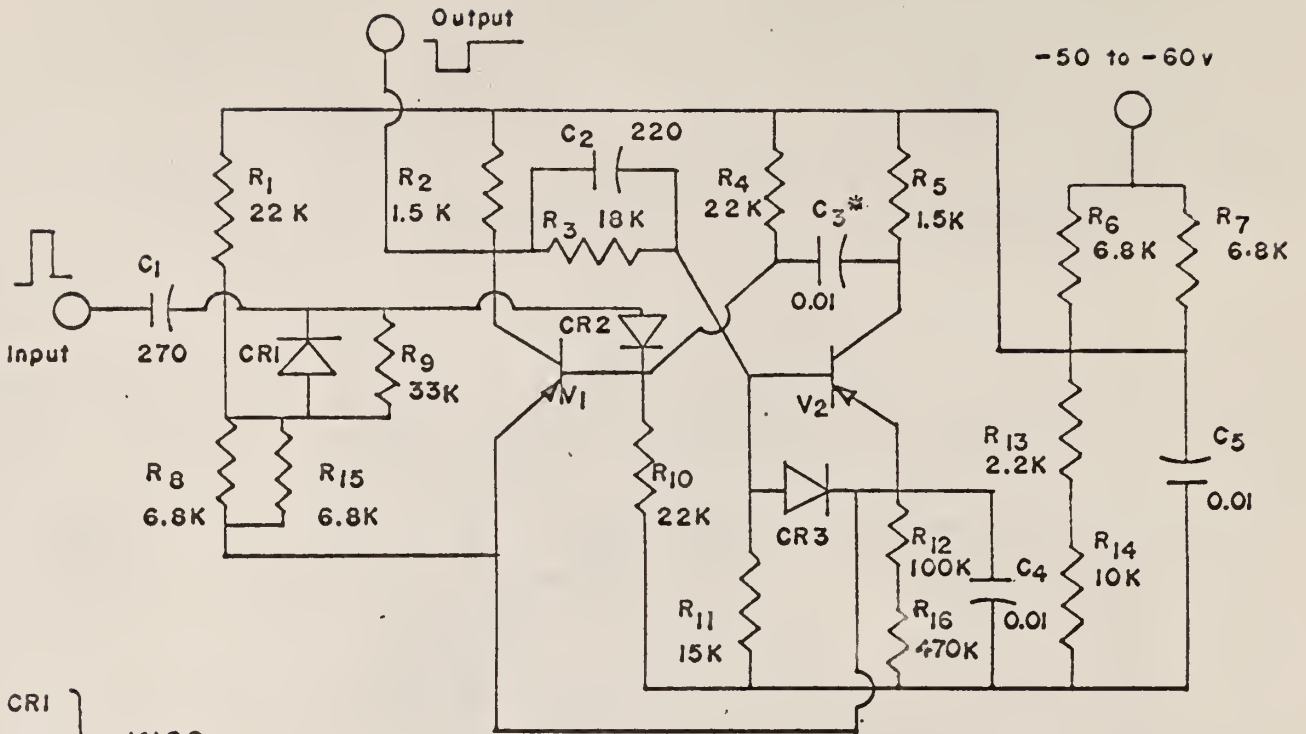


Figure 8. The Experimental Apparatus.

recorder. The output from the upper detector level was the input to the right-hand channel of the dual-channel recorder.

Time Interval Meter. The Time Interval Meter, shown below the ratemeters in Fig. 8, was a Beckman/Berkeley Model 7250R, NE 763. The counting rates from the ratemeters were fed to the input channel amplifiers of the Time Interval Meter for pulse shaping and amplification. Whenever a sharp change in the counting rate occurred, a positive pulse was generated at the output of the Time Interval Meter. The positive pulse output of each input channel of the Time Interval Meter was fed to a single, specially designed, transistorized, monostable multivibrator circuit, KSU-NE No. 009. The multivibrator circuit is shown in Fig. 9. The output from this circuit drove the external delta-t circuit of the Technical Measurements Corporation Multi-Channel Analyzer Multi-Scaler Logic Unit. All other outputs from the input channel circuits of the Time Interval Meter were disconnected. The gate times were stopped by the rapid change in the counting rate. To restart, the oscillator circuit in the Time Interval Meter was utilized. To provide the restart pulse, the following modifications were made to the Time Interval Meter. The output of pin 1 of V402 in the oscillator and shaper circuit in the Time Interval Meter was disconnected and reconnected to the top of R206 through a 470 mmfd capacitor. The circuit previously feeding R206 was disconnected by removing C201. These modifications can be seen by observing the schematic diagrams in the instruction manual for the Time Interval Meter. The Oscillator and Shaper Schematic Diagram and the Master Schematic Diagram are Beckman/Berkeley Division Drawing Numbers 7000 C 419 and 7250 D 21, respectively.

The oscillator in the Time Interval Meter also served as a fixed frequency pulse which acted as a time base generator and was fed into the amplifier input of the Multi-Channel Analyzer Multi-Scaler Logic Unit. A four-decade circuit



- CR1 } IN99
- CR2 } IN99
- CR3 } IN99
  
- V1 } 2N414
- V2 } 2N414

\* C<sub>3</sub> is chosen for pulse width desired

Figure 9. Wiring Diagram for KSU-NE 009 Multivibrator Circuit.

with an output jack for each decade was added to the output of the oscillator and shaper circuit so that a variable selection of frequencies could be used. Only one pulse frequency was used to obtain the experimental data.

Multi-Channel Analyzer. The Technical Measurements Corporation 256-channel Model CN-110 Analyzer, NE 630, utilizing the Multi-Scaler Logic Unit, served as a counter of the number of pulses from the Time Interval Meter oscillator over a period of time. The analyzer is shown in Fig. 10. The Pulse Height Logic Unit, NE 633, as shown in Fig. 10, was not used. Instead, as noted above, the Multi-Scaler Logic Unit, Model 214, NE 633, was used.

The output pulse from the mono-stable multivibrator circuit was connected to the external delta-t circuit of the Multi-Scaler Logic Unit and served as a trigger to switch channels in the multi-channel analyzer. Each channel, one-by-one, would accumulate and store the number of oscillator pulses counted before another rapid rise in counting rate from one of the ratemeters would cause storage to be transferred to the next channel. Therefore, the number of pulses counted from the Time Interval Meter oscillator was a measure of the time between rapid change in the output of the ratemeters, resulting from the radioactive source passing one of the detector level slits.

Digital Print Out. A Hewlet Packard, Model 561 B, NE 632, recorded the information stored in each of the 256 channels of the Multi-Channel Analyzer. The printer is shown directly above the Multi-Channel Analyzer in Fig. 10

## 2.2 Materials

Type 440-C stainless steel ball bearings of reject quality obtained from the Hartford Steel Ball Company were used exclusively for the solids in the fluidized bed. The balls had a sample mean diameter of 0.1876 inch, with a variance of  $0.0003 \text{ (inch)}^2$ , based on a random sample of 30 stainless steel

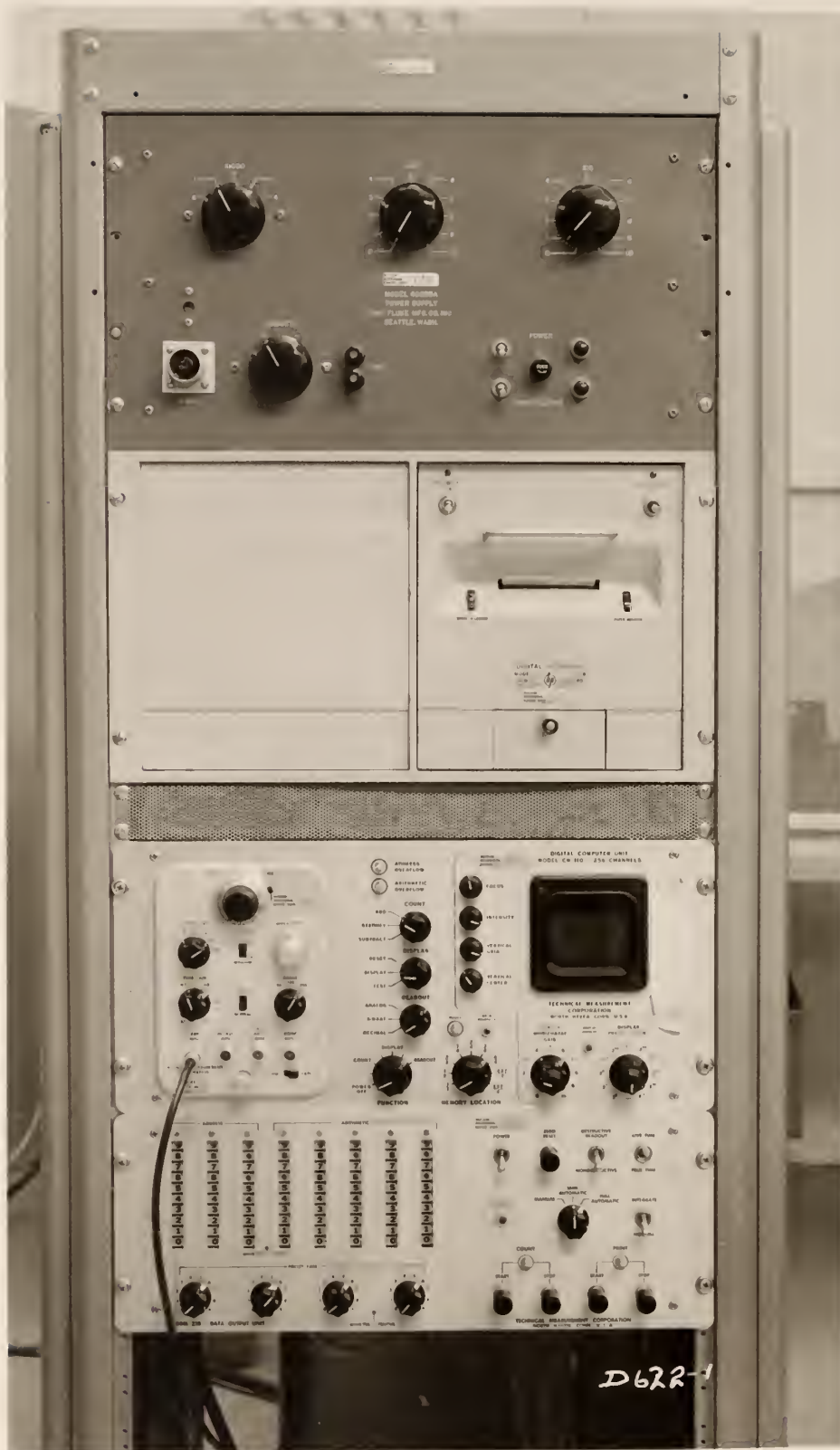


Figure 10. Multi - Channel Analyzer and Digital Printout Units.

balls removed from the fluidized bed. The mean sample weight of the balls was 0.4304 gram.

The radiation source was a type 316 stainless steel ball bearing, irradiated at a flux of  $10^{12}$  neutrons  $\text{cm}^{-2}\text{sec}^{-1}$  in the lazy susan irradiation facility of the Kansas State University Triga Mark II nuclear reactor. Irradiation for  $1\frac{1}{2}$  hours produced a Manganese-56 source strength of 12 to 14 millicuries.

A Type 316 stainless steel ball bearing was used because of the 2% manganese content by weight in Type 316 stainless steel. The diameter of the isotope was 0.1875 inch, and its weight was 0.450 gram. Industrial Tectonics, Inc. supplied the Type 316 stainless steel ball bearings. A different ball bearing was used as the radioactive source each day data were obtained. No detectable variations were found in the size and weight of the individual ball bearings.

Figure 3 is a photograph showing the stainless steel ball bearings inside the fluidizing column. The total weight of ball bearings in the column was 24.125 pounds, and the static bed height was 19.5 inches.

## 2.3 Calibrations

### 2.3.1 Half-life Determination

The half-life of the radioisotope produced upon neutron irradiation in the Kansas State University Triga Mark II nuclear reactor was determined by measuring the activity one yard from the source with a dose-rate meter, at various times after removal of the stainless steel ball bearing from the nuclear reactor. Figure 11 is a plot of the log of the dose rate at one yard from the source versus the time after removal of the ball bearing from the reactor. The half-life determined from this figure was found to be 2.5 hours. Manganese-56 has

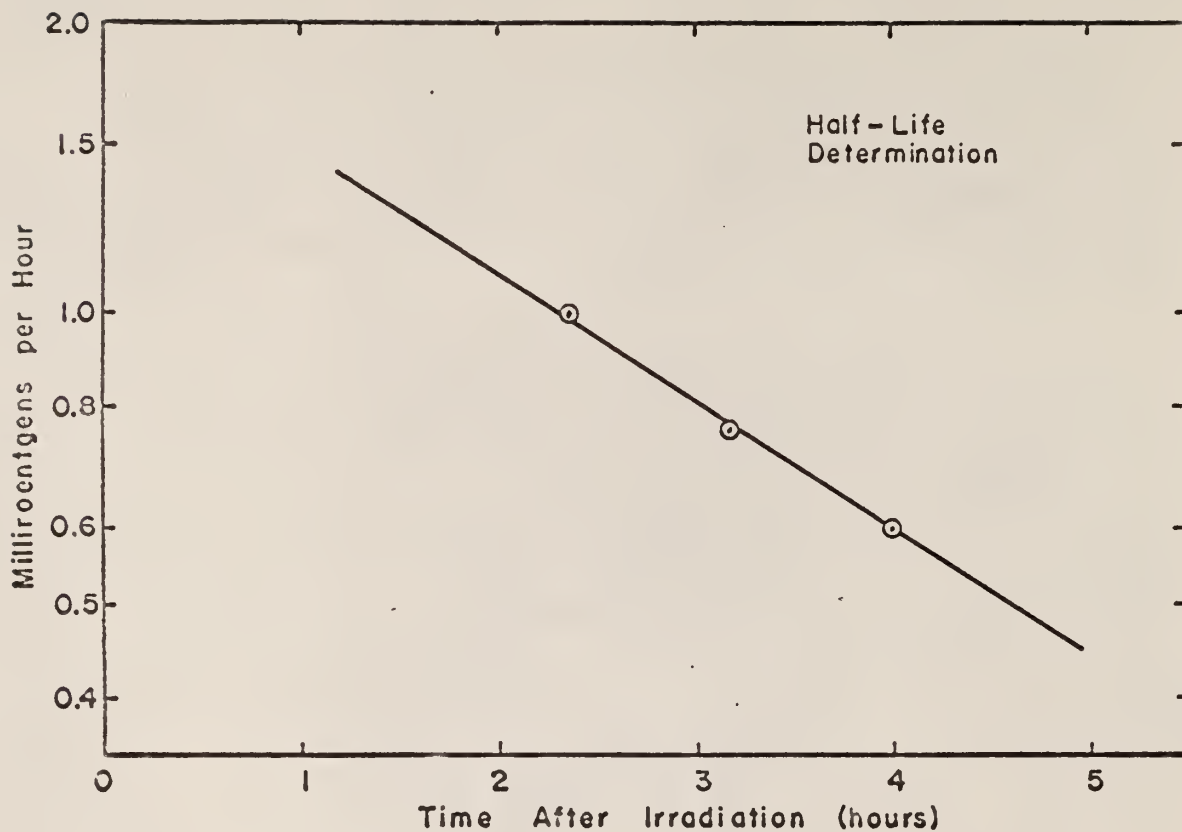


Figure II. Stainless Steel Ball Bearing Activity as a Function of Time After Removal From Reactor.

a gamma-ray half-life of 2.58 hours; therefore, the activity produced was primarily Manganese-56.

### 2.3.2 Calibration of the Orifice Meter

A length of  $1\frac{1}{2}$ -inch-inside diameter hose was connected to the outlet of the column, and the other end of the hose was placed in a 55-gallon barrel. Water was pumped from the supply tank, through the fluidizing column, and into the 55-gallon barrel. Two levels were marked off in the barrel. The water flow was adjusted. The height of the mercury in the manometer across the orifice meter and the time taken for the water level in the barrel to pass from the first mark to the second mark were recorded. Figure 12 shows a plot of gallons per minute versus the manometer reading. Figure 13 converts the manometer reading to superficial fluid velocity in the column.

### 2.3.3 Radial Effects

The scintillation detectors were paired off according to their operating voltage. It was found that of the scintillation probes available, NE 287 and NE 314, and NE 288 and NE 353 formed the best pairs.

The radioactive source, in its vertical movements, would rarely be moving in the center of the column during a data run. It was, therefore, necessary to determine the effect of radial position on the counting rates from each pair of detectors when the particle passed through the plane of each detector level.

The source was placed in each of the radial positions in the fluidizing column as shown in Fig. 14. For each radial position, counting rates were obtained at different vertical positions with respect to the detector level. Counting rate versus vertical position curves were plotted for each radial

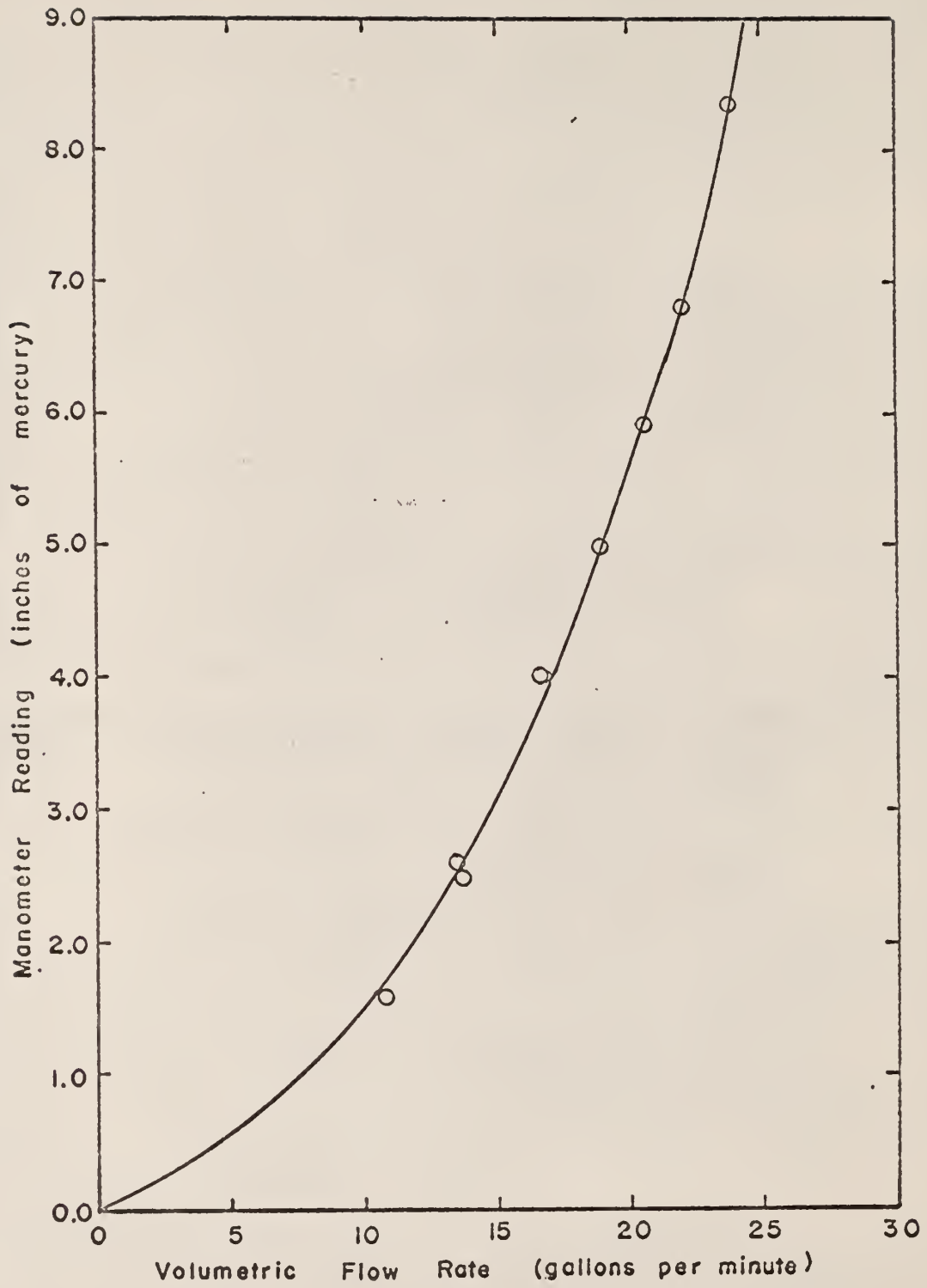


Figure 12. Calibration of the Orifice Meter.

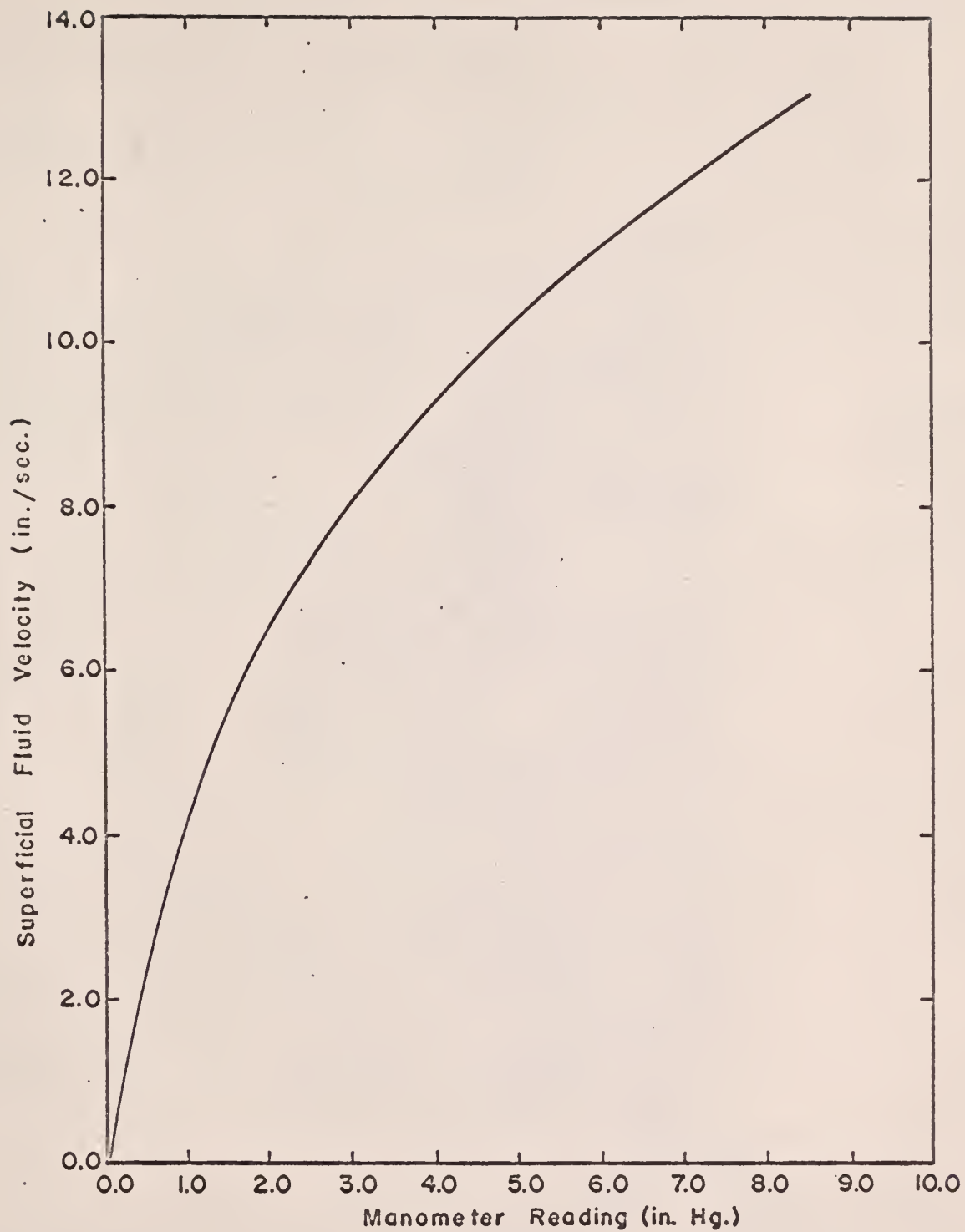


Figure 13. Superficial Fluid Velocity in Fluidizing Column.

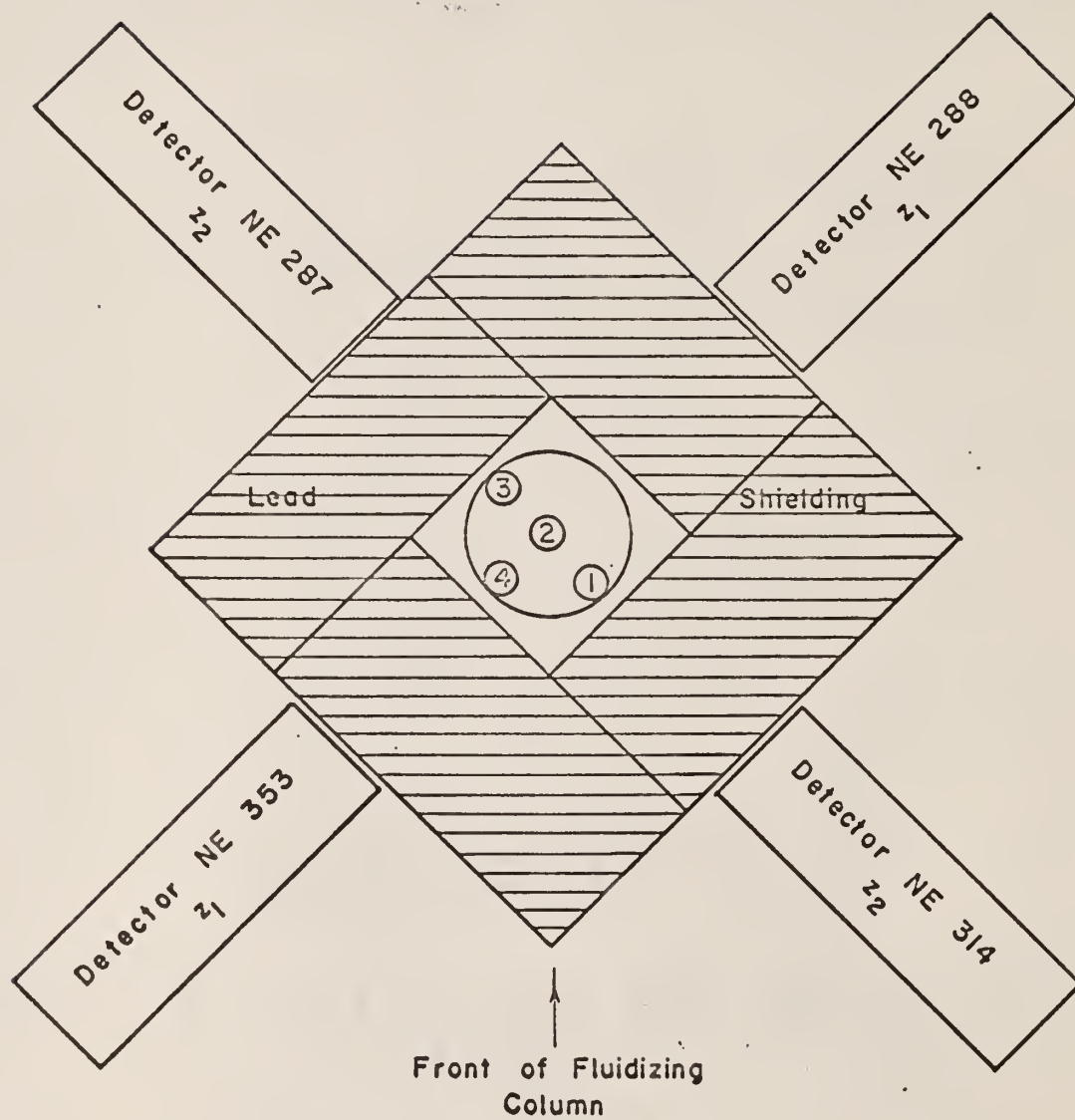


Figure 14. Arrangement of Probes and Shielding Around Fluidizing Column.

position and each pair of detectors. These curves are shown in Figs. 15, 16, 17, and 18. These figures show that, with the arrangement of detectors used, the radial position of the radioactive source had little effect on the output received from the scintillation probes. Detectors 288 and 353 gave a lower counting rate than detectors 287 and 314 at the same high voltage setting; therefore, during the data runs the high voltage to detectors 288 and 353 was adjusted to a higher value to equalize the sensitivity.

#### 2.3.4 Gap Width and Thickness of Shield Determination

It was necessary to determine the optimum gap width and shielding thickness to provide a high counting rate when the source was in front of the gap and a low counting rate when the source was not in front of the gap. The gap width and shielding thickness were determined experimentally by measuring the counting rate at different vertical distances with respect to the detector level for different gap widths and shielding thicknesses.

The source was placed in a plastic container and suspended into the water-filled column. It was moved vertically with a nylon cord. A graduated scale was placed alongside the column and the radioactive source was held at constant vertical positions while one-minute counts were obtained. Figures 19, 20, 21, 22, and 23 show the counting rates versus vertical position for different gap widths and shield thicknesses. The gap width and shield thickness selected are those shown in Fig. 23.

#### 2.3.5 Calibration of the Electronic System

As the source passed from one detector level to the other, the outputs from the ratemeters were recorded as a pulse on the dual-channel recorder. The right-hand channel of the recorder would map the output from the upper

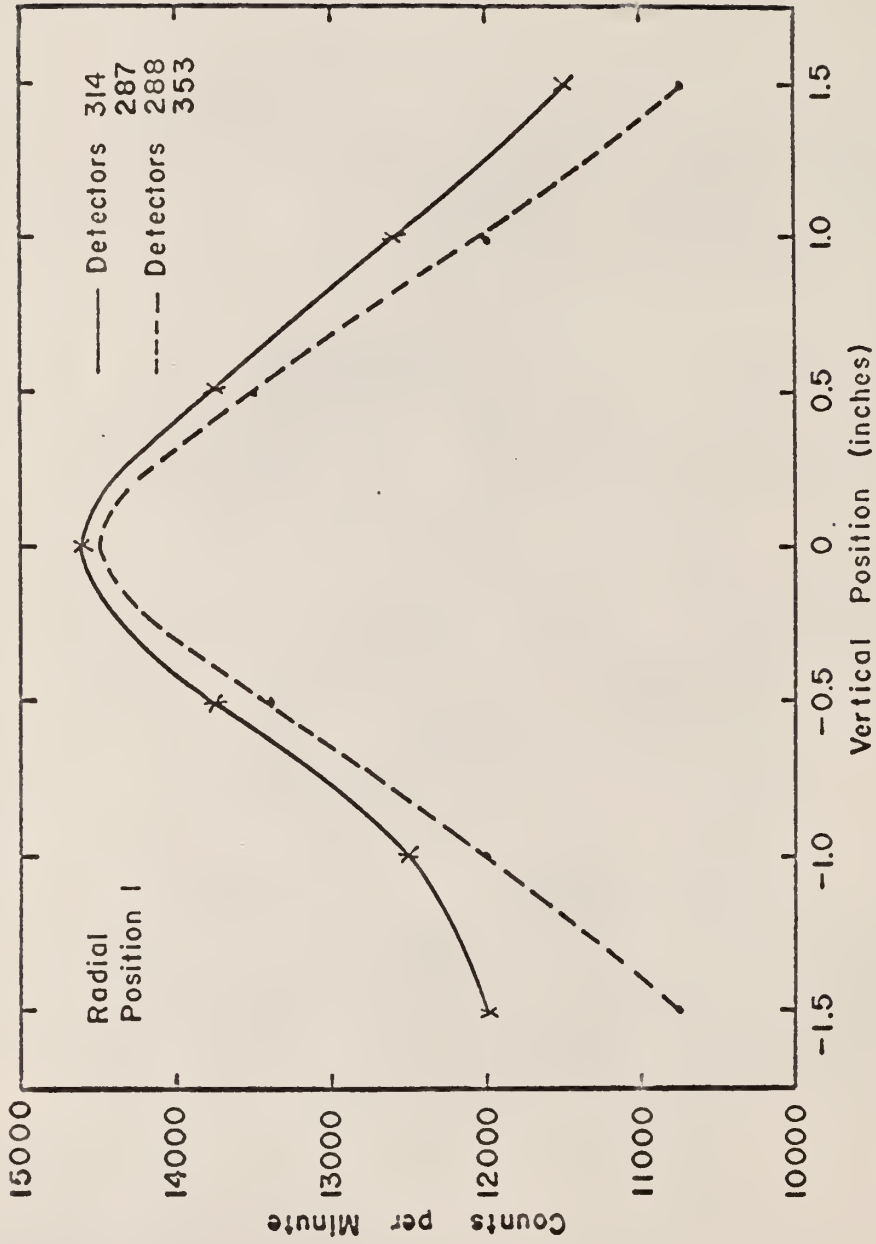


Figure 15. Counting Rate as a Function of Vertical Position of Radioactive Source, Radial Position I.

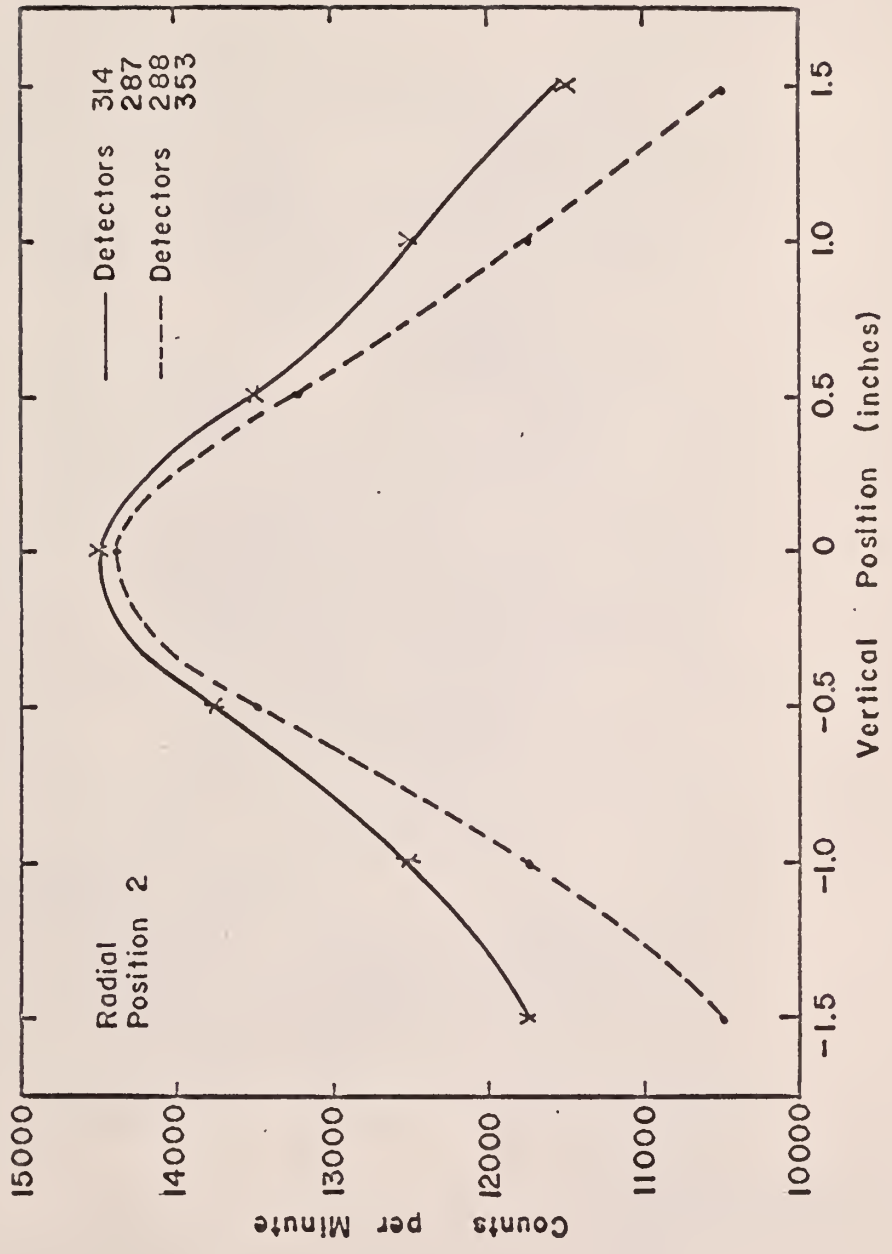


Figure 16. Counting Rate as a Function of Vertical Position of Radioactive Source, Radial Position 2.

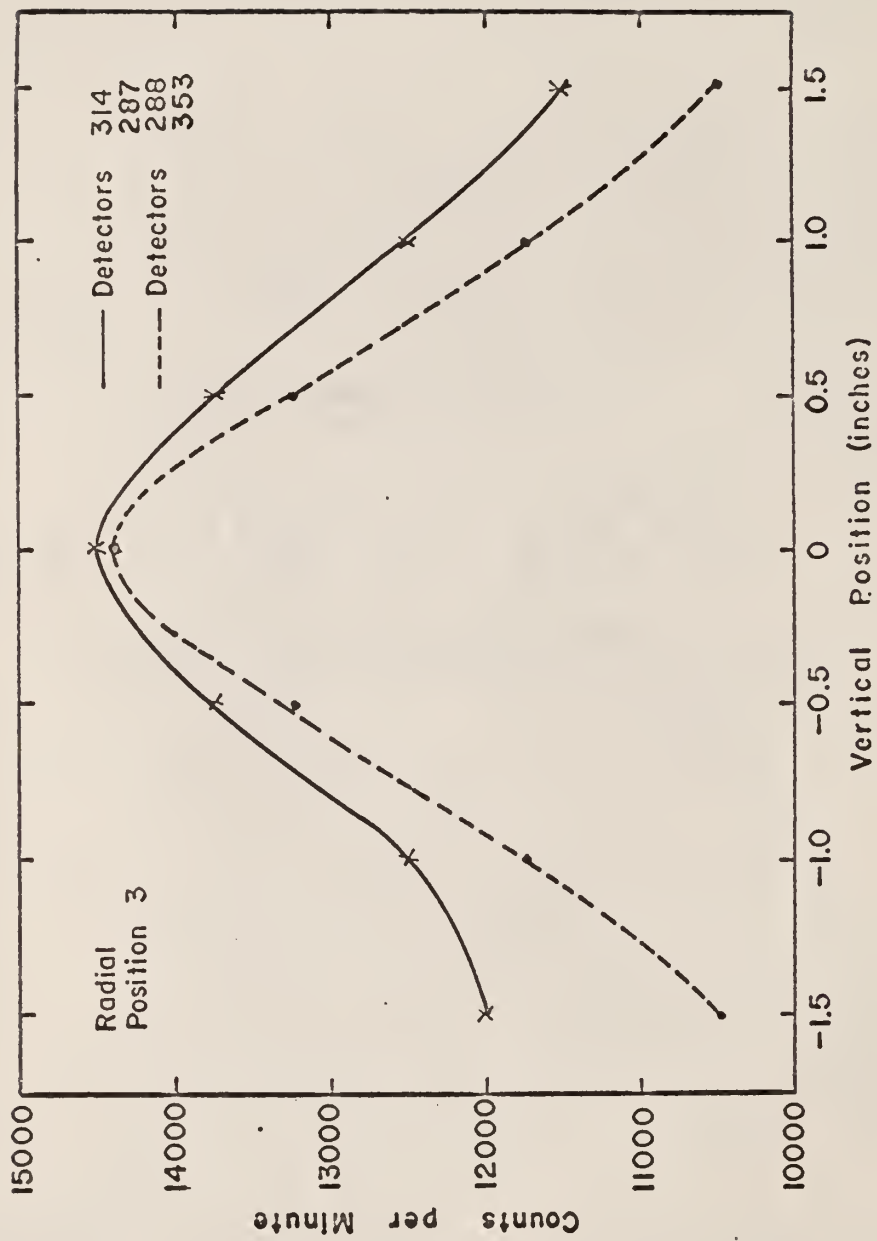


Figure 17. Counting Rate as a Function of Vertical Position of Radioactive Source, Radial Position 3.

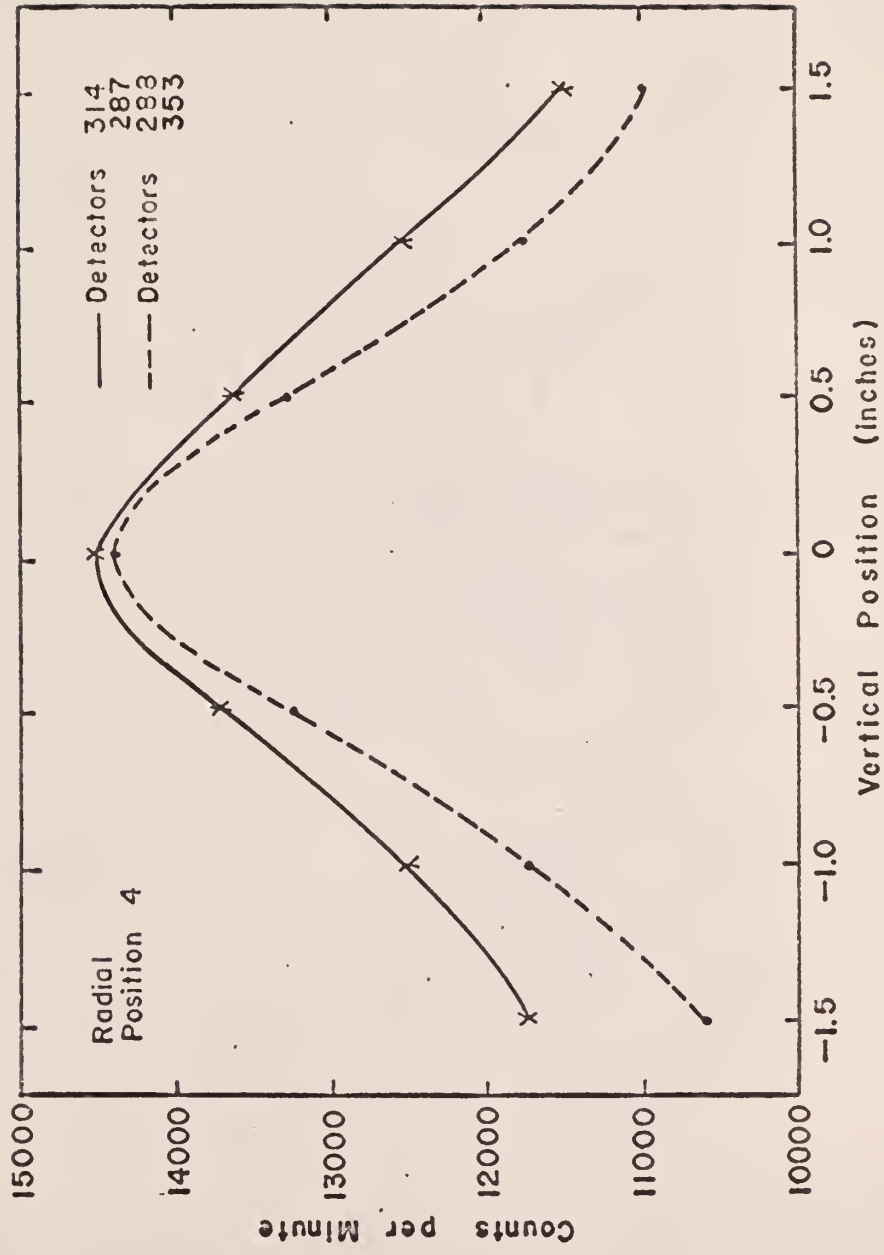


Figure 18. Counting Rate as a Function of Vertical Position of Radioactive Source, Radial Position 4.

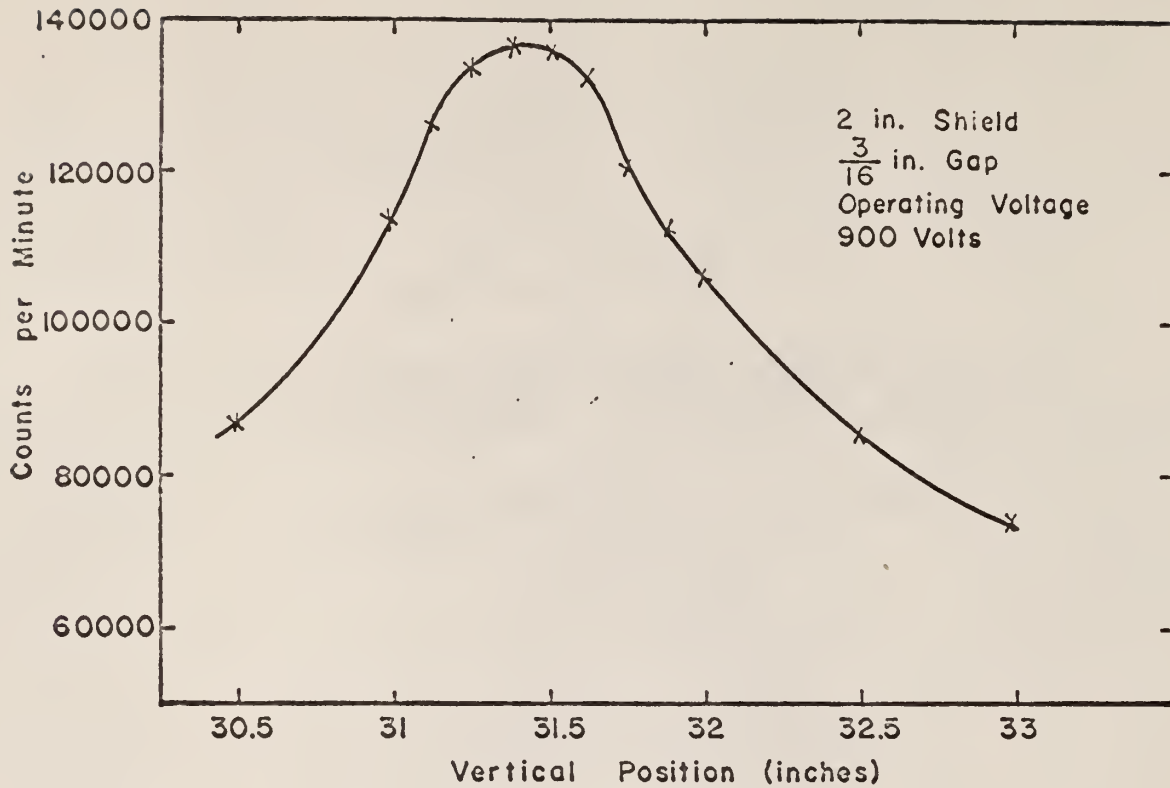


Figure 19. Counting Rate as a Function of Vertical Position of Radioactive Source, 2 in. Shield,  $\frac{3}{16}$  in. Gap.

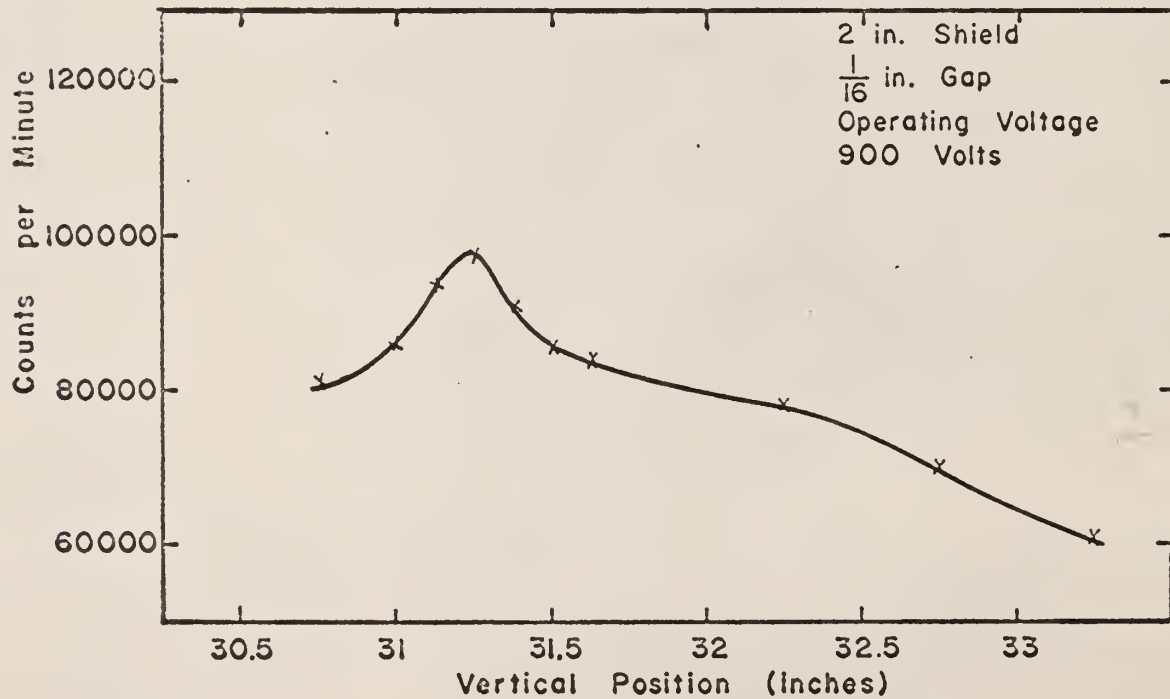


Figure 20. Counting Rate as a Function of Vertical Position of Radioactive Source, 2 in. Shield,  $\frac{1}{16}$  in. Gap.

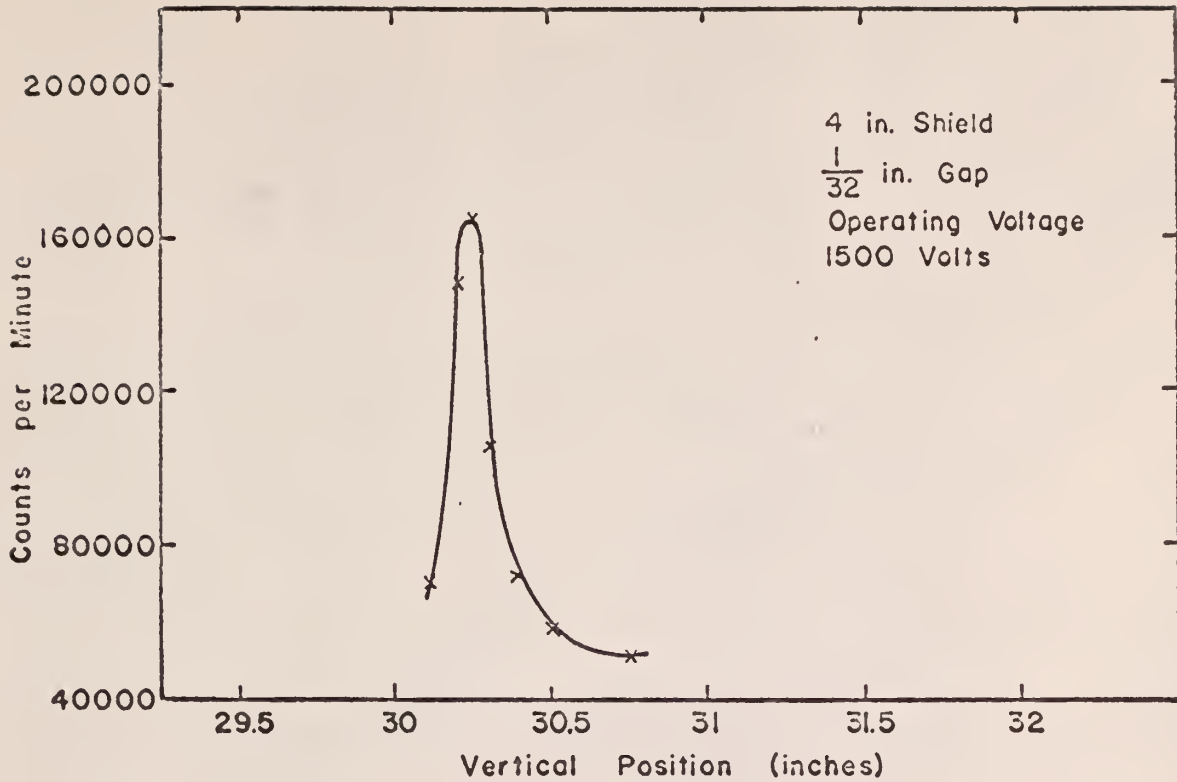


Figure 21. Counting Rate as a Function of Vertical Position of Radioactive Source, 4 in. Shield,  $\frac{1}{32}$  in. Gap.

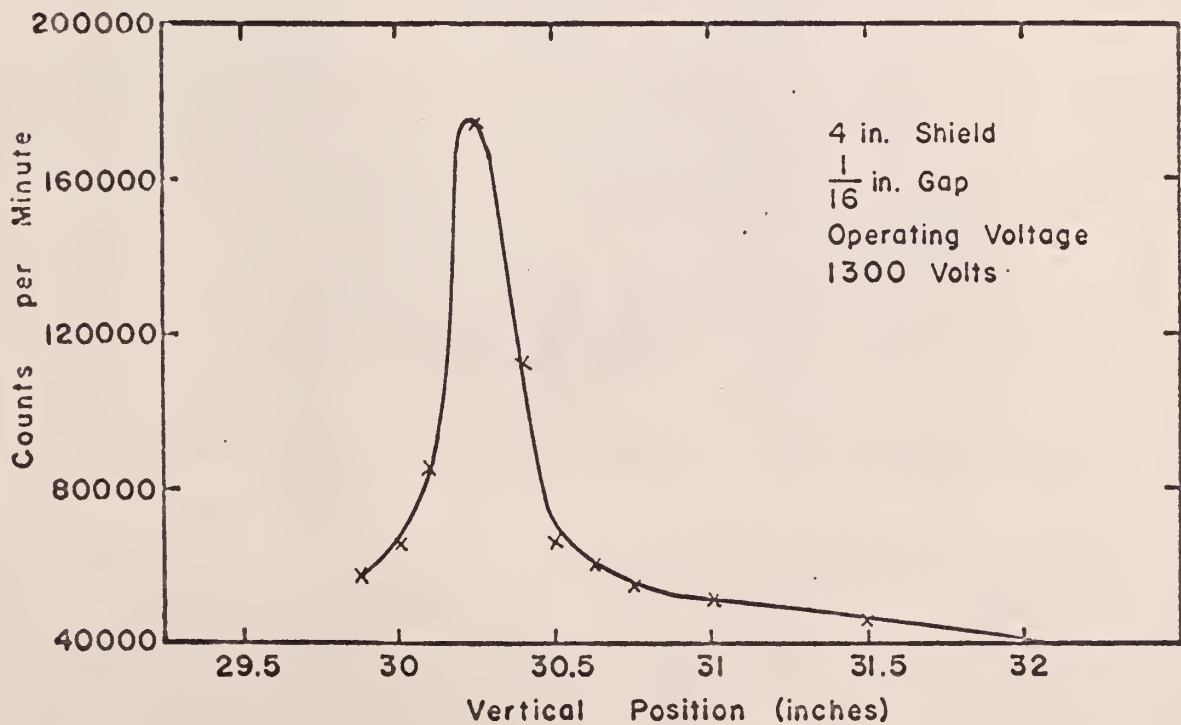


Figure 22. Counting Rate as a Function of Vertical Position of Radioactive Source, 4 in. Shield,  $\frac{1}{16}$  in. Gap.

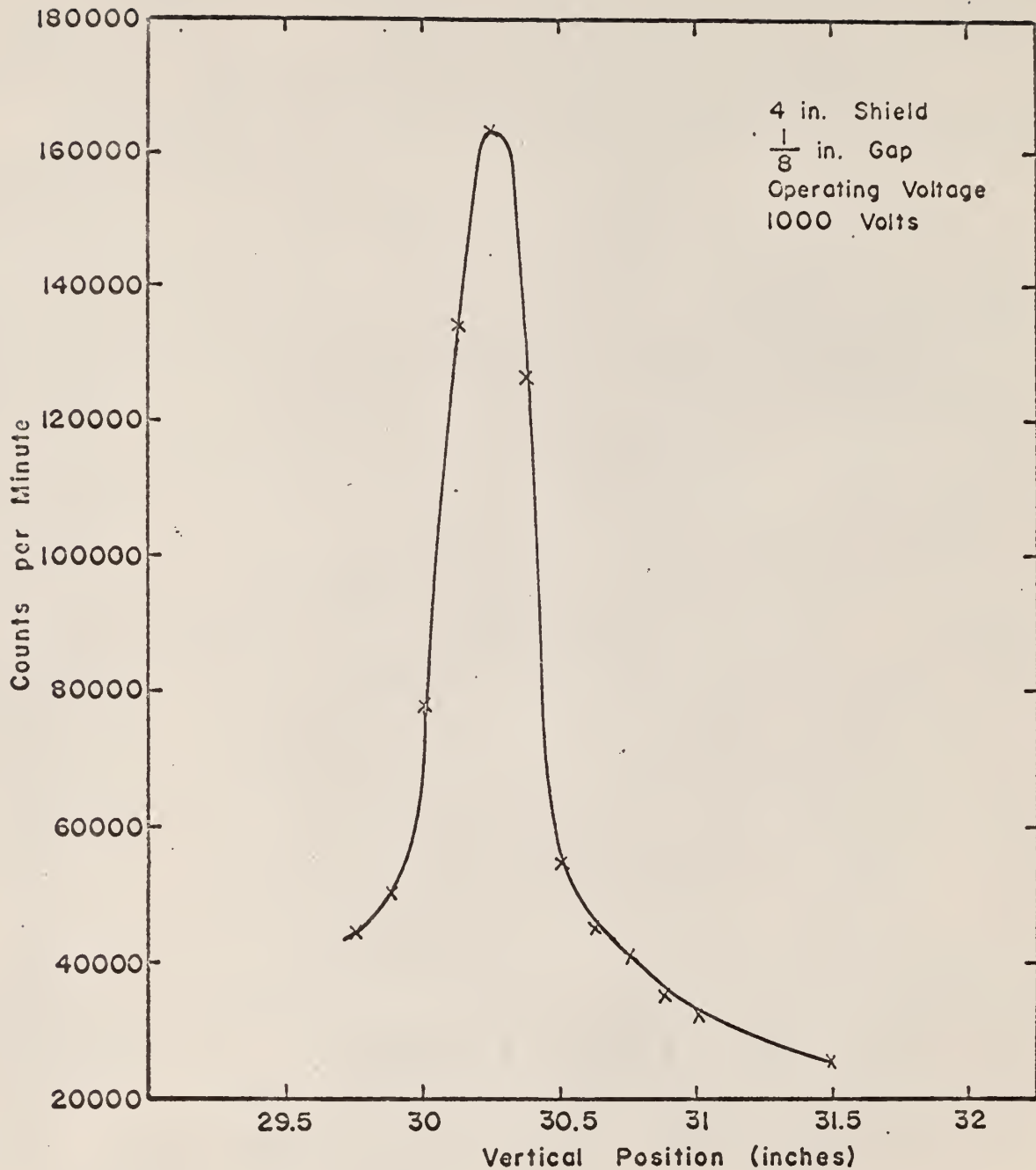


Figure 23. Counting Rate as a Function of Vertical Position of Radioactive Source, 4 in. Shield, 1/8 in. Gap.

detector level, and the left-hand channel would map the output from the lower detector level. Knowing the speed of the recorder, the distance between pulses was used to determine the elapsed time between the pulses. If the right-hand channel recorded a pulse, and the next pulse recorded was by the left-hand channel, the particle had passed from the upper to the lower detector level. By measuring the distance between the two pulses, the time to travel from upper to lower level was obtained.

The known fixed-frequency input to the Multi-Scaler Logic Unit of the Technical Measurements Corporation Multi-Channel Analyzer acted as a timer. When a pulse was recorded on either of the two recorder channels, the same pulse provided a trigger to switch channels in the multi-scaler. The number of counts stored in each channel of the multi-scaler was converted to elapsed time by dividing by the oscillator frequency.

The reliability of the measurement of elapsed time was determined experimentally. This was done by moving the source past the two detector levels at precisely known time increments and comparing this to the time increments obtained from the two methods outlined above. The experimental time was determined by finding the pulses on the chart recording and correlating these pulses to the correct channel locations given by the printout of the multi-scaler memory unit. Once the channel number of the printout tape was correlated to a pulse on the chart recording, the number of counts stored in that channel was divided by the frequency of the oscillator to obtain the time increment. This gave the experimentally measured times for the particle to pass from the lower-to-upper and upper-to-lower detector levels.

A Zero-Max motor and gearhead unit was used to move the source up and down in the column. The unit was capable of variable speeds from 0 to 400 revolutions per minute. A pulley was mounted at the top of the column, and a nylon cord was

passed over the pulley into the column. The source was suspended on the end of the cord. The other end of the cord was attached to the shaft of the gearhead. By winding the cord around the shaft until the source was at the top of the column and turning on the motor, the source would be lowered to the bottom of the column and returned to the top again. By this technique the source was lowered and raised at a constant speed past the two detector levels. A 30-inch section of the column was marked off, and the time for the source to be lowered through this section was taken as the best estimate of the time increment and was taken to be the true time.

Experimental runs were made at several gearhead speeds, and the time increments required to pass between the two levels obtained by the combination of the two methods discussed previously were compared to the visual observations.

Several sources of error were found. The multi-scaler occasionally skipped channels, thereby reducing the number of data values obtained from each data run. Due to mechanical malfunctions of the rotary printing head, the digital printer often printed incorrect numbers. For time increments of less than about one second required for the radioactive source to pass between the two detector levels, the time increments obtained from the experimental apparatus deviated largely from the actual time increments. To minimize the latter error, the following technique was used.

The times for the source to move from level  $Z_1$  to level  $Z_2$  and from level  $Z_2$  to level  $Z_1$  for a given source speed measured experimentally were averaged and plotted versus the true time for different true times. The results are shown in Fig. 24. At short time intervals the deviation from a one-to-one relationship is seen clearly in this figure. Figure 25 gives the same information, plotted as the ratio of the average experimental time to the true time versus the average experimental time. A significant deviation for time

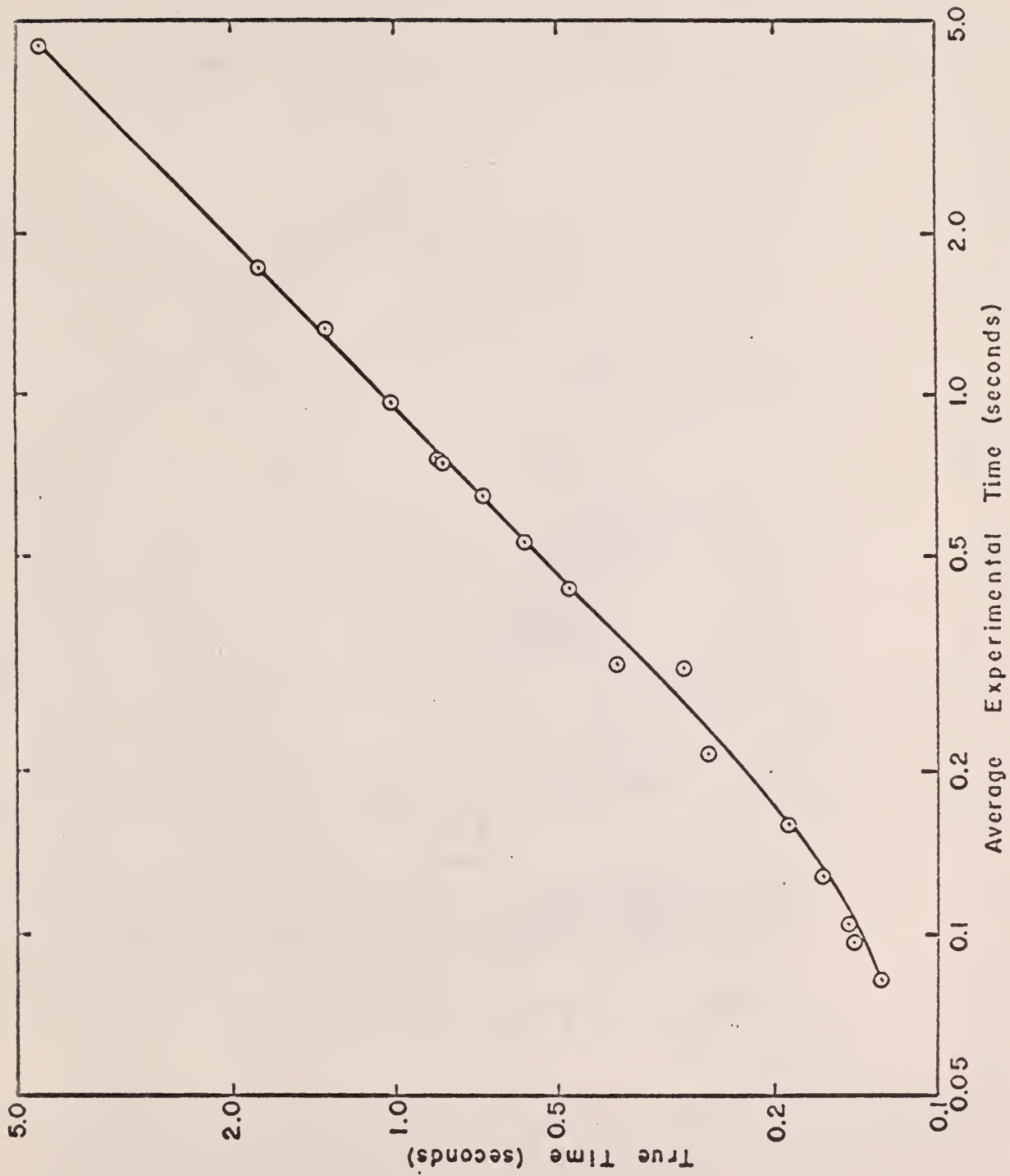


Figure 24. True Time Versus Average Experimental Time for the Radioactive Source to Pass Between Two Detector Levels.

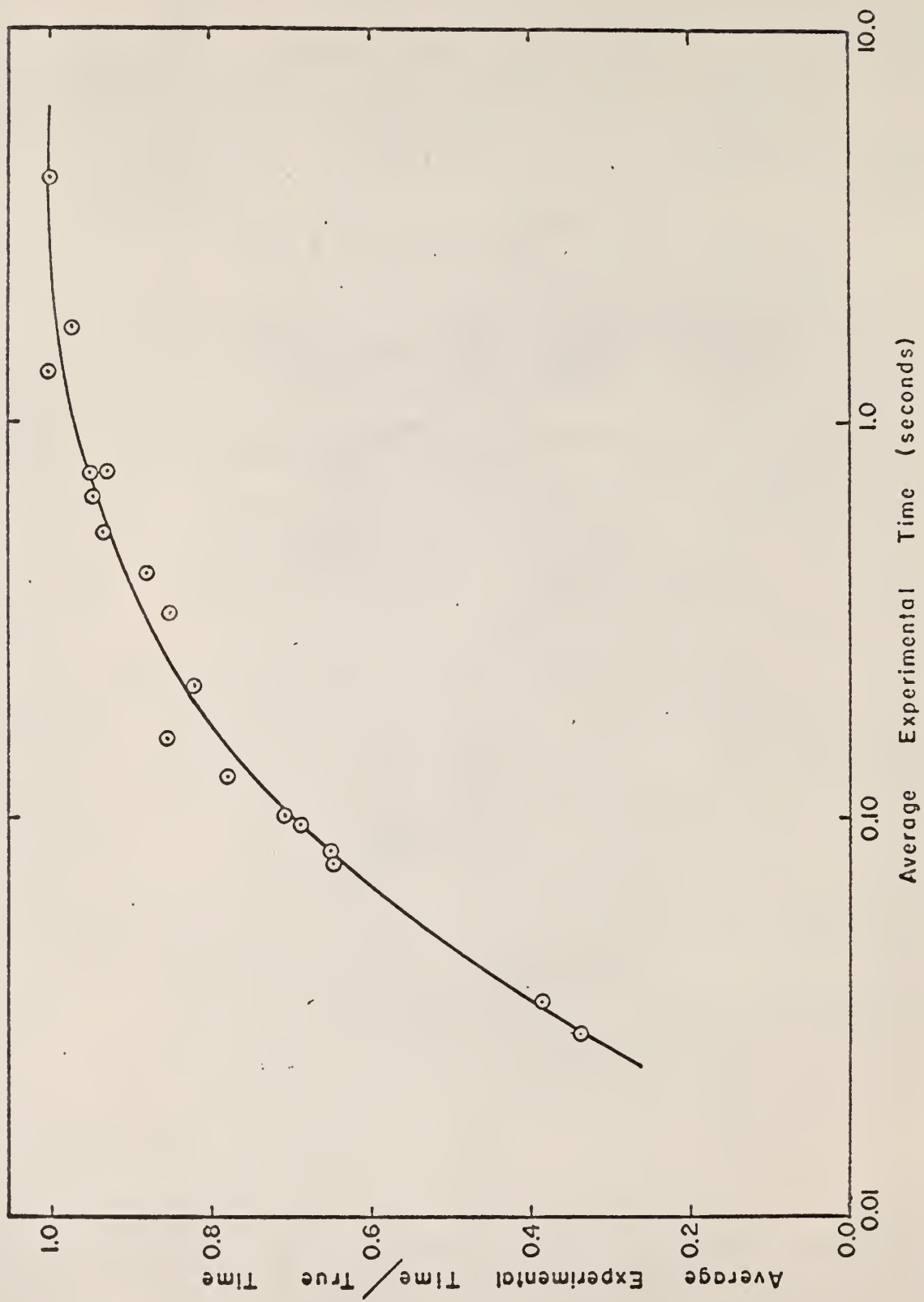


Figure 25. Ratio of Average Experimental Time to True Time as a Function of the Average Experimental Time for the Radioactive Source to Pass Between Two Detector Levels.

increments of less than one second is shown to be the case.

Figure 26 gives the ratio of experimental time to true time as a function of the experimental time before averaging the time increments obtained experimentally for the radioactive source to pass upward and downward between the two detector levels at a given source speed. The triangles represent the experimental time increments obtained for a given source speed when the source was moving downward between  $Z_2$  and  $Z_1$ , and the circles represent the experimental time increments obtained for a given source speed when the source was moving upward between  $Z_1$  and  $Z_2$ .

The time increment data obtained when the source was moving downward were fitted with three straight-line segments. A linear regression analysis was utilized to obtain the equation for each straight-line segment. A similar procedure was used to fit straight-line segments to the time increment data obtained when the source was moving upward. The equations resulting from the linear regression analysis of each straight-line segment are given in Table 1.

An IBM 1620 computer program in FORTRAN was developed to treat all of the lower-to-upper level and upper-to-lower level time increment data obtained from the experimental apparatus. For a given experimental time, the ratio of experimental time to true time was obtained from the appropriate equation shown in Table 1. To obtain the true time, the given experimental time increment was divided by that ratio.

The computer program developed to correct the experimental data is located in Appendix A.

### 2.3.6 Time Constants of the Ratemeters

The time constants for the ratemeters were determined by feeding a step input to each ratemeter and using a strip chart recorder to map the output of

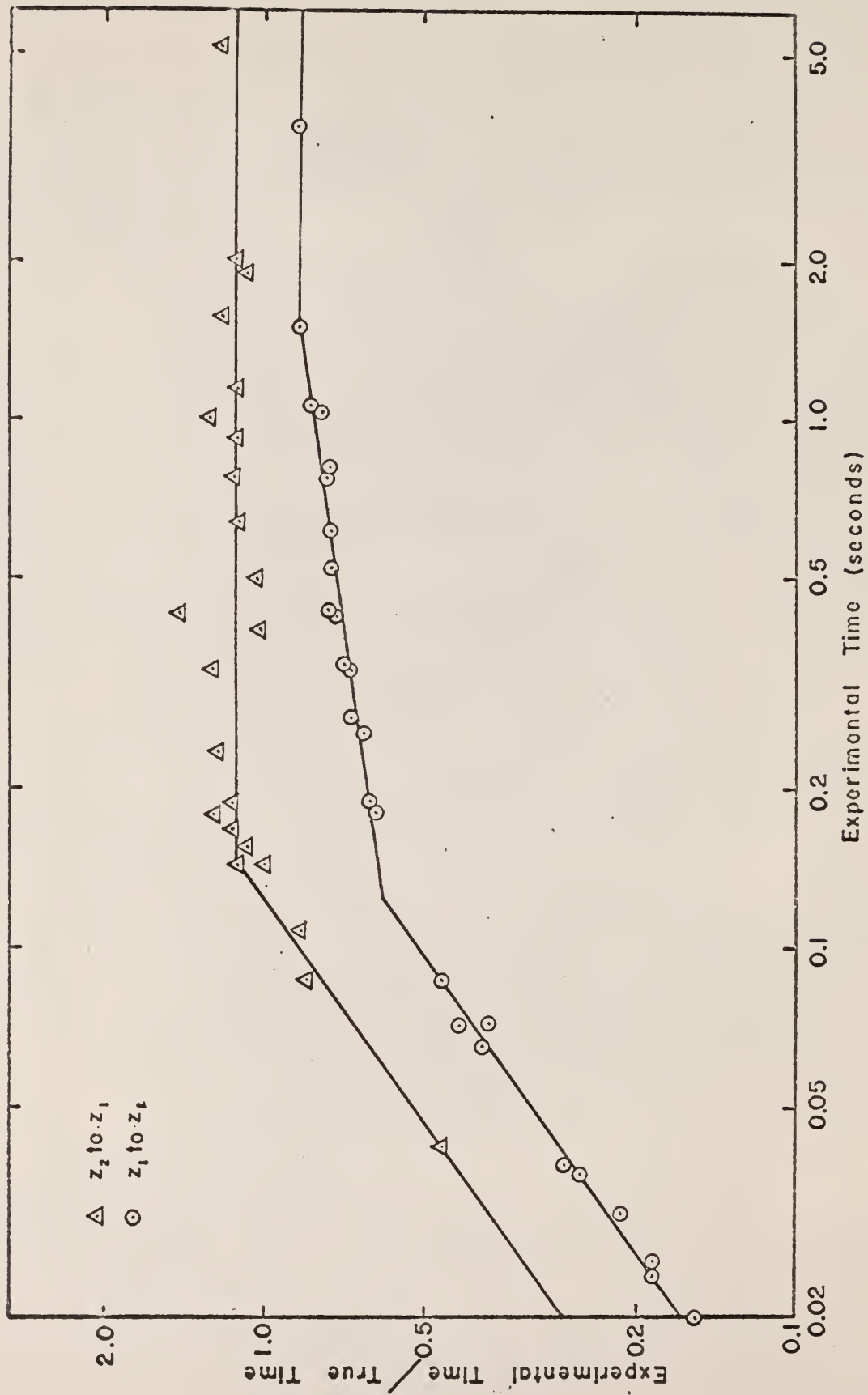


Figure 26. Ratio of Experimental Time to True Time as a Function of the Experimental Time for the Radioactive Source to Pass Between Two Detector Levels.

Table 1. Equations resulting from the linear regression analysis of the data from the calibration of the electronic system.

Detector level 1 to detector level 2	
Experimental time (seconds)	Equation
0.00 to 0.12	$\ln(R) = 1.006273 + 0.7186 \ln(t)$
0.12 to 1.50	$\ln(R) = -0.21715 + 0.13258 \ln(t)$
1.50 to infinity	$R = 0.85$
Detector level 2 to detector level 1	
0.00 to 0.14	$\ln(R) = 1.33479 + 0.65478 \ln(t)$
0.14 to infinity	$R = 1.1734$
$R = \text{Experimental time/True time}$	

each ratemeter. The procedure was as follows: a square-wave input was fed to each ratemeter, the sensitivities being so adjusted at first that the input would not be accepted; the sensitivity of each ratemeter was then increased to accept the square-wave input; the resulting output of each ratemeter, mapped by a strip chart recorder, was allowed to reach steady state; the sensitivity was then decreased so as not to accept the input, and the output was allowed to return to the original no-input value.

The time required to reach  $(1-1/e)$  of the steady state value is equal to the RC time constant for the rise in the output, and the time required to reach  $(1/e)$  of the steady state value is equal to the RC time constant for the decay of the output. Figures 27 and 28 illustrate the method of obtaining these time constants.

The time constants obtained for the two ratemeters in the experimental apparatus are given in Table 2.

Table 2. Time constants of the ratemeters.

Ratemeter	RC rise time	RC decay time
NE 901	0.492 second	0.300 second
NE 902	0.500 second	0.336 second

### 2.3.7 Pressure Drop Data

The pressure drop across the fluidized bed was determined by recording the pressure difference in inches of mercury across the column for different flow rates of water. Readings were taken arbitrarily as the flow rate was either increased or decreased. Figure 29 gives the pressure drop in inches of mercury as a function of the water flow rate in gallons per minute.

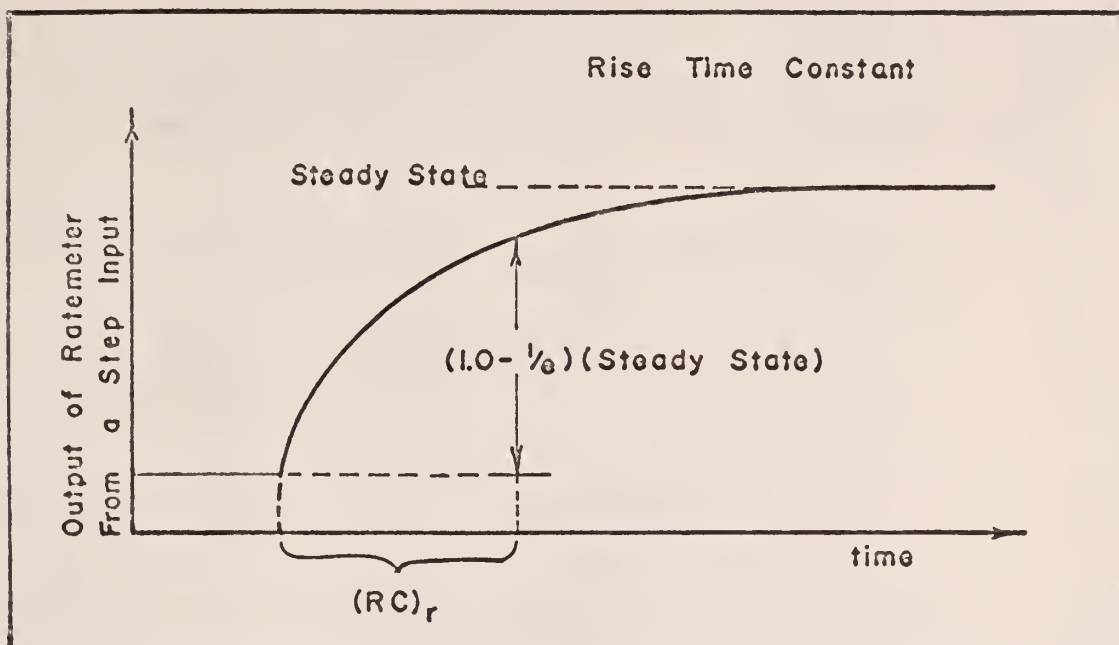


Figure 27. Method of Determining Rise Time of Ratemeters.

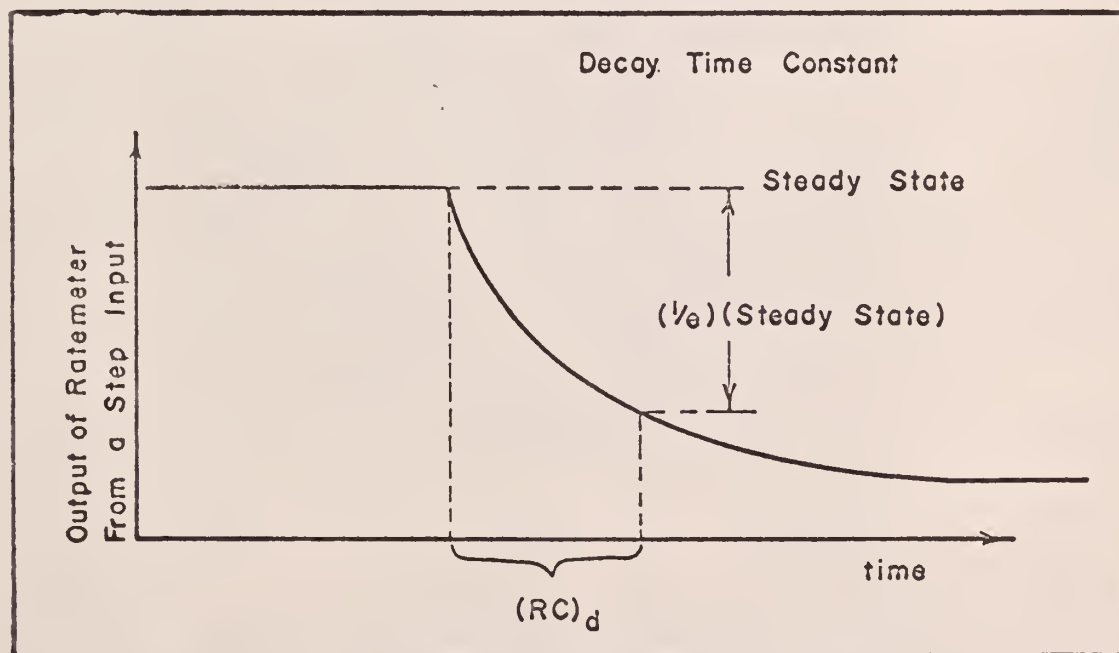


Figure 28. Method of Determining Decay Time of Ratemeters.

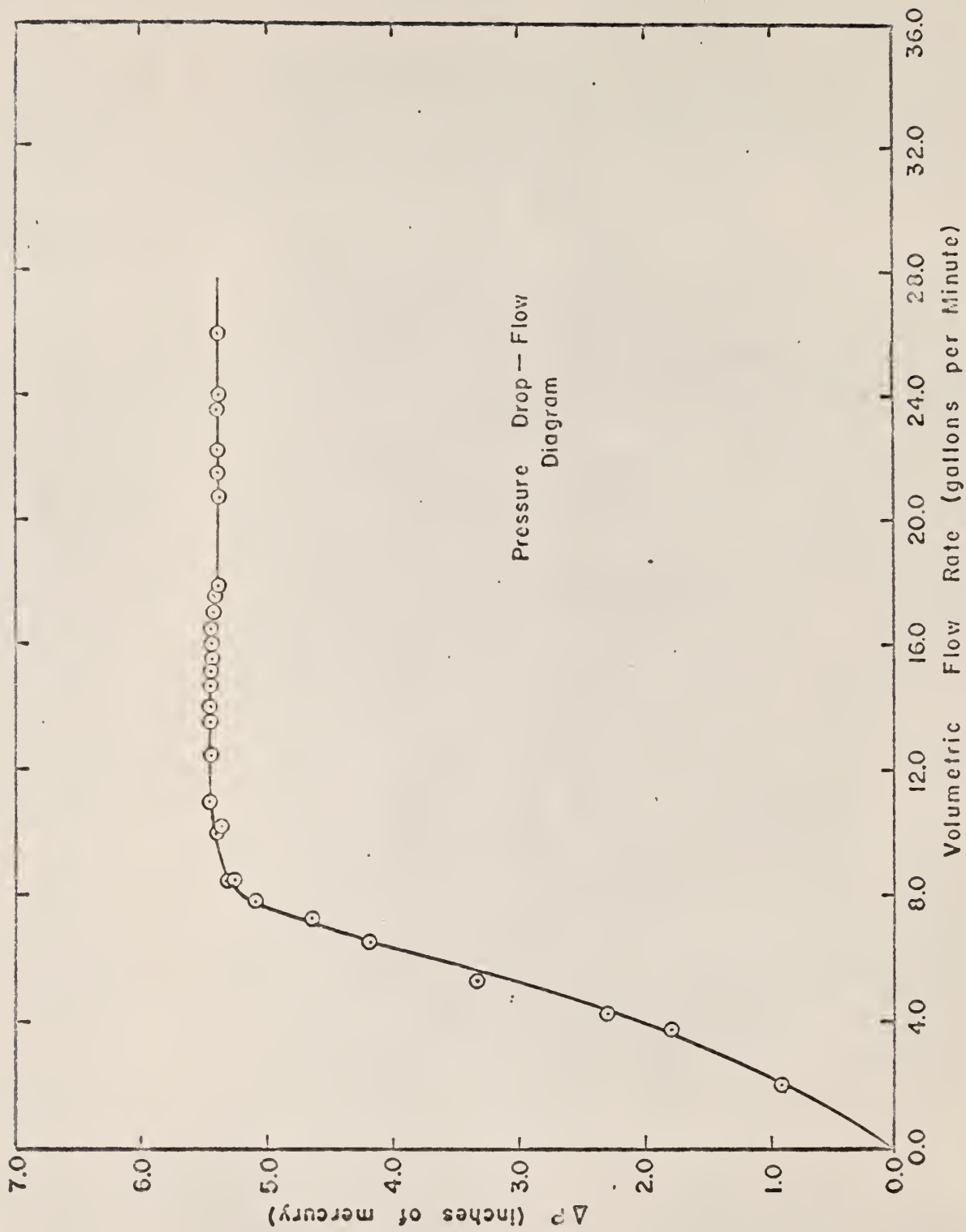


Figure 29. Pressure Drop Across Fluidized Bed as a Function of the Water Flow Rate.

## 2.4 Procedure

To determine if the equipment was operating properly, the nuclear instrumentation equipment was checked out prior to a day's run. The check-out procedure consisted of allowing the electronic apparatus to warm up and counting the pulses from a fixed-frequency input to the multi-scaler for one second in each channel of the multi-scaler. The digital printer was then used to print out the information in the memory of the multi-scaler. If the number stored in each channel was equal to the frequency input in cycles per second, the equipment was assumed to be operating properly. The high voltage to the photomultipliers of the scintillation probes was then adjusted, and a radioactive source was passed in front of the scintillation detectors to check proper operation of the dual-channel recorder used to measure the output of the two ratemeters. Next, another check of the multi-scaler was made by observing the cathode ray tube to determine if the source passing in front of the scintillation probes was triggering the unit properly. If the system was operating properly, a Type 316 stainless steel ball bearing was introduced into the Kansas State University Triga Mark II nuclear reactor and was irradiated at 100 kw for one and one-half hours. A surface dose rate of about 2 r/hr of gamma radiation was produced. The source was then inserted into the fluidizing column, and the pump was turned on to allow the water to circulate through the system.

The high voltage to the photomultipliers at each of the detector levels was adjusted until well-defined pulses with minimum background noise were obtained on each channel of the chart recorder.

The distance between the detector levels was set for the particular data run, and the water flow rate for the run was properly adjusted by setting to

the desired value the mercury height in the manometer across the orifice in the inlet line to the fluidizing column.

The chart recorder was then started. The multi-scaler was started, and the exact position of the pens on the chart recorder at the time of starting was noted.

During the data run, the water flow rate was maintained constant by making the necessary inlet valve adjustments to maintain the proper height of mercury in the manometer.

Observation of the cathode ray tube of the multi-channel analyzer provided a running check on the approximate amount of time left on a particular run. An illuminated dot on the face of the tube monitored the channel currently being used to store the frequency count. As soon as the source passed one of the detector levels, storage was transferred to the next channel. This could be visually observed by watching the dot jump to the right on the screen. When the 256 channels were filled, the dot would then move to an arbitrary position to the left on the screen. This indicated the end of the data run, and the position of the pens on the chart recorder was again noted.

The manometer reading, the distance between detector levels, the run number, and the data were then recorded on both the chart recording and the memory information of the multi-scaler printed out by the digital printer.

The detectors were positioned at different levels. Because of the strong gamma-ray source in the fluidized bed, changes were made as quickly as possible. The flow rate of the water was adjusted to a new value, and a new run was begun.

The length of time available for obtaining the data for each day's run was determined by the half-life of the radioactive source. As time passed, in order to maintain well-defined pulses on the dual-channel chart recorder,

the high voltage to the photomultipliers was increased to increase detector sensitivity, which compensated for the decreased activity of the source. When the high voltage was increased too high, the background noise would increase, resulting in difficulty in distinguishing between pulses that actually occurred when the source passed a detector level and background noise. This limited the time for taking data to about seven or eight hours after removal of the ball bearing from the reactor. The source would have decayed through about three half-lives by that time and was roughly  $1/8$  of its activity at the time of removal from the nuclear reactor.

### 3.0 ANALYSIS OF SINGLE PARTICLE EXPERIMENTS

#### 3.1 Experiment Arrangement

Figure 30 is an illustration of the fluidized column with specific vertical positions,  $Z_i$ , noted. Utilizing the experimental apparatus, the time a radioactive particle passed level  $Z_i$  was recorded. Only two levels of  $Z_i$  could be investigated at a time. The distance between the two  $Z_i$  levels was the distance between the two detector levels,  $\Delta Z$ .

The controlled variables were the fluidized bed height, determined by the water flow rate, the quantity of particles in the bed, and the distance between the two detector levels.

#### 3.2 Quantities Extracted from Data

The quantities obtainable from a single particle experiment are given below:

- |                            |   |
|----------------------------|---|
| $t(Z_i, Z_j)$              | Residence time, defined as the time required for a particle, after passing level $Z_i$ and moving into the region between $Z_i$ and $Z_j$ and not returning to $Z_i$ , to pass out of the region at $Z_j$ . |
| $r(Z_i)$                   | Particle traffic, defined as the number of times a particle passes level $Z_i$ per unit time.   |
| $\text{Pr}(Z_i, Z_j; Z_i)$ | Reflectivity, defined as the probability of a particle passing level $Z_i$ and not reaching level $Z_j$ before returning to level $Z_i$ .   |
| $I(Z_i, Z_j, t)$           | Particle concentration, defined as the number of times a particle passes level $Z_j$ in the time increment  |

$\Delta t$  at the time  $t$  per unit time, initially passing level  $Z_i$ .

$m(Z_i)$  The number of times a particle passes level  $Z_i$  before reaching level  $Z_j$ .

### 3.3 Determination of Fundamental Quantities from Experimental Data

Figure 31 is a simplified illustration of a data trace, showing the times at which a particle passed levels  $Z_i$  and  $Z_j$ . The fundamental quantities are determined from Fig. 31 as follows:

$$t(Z_i, Z_j) = 0.175; 0.175; 0.20$$

$$t(Z_j, Z_i) = 0.19; 0.125; 0.125; 0.18$$

$$r(Z_i) = 16/4 = 4.0$$

$$r(Z_j) = 18/4 = 4.5$$

Obtaining the reflectivity and particle concentration data requires some explanation. To obtain the reflectivity data  $Pr, m(Z)$  must be considered. For  $m$  particles passing level  $Z_i$ , in general, one half of them are headed toward  $Z_j$ , and one eventually reaches  $Z_j$ . Therefore, the probability of that particle reaching  $Z_j$  in  $m/2$  tries is  $1/(m/2)$  or  $2/m$ . The probability of not reaching  $Z_j$  but returning to  $Z_i$  is, therefore,  $1-(2/m)$  or  $(m-2)/m$ .

From Fig. 31, the probability of reflection of particles starting at level  $Z_i$  is, in the first instance,  $(4-2)/4$ , since the radioactive source passed the detector level  $Z_i$  four times before reaching level  $Z_j$ . The next time the source was detected at level  $Z_i$ , having been detected at level  $Z_j$  just prior to detection at level  $Z_i$ , it passed level  $Z_i$  six times before it

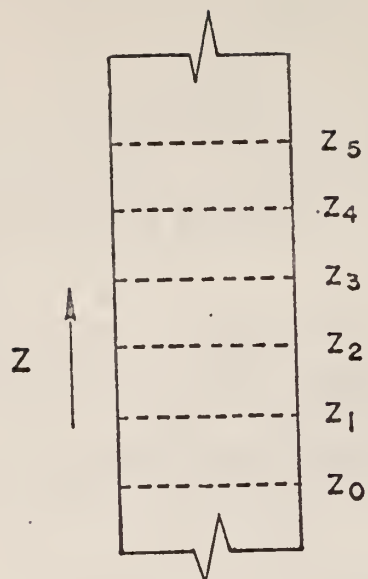


Figure 30. Vertical Arrangement of Detectors Adjacent to Fluidizing Column.

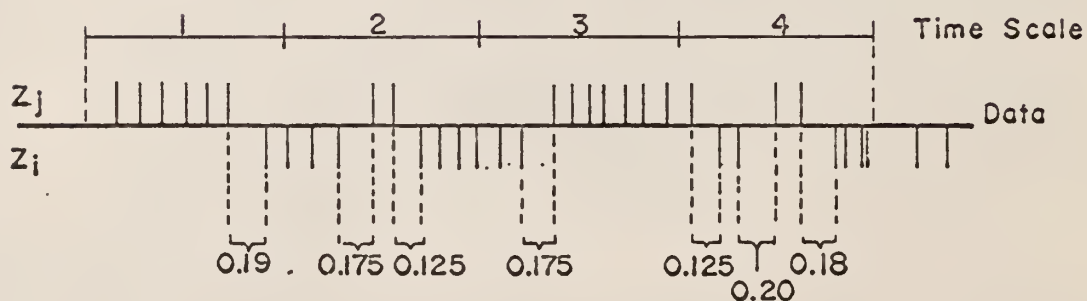


Figure 31. Simplified Data Trace.

reached  $Z_j$ , giving  $(6-2)/6$ . The third time the source was detected at level  $Z_i$ , having been detected at level  $Z_j$  just prior to detection at level  $Z_i$ , it passed level  $Z_i$  twice before being detected at level  $Z_j$ . The same analysis is used to determine the probability of reflection of particles starting at level  $Z_j$ .

$$\Pr(Z_i, Z_j; Z_i) = (4-2)/4 = 0.5; (6-2)/6 = 0.667; (2-2)/2 = 0.$$

$$\Pr(Z_j, Z_i; Z_j) = (6-2)/6 = 0.667; (2-2)/2 = 0; (8-2)/8 = 0.75; \\ (2-2)/2 = 0.$$

To obtain the particle concentration data, the number of times a particle passes a level per unit time within a time increment  $\Delta t$  is considered. Also considered is the level,  $Z_i$  or  $Z_j$ , at which the particle originated. As an example,  $I(Z_i, Z_j, t)$  and  $I(Z_i, Z_i, t)$  will be obtained step-by-step. For convenience,  $\Delta t$  will be set equal to 1. Since the second pulse at level  $Z_i$  shown in Fig. 31 occurs at the beginning of the second time increment, it will be used for the initial pulse. Considering  $I(Z_i, Z_j, t)$ , the number of pulses occurring at level  $Z_j$  within each time increment  $\Delta t$  with the time scale beginning at the initial pulse is

$$I(Z_i, Z_j, t_1) = 2, I(Z_i, Z_j, t_2) = 7, \text{ and } I(Z_i, Z_j, t_3) = 3.$$

Considering the number of pulses occurring at level  $Z_i$  in the same manner beginning with the initial pulse,

$$I(Z_i, Z_i, t_1) = 7, I(Z_i, Z_i, t_2) = 2, \text{ and } I(Z_i, Z_i, t_3) = 6.$$

## 4.0 DATA ANALYSIS

### 4.1 General Consideration

Figure 32 shows an example of a typical recorder trace, with arrows added to illustrate the upward or downward movement of the particle as it passed the two detector levels. Figure 32 also illustrates a typical digital printer recording of the first fifty channels of the multi-channel analyzer. The left-hand column of numbers indicates the channel number, and the right-hand column lists the number of pulses from the Time Interval Meter oscillator stored in each channel.

For each given flow rate and distance between detector levels, the recorder trace and the corresponding digital printer recording were correlated. This was done by using the recorder trace to determine when the particle passed either the bottom or the top detector level and by matching the time between pulses on the recorder trace to the numbers recorded by the digital printer. The dual channel recorder was always operated at 5 millimeters per second, so the graduations on the recorder trace were one second apart. The pulses from the Time Interval Meter to the Multiscaler Logic Unit amplitude input were always adjusted to 666 per second; therefore, one graduation on the recorder trace corresponded to the number 666 on the digital printer recording.

The channel number on the digital print-out recording was always equated to the pulse on the recorder trace that stopped the accumulation of Time Interval Meter pulses in that channel and transferred the storage to the next channel. Each pulse on the recorder trace that caused transfer of storage from one channel to the next, therefore, was identified by numbering it with the proper channel number.

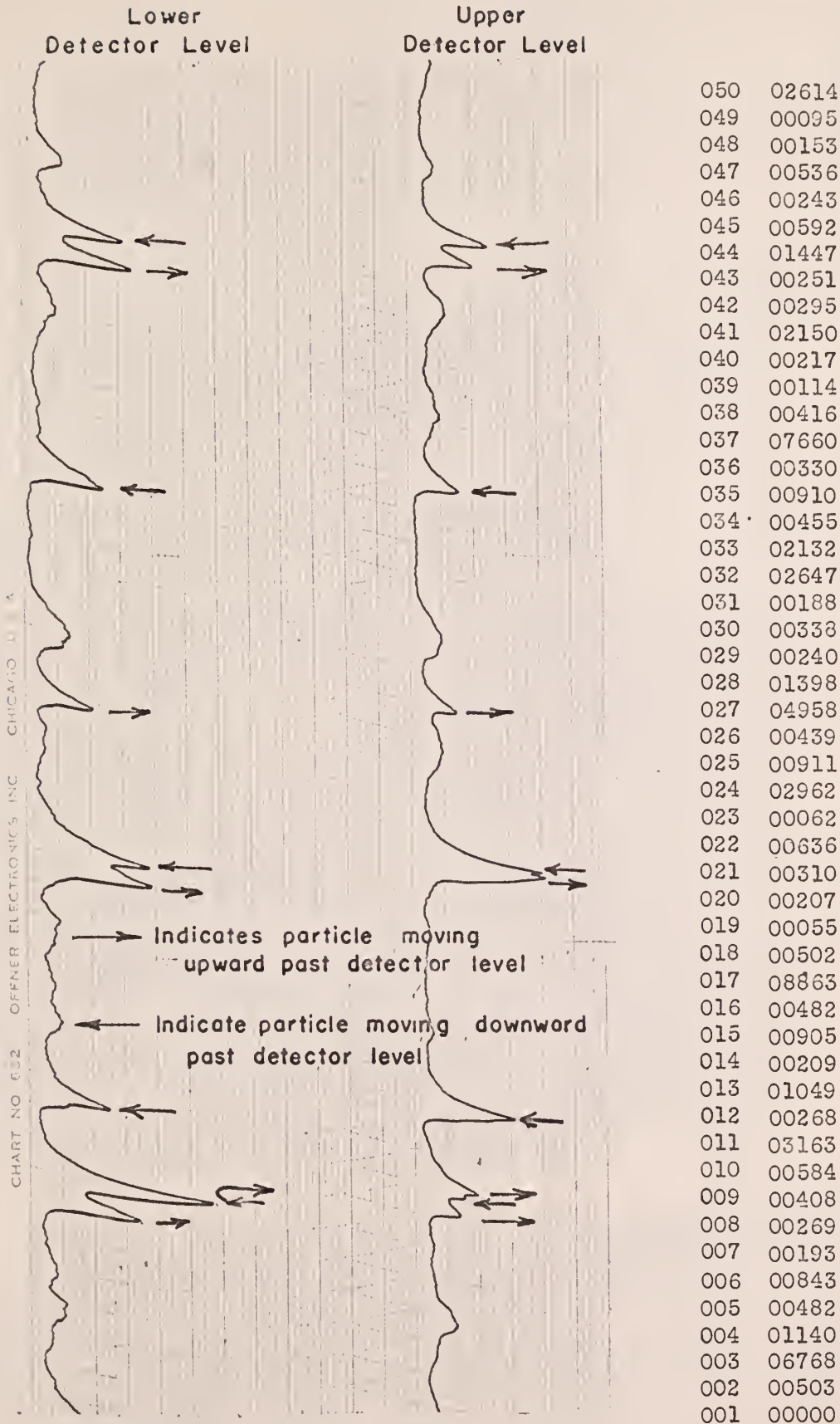
RECORDER OUTPUTDIGITAL PRINTER OUTPUT

Figure 32. Output of Recorder and Digital Printer.

The left-hand, or bottom detector level trace, was denoted by a minus sign, so that the number on the digital print-out recording corresponding to a pulse that occurred when the source passed the bottom detector level was identified by placing a minus sign beside it. The number on the digital print-out recording corresponding to a pulse that occurred when the source passed the top detector level was identified by placing a plus sign beside it. The digital print-out recording with a plus or minus sign beside the number stored in each channel in the multi-channel analyzer, therefore, contained all of the information obtained from the recorder trace and the digital printer recording. By observing the plus and minus signs, it was easy to determine when the source passed from one detector level to the other. For instance, when the isotope passed from lower to upper detector level, the sign would change from minus to plus. The time required to pass from lower to upper detector level was found by dividing by 666 the number of pulses counted and stored in the channel denoted by the plus sign. The resulting time would be in seconds.

The number in each channel location of the digital printer recording, along with its corresponding plus or minus sign, was then transferred to an IBM data card. To reduce the amount of data cards used, eight of the positive or negative numbers were typed per card.

Not all of the sets of data obtained from the experimental apparatus contained 256 data values, principally because the multi-channel analyzer would sometimes skip channels, causing no numbers to be recorded in the skipped channels. Therefore, each set of data was accompanied by the number of data values in the set. This value, denoted by JMAX, preceded the set of data on an IBM data card by itself.

Utilizing five water flow rates through the column and five distances between detector levels, seventy-six sets of data were obtained from the experiments.

Table 3 is a listing of the number of data runs obtained for each given water flow rate and distance between detector levels.  $B_k$  is the water flow rate corresponding to the height of mercury in the manometer that measured the pressure drop through the orifice meter, and  $\Delta Z$  is the distance between the two detector levels.

Table 4 is a listing of the data set numbers for given distances between detector levels and water flow rates.

#### 4.2 Statistical Analysis of Data

Sample variation was found to be useful in describing the frequency distribution of residence times obtained from the experimental data. Before any test of variance can be used on a sample taken from a population, however, the distribution upon which the test of variance is based must first be determined.

The simplest distribution for continuous data is the normal distribution, where the mean and median are the same and the distribution is symmetric with respect to the mean. The arithmetic mean is defined as  $(\sum f_i x_i / \sum f_i)$ , and the median is defined as the value equaled or exceeded by exactly half of the values  $x_i$  in the given list. An unbiased estimator of the population variance  $\sigma^2$  is

$$S^2 = \sum_{i=1}^n \frac{(x_i - \bar{x})^2}{n - 1} , \quad (1)$$

where  $x_i$  is the variable of which  $n$  observations are made, and  $\bar{x}$  is the average or mean of the  $n$  observations.

A measure of the skewness is given by

$$S^3 = \sum_{i=1}^n \frac{(x_i - \bar{x})^3}{n - 1} . \quad (2)$$

Table 3. Number of data sets obtained for each  $B_k$ ,  $\Delta Z$ .

$\Delta Z$ (inches)	$\frac{1}{2}$	1	2	4	6
$B_1$ (2.50 in. Hg)	2	3	4	4	2
$B_2$ (4.00 in. Hg)	2	4	4	3	2
$B_3$ (4.85 in. Hg)	2	4	4	4	2
$B_4$ (7.00 in. Hg)	2	4	4	4	2
$B_5$ (8.50 in. Hg)	2	4	4	2	2

Table 4. Data set numbers for given distances between detector levels  $\Delta Z$  and water flow rates  $B_k$ .

$\Delta Z$	$\frac{1}{2}$	1	2	4	6
$B_1$	1 2	3 4 5	6 7 8 9	10 11 12 13	14 15
$B_2$	16 17	18 19 20 21	22 23 24 25	26 27 28	29 30
$B_3$	31 32	33 34 35 36	37 38 39 40	41 42 43 44	45 46
$B_4$	47 48	49 50 51 52	53 54 55 56	57 58 59 60	61 62
$B_5$	63 64	65 66 67 68	69 70 71 72	73 74	75 76

The average fluid velocities for the given water flow rates through the fluidized bed are given below.

$B_1$	10.4 in./sec.
$B_2$	12.1 in./sec.
$B_3$	12.8 in./sec.
$B_4$	14.1 in./sec.
$B_5$	14.8 in./sec.

A positive value of  $S^3$  indicates that the mean is greater than the median, and a negative value of  $S^3$  indicates that the median is greater than the mean.

Figure 33 shows an example of a skewed distribution where the mean is greater than the median.

The function,

$$f(t) = \frac{t^{p-1} e^{-t/v}}{\Gamma(p) v^p}, \quad (3)$$

is an example of an analytical function that is skewed with a mean greater than the median for different values of the two parameters  $p$  and  $v$  (5). It is easy to observe that when  $v = 2$ , the above gamma distribution reduces to the well-known  $\chi^2$  frequency function with  $2p$  degrees of freedom. For the number of observations,  $n$ , greater than 5, this continuous distribution closely approximates the discrete frequency distribution,

$$\chi^2 = \sum_{i=1}^k \frac{(o_i - e_i)^2}{e_i}, \quad (4)$$

where  $k$  is the number of pairs of frequencies to be compared,  $o_i$  and  $e_i$  denote the  $i$  th pair of observed and expected frequencies, and  $\sum o_i = \sum e_i = n$ . The number of degrees of freedom is  $k-1.0$  (5).

The  $\chi^2$  statistic is a test to determine how well certain data fit a known or given hypothesis (11). K. Pearson established the distribution of  $\chi^2$  for any number of degrees of freedom, making it possible to test whether a sample came from an assumed distribution or not. This made it possible to calculate the probability,  $P$ , that a particular value of  $\chi^2$  would be exceeded,

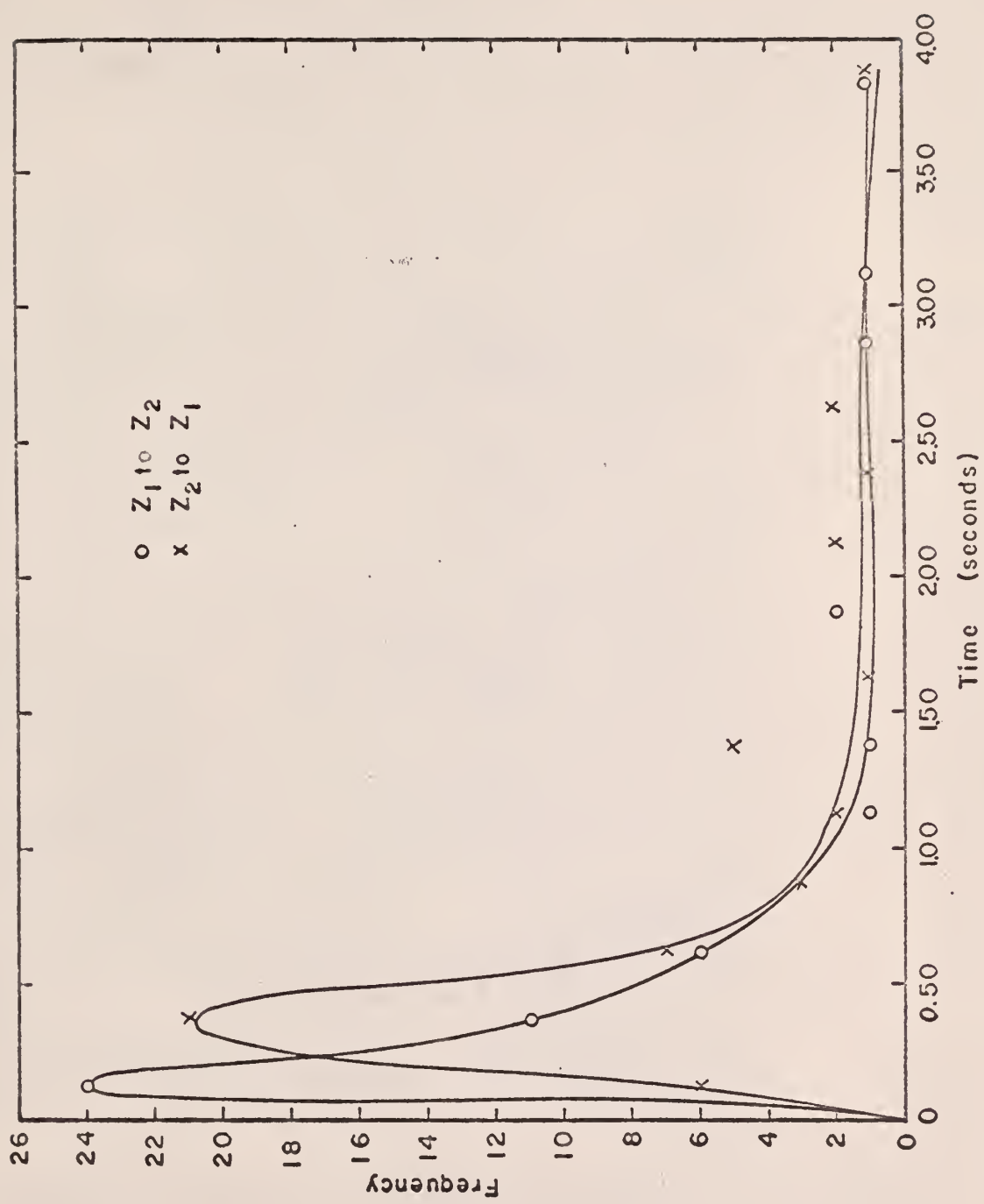


Figure 33. Frequency Distribution of Residence Times for a Typical Data Set.

by

$$\int_0^{\chi_0^2} \frac{(\chi^2)^{p-1} e^{-\chi^2/2}}{\Gamma(p) 2^p} d\chi^2 = 1-P. \quad (5)$$

The commonly accepted value for P is 0.05, or the five percent level of acceptability. If the observed value of  $\chi^2$  is less than the value from the distribution for the given degrees of freedom and P, the observed value is not suspected of not representing a sample from the distribution hypothesized. If, however, the observed value is greater than or equal to the  $\chi_0^2$  value from the distribution, the probability of this occurring is less than 0.05, and the hypothesis being tested is rejected, or, if the hypothesis is known to be correct, then the observed data is judged to be nonrepresentative of the known hypothesis.

#### 4.3 Analysis of the Residence Times Distribution

A frequency distribution of the residence times in a typical data set gave the frequency function  $f(t)$  versus the time  $t$  illustrated in Fig. 33. The two-parameter gamma distribution was used to develop the T statistic, analogous to the  $\chi^2$  statistic, to determine the data that were not representative of the  $f(t)$  distribution. It was concluded that the experimental times obtained at the right-hand end of the distribution in Fig. 33 were not representative of the residence times. This was primarily due to errors in correlating the recorder trace to the digital printer output. When the radioactive source passed the two detector levels at high speed, one of the resulting pulses may not have been strong enough to trigger the multi-scaler. The counts accumulated until the multi-scaler was again triggered would not be representative of the residence times distribution but would be far greater.

The data points that fell within the last five percent of the area under the  $f(t)$  distribution were rejected on the basis of the criteria mentioned above. The area under the total gamma distribution integrated from zero to infinity is 1.0. The area under the last five percent of the distribution is 0.05 and is equal to the probability  $P$ . The  $T$  statistic was determined by

$$\int_0^T \frac{t^{p-1} e^{-t/\nu} dt}{\Gamma(p) \nu^p} = 1-P \quad (6)$$

In each data set, all of the residence times that were greater than the  $T$  statistic were rejected.

An IBM-1620 FORTRAN computer program was developed to determine, for various values of the distribution parameters  $p$  and  $\nu$ , the area under the gamma distribution integrated from 0 to  $T$ . The computer program is discussed in Appendix G. A Gaussian quadrature numerical integration technique, discussed in Appendix H, was utilized to determine the area under the distribution for combinations of  $p, \nu$ , and  $T$ . The Gaussian quadrature approximation of  $\int_{-1}^1 f(x) dx$  is

$$\int_{-1}^1 f(x) dx = \sum_{k=1}^N a_k f(x_k) \quad (7)$$

A transformation of variables from  $\int_0^T f(t) dt$  to  $\int_{-1}^1 f(x) dx$ , where  $f(t)$  represents the gamma distribution, gives

$$\begin{aligned} \int_0^T f(t) dt &= \frac{(T/2)^p}{\Gamma(p) \nu^p} \sum_{k=1}^N a_k (x_k - 1)^{p-1} e^{-\frac{T}{2\nu}(x_k - 1)} \\ &= A \quad (8) \end{aligned}$$

The computer program gave the value of A for various values of p,  $\nu$ , and T. Interpolation of the answers obtained from constant values of p and  $\nu$  gave the time T required for the area A to equal 0.95.

Figure 34 gives the results of the T statistic corresponding to an area (A) under the curve  $\int f(t)dt$  equal to 0.95, for given gamma distribution parameters p and  $\nu$ .

The parameters p and  $\nu$  can be determined from the experimental data by utilizing the average,  $\bar{t}$ , and variance,  $\sigma^2$ , of the residence times.

$$\bar{t} = \frac{\int_0^{\infty} t f(t) dt}{\int_0^{\infty} f(t) dt} = \frac{-\nu t^p e^{-t/\nu} \Big|_0^{\infty} + p\nu \int_0^{\infty} t^{p-1} e^{-t/\nu} dt}{\int_0^{\infty} t^{p-1} e^{-t/\nu} dt} \quad (9)$$

$$\bar{t} = p\nu - \frac{\nu t^p e^{-t/\nu}}{\int_0^{\infty} t^{p-1} e^{-t/\nu} dt} = p\nu \quad (10)$$

$$\sigma^2 = \frac{\int_0^{\infty} (t-\bar{t})^2 f(t) dt}{\int_0^{\infty} f(t) dt} = \frac{\int_0^{\infty} (t^2 - 2t\bar{t} + \bar{t}^2) f(t) dt}{\int_0^{\infty} f(t) dt} \quad (11)$$

From the definition of  $\bar{t}$ , and since  $\bar{t}$  is a constant,

$$\sigma^2 = \frac{\int_0^{\infty} t^2 f(t) dt}{\int_0^{\infty} f(t) dt} - (\bar{t})^2 \quad (12)$$

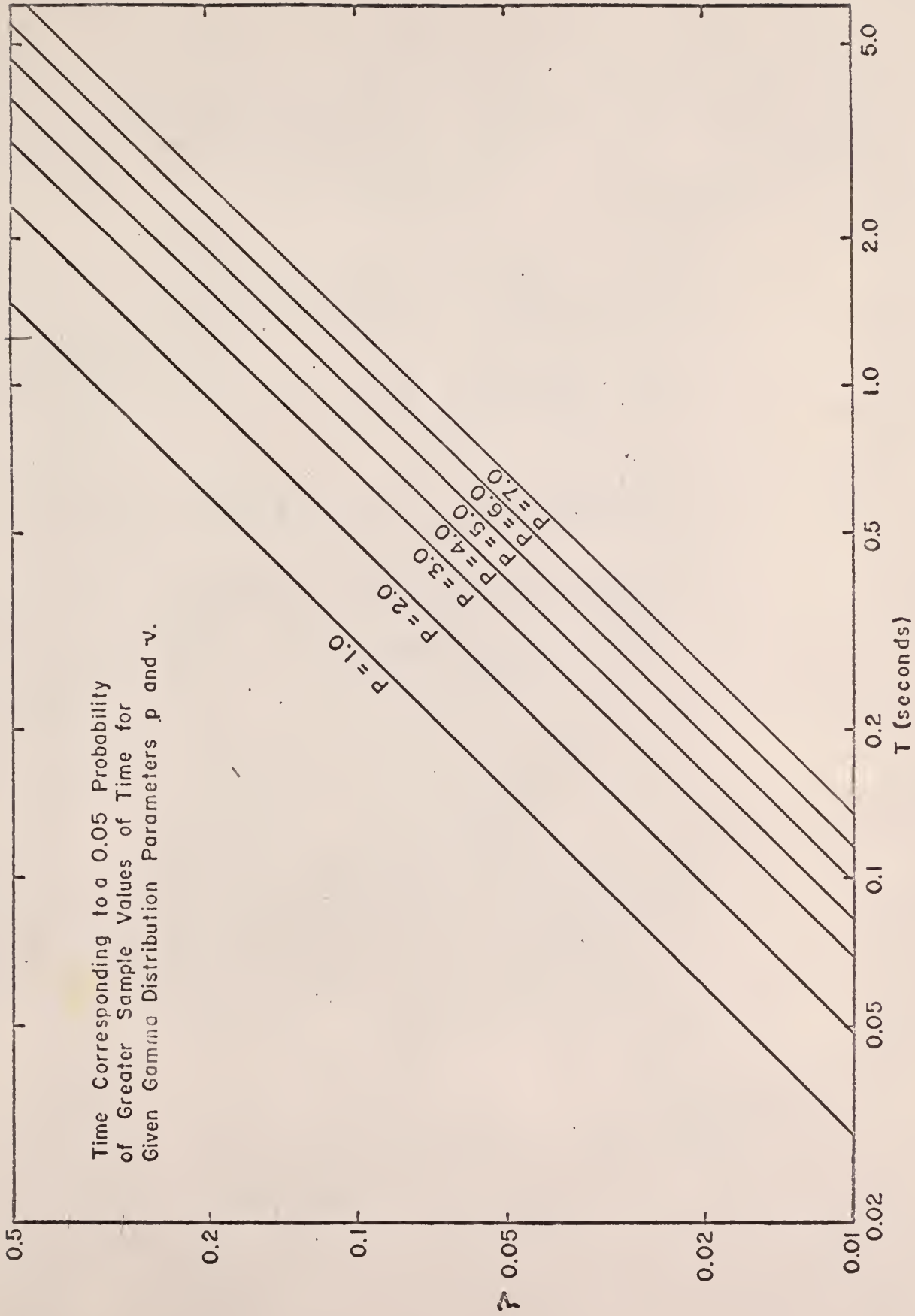


Figure 34. Plot of the T Statistic for the Gamma Distribution Parameters P and  $v$ .

or,

$$\sigma^2 = \frac{\int_0^{\infty} t^{p+1} e^{-t/\nu} dt}{\int_0^{\infty} t^{p-1} e^{-t/\nu} dt} - (p\nu)^2$$

Integrating by parts gives,

$$\sigma^2 = \frac{-\nu t^{p+1} e^{-t/\nu} \Big|_0^{\infty} + (p+1)\nu \int_0^{\infty} t^p e^{-t/\nu} dt}{\int_0^{\infty} t^{p-1} e^{-t/\nu} dt} - (p\nu)^2,$$

$$\sigma^2 = \frac{(p+1)\nu \left[ -\nu t^p e^{-t/\nu} \Big|_0^{\infty} + p\nu \int_0^{\infty} t^{p-1} e^{-t/\nu} dt \right]}{\int_0^{\infty} t^{p-1} e^{-t/\nu} dt} - (p\nu)^2,$$

$$\sigma^2 = (p+1)\nu (p\nu) - (p\nu)^2 = p\nu^2. \quad (13)$$

The average residence time obtained from the data is

$$\bar{t} = \sum_{i=1}^n \frac{t_i}{n}. \quad (14)$$

The corresponding unbiased estimate of the variance is

$$s^2 = \sum_{i=1}^n \frac{(t_i - \bar{t})^2}{n-1}, \quad (15)$$

where  $t_i$  is the  $i^{\text{th}}$  residence time and  $n$  is the number of residence times in each set of data.

The most probable residence time is determined when

$$\frac{d f(t)}{dt} = 0 . \quad (16)$$

This is equivalent to

$$\frac{1}{\Gamma(p)\nu^p} \frac{d}{dt} (t^{p-1} e^{-t/\nu}) = 0 ,$$

or,

$$\frac{d}{dt} f(t) = e^{-t/\nu} (p-1)t^{p-2} - \frac{t^{p-1}}{\nu} e^{-t/\nu} = 0 ,$$

$$e^{-t/\nu} t^p [(p-1)t^{-2} - t^{-1}\nu^{-1}] = 0 .$$

Solving for the most probable residence time, denoted by  $t_p$ , one has

$$t_p = (p-1)\nu . \quad (17)$$

An IBM-1620 FORTRAN computer program was developed to determine the average residence time,  $\bar{t}$ , the most probable residence time,  $t_p$ , and the variance of the residence time data for each water flow rate and distance between detector levels. The program also calculated the gamma distribution parameters  $p$  and  $\nu$ , determined from the average time and the variance. Once the gamma distribution parameters  $p$  and  $\nu$  were known, Fig. 34 was utilized to obtain the T statistic for the data set. All of the time increments in the data

set that were greater than T were discarded, and the data were rerun through the computer. A new pair of gamma distribution parameters was obtained, and a new T statistic was determined from Fig. 34. The procedure was repeated until none of the residence time data were greater than the T statistic. The average time, the most probable time, the variance,  $p$ , and  $\nu$ , computed by the final pass through the computer, were tabulated for each set of residence time distribution data.

The larger the number of data taken, the closer the sample mean value will be to the population mean. By observing a plot of the average sample mean versus the number of data taken, one can estimate the minimum amount of data needed to give a sample mean representative of the population mean.

Figures 35 and 36 give representations of the average residence time as a function of the number of data values used to compute the average. Appendix E gives a discussion of Computer Program No. 5 used to calculate the average residence time as a function of the number of data values used.

Figures 37 and 38 give sample representations of the variance of the residence time as a function of the number of data values used to compute the variance. Appendix E gives a discussion of Computer Program No. 6 used to calculate the variance as a function of the number of data values used.

Figures 39 through 46 give sample representations of the residence times data superimposed upon the computed gamma distribution using the parameters  $p$  and  $\nu$  determined from the experimental data.

Figures 47 through 56 give the gamma distribution parameters  $p$  and  $\nu$  as functions of the distance between detector levels.

The residence time data used in the final pass through the computer were also used for a FORTRAN program (Computer Program No. 8) to compute the average

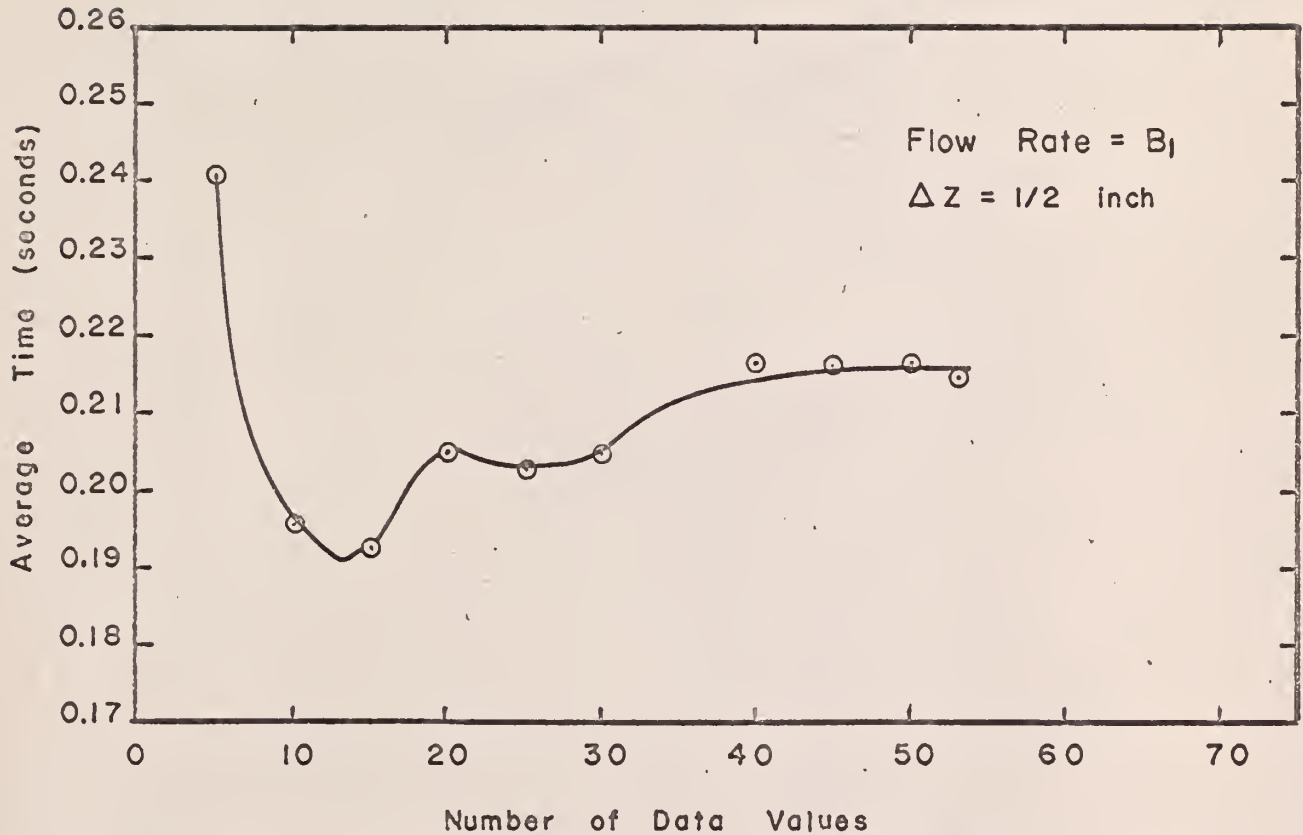


Figure 35. Average Residence Time as a Function of the Number of Data Values, Data Set No. 2.

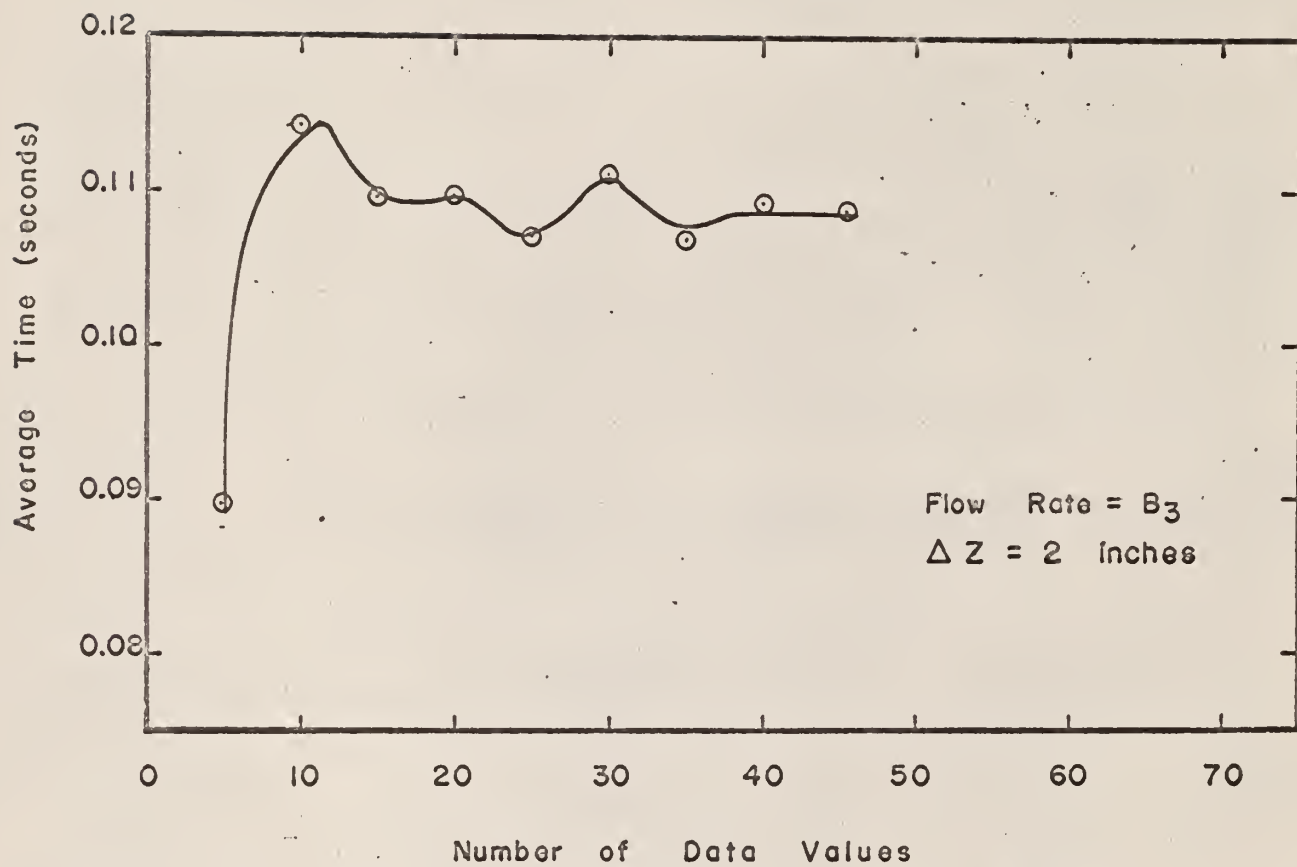


Figure 36. Average Residence Time as a Function of the Number of Data Values, Data Set No. 37.

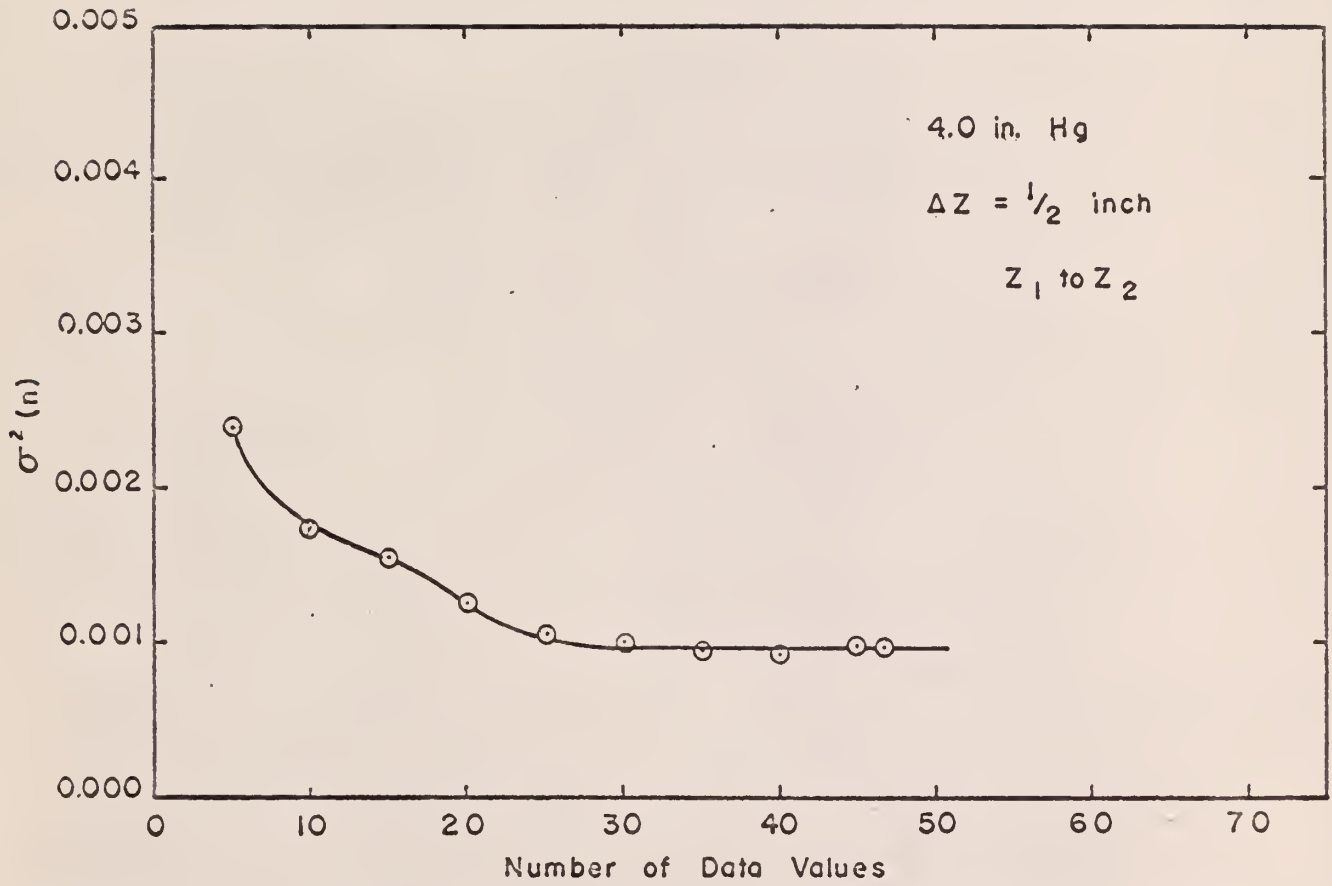


Figure 37. Variance of the Residence Times Data as a Function of the Number of Data Values, Data Set No. 16.

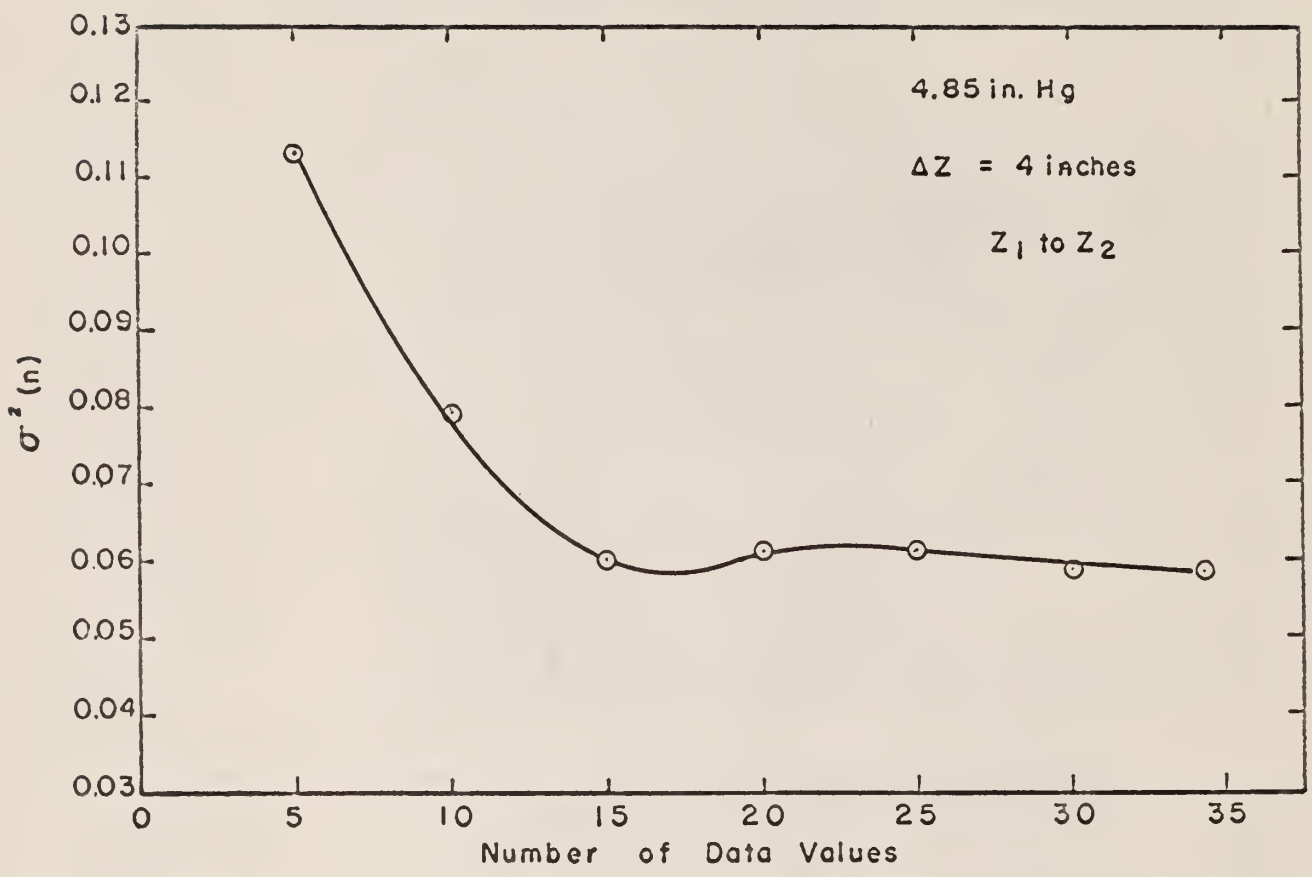


Figure 38. Variance of the Residence Times Data as a Function of the Number of Data Values, Data Set No. 42.

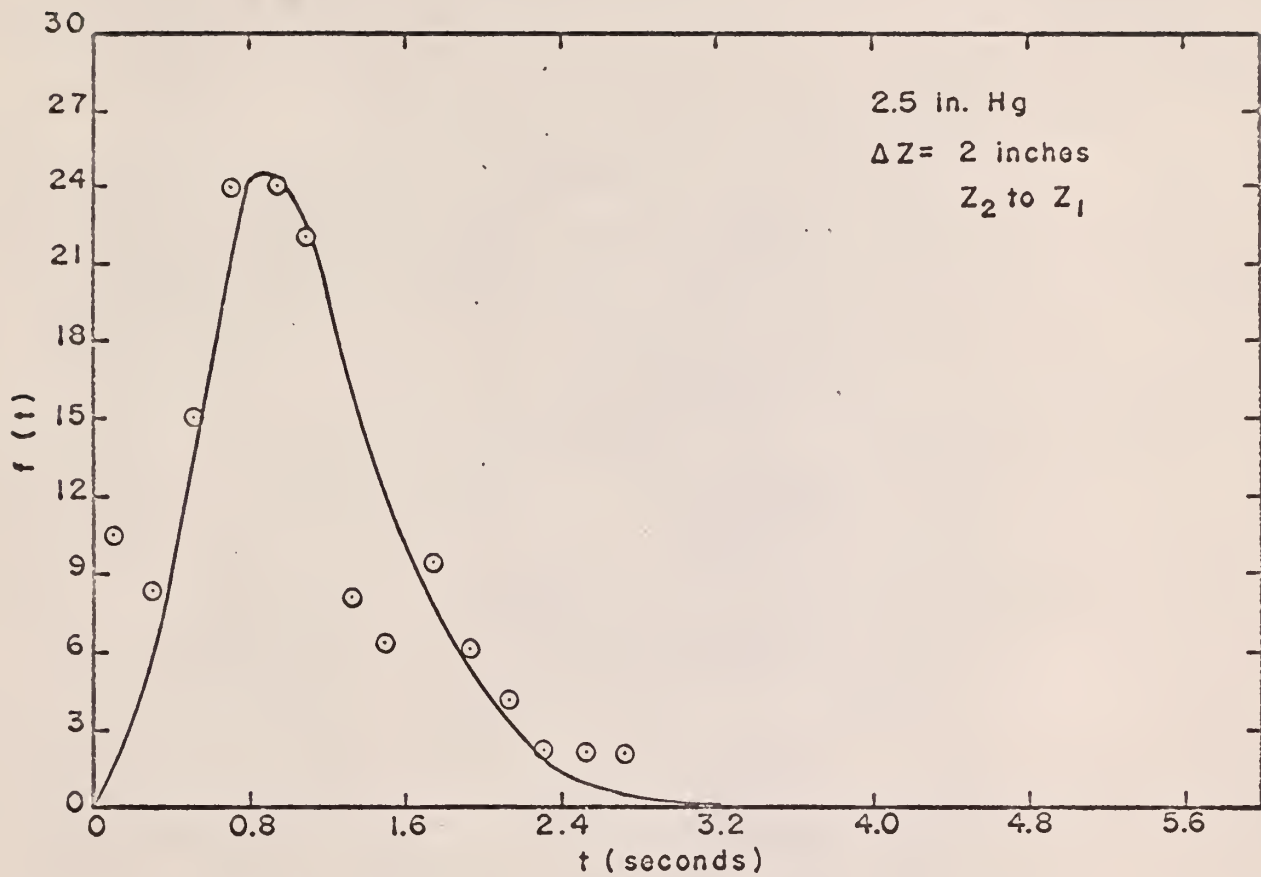


Figure 39. Frequency Distribution of the Residence Time Data and Theoretical Gamma Distribution, Data Set No. 8.

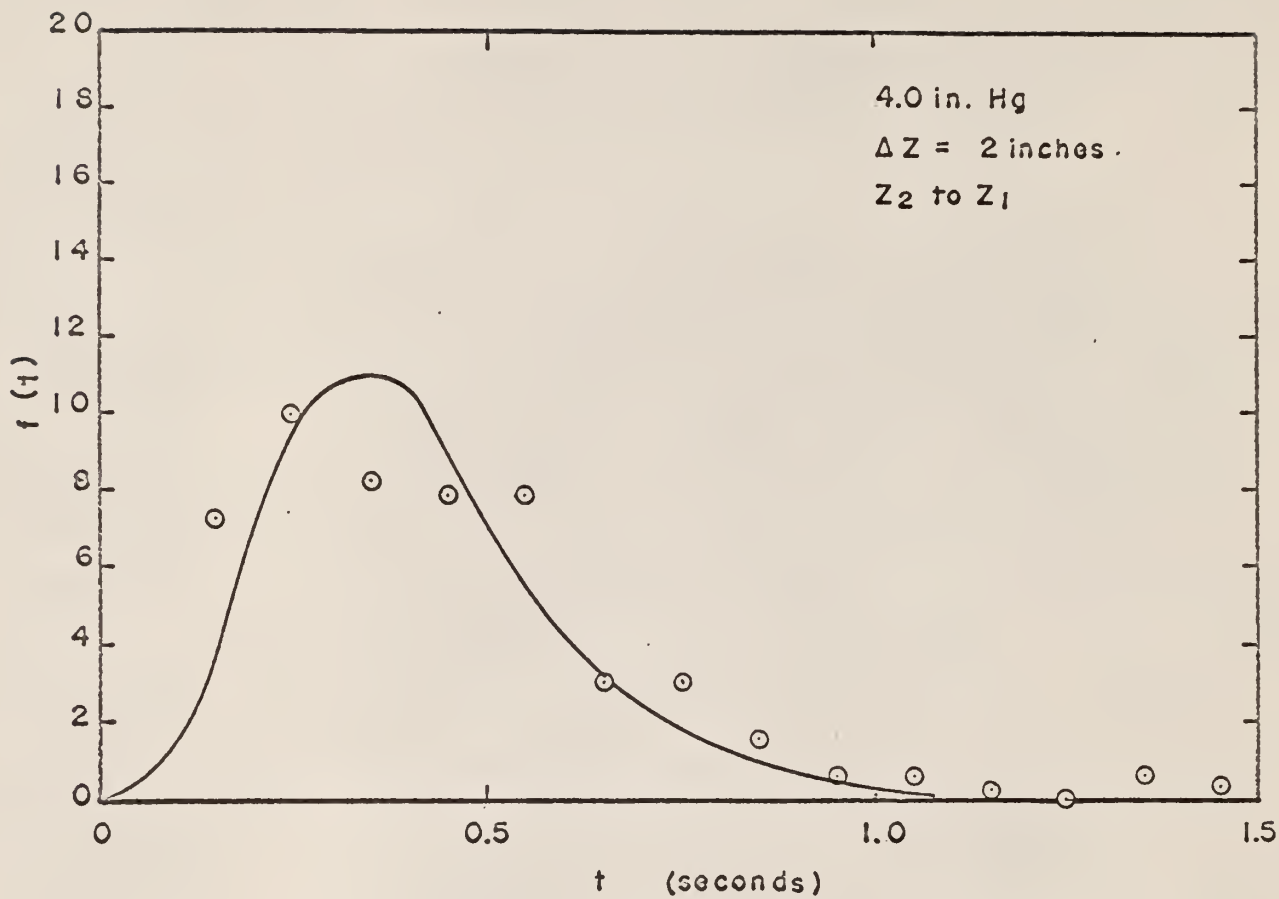


Figure 40. Frequency Distribution of the Residence Time Data and Theoretical Gamma Distribution, Data Set No. 22.

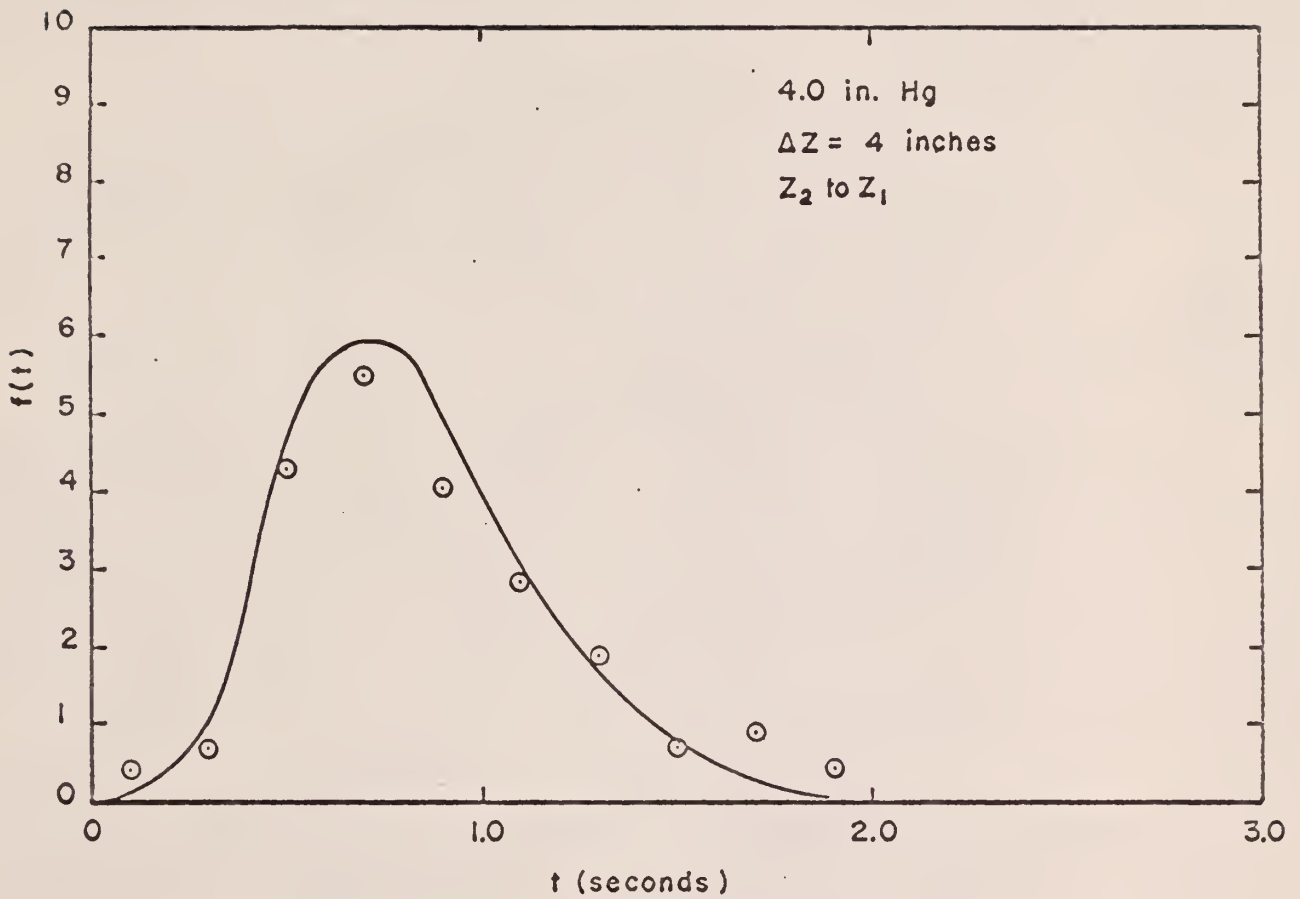


Figure 41. Frequency Distribution of the Residence Time Data and Theoretical Gamma Distribution, Data Set No. 27.

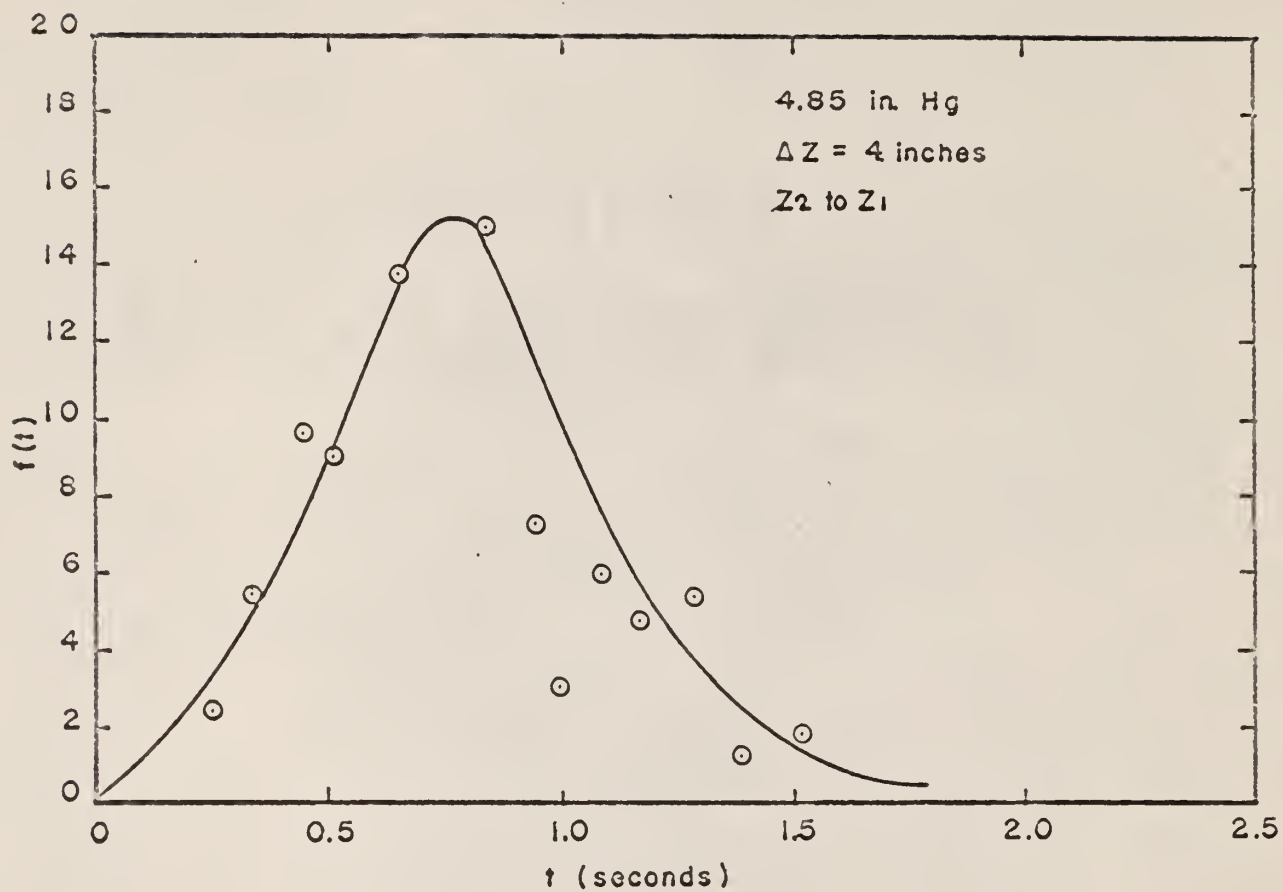


Figure 42. Frequency Distribution of the Residence Time Data and Theoretical Gamma Distribution, Data Set No. 44.

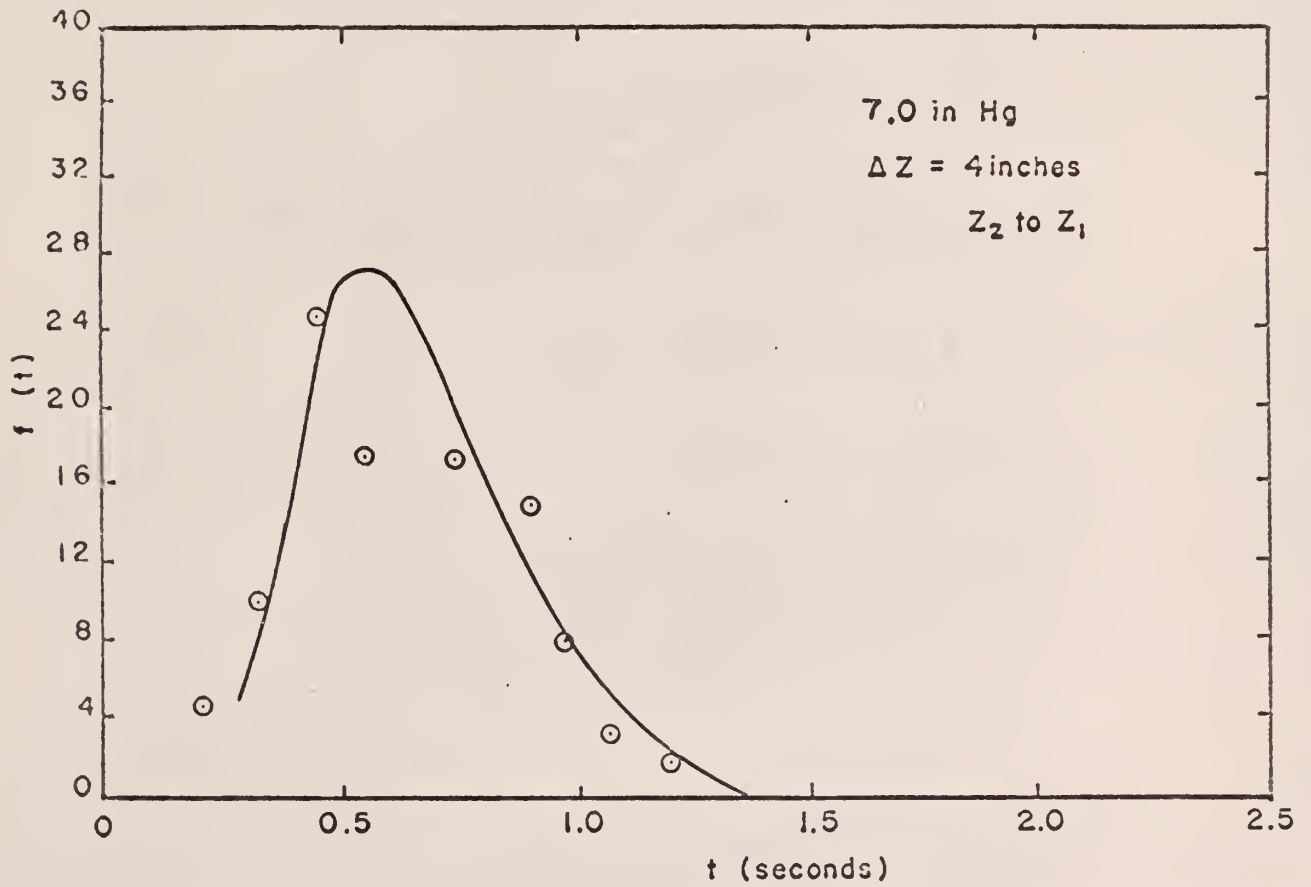


Figure 43. Frequency Distribution of the Residence Time Data and Theoretical Gamma Distribution, Data Set No. 59.

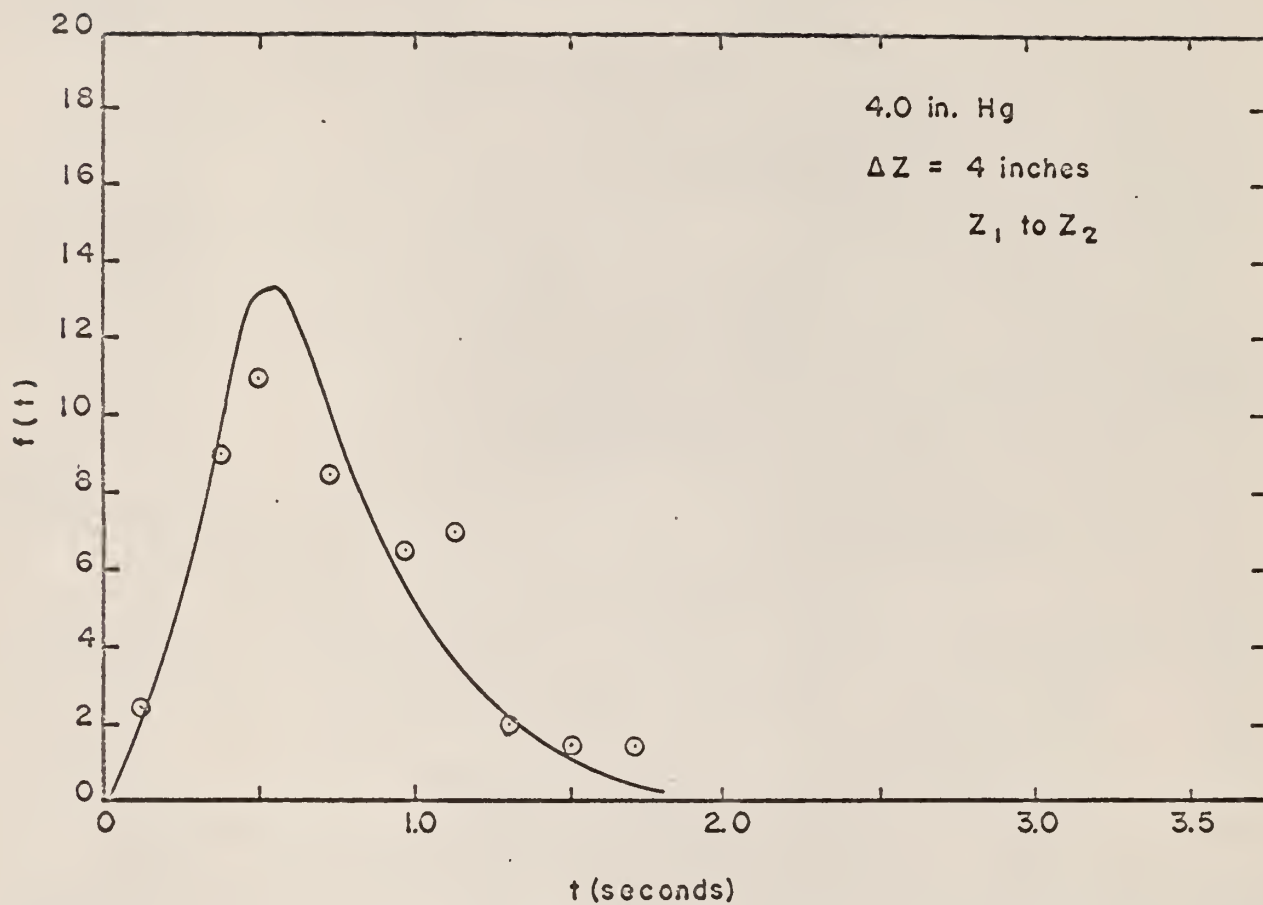


Figure 44. Frequency Distribution of Residence Time Data and Theoretical Gamma Distribution, Data Set No. 28.

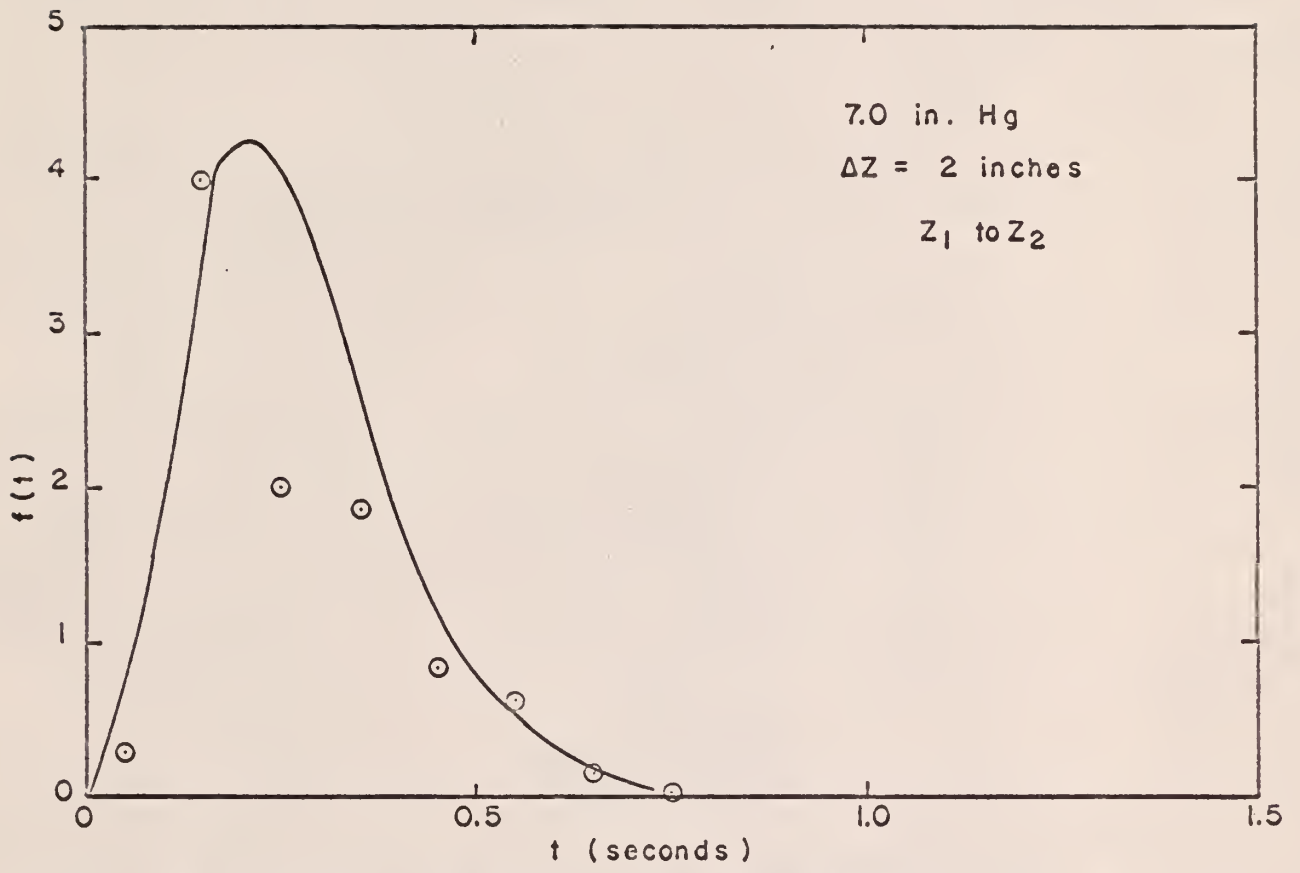


Figure 45. Frequency Distribution of the Residence Time Data and Theoretical Gamma Distribution, Data Set No. 53.

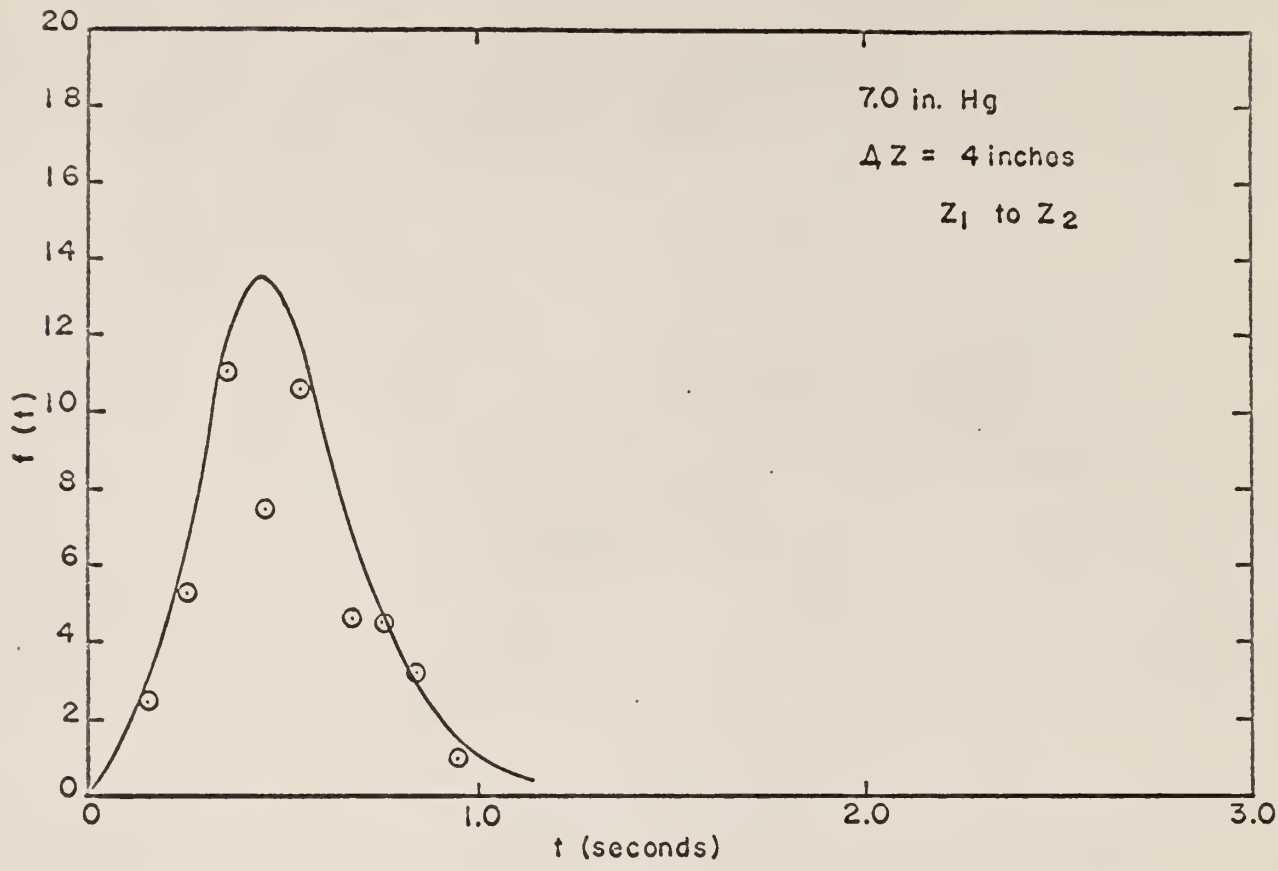


Figure 46. Frequency Distribution of the Residence Time Data and Theoretical Gamma Distribution, Data Set No. 58.

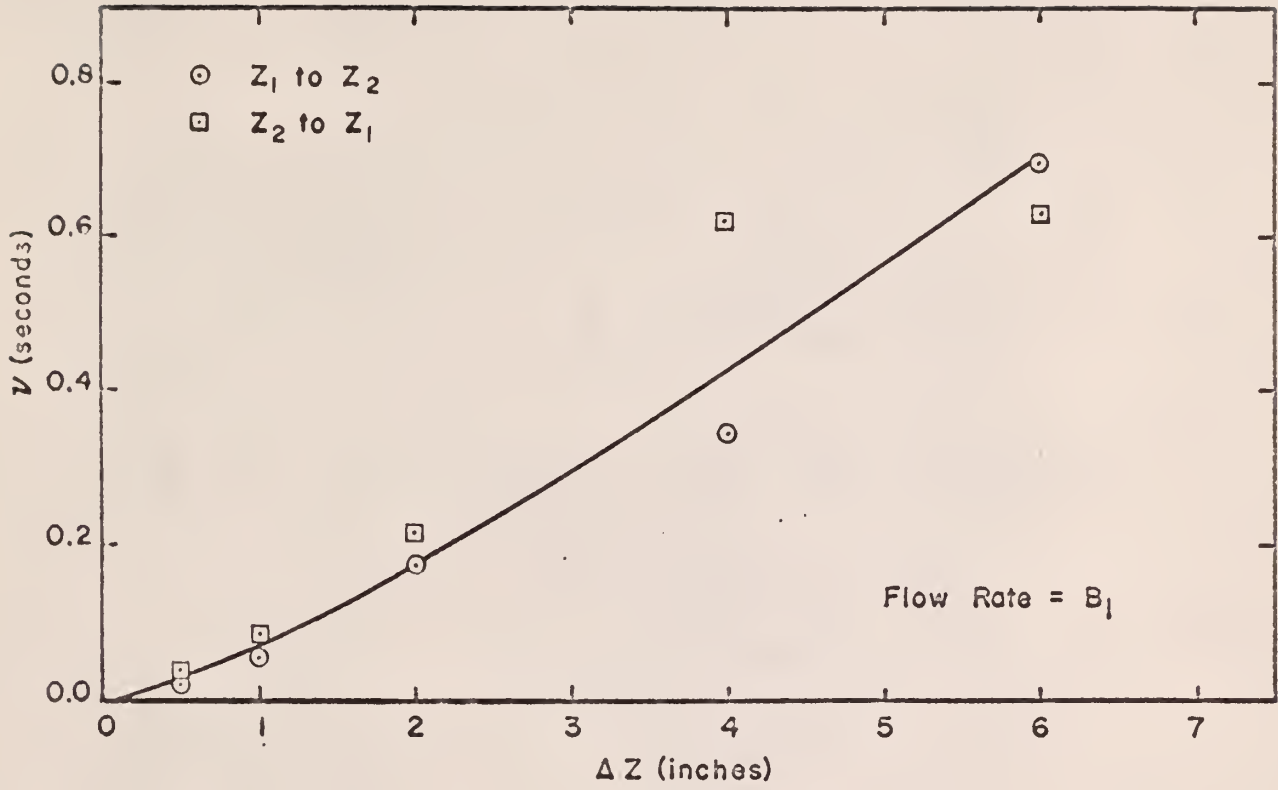


Figure 47. The Gamma Distribution Parameter  $\nu$ , at Flow Rate  $B_1$ .

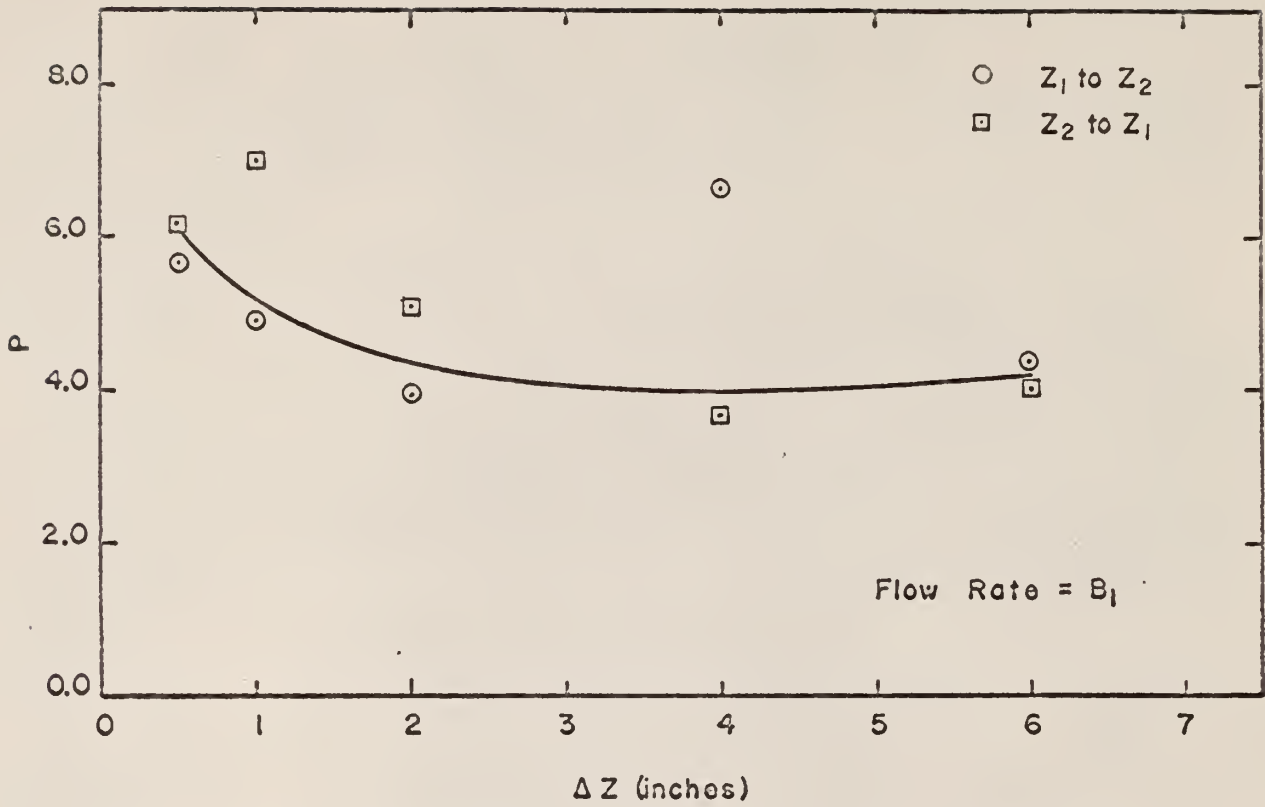


Figure 48. The Gamma Distribution Parameters P, at Flow Rate B<sub>1</sub>.

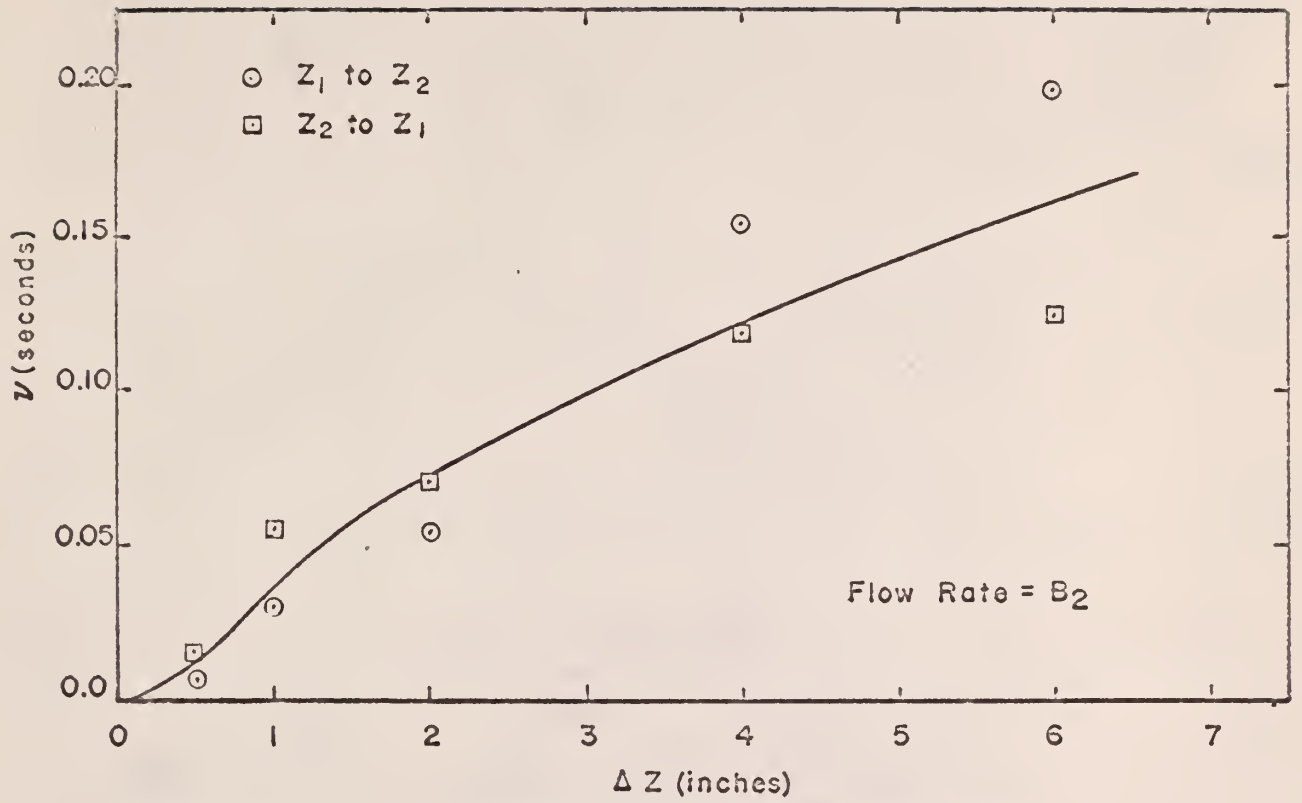


Figure 49. The Gamma Distribution Parameter  $\nu$ , at Flow Rate  $B_2$ .

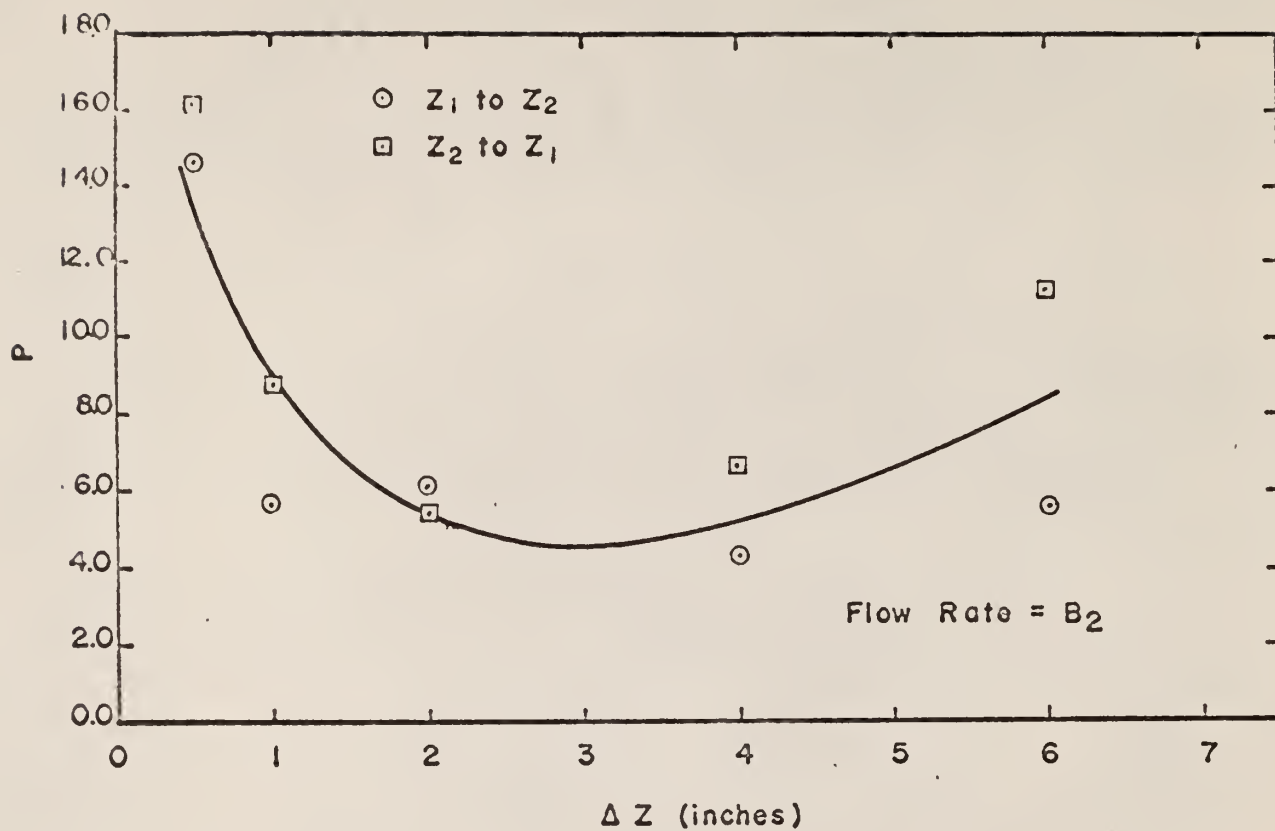


Figure 50. The Gamma Distribution Parameter  $P$ , at Flow Rate  $B_2$ .

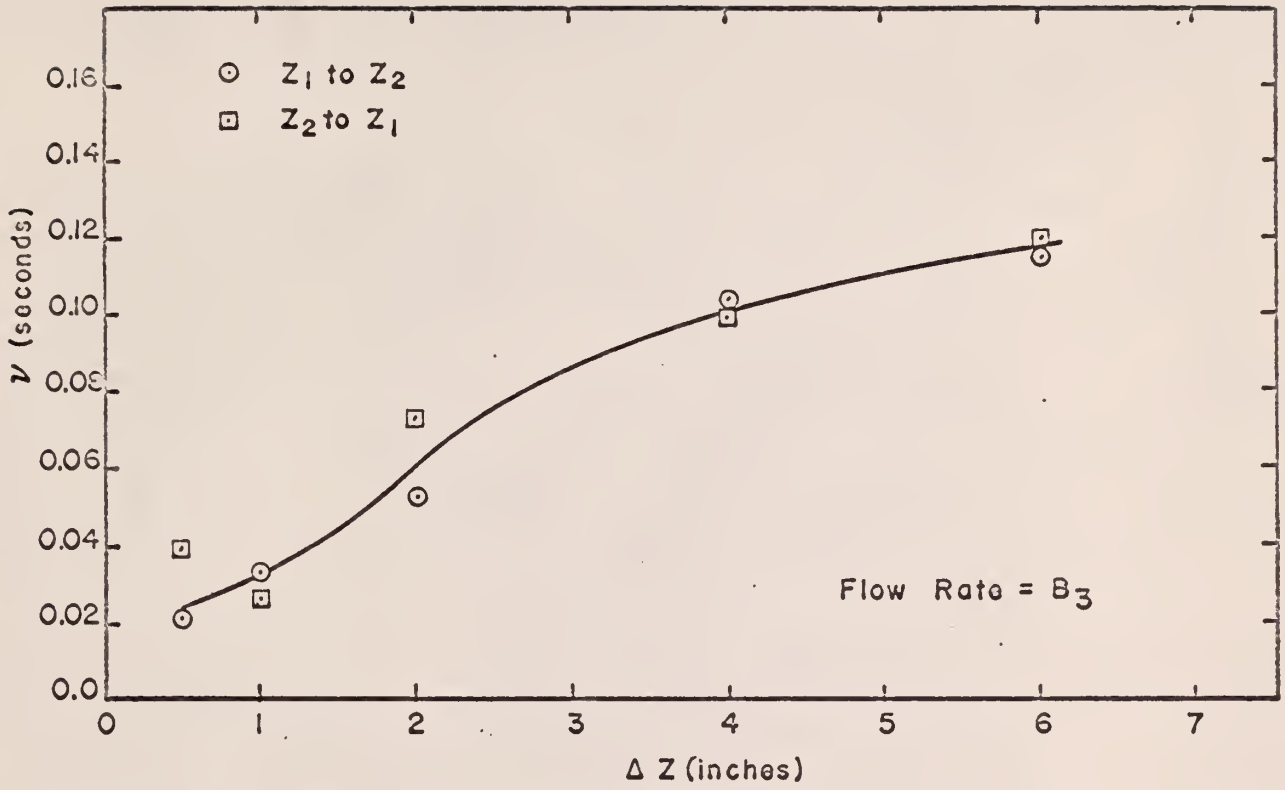


Figure 51. The Gamma Distribution Parameter  $\nu$ , at Flow Rate  $B_3$ .

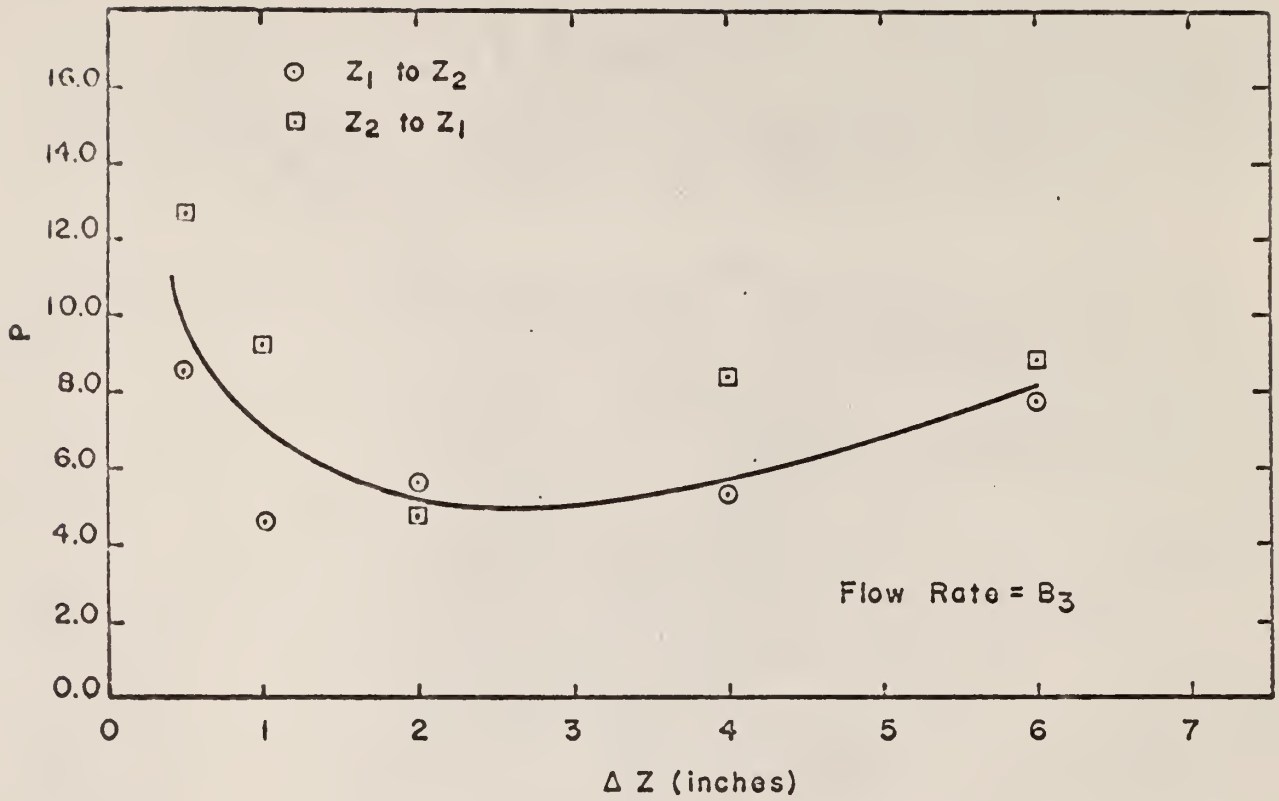


Figure 52. The Gamma Distribution Parameter  $P$ , at Flow Rate  $B_3$ .

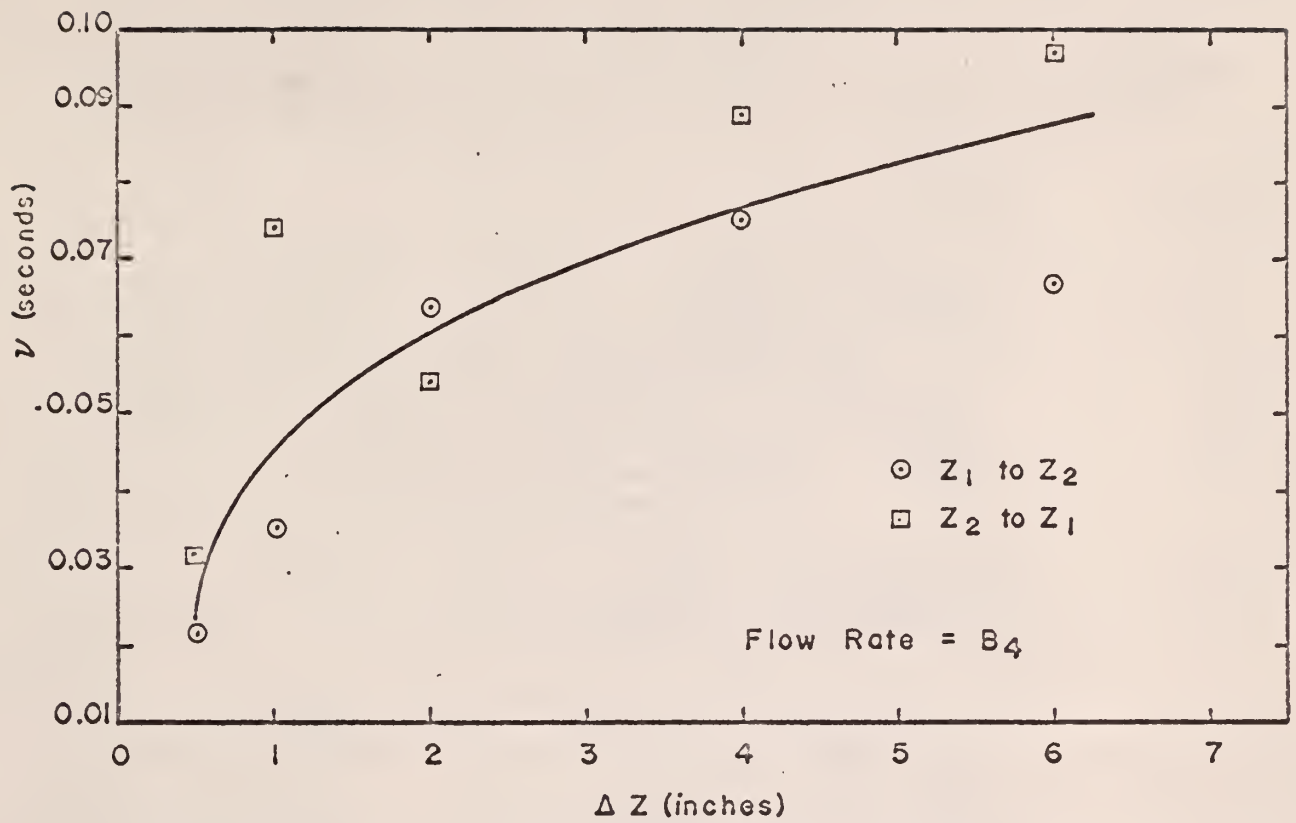


Figure 53. The Gamma Distribution Parameter  $\nu$ , at Flow Rate  $B_4$ .

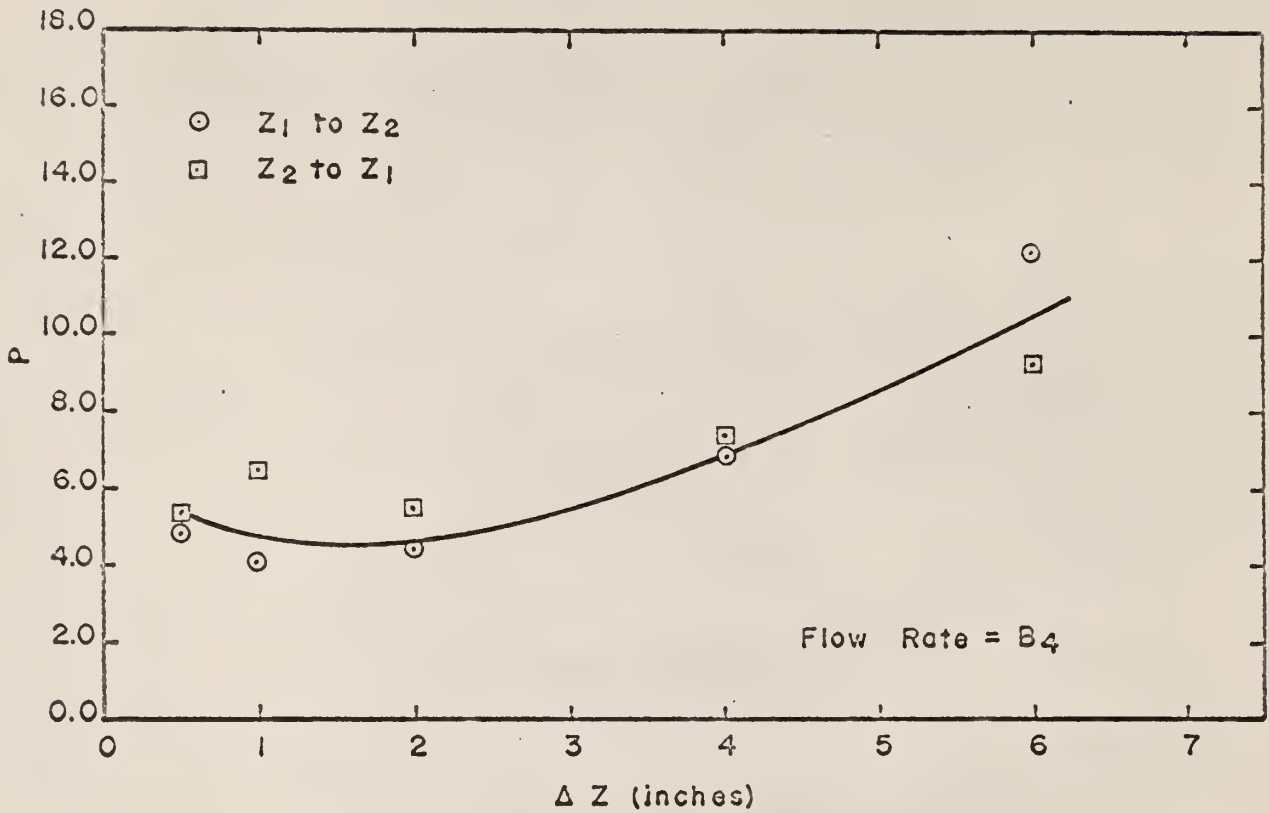


Figure 54. The Gamma Distribution Parameter  $P$ , at Flow Rate  $B_4$ .

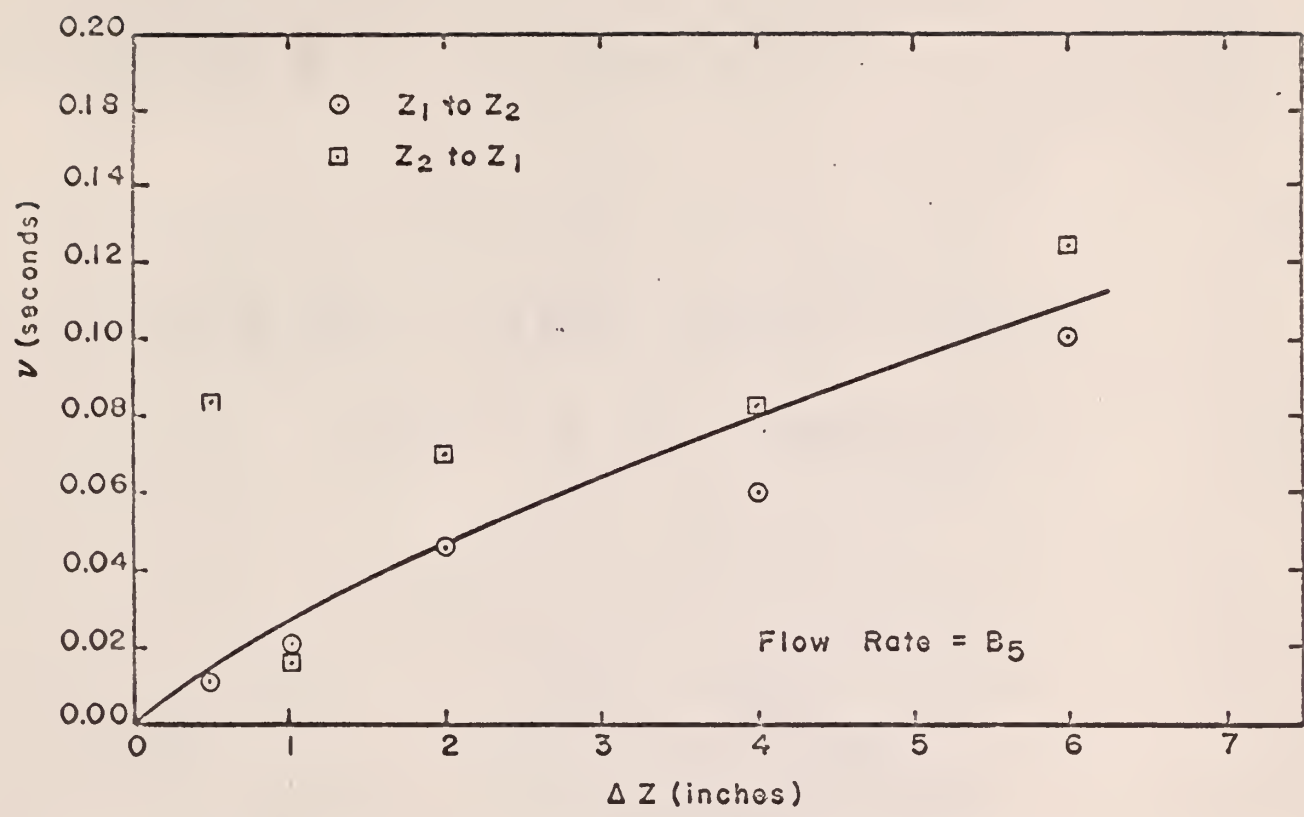


Figure 55. The Gamma Distribution Parameter  $\nu$ , at Flow Rate B5.

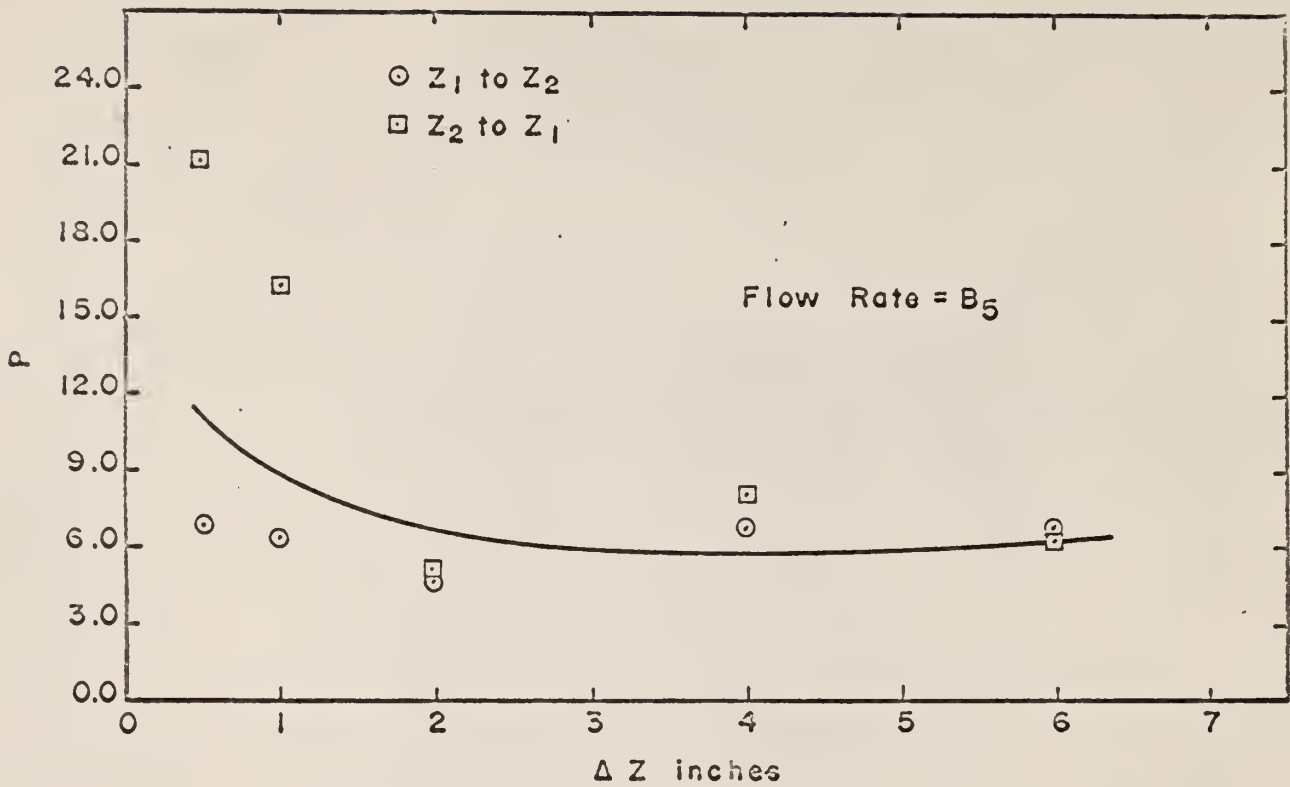


Figure 56. The Gamma Distribution Parameter P, at Flow Rate B<sub>5</sub>.

speed of the tagged particle for each set of data in the following manner:

$$\bar{v} = \sum_{i=1}^n \frac{\Delta Z}{t_i n} = \frac{\Delta Z}{n} \sum_{i=1}^n \frac{1}{t_i} \quad (18)$$

The output of Computer Program No. 8 is given in Appendix F.

The speed of the tagged particle for each distance between detector levels and water flow rate was determined by the following three methods:

$$v(t_p) = \frac{\Delta Z}{t_p} = \frac{\Delta Z}{(p-1)\mathcal{V}} \quad (19)$$

$$v(\bar{t}) = \frac{\Delta Z}{\bar{t}} = \frac{\Delta Z n}{\sum_{i=1}^n t_i} \quad (20)$$

$$\bar{v} = \frac{\Delta Z}{n} \sum_{i=1}^n \frac{1}{t_i} \quad (18)$$

The quantity  $v(t_p)$  is the speed of the tagged particle corresponding to the most probable residence time,  $v(\bar{t})$  is the speed of the tagged particle corresponding to the average residence time, and  $\bar{v}$  is the average speed of the tagged particle.

Figures 57 through 71 give the results of  $v(t_p)$ ,  $v(\bar{t})$ , and  $\bar{v}$  as functions of the distance between detector levels.

Figures 72, 73, and 74 give straight-line extrapolations to  $\Delta Z = 0$  values (obtained from Figs. 57 through 71) for the speed of the tagged particle as a function of the mean fluid velocity through the fluidized bed.

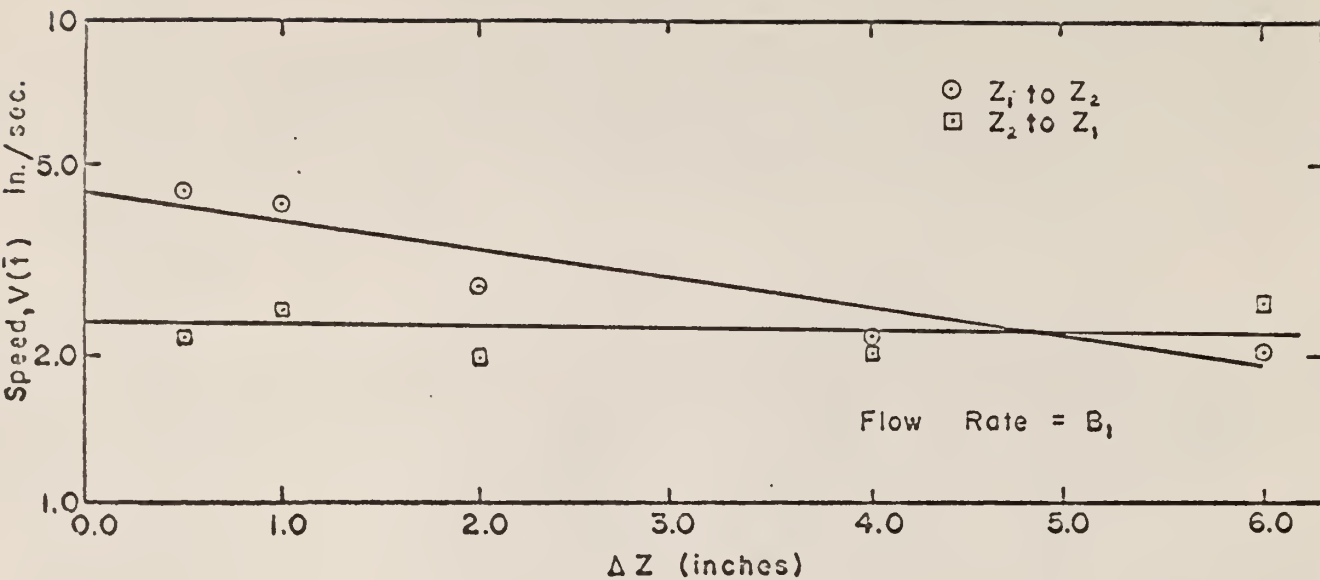


Figure 57. Particle Speed Corresponding to the Average Residence Time, at Flow Rate  $B_1$ .

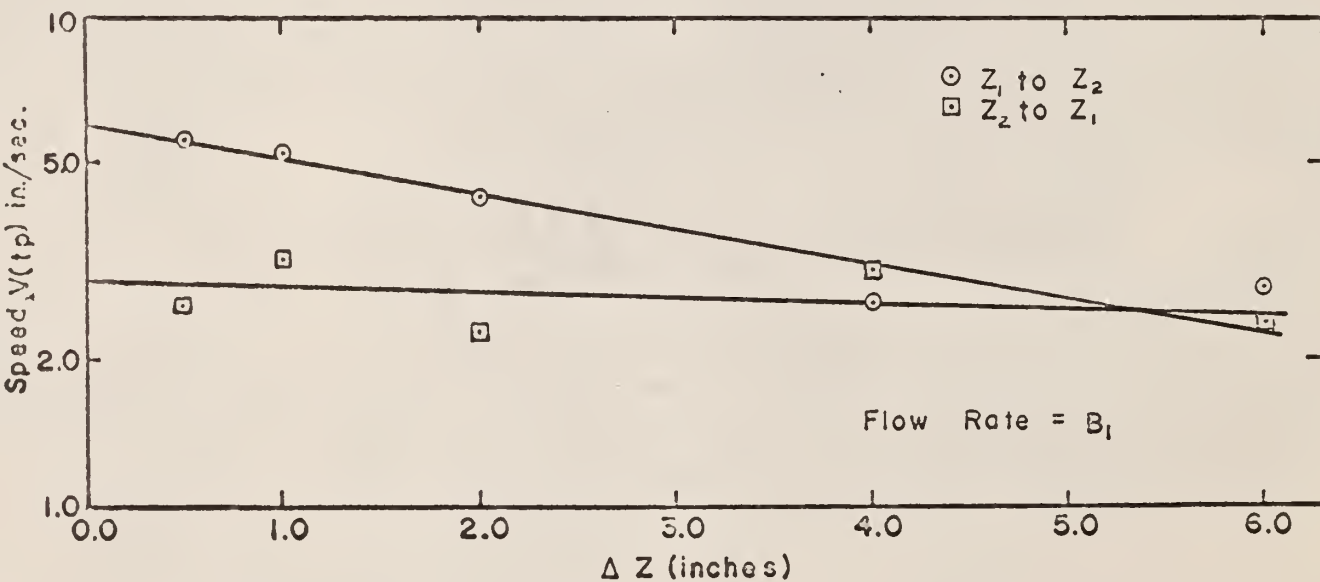


Figure 58. Particle Speed Corresponding to the Most Probable Residence Time, at Flow Rate  $B_1$ .

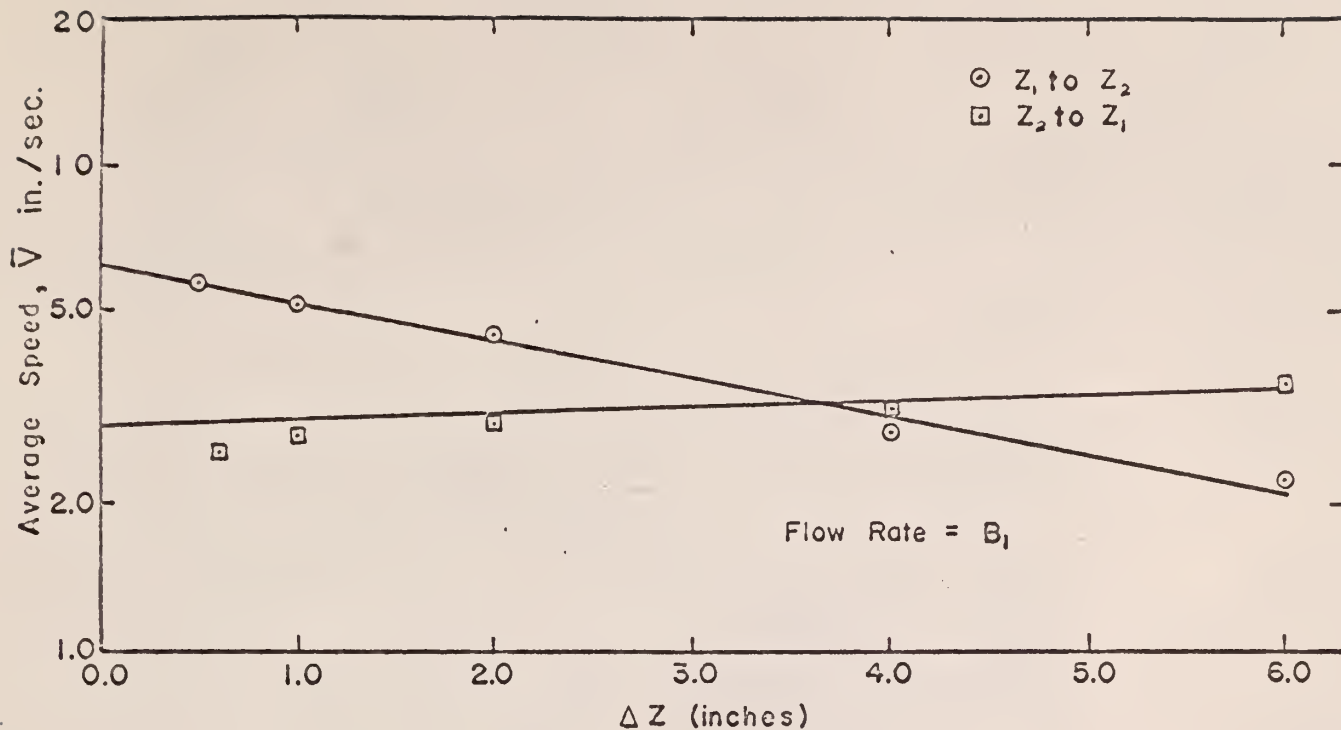


Figure 59. Average Particle Speed, at Flow Rate  $B_1$ .

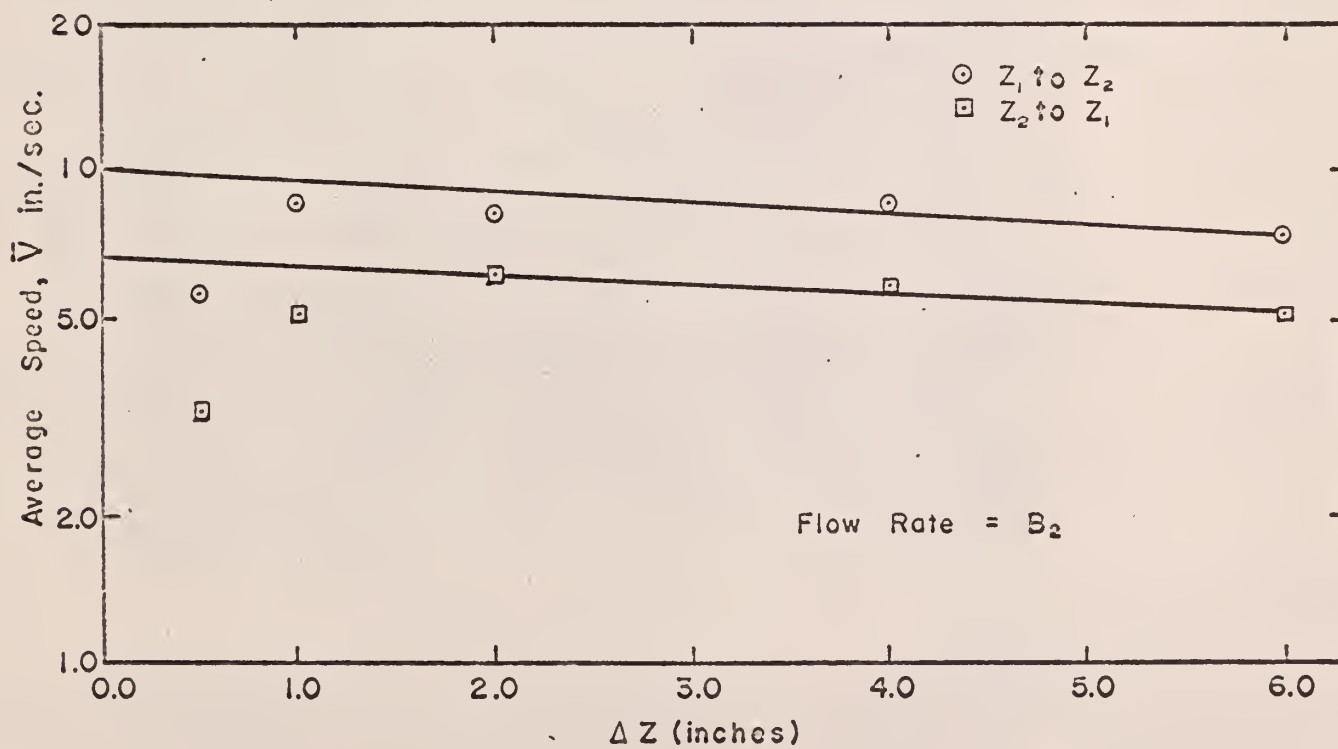


Figure 60. Average Particle Speed, at Flow Rate  $B_2$ .

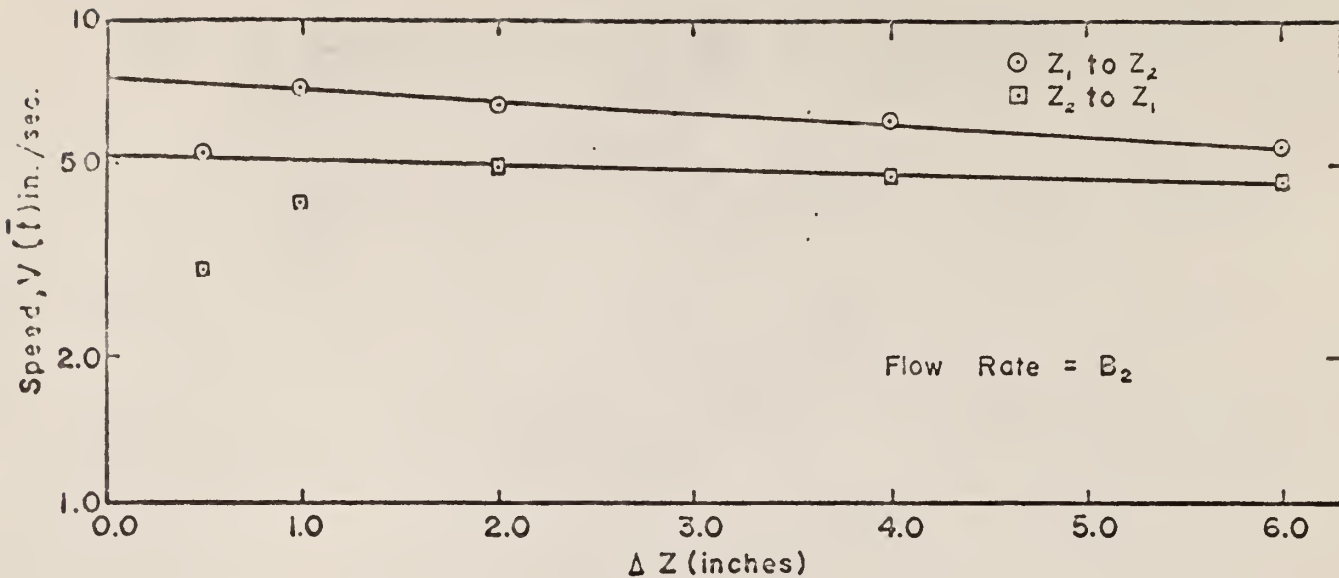


Figure 61. Particle Speed Corresponding to the Average Residence Time, at Flow Rate  $B_2$ .

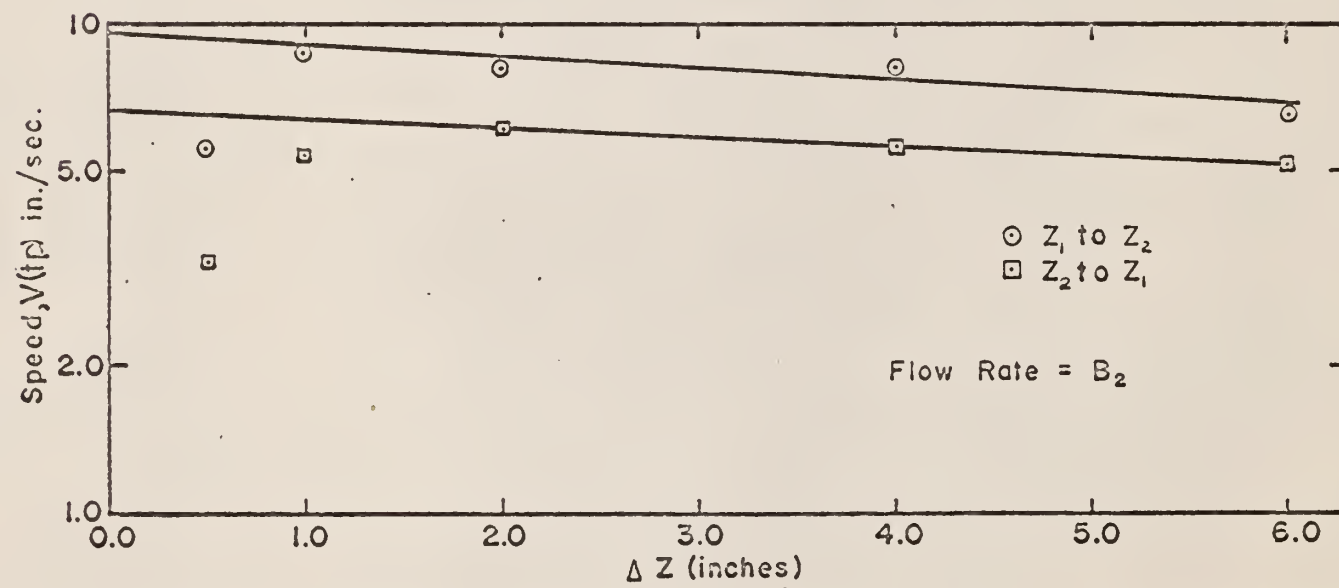


Figure 62. Particle Speed Corresponding to the Most Probable Residence Time, at Flow Rate  $B_2$ .

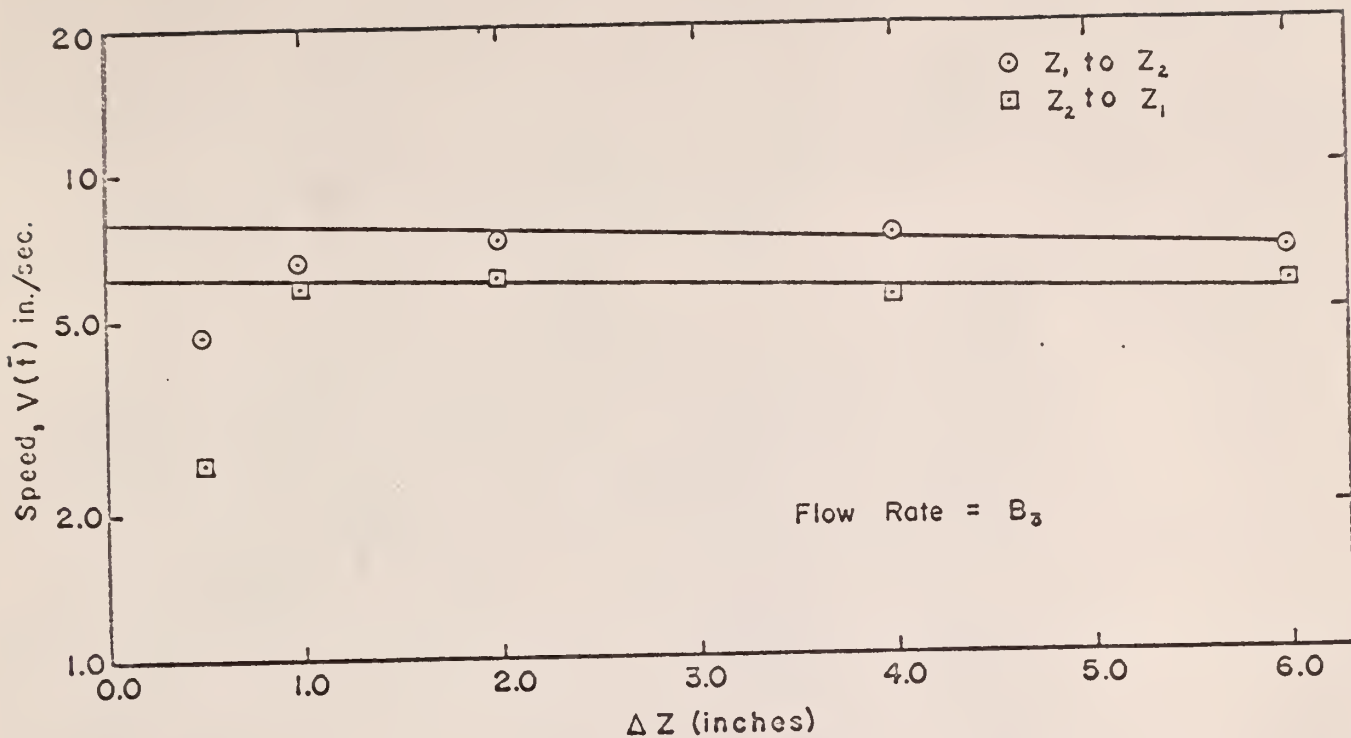


Figure 63. Particle Speed Corresponding to the Average Residence Time, at Flow Rate  $B_3$ .

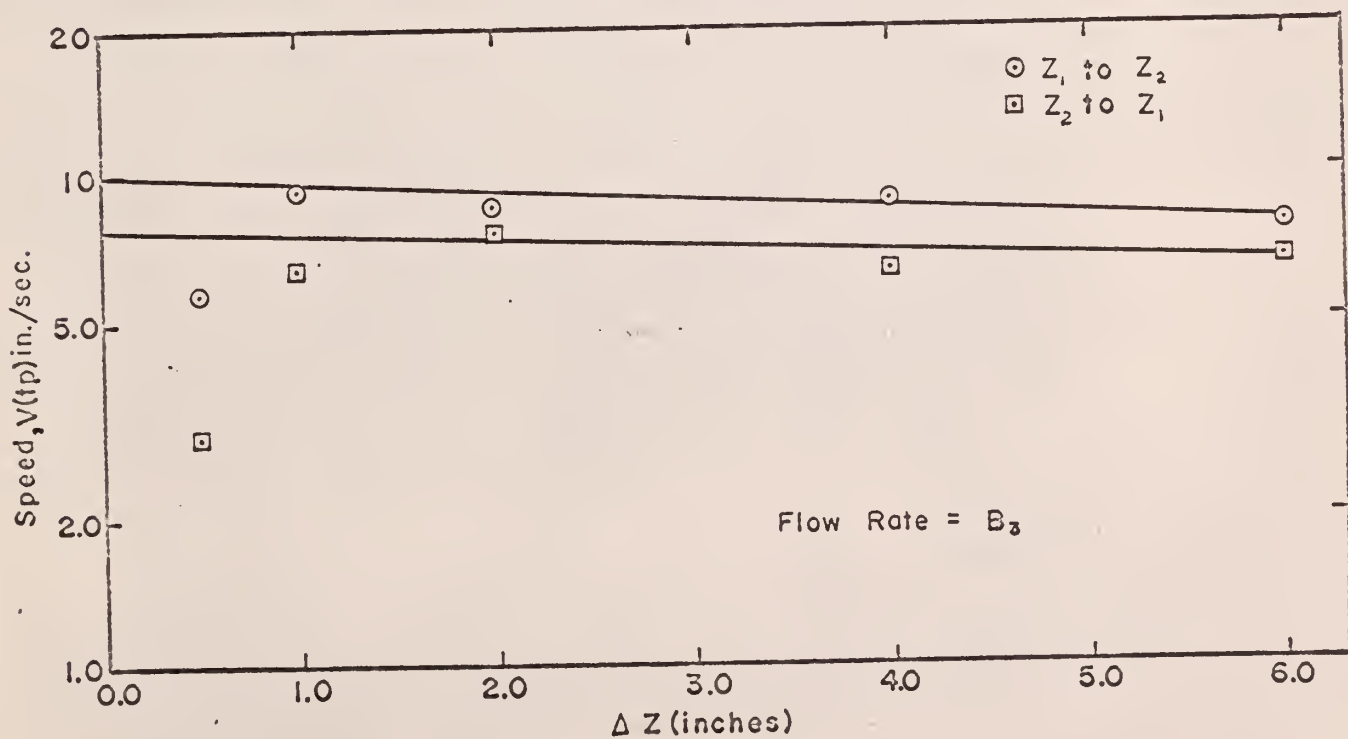


Figure 64. Particle Speed Corresponding to the Most Probable Residence Time, at Flow Rate  $B_3$ .

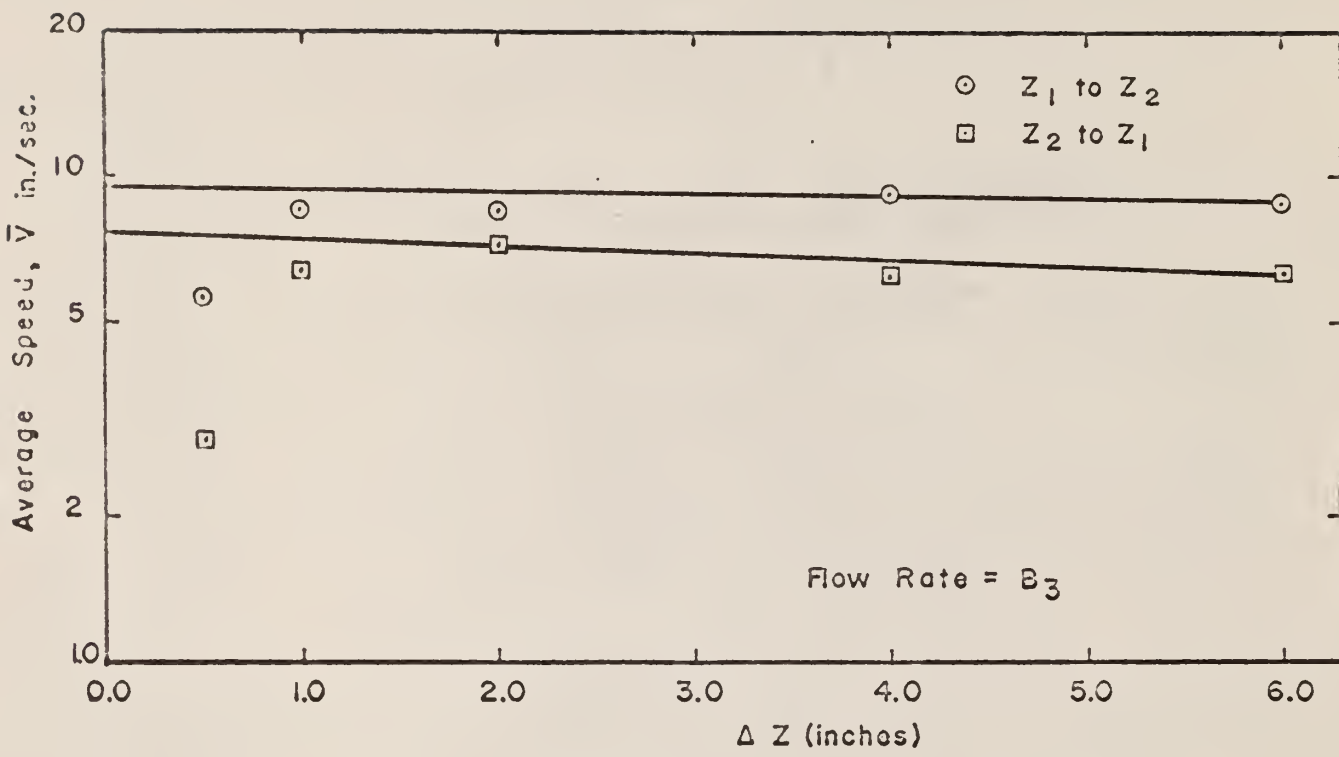


Figure 65. Average Particle Speed, at Flow Rate B<sub>3</sub>.

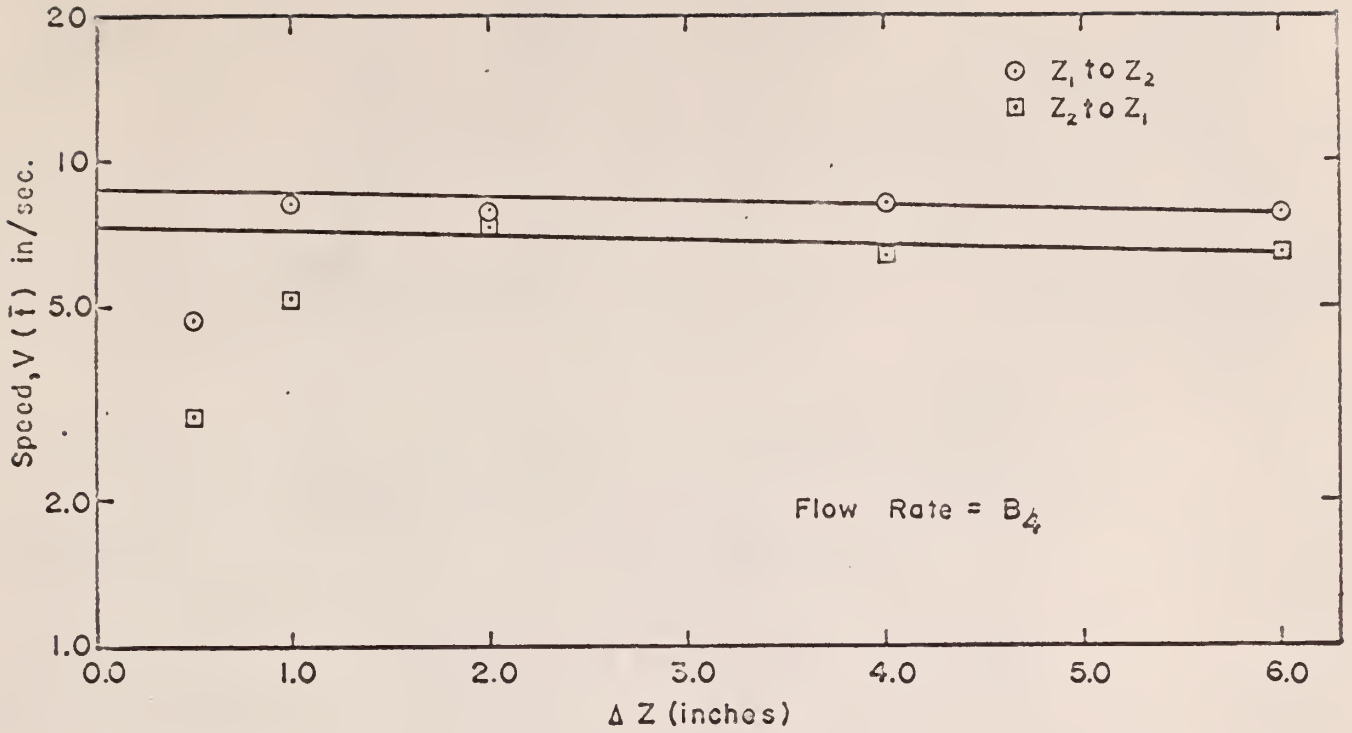


Figure 66. Particle Speed Corresponding to the Average Residence Time, at Flow Rate  $B_4$ .

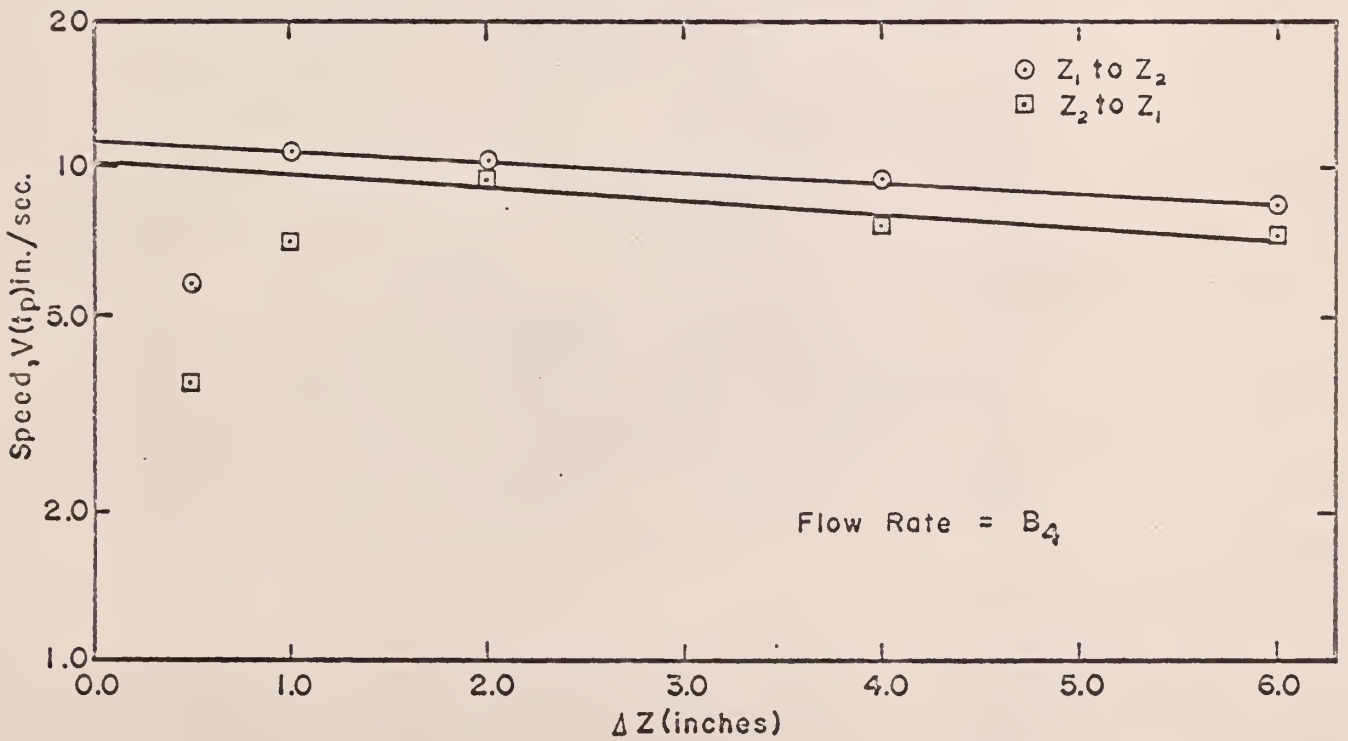


Figure 67. Particle Speed Corresponding to the Most Probable Residence Time, at Flow Rate  $B_4$ .

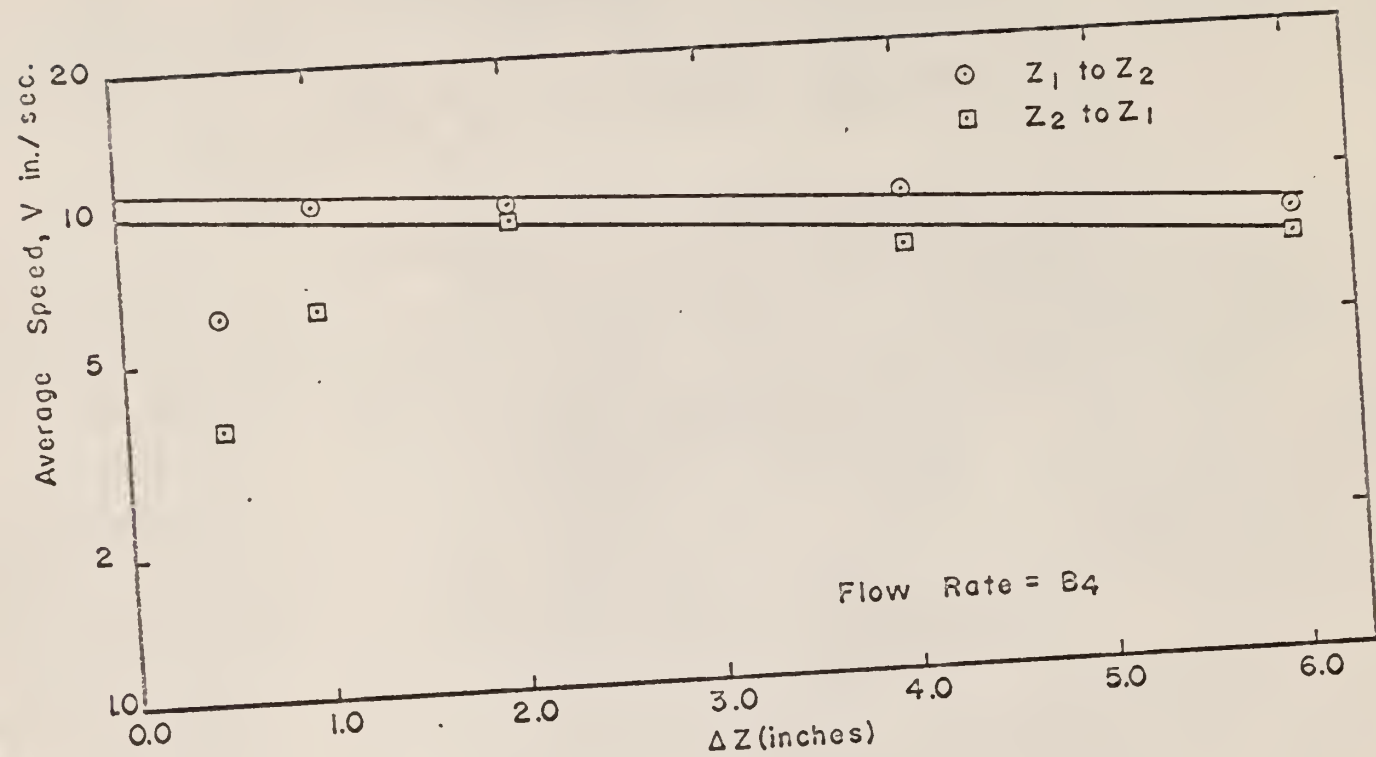


Figure 68. Average Particle Speed, at Flow Rate B4.

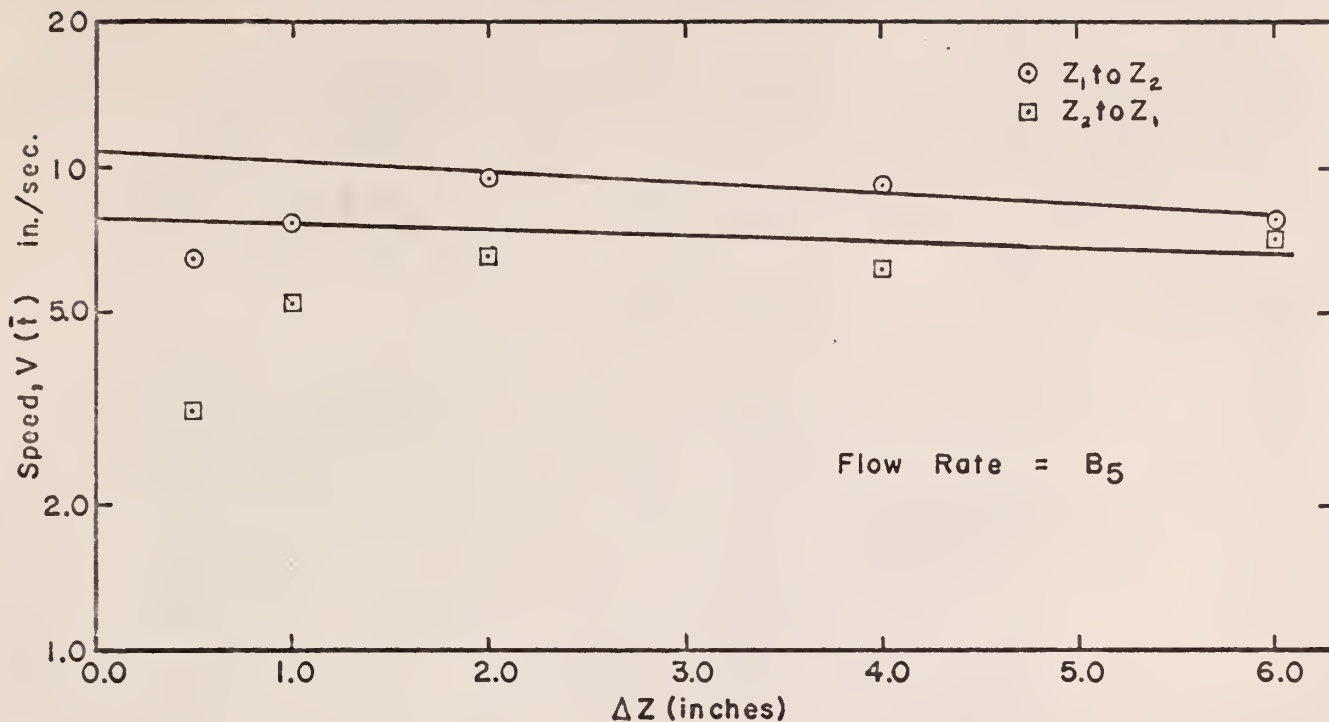


Figure 69. Particle Speed Corresponding to the Average Residence Time, at Flow Rate  $B_5$ .

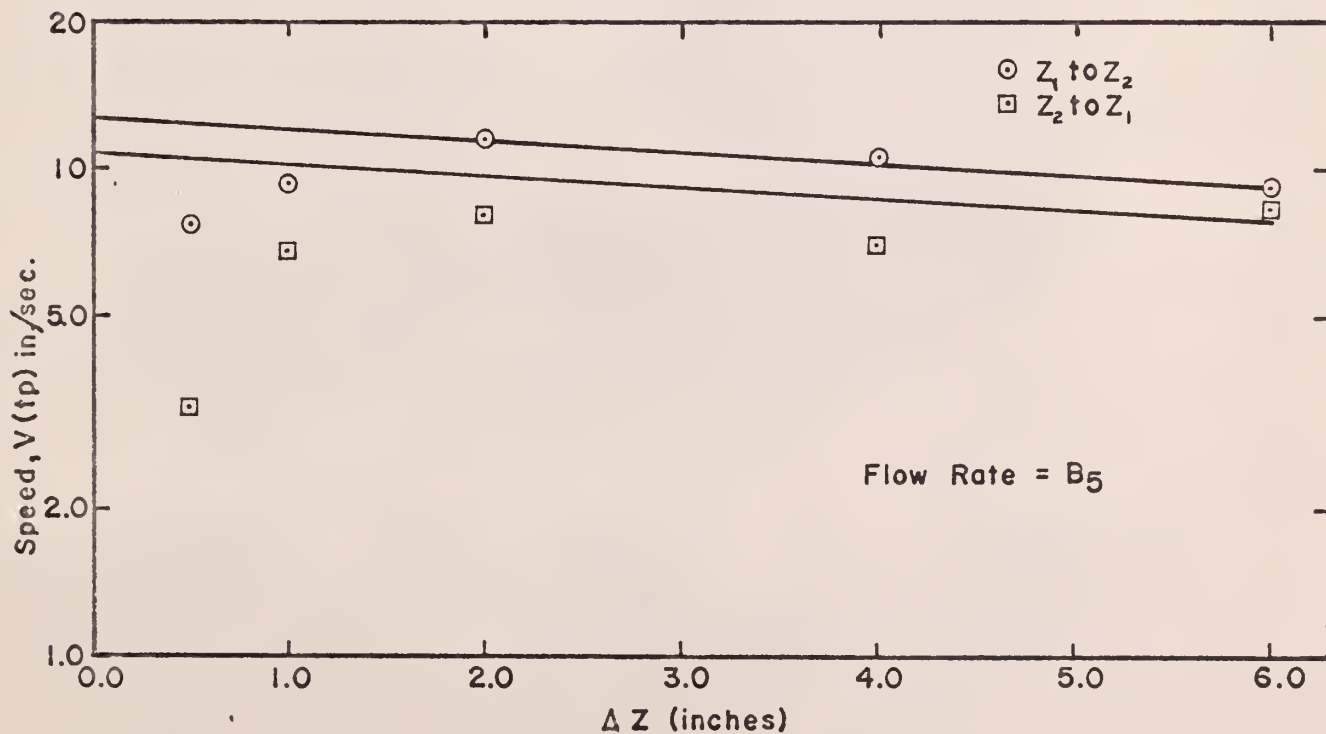


Figure 70. Particle Speed Corresponding to the Most Probable Residence Time at Flow Rate  $B_5$ .

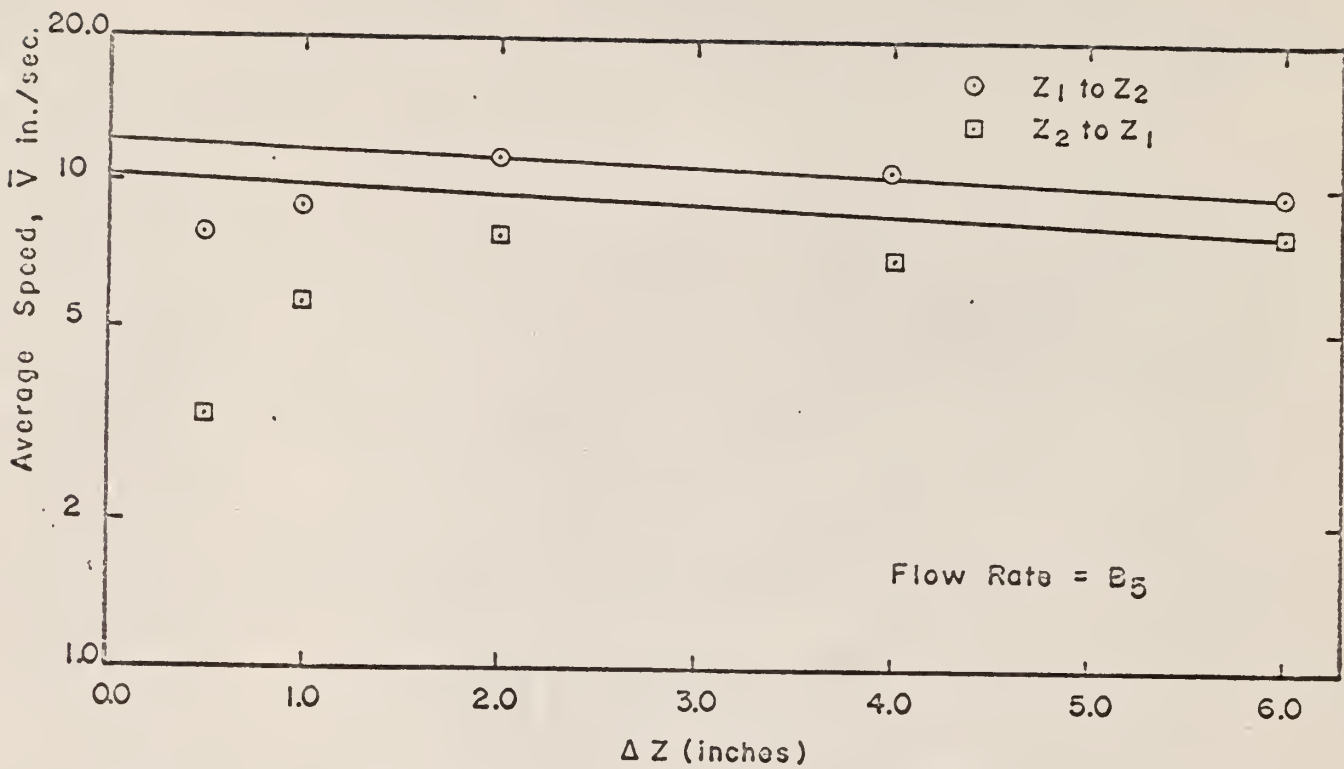


Figure 71. Average Particle Speed, at Flow Rate B<sub>5</sub>.

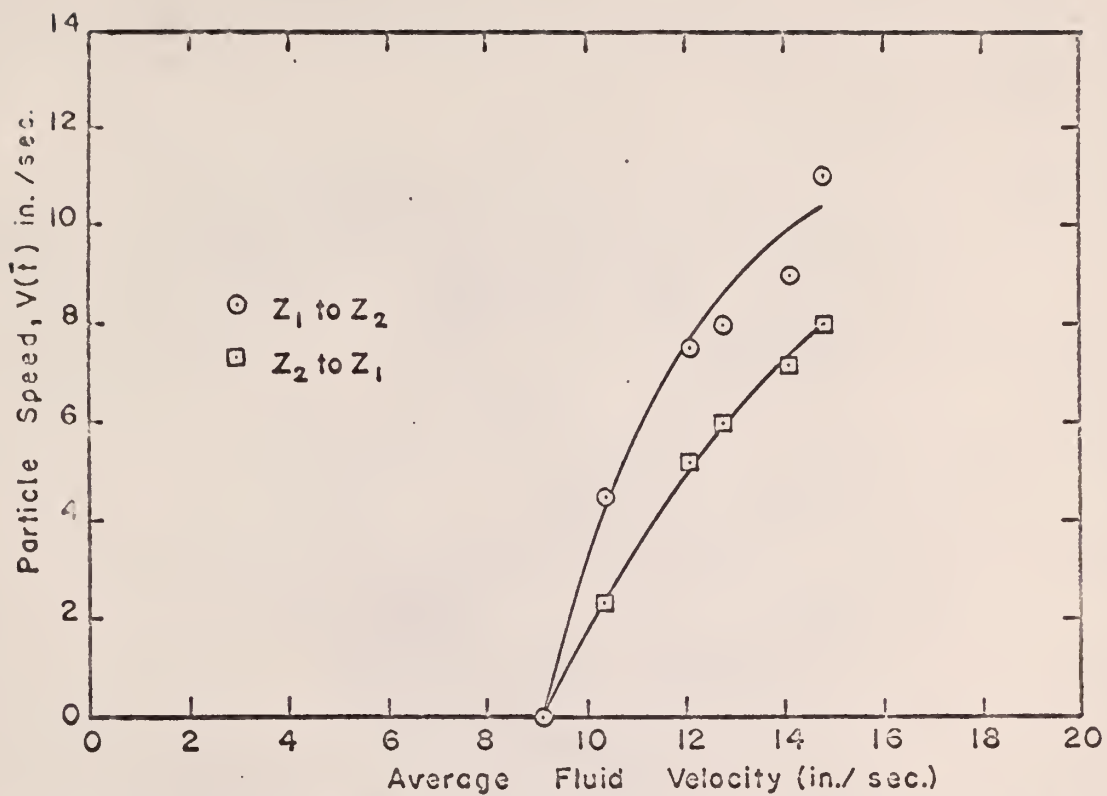


Figure 72. Particle Speed Corresponding to the Average Residence Time as a Function of the Mean Fluid Velocity.

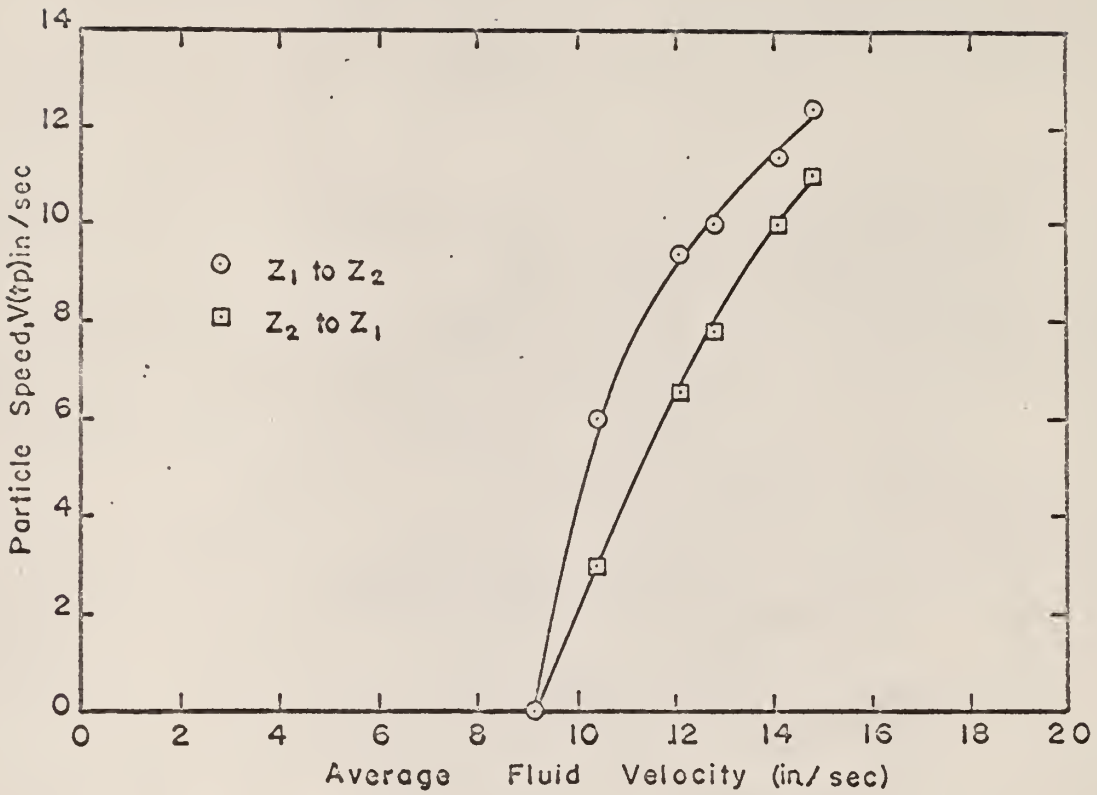


Figure 73. Particle Speed Corresponding to the Most Probable Residence Time as a Function of the Mean Fluid Velocity.

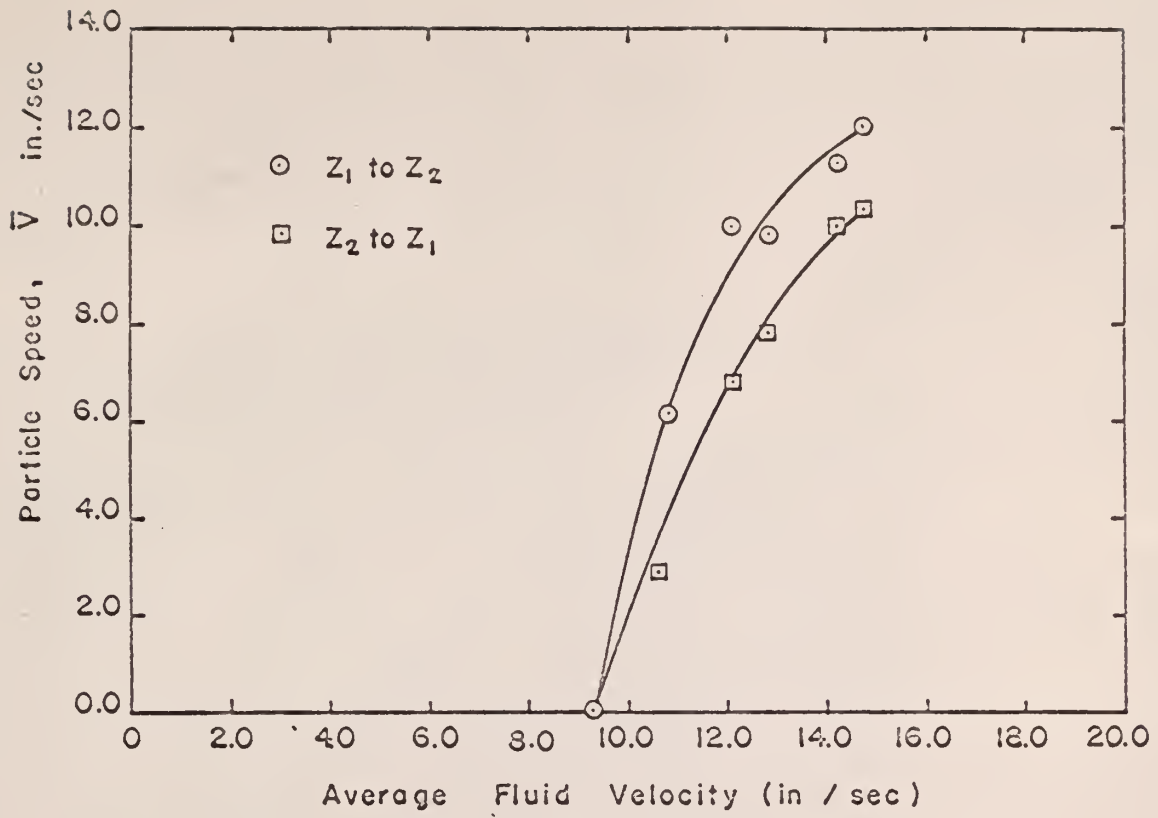


Figure 74. Average Particle Speed as a Function of the Mean Fluid Velocity.

#### 4.4 Analysis of the Particle Traffic

The number of times a particle passes a level  $Z_i$  per unit time is defined as the particle traffic,  $r(Z_i)$ , and was determined by counting the number of times the tagged particle passed each detector level in each data set and dividing by the total time required to obtain the data as described previously.

An IBM-1620 FORTRAN computer program was developed to determine the particle traffic, and it is discussed in Appendix B.

Figure 75 is a plot of the particle traffic data obtained from each detector level as a function of the mean fluid velocity through the fluidizing column.

#### 4.5 Analysis of the Reflectivity Data

The reflectivity,  $Pr$ , was previously defined as the probability of a particle passing level  $Z_i$  and failing to reach a different level ( $Z_j$ ) a given distance ( $\Delta Z$ ) away from  $Z_i$  before returning to  $Z_i$ . This probability is represented by  $Pr(Z_i, Z_j; Z_i)$  and is equal to  $(m-2)/m$ , where  $m$  is the number of times the particle passed  $Z_i$  before reaching  $Z_j$ . The reflectivity is equivalent to the reflection coefficient or albedo used by some authors (3).

The transmissivity is the probability of a particle passing level  $Z_i$  and reaching a different level ( $Z_j$ ) a given distance ( $\Delta Z$ ) away from  $Z_i$  before returning to  $Z_i$ . This probability is represented by  $Pr(Z_i, Z_j; Z_j)$ . The sum of the reflectivity and transmissivity probabilities must equal 1.0; therefore,

$$Pr(Z_i, Z_j; Z_i) = 1 - Pr(Z_i, Z_j; Z_j) \quad . \quad (21)$$

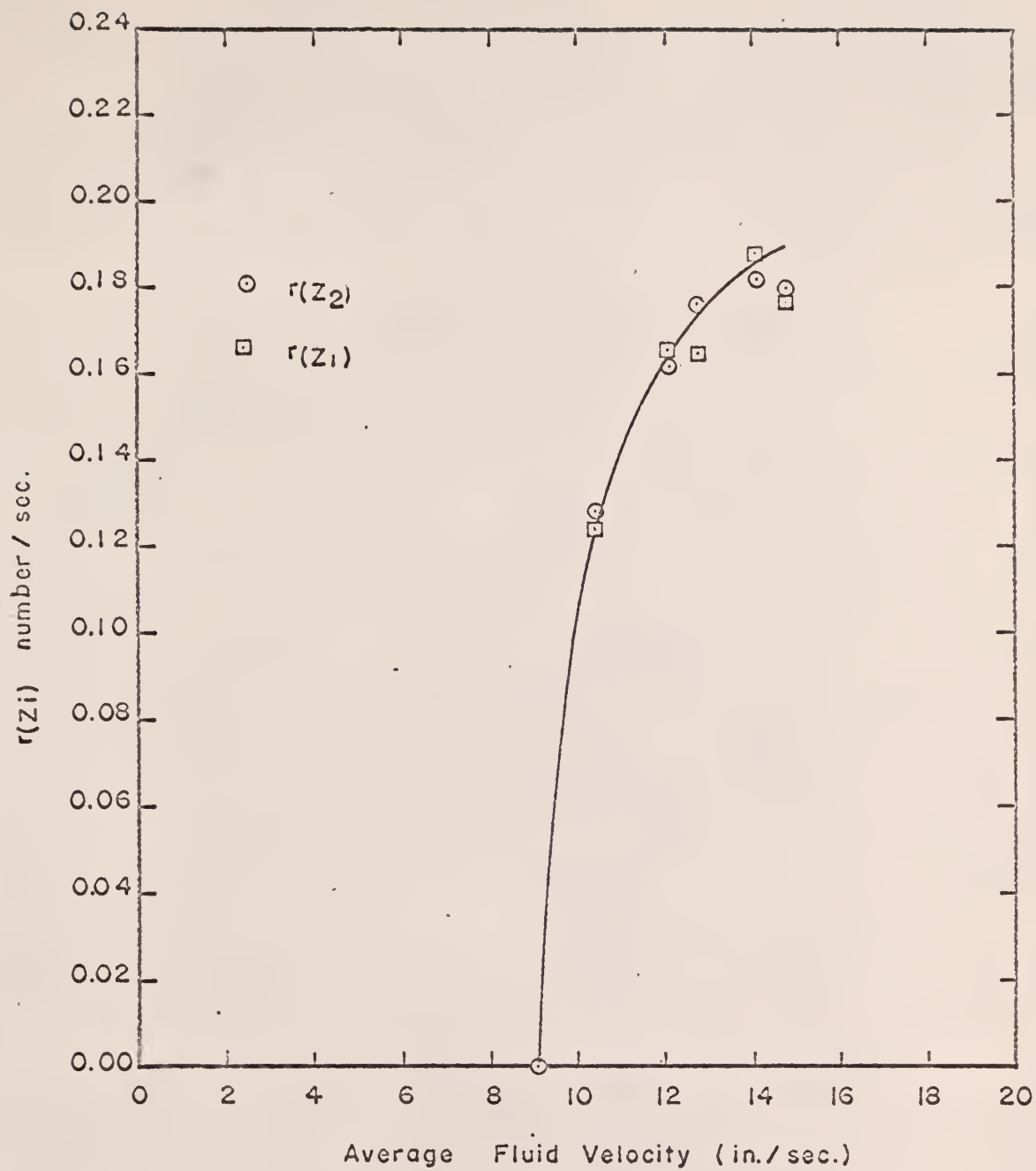


Figure 75. Particle Traffic as a Function of the Mean Fluid Velocity.

The reflectivity and transmissivity probabilities are easily derived by noting that for  $m$  particles passing  $Z_i$ ,  $m/2$  of the particles are moving in the direction toward  $Z_j$ , and one particle eventually reaches  $Z_j$ . The probability of transmission to  $Z_j$  is  $1/(m/2)$  or  $2/m$ . The probability of reflection is  $1 - (2/m)$  or  $(m-2)/m$ .

The following analysis was used to attempt to express analytically the reflectivity as a function of the distance between detector levels ( $\Delta Z$ ) and the position of the lower detector level ( $Z_i$ ).

The probability of a particle passing  $Z_i$  and reaching  $Z_j$  before returning to  $Z_i$  has been represented by

$$\Pr(Z_i, Z_j; Z_j) .$$

Generalizing, the probability of a particle passing  $Z_i$  and reaching  $Z$  before returning to  $Z_i$  is

$$\Pr(Z_i, Z; Z) .$$

The probability of a particle passing  $Z$  and reaching  $Z+\Delta Z$  before returning to  $Z$  is

$$\Pr(Z, Z+\Delta Z; Z+\Delta Z) ,$$

and the probability of a particle passing  $Z_i$  and reaching  $Z+\Delta Z$  before returning to  $Z_i$  is

$$\Pr(Z_i, Z+\Delta Z; Z+\Delta Z) .$$

These two probabilities are related by

$$\Pr(Z_i, Z+\Delta Z; Z+\Delta Z) = \Pr(Z_i, Z; Z)\Pr(Z, Z+\Delta Z; Z+\Delta Z). \quad (22)$$

The probability of a particle passing  $Z_i$  and reaching  $Z$  but not  $Z+\Delta Z$  before returning to  $Z_i$  is

$$\Pr(Z_i, Z; Z) \left[ 1 - \Pr(Z, Z+\Delta Z; Z+\Delta Z) \right] .$$

Assuming the relationship

$$1 - \Pr(Z, Z+\Delta Z; Z+\Delta Z) = \beta \Delta Z , \quad (23)$$

where  $\beta$  is defined as the reflection coefficient, and substituting it into Equation 22 gives

$$\Pr(Z_i, Z+\Delta Z; Z+\Delta Z) = \Pr(Z_i, Z; Z) (1 - \beta \Delta Z) . \quad (24)$$

Rearranging gives

$$\frac{\Pr(Z_i, Z+\Delta Z; Z+\Delta Z) - \Pr(Z_i, Z; Z)}{\Delta Z} = -\beta \Pr(Z_i, Z; Z) .$$

Taking the limit as  $\Delta Z \rightarrow 0$ ,

$$\frac{d \Pr(Z_i, Z; Z)}{dZ} = -\beta \Pr(Z_i, Z; Z) .$$

Integrating gives

$$\int \frac{d \Pr(Z_i, Z; Z)}{\Pr(Z_i, Z; Z)} = -\beta \int_{Z_i}^Z dZ ,$$

$$\ln \Pr(Z_i, Z; Z) = -\beta (Z - Z_i) + K \quad (25)$$

or,

$$\Pr(Z_i, Z; Z) = K e^{-\beta (Z - Z_i)} . \quad (26)$$

When  $Z = Z_i$ ,  $\Pr(Z_i, Z; Z) = 1.0$ . Therefore,

$$K = 1.$$

$Z$  is limited to the height of the fluidized bed,  $L$ . The probability of transmission from  $Z_i$  to  $L$ ,

$$\Pr(Z_i, L; L) = e^{-\beta(L-Z_i)},$$

is never zero for the range of experiments; therefore,  $\Pr(Z_i, Z; Z)$  ranges from  $e^{-\beta(L-Z_i)}$  to 1. The probability of reflection, therefore, ranges from zero to  $1 - e^{-\beta(L-Z_i)}$ .

Figures 76, 77, and 78 give illustrations of the frequency distribution of  $\Pr(Z_i, Z_j; Z_i)$  for different data sets, where  $f(\Pr)$  is the number of occurrences of each value of  $\Pr(Z_i, Z_j; Z_i)$ . Only discrete values of the reflectivity occur, since the reflectivity is defined as  $(m-2)/m$ , where  $m$  represents integers 2, 3, ..., etc. Note that the frequency distributions of  $\Pr(Z_i, Z_j; Z_i)$  compare very closely for  $Z_i$  being either the upper or lower detector level.

The average  $m$  for each set of data was determined, and the average  $\Pr(Z_i, Z_j; Z_i)$  for each set of data was defined as

$$\overline{\Pr}(Z_i, Z_j; Z_i) = (\overline{m}-2)/\overline{m} . \quad (27)$$

A least squares analysis was used to fit the analytical expression  $\Pr(Z_i, Z_j; Z_i) = 1 - e^{-\beta(Z_j-Z_i)}$  to the experimental data,  $\overline{\Pr}(Z_i, Z_j; Z_i)$ . The following method was used.

Since the probability of transmission is given by

$$\Pr(Z_i, Z_j; Z_j) = e^{-\beta(Z_j - Z_i)},$$

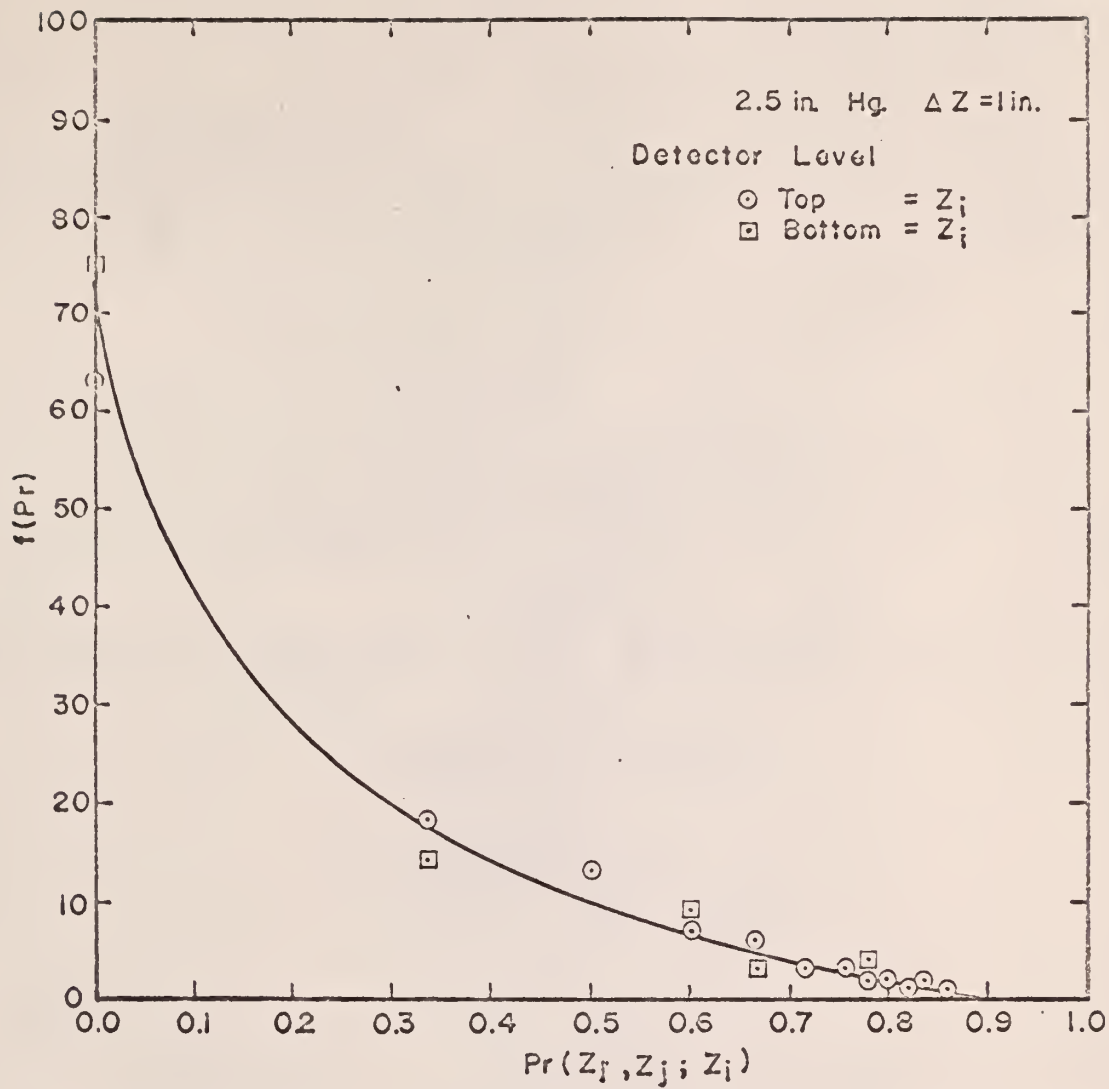


Figure 76. Frequency Distribution of the Reflectivity Data, Data Set No. 4.

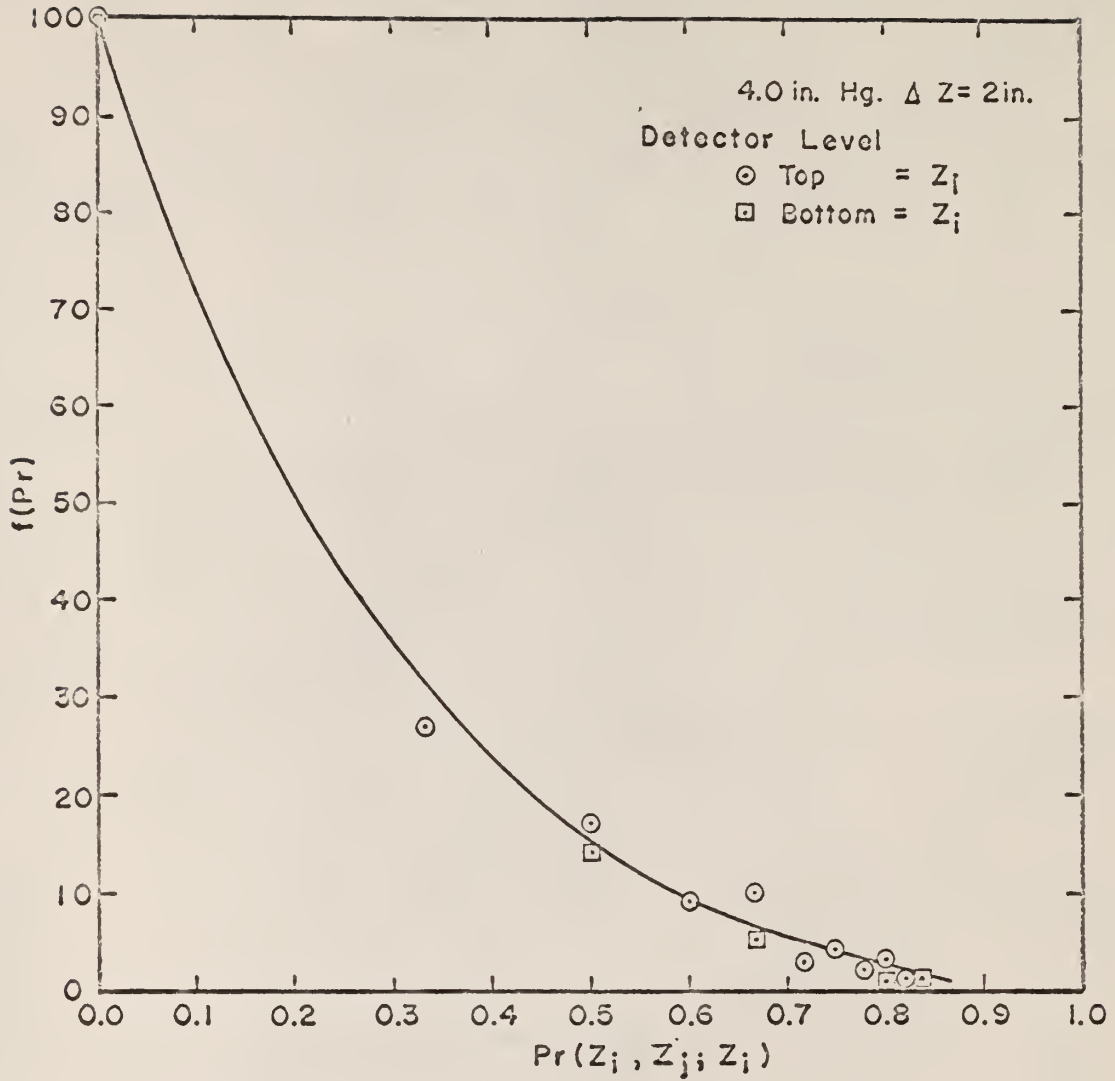


Figure 77. Frequency Distribution of the Reflectivity Data, Data Set No. 23.

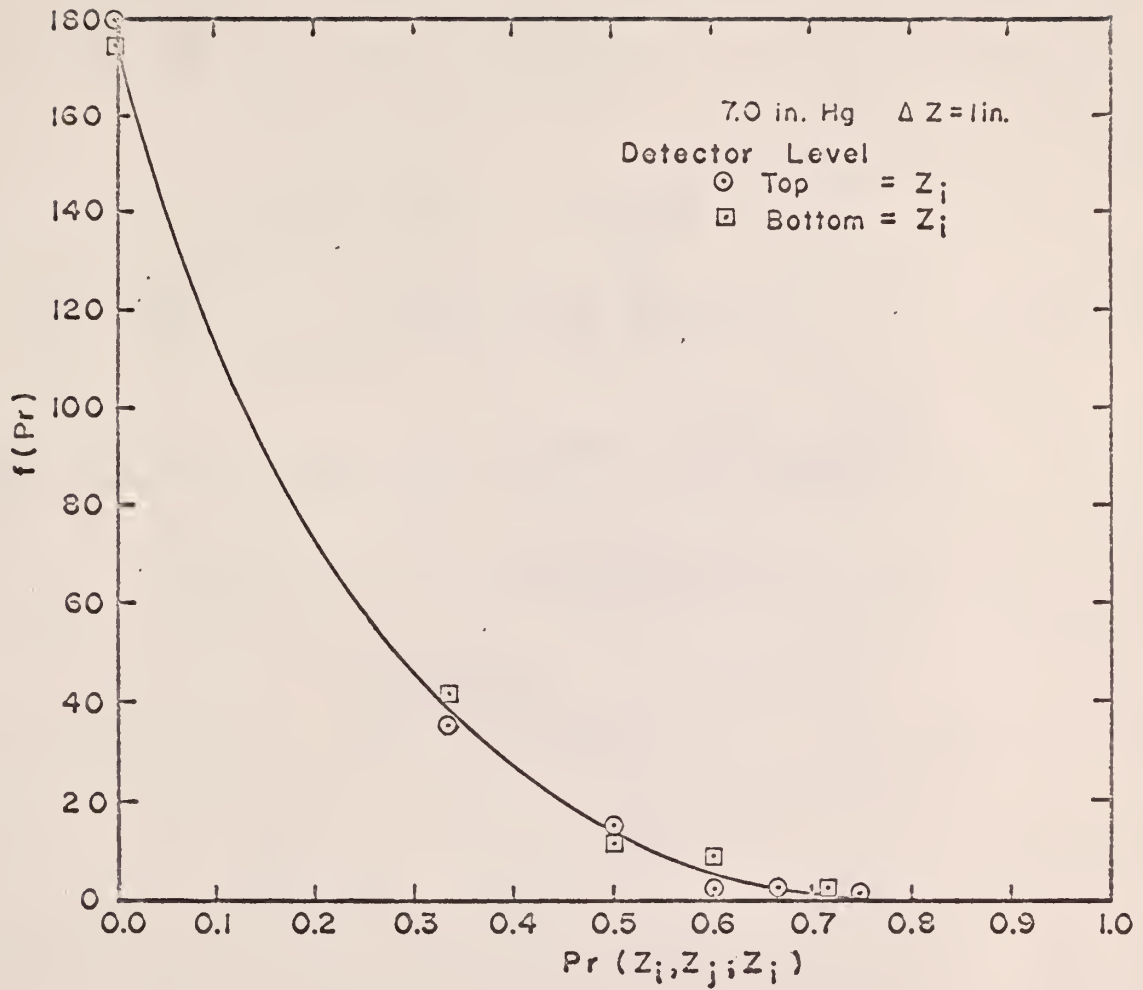


Figure 78. Frequency Distribution of the Reflectivity Data, Data Set No. 48.

the average probability of transmission determined from the experimental data is

$$\overline{\text{Pr}}(Z_i, Z_j; Z_j) = 1 - \overline{\text{Pr}}(Z_i, Z_j; Z_i) . \quad (28)$$

To simplify the nomenclature, let

$$\overline{\text{Pr}}(Z_i, Z_j; Z_j) \equiv \overline{\text{Pr}} . \quad (29)$$

For each water flow rate, the difference between experiment and correlation for each data value was computed. Forming the sum of the squares of the deviations gives a measure of how well data values fit an analytical expression as a whole. Therefore, the sum of the squares of the deviations of the experiment from correlation for each water flow rate is

$$\sum_{\text{all data}} \sum_{k=1} \left[ e^{-\beta(Z_k - Z_i)} - \overline{\text{Pr}}_k \right]^2 , \quad (30)$$

or

$$\sum_k \left[ -\beta \Delta Z_k - \ln \overline{\text{Pr}}_k \right]^2 . \quad (31)$$

The parameter  $\beta$  should be chosen so as to minimize the sum of the squares of the deviations. To do this,

$$\frac{d}{d\beta} \left[ \sum_k (-\beta \Delta Z_k - \ln \overline{\text{Pr}}_k)^2 \right] = 0 . \quad (32)$$

Solving for the best estimate of  $\beta$  gives

$$\beta \sum_k \Delta Z_k^2 + \sum_k \Delta Z_k \ln \bar{Pr}_k = 0 ,$$

$$\beta = \frac{- \sum_k \Delta Z_k \ln \bar{Pr}_k}{\sum_k \Delta Z_k^2} . \quad (33)$$

Figure 79 presents the average reflectivity data as a function of the distance between detector levels and water flow rate, along with the theoretical curves determined from the least squares analysis of the data to determine the best estimate of  $\beta$ . The lower detector level was  $Z_1$ .

Figure 80 presents the theoretical reflectivity curves normalized to the reflectivity at the top of the fluidized bed as a function of the distance from the bottom of the fluidized bed for a particle initially passing the lower detector level.

Table 5 presents the values of  $\beta$  determined from the least squares analysis of the reflectivity data for the water flow rates studied.

Table 5. Reflection Coefficient determined from the least squares analysis of the reflectivity data.

WATER FLOW RATE	$\beta$
B <sub>1</sub> (13.5 gal/min.)	0.300/in.
B <sub>2</sub> (17.0 gal/min.)	0.125/in.
B <sub>3</sub> (18.8 gal/min.)	0.087/in.
B <sub>4</sub> (22.3 gal/min.)	0.088/in.
B <sub>5</sub> (24.0 gal/min.)	0.100/in.

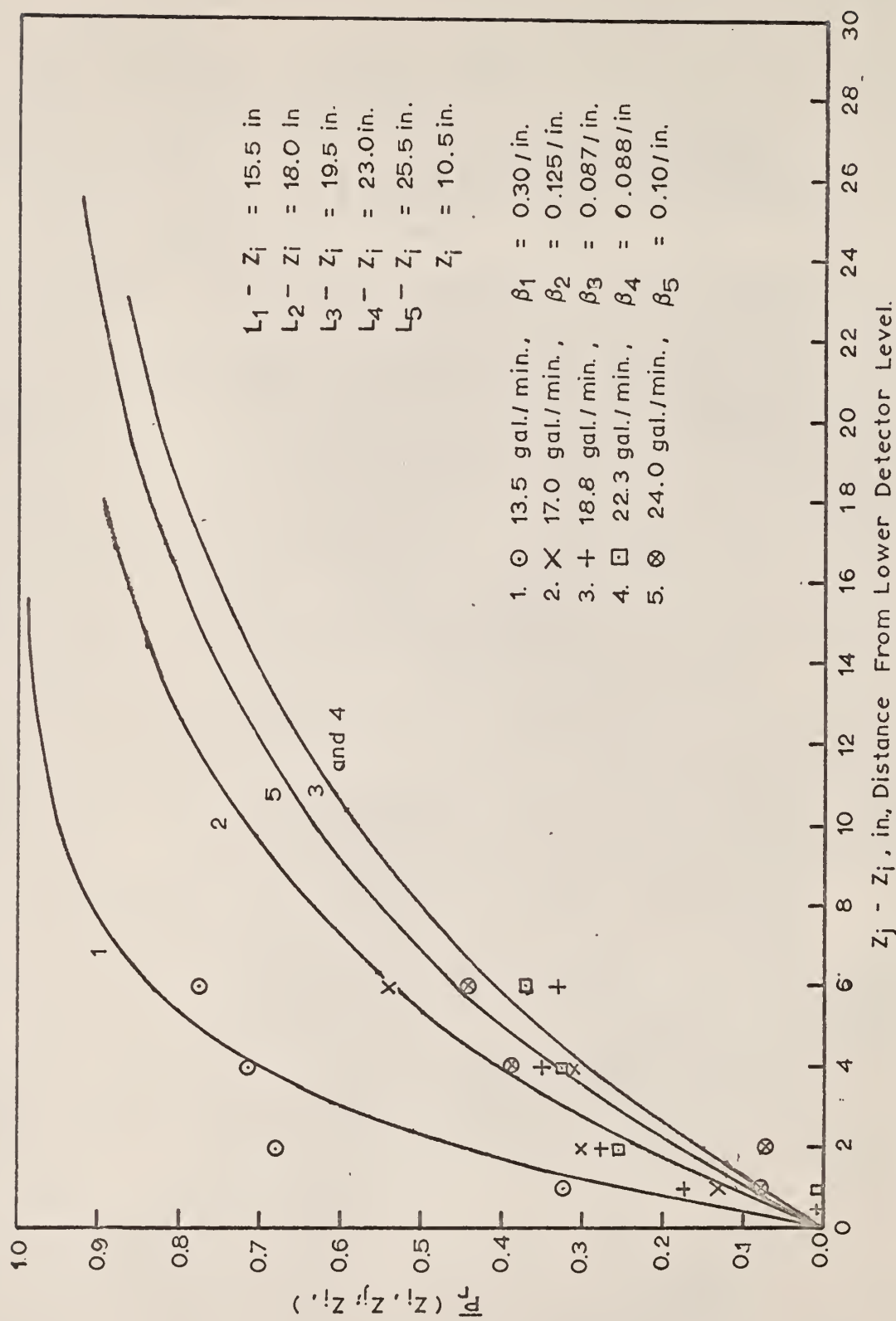


Figure 79. Average Reflectivity as a Function of Water Flow Rate and Distance Above Lower Detector Level.

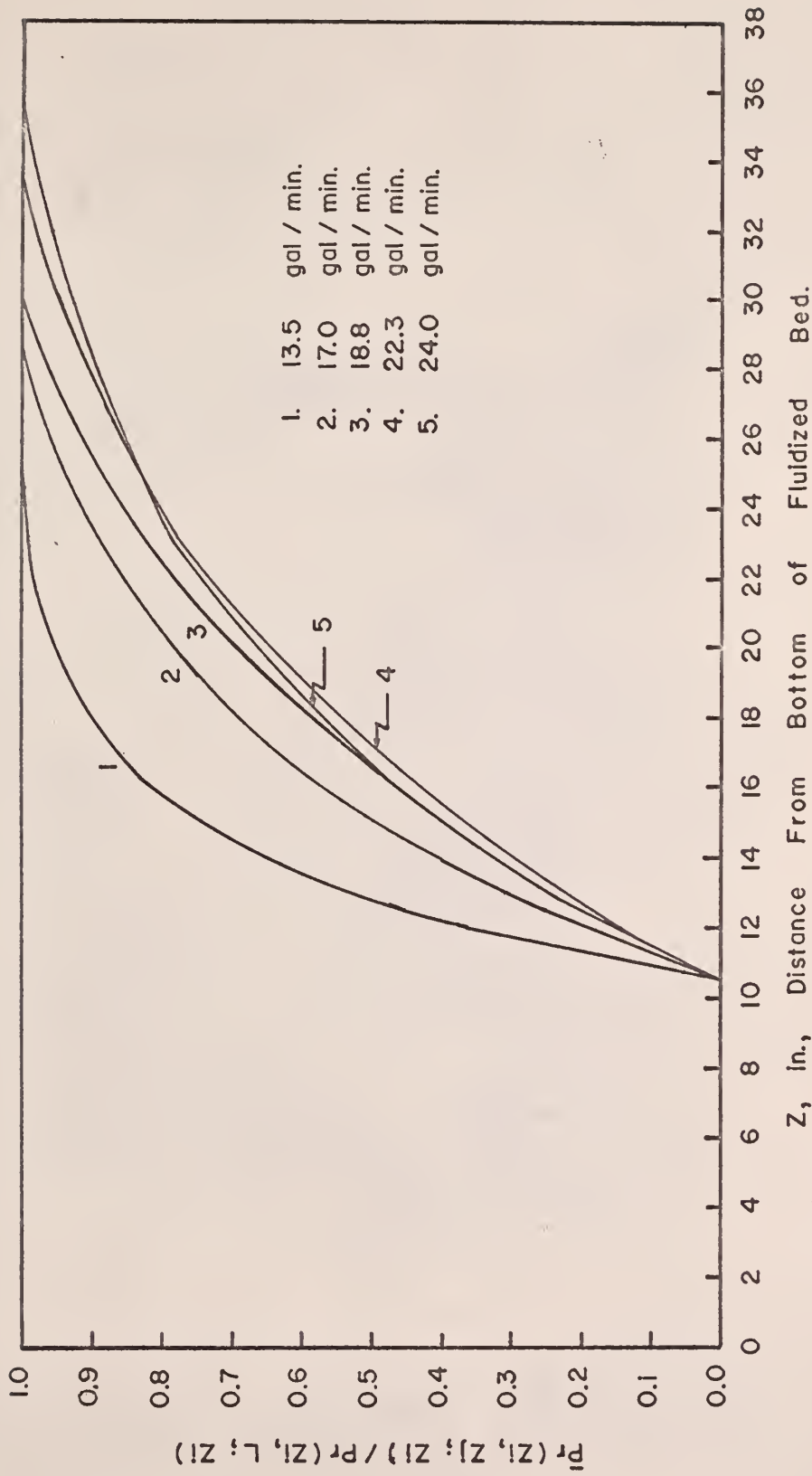


Figure 80. Ratio of Computed Reflectivity to Reflectivity at Top of Fluidized Bed as a Function of the Distance From the Bottom of the Fluidized Bed for a Particle Initially Passing the Lower Detector Level.

## 4.6 Analysis of the Particle Concentrations

### 4.6.1 Theoretical Development

A knowledge of the concentration of particles with respect to time and position for the given source condition and boundary conditions is of particular interest in the study of fluidized beds. If the assumption is made that the concentration of particles can be represented by a solution of the diffusion equation applying the source and boundary conditions of the fluidized bed, a dispersion coefficient based upon the experimental data can be obtained.

The diffusion equation for no absorption may be written

$$E \nabla^2 C + Q = \partial C / \partial t, \quad (34)$$

$$\left( \begin{array}{l} - \text{Leakage} + \text{Source} \\ \text{Particle Density} \end{array} \right) = \text{Time rate of change of}$$

where  $E$  is the diffusion coefficient. When the diffusion is one-dimensional this reduces to

$$E_z \frac{\partial^2 C}{\partial Z^2} + Q = \partial C / \partial t, \quad (35)$$

where  $E_z$  is defined as the dispersion coefficient. The  $Z$ -dependent diffusion equation must be solved subject to the following boundary conditions and source:

$$\left. \frac{\partial C}{\partial Z} \right|_{Z=L} = 0, \quad (36)$$

$$\left. \frac{\partial C}{\partial z} \right|_{z=0} = 0, \quad (37)$$

$$C_{t=0} = 0, \quad (38)$$

at  $t=0$ ,  $Q$  particles per  $\text{in}^2$  are injected at  $z = z_0$ ,  $= Q \delta(z-z_0) \delta(t)$

The method used to solve the diffusion equation for the given source and boundary conditions is outlined as follows:

Taking the Laplace transform with respect to time, Equation 35 gives

$$E_z \frac{d^2 \bar{C}}{dz^2} - s \bar{C} = -Q \delta(z-z_0). \quad (39)$$

Letting

$$\frac{s}{E_z} = \lambda^2, \quad (40)$$

and substituting Equation 40 into Equation 39 gives

$$\frac{d^2 \bar{C}}{dz^2} - \lambda^2 \bar{C} = -\frac{Q}{E_z} \delta(z-z_0). \quad (41)$$

Taking the Laplace transform of Equation 41 with respect to Z yields

$$p^2 \bar{c} - p\bar{c}(0) - \bar{c}'(0) - \lambda^2 \bar{c} = - \frac{Q}{E_z} e^{-pZ_0} . \quad (42)$$

Applying Equation 36, and solving  $\bar{c}$  gives Equation 43.

$$\bar{c} = \frac{p\bar{c}(0)}{p^2 - \lambda^2} - \frac{Q e^{-pZ_0}}{E_z(p^2 - \lambda^2)} . \quad (43)$$

The first term on the right-hand side of Equation 43 represents the homogeneous or steady-state term. The homogeneous solution of Equation 43 is given by Equation 44.

$$\bar{c} = A e^{\lambda Z} + B e^{-\lambda Z} . \quad (44)$$

The inverse Laplace transform of the second term on the right-hand side of Equation 43 is determined by utilizing the Second Shifting Theorem (12). Any function  $f(x-a)$  multiplied by  $H(x-a)$  has the value of zero for  $x < a$  and  $f(x-a)$  for  $x > a$ . The Second Shifting Theorem is

$$\mathcal{L}^{-1} \left[ e^{-as} \bar{f}(s) \right] = f(x-a) H(x-a), \quad (45)$$

where  $H(x-a)$  is the unit step function defined above. Applying this theorem, one has

$$\mathcal{L}^{-1} \left[ \frac{Q e^{-pZ_0}}{E_z(p^2 - \lambda^2)} \right] = \frac{Q}{E_z} \mathcal{L}^{-1} \left[ \frac{1}{p^2 - \lambda^2} \right] H(Z - Z_0) . \quad (46)$$

The inverse Laplace transform of  $1/(p^2 - \lambda^2)$  with the argument  $(Z - Z_0)$  is given by Equation 47.

$$\mathcal{L}^{-1} \left[ \frac{1}{p^2 - \lambda^2} \right] = \frac{\sinh \lambda(Z - Z_0)}{\lambda} . \quad (47)$$

Substituting Equation 47 into Equation 46 gives

$$\mathcal{L}^{-1} \left[ \frac{Q e^{-pZ_0}}{E_z(p^2 - \lambda^2)} \right] = \frac{Q}{\lambda E_z} \sinh \lambda(Z - Z_0) H(Z - Z_0) . \quad (48)$$

Noting the identity

$$\sinh \lambda(Z - Z_0) = \frac{e^{\lambda(Z - Z_0)} - e^{-\lambda(Z - Z_0)}}{2} ,$$

and substituting into Equation 48 one can obtain

$$\mathcal{L}^{-1} \left[ \frac{Q e^{-pZ_0}}{E_z(p^2 - \lambda^2)} \right] = \frac{Q}{2\lambda E_z} \left[ e^{\lambda(Z - Z_0)} - e^{-\lambda(Z - Z_0)} \right] H(Z - Z_0) . \quad (49)$$

For  $Z > Z_0$ , only the second term of Equation 49 is applicable, since the concentration of particles beyond the fluidized bed height ( $L$ ) is zero. Equation 50 below represents the solution of the second term in Equation 43 for  $Z > Z_0$ .

$$\mathcal{L}^{-1} \left[ \frac{Q e^{-pZ_0}}{E_z(p^2 - \lambda^2)} \right] = - \frac{Q}{2\lambda E_z} e^{-\lambda(Z - Z_0)} H(Z - Z_0) . \quad (50)$$

Since the particles injected at  $Z_0$  will also move downward, the solution of the second term of Equation 43 must also account for the downward movement. The solution is the same as for  $Z > Z_0$ . The equation applicable is, therefore, Equation 50, except the  $Z_0$  and  $Z$  are interchanged in the exponential function, and the unit step function  $H(Z-Z_0)$  is changed to  $H(Z_0-Z)$  for its proper operation when  $Z < Z_0$ . Equation 51 below is the result.

$$\mathcal{L}^{-1} \left[ \frac{q e^{-pZ_0}}{E_z(p^2 - \lambda^2)} \right] = - \frac{q}{2\lambda E_z} e^{-\lambda(Z_0-Z)} H(Z_0-Z). \quad (51)$$

The general solution for  $\bar{C}$  is the sum of Equations 44, 50, and 51.

$$\bar{C} = A e^{\lambda Z} + B e^{-\lambda Z} + \frac{q}{2\lambda E_z} \left[ e^{-\lambda(Z-Z_0)} H(Z-Z_0) + e^{-\lambda(Z_0-Z)} H(Z_0-Z) \right]. \quad (52)$$

If  $(Z-Z_0)$  is changed to the magnitude of  $Z-Z_0$  in Equation 52, the operators  $H(Z-Z_0)$  and  $H(Z_0-Z)$  may be removed, giving Equation 53.

$$\bar{C} = A e^{\lambda Z} + B e^{-\lambda Z} + \frac{q}{2\lambda E_z} e^{-\lambda|Z-Z_0|}. \quad (53)$$

The constants, A and B, are determined by applying the boundary conditions given in Equations 36 and 37 as follows:

$$\left[ \frac{d\bar{C}}{dZ} \right]_L = A\lambda e^{\lambda L} - B\lambda e^{-\lambda L} - \frac{q}{2E_z} e^{-\lambda|L-Z_0|} = 0. \quad (54)$$

$$\left[ \frac{d\bar{C}}{dZ} \right]_0 = A\lambda - B\lambda + \frac{q}{2E_z} e^{-\lambda Z_0} = 0. \quad (55)$$

Solving Equations 54 and 55 for A and B, one obtains

$$A = \frac{\begin{vmatrix} \frac{Q}{2E_z} e^{-\lambda(L-Z_0)} & -\lambda e^{-\lambda L} \\ -\frac{Q}{2E_z} e^{-\lambda Z_0} & -\lambda \end{vmatrix}}{\begin{vmatrix} \lambda e^{\lambda L} & -\lambda e^{-\lambda L} \\ \lambda & -\lambda \end{vmatrix}} \quad (56)$$

Expanding the determinants in Equation 56 gives

$$A = \frac{\frac{\lambda Q}{2E_z} \left[ e^{-\lambda(L-Z_0)} + e^{-\lambda(L+Z_0)} \right]}{\lambda^2 (e^{\lambda L} - e^{-\lambda L})} \quad (57)$$

Factoring  $e^{-\lambda L}$  in the numerator of Equation 57, and applying the following identities,

$$\cosh \lambda Z_0 = \frac{e^{\lambda Z_0} + e^{-\lambda Z_0}}{2} \quad (58)$$

$$\sinh \lambda L = \frac{e^{\lambda L} - e^{-\lambda L}}{2},$$

one obtains

$$A = \frac{Q e^{-\lambda L} \cosh \lambda Z_0}{2E_z \lambda \sinh \lambda L} \quad (59)$$

$$B = \frac{\begin{vmatrix} \lambda e^{\lambda L} & -\frac{Q}{2E_z} e^{-\lambda(L-Z_0)} \\ \lambda & \frac{Q}{2E_z} e^{-\lambda Z_0} \end{vmatrix}}{2\lambda^2 \sinh \lambda L} \quad (60)$$

Expanding the determinant in Equation 60, and applying Equation 58 give

$$B = \frac{Q \cosh \lambda (L-Z_0)}{2E_z \lambda \sinh \lambda L} \quad (61)$$

To obtain the final solution for the particle concentrations,  $C$ , the inverse Laplace transformation of Equation 53 must be performed. To do this, Equation 53 is separated into the sum of the complementary and particular parts as,

$$\bar{C} = \bar{C}_{\text{comp}} + \bar{C}_p \quad (62)$$

where

$$\bar{C}_{\text{comp}} = \frac{Q}{2E_z} \left[ \frac{e^{-\lambda(L-Z)} \cosh \lambda Z_0 + e^{-\lambda Z} \cosh \lambda (L-Z_0)}{\lambda \sinh \lambda L} \right], \quad (63)$$

and

$$\bar{C}_p = \frac{Q}{2\lambda E_z} e^{-\lambda(Z-Z_0)} \quad (64)$$

For the complementary part, note that there are poles at  $\lambda = 0$  and  $\frac{n\pi i}{L}$ . The inverse Laplace transform for the case of simple poles is given by the sum of the residues (12). Thus,

$$f(t) = \sum_{k=1}^n \lim_{s \rightarrow a_k} (s - a_k) \bar{f}(s) e^{st} . \quad (65)$$

The relation of  $(s)$  to  $\lambda$  is given by Equation 40, but, for simplicity,  $\lambda$  will still be used in the equations. Operating on Equation 63 as indicated in Equation 65 produces the indeterminate form  $0/0$  for  $\lambda = 0$  and  $\frac{n\pi i}{L}$ , where

$$\bar{f}(s) = \frac{e^{-\lambda(L-Z)} \cosh \lambda Z_0 + e^{-\lambda Z} \cosh \lambda(L-Z_0)}{\lambda \sinh \lambda L} . \quad (66)$$

The application of L'Hospital's rule will produce a solution. Let

$$\bar{f}(s) = \frac{N(s)}{D(s)} , \quad (67)$$

where

$$N(s) = e^{-\lambda(L-Z)} \cosh \lambda Z_0 + e^{-\lambda Z} \cosh \lambda(L-Z_0) , \quad (68)$$

and

$$D(s) = \lambda \sinh \lambda L . \quad (69)$$

Equation 65 becomes

$$f(t) = \sum_{k=1}^n \lim_{s \rightarrow a_k} (s - a_k) \frac{N(s)}{D(s)} e^{st} . \quad (70)$$

Differentiating the numerator and denominator of  $(s-a_k) \frac{N(s)}{D(s)}$  with respect to  $s$  gives

$$\frac{d}{ds}(s-a_k)N(s) / \frac{d}{ds} D(s) = \frac{N(s) + (s-a_k)N'(s)}{D'(s)} . \quad (71)$$

Therefore, Equation 70 becomes

$$f(t) = \sum_{k=1}^n \lim_{s \rightarrow a_k} \left[ \frac{N(s) + (s-a_k)N'(s)}{D'(s)} \right] e^{st} , \quad (72)$$

where

$$D'(s) = \frac{d\lambda}{ds} \frac{d}{d\lambda} (\lambda \sinh \lambda L) . \quad (73)$$

From Equation 40,

$$\frac{d\lambda}{ds} = \frac{1}{2\lambda E_z} . \quad (74)$$

Therefore, Equation 73 becomes

$$D'(s) = \frac{1}{2\lambda E_z} (\sinh \lambda L + \lambda L \cosh \lambda L) . \quad (75)$$

The residues at  $\lambda = 0$  and  $\frac{n\pi i}{L}$  are given by utilizing Equations 63, 68, and 75 in Equation 72.

At  $\lambda=0$ ,

$$C_{\text{comp}} \Big|_{\lambda=0} = \frac{Q}{E_z} \left[ \frac{2E_z}{\frac{\sinh \lambda L}{\lambda} + L \cosh \lambda L} \right] = \frac{Q}{L}, \quad (76)$$

where

$$\frac{\sinh \lambda L}{\lambda} \Big|_{\lambda=0} = \frac{\frac{d}{d\lambda} \sinh \lambda L}{\frac{d}{d\lambda} \lambda} = L \cosh \lambda L = L.$$

At  $\lambda = \frac{n\pi i}{L}$ ,

$$C_{\text{comp}} \Big|_{\lambda = \frac{n\pi i}{L}} = \frac{Q}{2E_z} \sum_{n=1}^{\infty} \left[ \frac{e^{-\frac{n\pi i}{L}(L-Z)} \cos \frac{n\pi Z_0}{L}}{\frac{1}{2E_z} \left[ \frac{\sinh n\pi i}{n\pi i} + L \cos n\pi \right]} \right]$$

$$+ \frac{e^{-\frac{n\pi i}{L} Z} \cos n\pi \left(1 - \frac{Z_0}{L}\right)}{\frac{1}{2E_z} \left[ \frac{\sinh n\pi i}{n\pi i} + L \cos n\pi \right]} \Big] e^{-\frac{n^2 \pi^2 t}{L^2}} E_z,$$

(77)

where

$$\cosh \frac{n\pi i}{L} = \cos \frac{n\pi}{L}.$$

Noting that

$$\sinh n\pi i = i \sin n\pi = 0 ,$$

Equation 77 becomes

$$C_{\text{comp}} \Big|_{\lambda = \frac{n\pi i}{L}} = \frac{Q}{L} \sum_{n=1}^{\infty} \left[ \frac{e^{-\frac{n\pi i(L-Z)}{L}} \cos \frac{n\pi Z_0}{L}}{\cos n\pi} + \frac{e^{-\frac{n\pi i}{L} Z} \cos n\pi(1 - \frac{Z_0}{L})}{\cos n\pi} \right] e^{-\frac{n^2 \pi^2 t}{L^2}} E_z \quad (78)$$

Substituting the identities

$$\cos n\pi(1-x) = \cos n\pi \cos n\pi x , \quad (79)$$

and

$$e^{i\theta} = \cos \theta + i \sin \theta \quad (80)$$

into Equation 78 gives

$$C_{\text{comp}} \Big|_{\lambda = \frac{n\pi i}{L}} = \frac{2Q}{L} \sum_{n=1}^{\infty} \cos \frac{n\pi Z_0}{L} \cos \frac{n\pi Z}{L} e^{-\frac{n^2 \pi^2 t}{L^2}} E_z . \quad (81)$$

The inverse Laplace transform of the particular part, Equation 64, obtained from a table of Laplace transforms, is given in the following equation:

$$C_p = \frac{Q}{2(E_z \pi t)^{\frac{1}{2}}} e^{-\frac{(z-z_0)^2}{4E_z t}} \quad (82)$$

The complete solution for C becomes

$$C = \sum C_{\text{comp}} + C_p \quad (83)$$

Defining the following dimensionless variables,

$$\begin{aligned} x &= \frac{z}{L} \quad , \\ x_0 &= \frac{z_0}{L} \quad , \\ \tau &= \frac{t E_z}{L^2} \quad , \end{aligned} \quad (84)$$

and substituting them into Equations 76, 81, 82, and 83, and rearranging, one obtains

$$\frac{C L}{Q} = 1 + 2 \sum_{n=1}^{\infty} e^{-n^2 \pi^2 \tau} \cos(n \pi x) \cos(n \pi x_0) + \frac{e^{-\frac{(x-x_0)^2}{4\tau}}}{2(\pi \tau)^{\frac{1}{2}}} \quad (85)$$

The equilibrium concentration obtained a long period of time after introduction of the quantity of tracer Q is

$$\frac{Q}{L} = C_{\infty} \quad , \quad (86)$$

or

$$\frac{C}{C_{\infty}} = \frac{C I}{Q} \cdot \quad (87)$$

#### 4.6.2 Analysis of Experimental Results

The concentration of tagged particles,  $C$ , is assumed to be proportional to the number of times that a tagged particle passes a horizontal plane per unit time,  $I$ , after it has been introduced into the fluidized bed. Since  $C$  is assumed proportional to  $I$ ,

$$\frac{C}{C_{\infty}} = \frac{I}{I_{\infty}} \cdot \quad (88)$$

The data obtained from a single radioactive particle were used to determine the concentration due to  $Q$  particles being injected at one time. A tagged particle is considered to be injected into the fluidized bed at a detector level every time the tagged particle is detected at that detector level. Each time a tagged particle passed one detector level a

time scale was started, and, every time it passed the other detector level, the time was recorded. This was done for a finite length of time. These data were used to obtain the number of times a particle passed a detector level per unit time as a function of the time since it was first detected at a detector level. Summing  $Q$  such occurrences in the set of data will result in the same distribution as injecting  $Q$  particles at a detector level at the same instant.

Figure 81 illustrates a modified dual channel recorder trace for a typical set of data. The minus sign represents the pulses obtained from the lower detector level, and the plus sign represents the pulses from the upper detector level. The particle concentration data,  $I$ , is obtained as described previously. The time span,  $W$ , in Fig. 81, is chosen of great enough length to obtain the equilibrium concentration,  $I_{\infty}$ . The time span,  $W$ , is then divided into  $q$  increments of time  $\Delta t$ , giving

$$\sum_{i=1}^q \Delta t_i = W .$$

The time increments do not necessarily have to be equal.

The time span,  $W$ , is begun initially with the first pulse in the data set, which may be either positive or negative. The number of positive or negative pulses within each time increment  $\Delta t$  are recorded until the time  $W$  is reached. At this point the time span  $W$  is then initialized at the next pulse in the data set, which may be either positive or negative, and the number of positive or negative pulses within each time increment  $\Delta t$  are recorded until the time  $W$  is reached. This stepping-ahead from pulse-to-pulse procedure in initializing the time span  $W$  is continued until the last data pulse in the data set falls within the last time increment  $\Delta t$  at the time  $W$  from the initialized pulse.

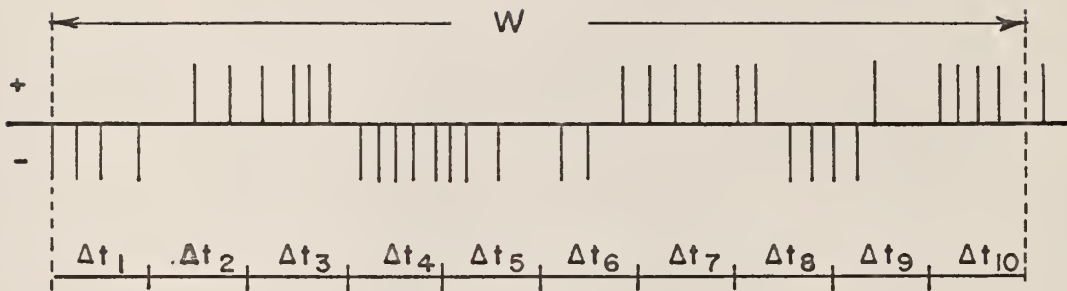


Figure 81. Modified Two-Channel Recorder Output Trace.

By this method, four sets of frequency distributions are obtained. The number of occurrences of the radioactive source being detected at the upper (or lower) detector level per unit time at the time  $t$ , initially being detected at the lower (or upper) detector level yield the frequency distributions  $I(Z_1, Z_2, t)$  and  $I(Z_2, Z_1, t)$ . Also, the number of occurrences of the radioactive source being detected at the upper (or lower) detector level per unit time at the time  $t$ , initially being detected at the upper (or lower) detector level yield the frequency distributions  $I(Z_2, Z_2, t)$  and  $I(Z_1, Z_1, t)$ .

Figures 82 through 85 represent examples of the particle concentration frequency distributions obtained from the experimental data. Computer Program No. 4, explained in Appendix D, was used to obtain the experimental particle concentrations.

An attempt was made to determine the diffusion coefficient,  $E_z$ , for each water flow rate by two methods of applying a least squares analysis to the experimental particle concentration data. The first method produced dispersion coefficients for each water flow rate, but the second method was unsuccessful. An attempt to explain the reason for lack of success in determining dispersion coefficients by the second method will be given in Section 5.4. An explanation of each method will first be given.

Method 1. The first method minimized the sum of the squares of the errors in the time corresponding to the maximum experimental  $I/I_\infty$  for five distances between detector levels for a given water flow rate.

The maximum value for the correlated  $C/C_\infty$  occurs at the time corresponding to

$$\frac{\partial (C/C_\infty)}{\partial t} = 0 \quad . \quad (89)$$

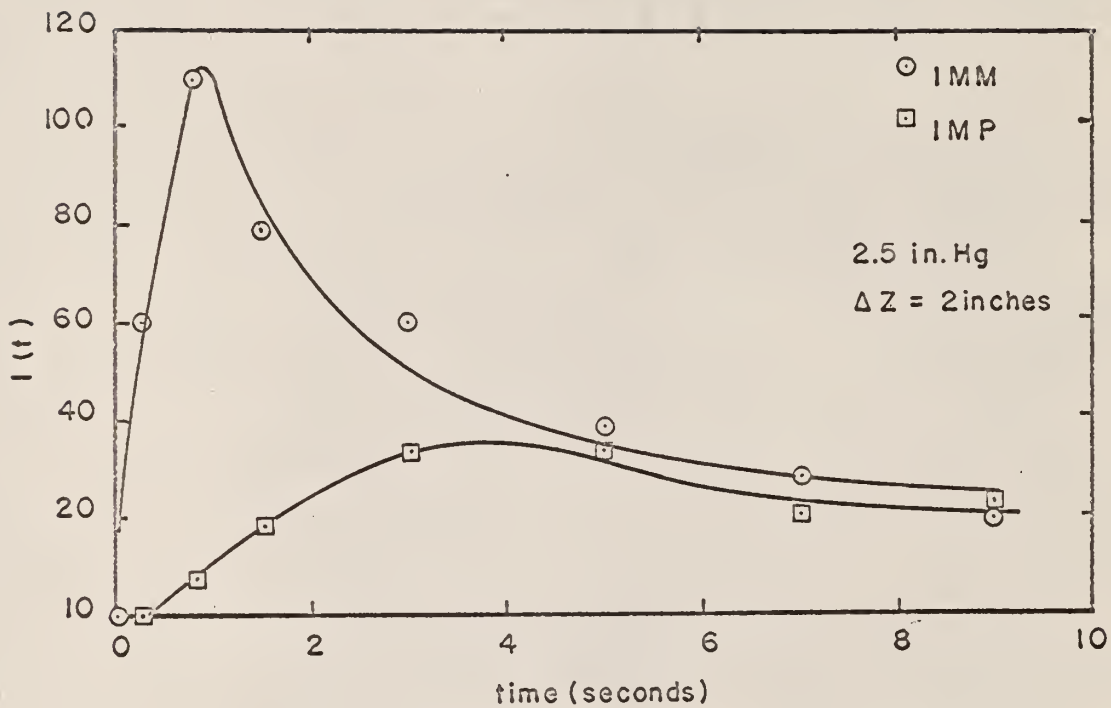


Figure 82. Particle Concentration Data, at Flow Rate  $B_1$ , Particles Initially at Lower Detector Level.

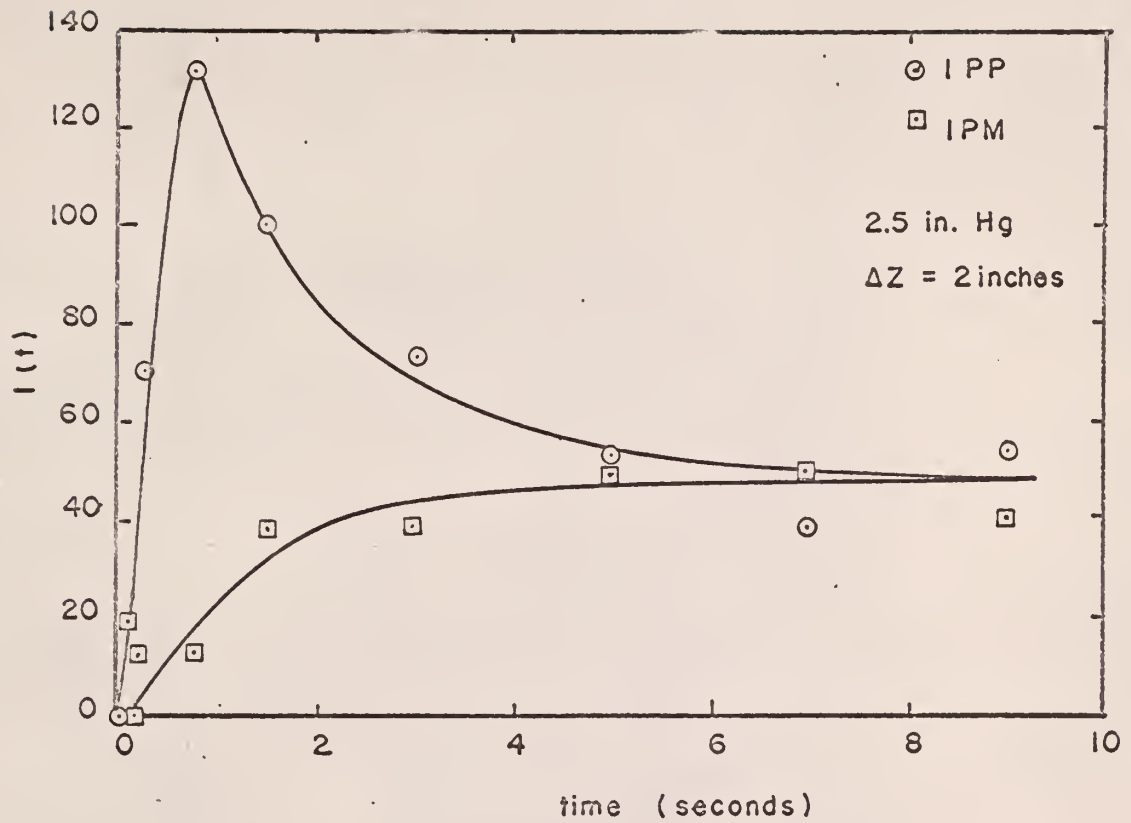


Figure 83. Particle Concentration Data, at Flow Rate  $B_1$ , Particles Initially at Upper Detector Level.

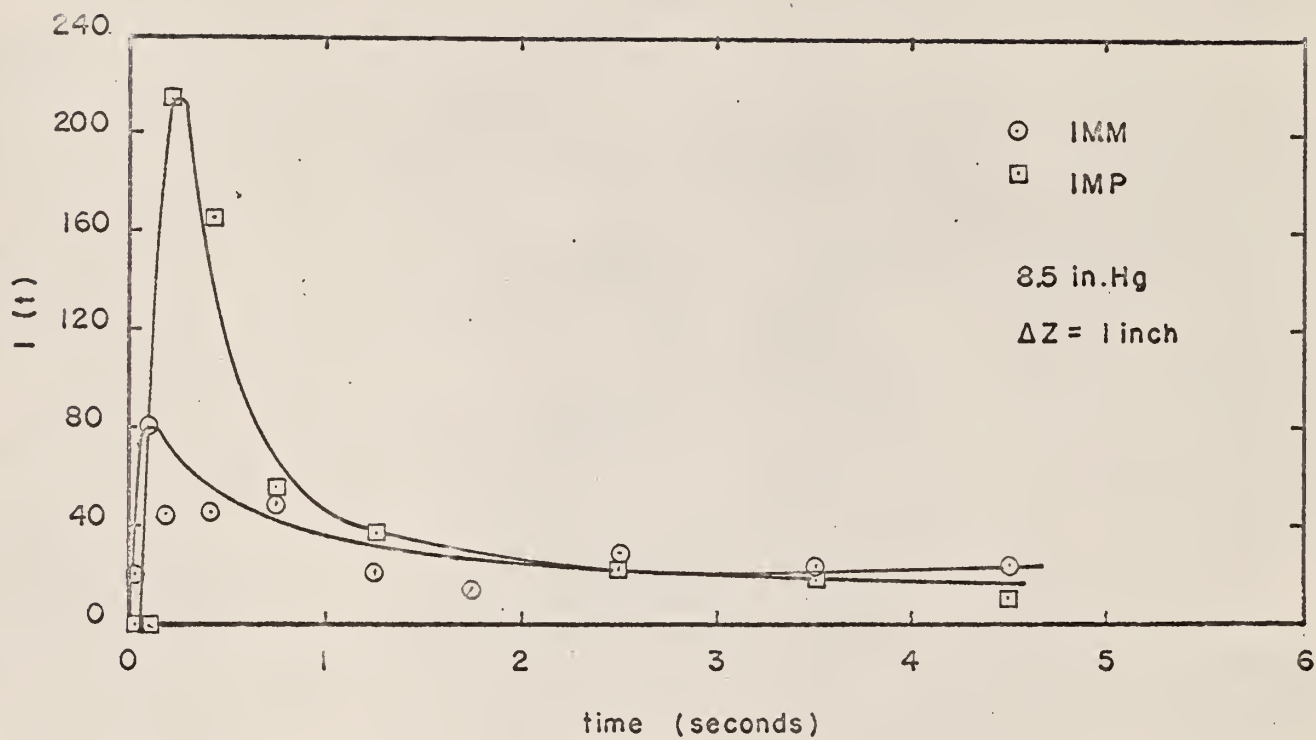


Figure 84. Particle Concentration Data, at Flow Rate  $B_5$ , Particles Initially at Lower Detector Level.

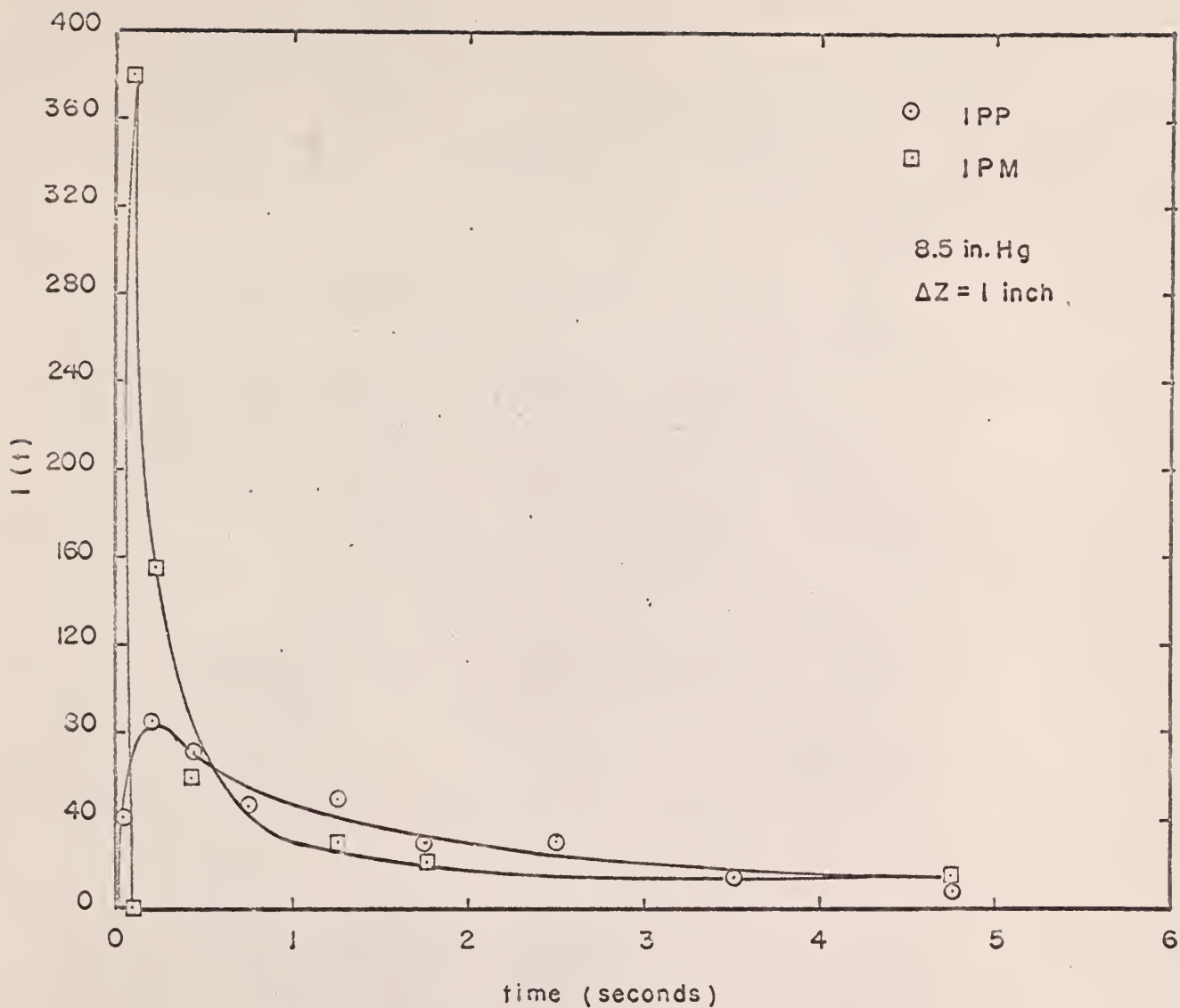


Figure 85. Particle Concentration Data, at Flow Rate B5, Particles Initially at Upper Detector Level.

Therefore, from Equation 85, one has

$$\frac{(C/C_\infty)-1}{2} = \sum_{n=1}^{\infty} e^{-n^2 \pi^2 \tau} \cos(n\pi x) \cos(n\pi x_0) + \frac{1}{4(\pi\tau)^{1/2}} e^{-(x-x_0)^2/4\tau} \quad (90)$$

Differentiating with respect to time gives

$$\frac{\partial \left[ \frac{(C/C_\infty)-1}{2} \right]}{\partial t} = 0 = \sum_{n=1}^{\infty} \left[ \frac{-n^2 \pi^2 E_z}{L^2} \right] \cos(n\pi x) \cos(n\pi x_0) e^{-n^2 \pi^2 \tau} - \frac{L e^{-(x-x_0)^2/4\tau}}{8\pi^{1/2} E_z^{1/2} t^{3/2}} + \frac{L^3 (x-x_0)^2 e^{-(x-x_0)^2/4\tau}}{16\pi^{1/2} E_z^{3/2} t^{5/2}} \quad (91)$$

Solving for the time corresponding to  $(C/C_\infty)_{\max}$ , one obtains

$$t = \frac{(2E_z)^{-1} (\Delta Z)^2}{\left[ \frac{8\pi^{5/2} (\Delta Z)^2/4 E_z t}{L^3 (E_z t)^{-3/2}} \right] \sum_{n=1}^{\infty} n^2 \cos(n\pi x) \cos(n\pi x_0) e^{-n^2 \pi^2 \tau} + 1} \quad (92)$$

where

$$\Delta Z = (x-x_0)L \quad (93)$$

For a given flow rate of water and five distances between detector levels,

$\Delta Z$ , one has

$$\sum_{m=1}^5 \frac{\partial \tau_m}{\partial E_Z} \frac{\partial [t_m - (t_{\text{exp}})_m]^2}{\partial \tau_m} = 0, \quad (94)$$

where  $(t_{\text{exp}})_m$  is the time corresponding to  $(I/I_{\infty})_{\text{max}}$ .

The particle concentration frequency distributions obtained from considering the source plane at the lower detector level,  $I(Z_1, Z_2, t)$ , for all data sets were normalized and combined for each distance between detector levels and water flow rate, and are shown in Figs. 86 through 90. The experimental values,  $(t_{\text{exp}})_m$  were obtained from these figures. Thus,

$$\frac{\partial}{\partial \tau_m} [t_m - (t_{\text{exp}})_m]^2 = 2 [t_m - (t_{\text{exp}})_m] \frac{\partial t_m}{\partial \tau_m}, \quad (95)$$

where

$$\begin{aligned} \frac{\partial t_m}{\partial \tau_m} = & \frac{(\Delta Z)_m^2}{2E_Z} \left[ \frac{2e^{(x-x_0)_m^2/4\tau_m}}{\pi^{-5/2} \tau_m^{1/2} (x-x_0)_m^2} \sum_{n=1}^{\infty} n^2 \cos(n\pi x_m) \cos(n\pi x_0) e^{-n^2 \pi^2 \tau_m} \right. \\ & + \frac{8e^{(x-x_0)_m^2/4\tau_m}}{\pi^{-9/2} \tau_m^{-3/2}} \sum_{n=1}^{\infty} n^4 \cos(n\pi x_m) \cos(n\pi x_0) e^{-n^2 \pi^2 \tau_m} \\ & \left. - \frac{12e^{(x-x_0)_m^2/4\tau_m}}{\pi^{-5/2} \tau_m^{-1/2}} \sum_{n=1}^{\infty} n^2 \cos(n\pi x_m) \cos(n\pi x_0) e^{-n^2 \pi^2 \tau_m} \right] \\ & \left[ \frac{8e^{(x-x_0)_m^2/4\tau_m}}{\pi^{-5/2} \tau_m^{-3/2}} \sum_{n=1}^{\infty} n^2 \cos(n\pi x_m) \cos(n\pi x_0) e^{-n^2 \pi^2 \tau_m} + 1 \right]^{-2}. \end{aligned} \quad (96)$$

inaccuracy was the fact that the time constants of the ratemeters were greater than one-third of a second. Observing Figs. 57 through 71, except in the cases of high fluid velocity and a small distance between detector levels where the residence times were very short, an exponential relationship is seen to exist between particle speed and the distance between detector levels. Because of errors in measurement of short residence times, only the data obtained when the distance between detector levels was greater than one inch were used for an extrapolation to zero distance between detector levels to produce the results shown in Figs. 72, 73, and 74.

Figures 72, 73, and 74 clearly illustrate that the speed of the particles within the fluidized bed is greater for upward movement ( $Z_1$  to  $Z_2$ ) than for downward movement ( $Z_2$  to  $Z_1$ ). Since, on the average, the same number of particles move upward as downward, this means that greater than fifty percent of the cross-sectional area of the fluidized bed must be utilized for downward particle movement.

## 5.2 Particle Traffic

Figure 75 presents the particle traffic data as a function of the average fluid velocity. The data  $r(Z_1)$  were obtained at one vertical height for all of the data, but the data  $r(Z_2)$  were actually obtained at five different vertical heights. No trend dependent upon vertical height was obtained, so all of the data at  $Z_2$  were combined and are shown in Fig. 75 as a single data value at each water flow rate studied. It was concluded that  $r(Z)$  had no dependence on  $Z$  over the range of vertical heights studied. However, the particle traffic was measured only in the middle sections of the fluidized bed, and thus, no data were available to determine the effect on particle traffic measurements close to the top or bottom of the fluidized bed.

### 5.3 Reflectivity Data

Figure 79 presents the experimental reflectivity data based on an average  $m(Z_i)$  for each data set. Also shown are the correlated probability of reflection curves  $(1 - e^{-\beta \Delta Z})$  determined from the data by least squares analyses, limited to the height of the fluidized bed for each water flow rate. Since no data were obtained for  $\Delta Z$  greater than six inches, no comparison is available between experiment and theory for large  $\Delta Z$ . For the lowest water flow studied,  $B_1$ , data were obtained over a larger percentage of the distance from  $Z_1$  to  $L$  than for the other flow rates studied, and the data appear to support the theory, as shown in Fig. 79.

### 5.4 Particle Concentrations

Two methods of determining the dispersion coefficient,  $E_z$ , were given in Section 4.6, based upon a diffusion theory model. The first method produced results reported in this section. The second method gave no results. Before attempting to determine the reason for this, the correlated distribution  $(C/C_\infty)$  was calculated for the five water flow rates studied by assuming different values of the dispersion coefficient and comparing the resulting distributions for each dispersion coefficient with the experimental data  $(I/I_\infty)$  determined from Figs. 86 through 90. The effect on the correlated distributions as a result of varying  $E_z$  for each water flow rate was as follows. As  $E_z$  was increased, the maximum value of  $C/C_\infty$  was decreased for each distance between detector levels, and the maximum values occurred at lesser time increments. The dispersion coefficients that produced the correlated distributions that came closest to representing the experimental distributions for each water flow rate were then tabulated.

It was noted that for time increments less than about 0.3 second, the correlated  $(C/C_\infty)$  distribution did not compare very closely with the experimental  $(I/I_\infty)$  distribution, even though the distribution for time increments greater than 0.3 second were closely matched. This would indicate that the data for short time increments (less than 0.3 second) were incompatible with the rest of the data in each experiment, and, in attempting to determine a dispersion coefficient by Method 2 using all of the data in each experiment, results, if any could be obtained, would be highly questionable.

Figure 91 presents the experimental  $(I/I_\infty)$  data for the lowest water flow rate studied, with the correlated  $(C/C_\infty)$  distribution for a dispersion coefficient of  $1 \text{ in}^2/\text{sec}$  superimposed. The data below about 0.3 second are not compatible with the correlated distribution. Figure 92 presents the correlated  $(C/C_\infty)$  distribution for a water flow rate of 18.8 gal/min., using a dispersion coefficient of  $10 \text{ in}^2/\text{sec}$ . Comparison of this figure with Figure 88 illustrates the marked difference below a 0.3 second time increment, although the dispersion coefficient used gave the best representation at greater time increments.

Table 6 gives the dispersion coefficients determined as outlined above. Table 6 also gives values of dispersion coefficients determined from a microscopic viewpoint, as discussed below.

In a medium where only scattering reactions occur, expressions for particle current density have been developed (3). Assuming only Z-dependence and that the particles move with average speed  $\bar{v}$ , the following current densities result.

$$J_+ = \frac{C \bar{v}}{4} - \frac{\bar{v}}{6 \Sigma} \left[ \frac{\partial C}{\partial Z} \right]_0, \quad (101)$$

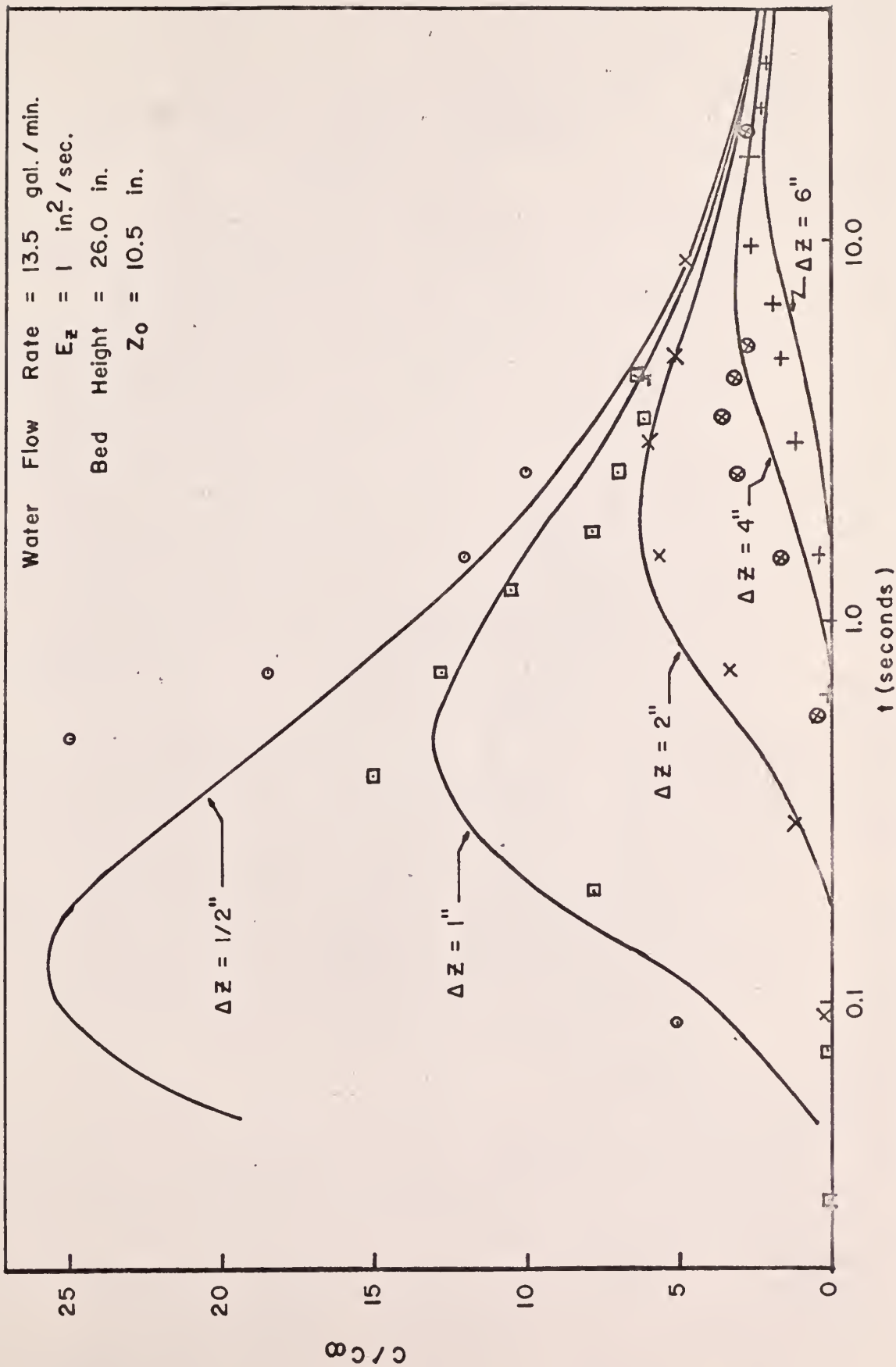


Figure 91. Correlated Particle Concentration Distribution  $C/C_\infty$  and Experimental  $I/I_\infty$ , at Flow Rate  $B_1$ .

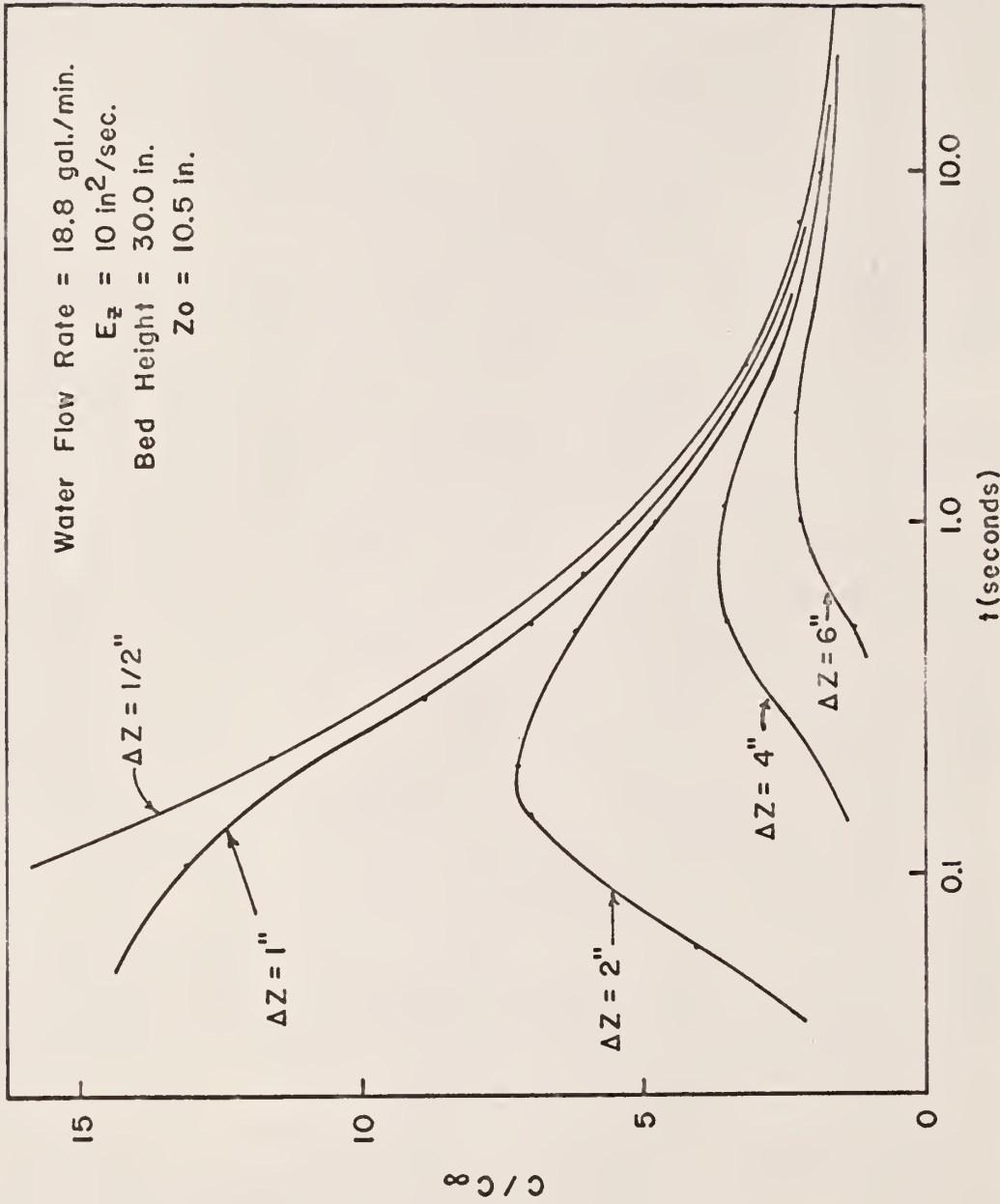


Figure 92. Correlated Particle Concentration Distribution, at Flow Rate B<sub>3</sub>.

Table 6. Dispersion Coefficient  $E_z$  as Determined by Single and Multi-Particle Experiments.

Dispersion Coefficient (in <sup>2</sup> /sec)	Water Flow Rate (gal/min)				
	13.5	17.0	18.8	22.3	24.0
Method 1	13.6	11.9	24.0	23.6	23.6
Method 2	-	-	-	-	-
Estimated from Correlated Distribution	1.0	8.0	10.0	11.0	12.0
Determined from Single Particle Experiments	6.7	25.3	38.3	41.6	41.7

and

$$J_- = \frac{C \bar{v}}{4} + \frac{\bar{v}}{6\Sigma} \left[ \frac{\partial C}{\partial Z} \right]_0 \quad (102)$$

where  $\Sigma$  is the probability of interaction. Applying Equations 101 and 102 to fluidized beds,  $\Sigma$  is equivalent to the reflection coefficient ( $\beta$ ), for  $\beta$  is an interaction probability, as implied in Equation 26, and is determined from single particle experiments.

In experiments with more than one particle, determination of  $J_+$  and  $J_-$  cannot be made; only the net movement of particles through the area studied can be made. The net movement is given by

$$J_{\text{net}} = J_+ - J_- \quad (103)$$

Substituting Equations 101 and 102 into Equation 103 give

$$J_{\text{net}} = - \frac{\bar{v}}{3\beta} \left[ \frac{\partial C}{\partial Z} \right]_0 \quad (104)$$

In diffusion theory, Equation 104 is Fick's law of diffusion,

$$J_{\text{net}} = - E_z \text{ grad } C \quad (105)$$

where  $E_z$  is the diffusion coefficient. From Equations 104 and 105,

$$E_z = \frac{\bar{v}}{3\beta} \quad (106)$$

Thus, we have a means of comparing results based on single particle experiments with multi-particle experimental results. The quantities  $\bar{v}$  and  $\beta$  were determined from microscopic investigations (Sections 4.3 and 4.5), and  $E_2$  has been determined from macroscopic investigations.

## 6.0 CONCLUSIONS

The results of this investigation have led to the following conclusions about fluid-solids fluidized beds.

Frequency distributions of residence times agree very well with gamma distribution correlations based on the parameters  $p$  and  $\nu$  determined from the experimental data. The gamma distribution parameter  $\nu$  increases with increasing distance between detector levels, while the parameter  $p$  tends to have a minimum value at about three inches distance between detector levels for all water flow rates studied, as illustrated in Figs. 47 through 56.

The logarithm of the vertical speed of the particles tends to increase linearly with decreasing distance between detector levels for all water flow rates studied, as illustrated in Figs. 57 through 71.

The vertical speed of the particles increases with increasing fluid velocity, as illustrated in Figs. 72, 73, and 74.

More than fifty percent of the cross-sectional area of the fluidized bed is used for downward particle movement.

About fifty residence times per data set are sufficient to study particle speeds.

In the middle sections of the fluidized bed, the particle traffic increases with increased fluid velocity, as illustrated in Fig. 75.

A frequency distribution of the probability of reflection for downward particle movement is the same as for upward particle movement, as illustrated in Figs. 76, 77, and 78. The probability of reflection increases with increased distance between detector levels for all water flow rates studied, as illustrated in Fig. 79.

The analytical model developed to determine the concentration of particles with respect to time and distance from the source plane gives distributions

that are in good agreement with the experimental frequency distributions of particle concentrations for distances between detector levels greater than one inch, as illustrated in Fig. 91.

The determination of particle dispersion properties by microscopic and macroscopic investigations has given particle dispersion coefficients with differences of less than an order of magnitude for all water flow rates studied.

The study of individual particle mobility by the method developed in this thesis, utilizing the apparatus used in this thesis to obtain the experimental data, led to the following conclusions.

Residence times obtained from the experimental apparatus which were less than 0.2 second were not reliable.

Measurements at the top and bottom of the fluidized bed should be made to determine how end effects affect the particle traffic.

For low water flow rates, a data correlation was obtained to enable a prediction of particle reflection characteristics.

Experimental measurements with greater distances between detector levels and higher water flow rates are needed to produce more particle reflection data to compare with the analytical expression for particle reflectivity developed in this thesis.

Analyses of the residence time, reflectivity, and particle concentration data led to the conclusion that the data obtained for distances between detector levels of less than one inch were not representative of the rest of the data, and this was attributed to the limitations of the ratemeters used in the experimental study. Better instrumentation sensitivity and recovery times are needed to obtain data at high water flow rates and small distances between detector levels.

Additional experiments with different fixed bed heights and different particle sizes and densities using the radioactive tracer technique should prove worthwhile.

A large amount of labor was expended in reducing and correlating the raw data from the dual-channel recorder trace and digital printout, and transferring the data to IBM cards. It is suggested that should further experiments occur, a method should be developed that will enable more data collection at reduced labor by automatically recording the raw data in a form suitable for digital computation.

The preliminary data obtained in this thesis indicate that the use of the methods of data collection and analysis developed and presented, is feasible in assisting in the determination of the behavior of individual particles in fluidized beds.

## 7.0 ACKNOWLEDGMENT

The author wishes to express his sincere appreciation to the following persons: Professor Richard C. Bailie, under whose direction and counsel this study has been accomplished; Dr. Liang-tseng Fan, for his advice and guidance throughout this investigation; Dr. William R. Kimel, Head of the Kansas State University Department of Nuclear Engineering, for his help and encouragement; Mr. Ray E. Hightower, for his assistance in the development of the electronic systems; Mr. Eldon J. Linnebur, undergraduate student in the Department of Nuclear Engineering, for his assistance in the use of the IBM 1620 Computer for data evaluation; and the staffs and students of both the Nuclear Engineering and Chemical Engineering Departments for their assistance when called upon.

## 8.0 LITERATURE CITED

1. Bellman, R. E., and Dreyfus, S. E.  
Applied Dynamic Programming. Princeton University Press, Princeton,  
New Jersey (1962).
2. Bellman, R. E., Kalaba, R. E. and Prestrud, M. C.  
Invariant Imbedding and Radiation Transfer in Slabs of Finite Thickness.  
The Rand Corporation R-388-ARPA (February, 1962).
3. Glasstone, W., and M. E. Edlund.  
The Elements of Nuclear Reactor Theory. Princeton: Van Nostrand (1952).
4. Gordon, L.  
Unpublished Ph. D. Thesis, University of Washington (1964).
5. Hoel, P. G.  
Introduction to Mathematical Statistics. John Wiley and Sons, Inc.,  
New York (1954).
6. Lapidus, L.  
Digital Computation for Chemical Engineers. McGraw-Hill Book Company,  
Inc., New York (1962).
7. Leva, M.  
Fluidization. McGraw-Hill Book Company, Inc., New York (1959).
8. Martin Nuclear  
Fluidized Bed Reactor Study. Phase I - Feasibility. MND-FBR-1696  
(February, 1959).
9. Morris, J. B., Nicholls, C. M., and Feninng, F. W.  
The Application of Fluidisation Techniques to Nuclear Reactors - A  
Preliminary Assessment. Transactions of the Institution of Chemical  
Engineers. The Institution of Chemical Engineers. 56 Victoria Street,  
Westminster, London SW1, Volume 34, Number 2 (1956).
10. Silverstein, C. C.  
Nucleonics. Volume 15, Number 3, March (1957).
11. Snedecor, G. W.  
Statistical Methods. Fifth Edition. Iowa State University Press,  
Ames, Iowa (1956).
12. Thomson, W. T.  
Laplace Transformation. Second Edition. Prentice-Hall, Inc.,  
Englewood Cliffs, New Jersey (1960).
13. Wilde, D. J.  
Unpublished Master's Thesis. University of Washington (1956).
14. Zenz, F. A., and Othmer, D. F.  
Fluidization and Fluid-Particle Systems. Reinhold, New York (1956).

## 9.0 APPENDICES

## APPENDIX A

Description and Explanation of the IBM  
1620 Computer FORTRAN Program No. 1 for  
Correcting the Time Increment Data

This computer program was written to correct the experimental time increments obtained when the tagged particle passed from the upper-to-lower and lower-to-upper detector levels. The corrections were applied on the basis of Table 1. Table 7 defines the various symbols utilized in this computer code.

Table 7. Input data and variables required for  
the IBM 1620 Computer Program No. 1.

SYMBOL	EXPLANATION
JMAX	Number of time increment data for given set
D(J)	Individual time increment data in given set, J=1 to JMAX, in pulses per channel $\times 10^{-3}$
P(J)	Individual time increment data converted to time in seconds
I	Time increment data set in the process of correction

First the program reads the experimental data D(J) and the number of individual data values JMAX in the Set I. The program then converts the data to time in seconds P(J).

The program determines which data represents upper-to-lower and lower-to-upper detector level time increments. By applying the equation necessary from Table 1, each time increment for both the upper-to-lower and lower-to-upper detector level is then corrected to true time.

After each time increment in the set has been so treated, the program punches IBM cards containing the data set I, the number of data values in

the set JMAX, and the individual values of corrected time increments.

Input to Computer Program No. 1

The data obtained from the fluidized bed apparatus was transferred to IBM cards and served as the input to Computer Program No. 1. Eight individual time increments were typed per card. A plus or minus sign preceded each time increment to designate detection of the tagged particle at either the upper or lower detector level respectively.

Seventy-six sets of data, with water flow rates and distances between detector levels for each data set, are given in Table 4. Table 8 gives the input data to Computer Program No. 1. Each data set is indicated by Data Set I. The first number shown in each data set is the number of time increments in the set (JMAX). Each data card is read into the computer as FORMAT (I4, I4, 8E7.3). The first four columns give the card number. The next four columns give the subscript J of the first time increment D(J) on each data card. J = 1, 2, ..., JMAX. The individual time increments are recorded as the number of pulses from the Time Interval Meter x 10<sup>-3</sup> stored in each channel of the multi-channel analyzer before rapid change in the counting rate caused transfer of storage to the next channel.

Output of Computer Program No. 1

The output of Computer Program No. 1 is given in Table 9. The output was punched as FORMAT (I4, I4, 8F8.3). Each data set is given as Data Set I. The first number shown in each data set is the number of time increments in the set (JMAX). The first four columns per card indicate

Table 8. Input to Computer Program No. 1.

## Data Set 6

232

10001	+00001	+00491	+01371	+00356	-00209	+00077	-00197	-00077
20009	-00168	-00170	-00300	-00113	-00648	-00576	-07350	-00139
30017	-06000	-00312	+00280	-00961	-00700	-00100	-00140	-00594
40025	-00656	-00431	-00200	-00233	+03330	+04332	+00212	+00586
50033	+00278	-00212	-00358	-00579	-05909	-00934	-03928	-00507
60041	-00253	-00220	-00409	-00162	-00185	-00407	-00121	-00790
70049	-00134	-00300	-00841	+00150	+00363	+00559	+00606	+00263
80057	+00333	+00672	+00124	+00061	+00299	+00267	+00152	+00224
90065	+00147	+00585	+00389	-00207	-00400	-00375	-00300	-02788
100073	+00300	-00400	-00579	-00192	-00400	-00200	-00200	-00422
110081	-00259	-00747	+00200	+00300	+00233	+00141	-00426	-00113
120089	-00190	-00279	-00067	-16147	+00300	+99999	+00156	+00211
130097	+00486	+00593	-00158	-00400	-00300	-00172	-03370	-24476
140105	+00160	+00700	+00152	+00299	+00508	-00322	+00608	+00636
150113	+00625	+00571	+00724	+00395	+00184	-00167	+00195	+04331
160121	+01152	+01204	-00174	-00676	-00519	-00348	-02068	-00552
170129	-00132	-00215	-00889	+00529	+00561	+00414	-00440	-14596
180137	-00077	-00274	-00107	-00135	-00003	-00136	-21451	-00147
190145	-00398	-00300	-00490	+00200	-00600	-00240	-00347	-03126
200153	+00900	+00079	+00835	-00311	-00938	+00937	+00168	+00148
210161	-07183	-00334	-00332	-00971	-04928	-00425	-00195	+00376
220169	+00232	+18067	+00299	+00120	+00568	-01010	-00097	+00427
220177	+00269	+00329	+00136	+00278	+00885	+00452	+07963	+01218
240185	+00524	-00497	-00421	-04827	-00141	-00288	-00244	+01064
250193	+04504	+00514	-00572	-00684	-01793	-00313	-00021	-07406
260201	-00752	-00240	-00109	-00320	-00386	+00080	+00125	+10097
270209	+01200	+00560	+00444	+00490	+00597	+01188	+16486	+00310
280217	+01184	+02718	+00989	+00099	-00644	-00171	+00730	-00384
290225	-00060	-00252	-00188	-02753	+00128	+00559	+00187	+00309

Table 8 (cont.)

## Data Set 7

232

10001	-00001	-00104	-00472	-00595	-00248	-00338	-00357	-00053
20009	-00522	-01229	-00572	-00499	-01043	-00260	-00599	-00122
30017	-20055	-00440	-00469	-00277	-00131	-00431	-00389	-00691
40025	-00074	-01183	-00616	-00601	-00761	-00148	-01074	+00696
50033	+00220	+00372	+00232	+00687	-00355	-00354	-00085	+00423
60041	+00344	+00586	-00300	-00100	-01394	-01103	-01778	-04202
70049	-00871	-00370	-00359	-08466	+00439	+97715	+00487	-00669
80057	+00531	+00352	+00091	+00717	+00151	+00140	+00474	+01705
90065	+00700	+00968	+00200	-02027	-00600	-00200	-00090	-00090
100073	-00086	-00642	-00183	+00346	-00595	-14012	+00072	+00524
110081	+01200	+00529	+28747	+00659	+01399	-00751	+00373	+00247
120089	+00244	+00188	+00712	+00123	+00367	+01336	+00311	+00245
130097	+00481	-00645	+00392	-00300	-00188	-00146	-00200	-38400
140105	-00600	-00300	-01293	-01507	-00120	-00807	-02559	-00392
150113	+01499	+00830	+00157	+00860	+00247	+00253	+06908	+00546
160121	+01124	+00292	+00315	+00191	+00526	+00786	+00826	-00337
170129	-00270	-00210	-00392	-00246	-00213	-00368	-00090	+00448
180137	-00141	+00281	+00655	-00831	+00839	+00285	+00097	+00457
190145	+00545	+00205	+16883	+00220	+02912	+00331	+00502	+00068
200153	-00962	-00214	-08572	+00387	+00644	+00243	+00454	+00914
210161	+00869	+00451	-00184	-00274	-00519	-01339	-04105	-00424
220169	-00544	-00098	+00443	+00313	+00144	+00114	+01232	+00447
230177	+00689	+00315	+00124	+00372	+00251	+00455	-00267	+00576
240185	-07247	+00560	+01171	+00520	+00177	+00376	+00434	+00145
250193	+00094	+00526	+00067	+00535	+00684	+00470	+00513	+00673
260201	+00172	-00072	-00285	-00200	-01060	-00093	-00422	-00547
270209	-00118	-00931	+00873	-00114	-00315	-00315	-00077	-01381
280217	+00065	-00494	-00662	-00381	-00146	-00351	-00813	-00056
290225	-00092	-00074	-06216	-00368	-07730	-00244	-00168	-17801

---

Table 9. Output of Computer Program No. 1.

## Data Set 6

232

6	1	.001	.736	2.056	.534	-.267	.199	-.251	-.115
6	9	-.252	-.255	-.450	-.169	-.972	-.864	-11.025	-.208
6	17	-9.000	-.468	.585	-1.228	-1.050	-.150	-.210	-.891
6	25	-.984	-.646	-.300	-.349	5.876	6.498	1.218	.379
6	33	.417	-.271	-.537	-.868	-8.863	-1.401	-5.892	-.760
6	41	-.379	-.330	-.613	-.243	-.277	-.610	-.181	-1.185
6	49	-.201	-.450	-1.261	.340	.544	.838	.909	.394
6	57	.499	1.008	.186	.091	.448	.400	.228	.336
6	65	.220	.877	.583	-.264	-.600	-.562	-.450	-13.182
6	73	.621	-.511	-.868	-.288	-.600	-.300	-.300	-.633
6	81	-.388	-1.120	.437	.450	.349	.211	-.544	-.169
6	89	-.285	-.418	-.100	-24.220	.621	149.998	.234	.316
6	97	.729	.889	-.201	-.600	-.450	-.258	-5.055	-36.714
6	105	.360	1.050	.228	.448	.762	-.411	1.147	.954
6	113	.937	.856	1.086	.592	.276	-.213	.427	6.496
6	121	1.728	1.806	-.222	-1.014	-.778	-.522	-3.102	-.828
6	129	-.198	-.322	-1.333	1.016	.841	.621	-.562	-21.894
6	137	-.115	-.411	-.160	-.202	-.004	-.204	-32.191	-.220
6	145	-.597	-.450	-.735	.437	-.767	-.360	-.520	-4.689
6	153	1.611	.118	1.252	-.397	-1.407	1.669	.252	.222
6	161	-9.182	-.501	-.496	-1.456	-7.392	-.637	-.292	.756
6	169	.348	27.100	.448	.180	.852	-1.291	-.145	.844
6	177	.403	.493	.204	.417	1.327	.678	11.944	1.827
6	185	.786	-.635	-.631	-7.240	-.211	-.432	-.366	1.877
6	193	6.756	.771	-.731	-1.026	-2.689	-.469	-.031	-11.109
6	201	-1.128	-.360	-.163	-.480	-.579	.197	.187	15.145
6	209	1.800	.840	.666	.735	.895	1.782	24.729	.465
6	217	1.776	4.077	1.483	.148	-.823	-.256	1.344	-.490
6	225	-.103	-.378	-.282	-4.129	.296	.838	.280	.463

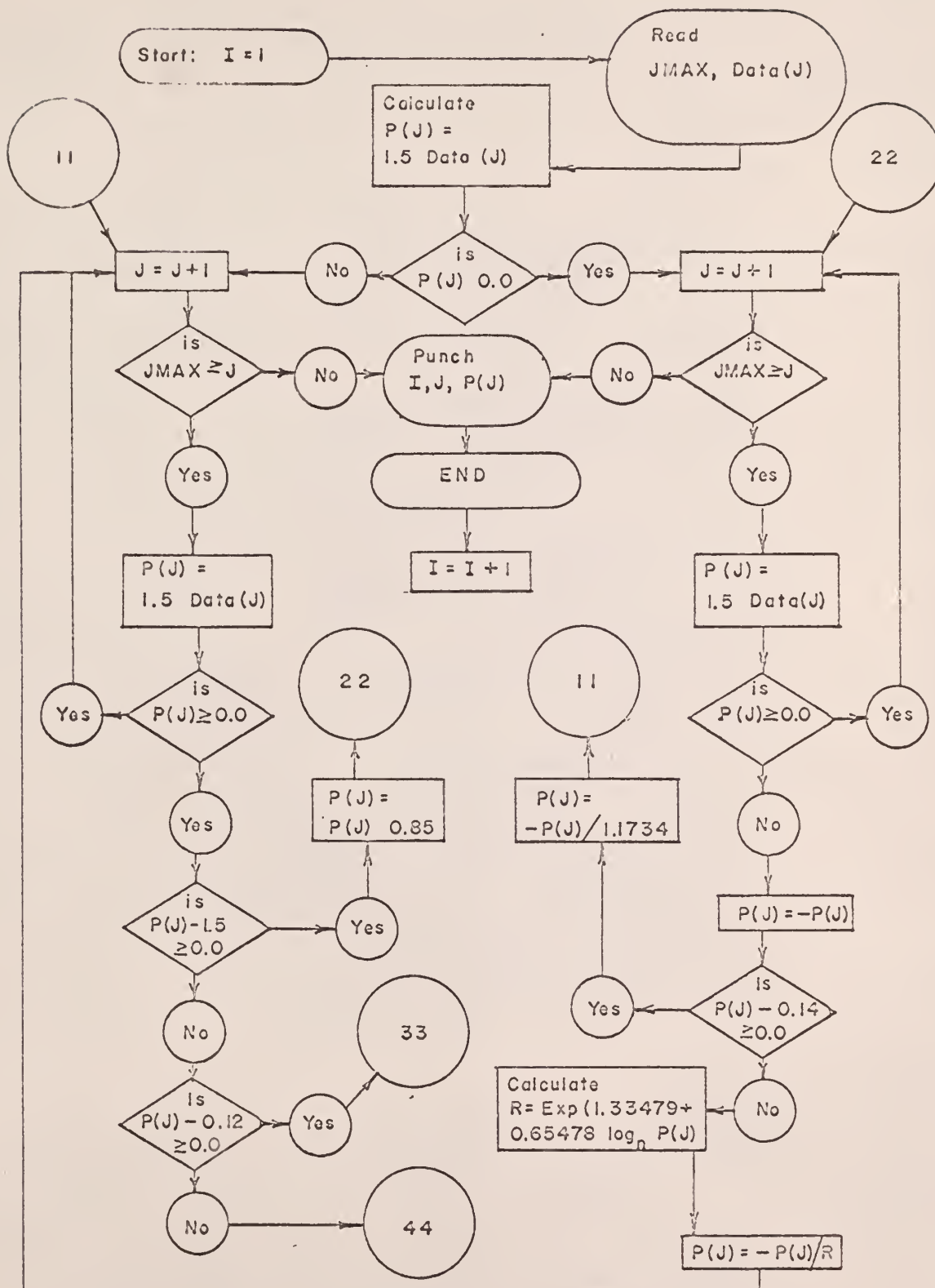
Table 9 (cont.)

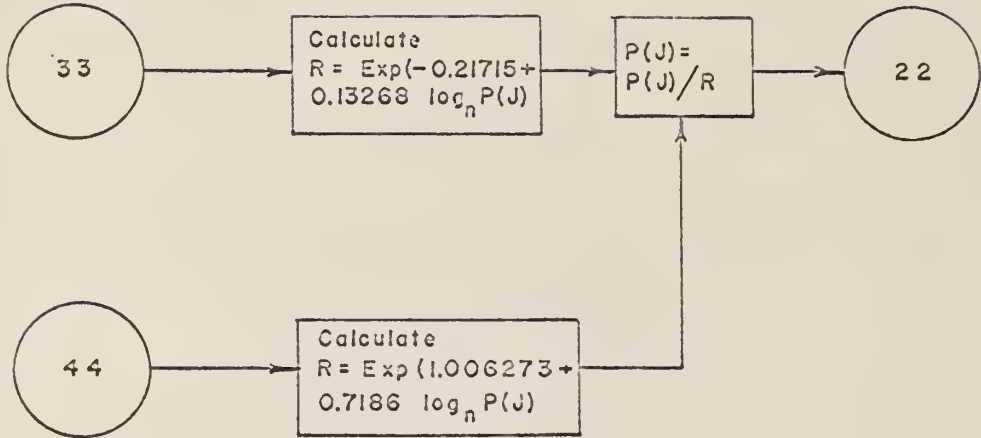
## Data Set 7

232										
7	1	-.001	-.156	-.708	-.892	-.372	-.507	-.535	-.079	
7	9	-.783	-1.843	-.858	-.748	-1.564	-.390	-.898	-.183	
7	17	-30.082	-.660	-.703	-.415	-.196	-.646	-.583	-1.036	
7	25	-.111	-1.774	-.924	-.901	-1.141	-.222	-1.611	1.289	
7	33	.330	.558	.348	1.030	-.453	-.531	-.127	.837	
7	41	.516	.879	-.383	-.150	-2.091	-1.654	-2.667	-6.303	
7	49	-1.306	-.555	-.538	-12.699	.864	146.572	.730	-.855	
7	57	1.020	.528	.136	1.075	.226	.210	.711	2.557	
7	65	1.050	1.452	.300	-2.591	-.900	-.300	-.135	-.135	
7	73	-.129	-.963	-.274	.703	-.760	-21.018	.195	.786	
7	81	1.800	.793	43.120	.988	2.098	-.960	.750	.370	
7	89	.366	.282	1.068	.184	.550	2.004	.466	.367	
7	97	.721	-.824	.783	-.383	-.282	-.219	-.300	-57.600	
7	105	-.900	-.450	-1.939	-2.260	-.180	-1.210	-3.838	-.588	
7	113	2.645	1.245	.235	1.290	.370	.379	10.362	.819	
7	121	1.636	.438	.472	.286	.789	1.179	1.239	-.430	
7	129	-.405	-.315	-.588	-.369	-.319	-.552	-.135	.820	
7	137	-.180	.587	.982	-1.062	1.516	.427	.145	.585	
7	145	.817	.307	25.324	.330	4.368	.496	.753	.102	
7	153	-1.229	-.321	-12.858	.775	.966	.364	.681	1.371	
7	161	1.303	.676	-.235	-.411	-.778	-2.008	-6.157	-.636	
7	169	-.816	-.147	.871	.469	.216	.171	1.848	.670	
7	177	1.033	.472	.186	.558	.376	.682	-.341	1.094	
7	185	-9.264	1.068	1.756	.780	.265	.564	.651	.217	
7	193	.141	.789	.100	.802	1.026	.705	.769	1.009	
7	201	.258	-.122	-.427	-.300	-1.590	-.139	-.633	-.820	
7	209	-.177	-1.396	1.569	-.145	-.472	-.472	-.115	-2.071	
7	217	.189	-.631	-.993	-.571	-.219	-.526	-1.219	-.084	
7	225	-1.338	-.111	-9.324	-.552	-11.595	-.366	-.252	-26.701	

the data set. The next four columns indicate the subscript  $J$  of the first time increment  $D(J)$  on each data card. The individual time increments are given in seconds, with eight time increments per card. A plus or minus sign preceded each time increment to designate detection of the tagged particle at either the upper or lower detector level respectively.

Logic Diagram for Computer Program No. 1





## FORTRAN Source Program for Computer Program No. 1

```
C PROGRAM FOR CORRECTING ALL DATA
  DIMENSION D(300),P(300)
101 FORMAT(I4,I4,E7.3,E7.3,E7.3,E7.3,E7.3,E7.3,E7.3,E7.3)
103 FORMAT(I5)
105 FORMAT(I4,I4,F8.3,F8.3,F8.3,F8.3,F8.3,F8.3,F8.3,F8.3)
  READ 103,K
  I=1
200 READ 103,JMAX
  PUNCH 103,JMAX
201 J=1
202 READ 101,M,N,D(J),D(J+1),D(J+2),D(J+3),D(J+4),D(J+5),D(J+6),D(J+7)
  J=J+8
  IF(JMAX-J)1,1,202
  1 J=1
  P(J)=1.5*D(J)
  IF(P(J))3,2,2
  2 J=J+1
  IF(JMAX-J)203,4,4
  4 P(J)=1.5*D(J)
  IF(P(J))5,2,2
  5 P(J)=-P(J)
  IF(P(J)-0.14)7,6,6
  6 P(J)=-P(J)/1.1734
  GO TO 3
  7 X=LOGF(P(J))
  Y=1.33479+(0.65478)*X
  R=EXPF(Y)
  P(J)=-P(J)/R
  GO TO 3
  3 J=J+1
  IF(JMAX-J)203,8,8
  8 P(J)=1.5*D(J)
  IF(P(J))3,9,9
  9 IF(P(J)-1.5)11,10,10
10 P(J)=P(J)/0.85
  GO TO 2
11 IF(P(J)-0.12)12,13,13
```

```
13 X=LOGF(P(J))
   Y=-0.21715+(0.13268)*X
   R=EXPF(Y)
   P(J)=P(J)/R
   GO TO 2
12 X=LOGF(P(J))
   Y=1.006273+(0.7186)*X
   R=EXPF(Y)
   P(J)=P(J)/R
   GO TO 2
203 J=1
204 PUNCH105,K,J,P(J),P(J+1),P(J+2),P(J+3),P(J+4),P(J+5),P(J+6),P(J+7)
   J=J+8
   IF(JMAX-J)300,204,204
300 K=K+1
   GO TO 200
   END
```

## APPENDIX B

Description and Explanation of the IBM  
1620 Computer FORTRAN Program No. 2 for  
Computing the Average Number of Times a  
Particle Passed a Detector Level per  
Unit Time

This computer code was written to determine the average number of times per unit time a tagged particle in the fluidized bed passed a given horizontal plane. This calculation was done by counting the number of times the tagged particle passed each of the two detector levels in a given set of data and dividing each number by the total time required to obtain the data. Figure 75 illustrates the results obtained from this program. Table 10 defines the various symbols utilized in this computer code.

Table 10. Input data and variables required for  
the IBM 1620 Computer Program No. 2.

SYMBOL	EXPLANATION
JMAX	Number of time increment data for given set
D(J)	Individual time increment data in given set, J = 1 to JMAX, in seconds
M	Data set
SUMT	Total time required to obtain data set
ZT	Number of times particle passed upper level
ZB	Number of times particle passed lower level
RT	Average number of times particle passed upper level
RB	Average number of times particle passed lower level

Input to Computer Program No. 2

The input to Computer Program No. 2 is the output of Computer Program No. 1. The input is read into the computer as FORMAT (I4, I4, 8F8.3).

Output of Computer Program No. 2

Table 11 gives the output of Computer Program No. 2. The left-hand column designates the data set number. RB is the average number of times the tagged particle passed the lower detector level per second, and RT is the average number of times the tagged particle passed the upper detector level per second. SUMT is the sum in seconds of the absolute values of the individual time increments for the given data set and is, therefore, the time required to obtain the data set.

Table 11. Output of Computer Program No. 2.

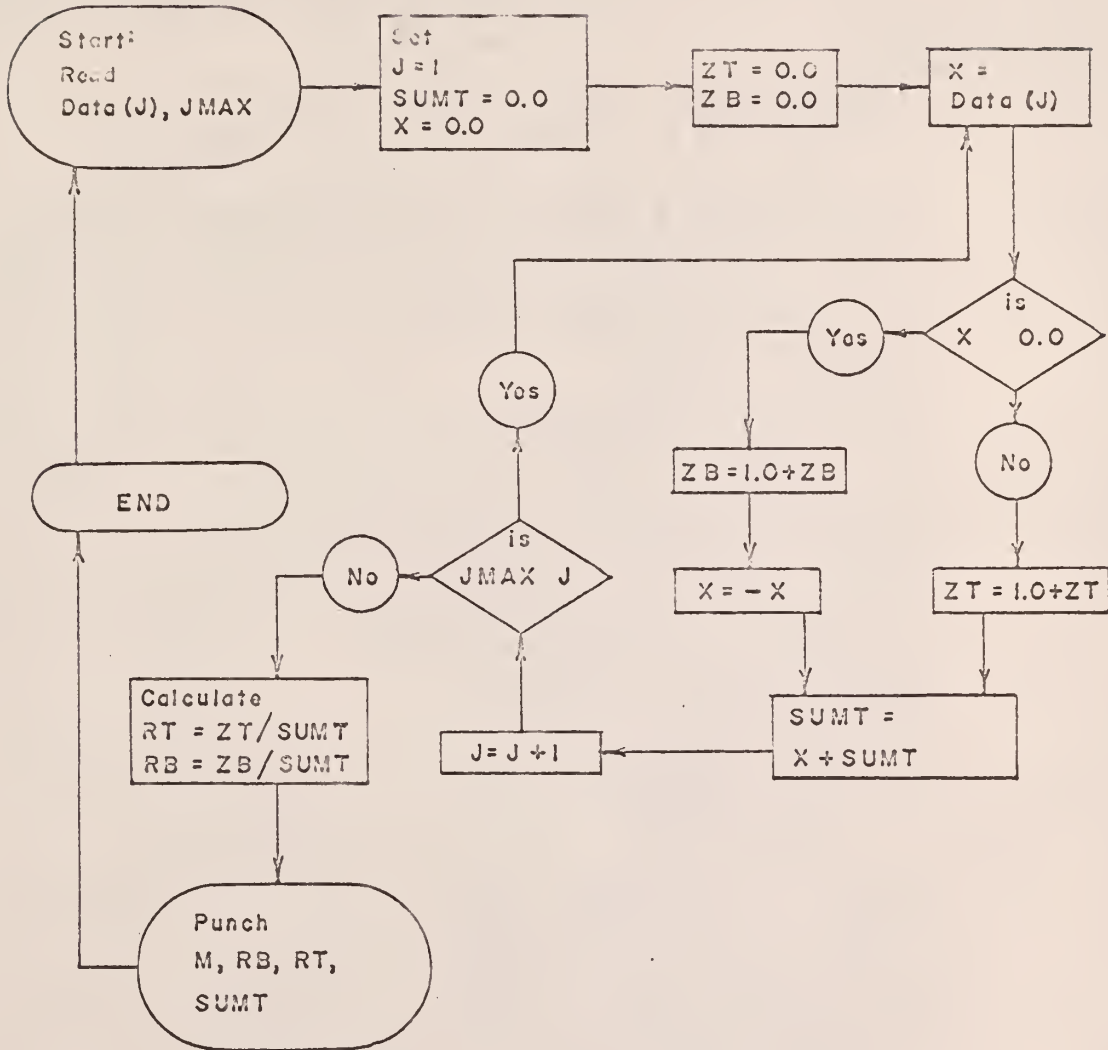
SET NO	RB	RT	SUMT
1	.16672560	.15737650	641.77300000
2	.09450548	.09093924	1121.62800000
3	.11695540	.13592120	949.07900000
4	.13426900	.15090410	841.59400000
5	.05934301	.10981867	1466.05300000
6	.21515310	.17178890	599.57300000
7	.20535470	.18515580	594.09400000
8	.08815150	.08958486	1395.32500000
9	.08581589	.09765256	1351.73100000
10	.09155243	.08176820	1430.87400000
11	.08233181	.10328900	1236.05700000
12	.14307640	.09745790	964.51900000
13	.17278970	.08228082	972.28000000
14	.11348069	.17369490	863.58300000
15	.12455340	.14173320	931.32700000
16	.14613030	.13569240	766.43900000
17	.22857180	.21664630	503.12400000
18	.18476280	.16501710	709.01700000
19	.24350410	.19590180	546.19200000
20	.11517251	.13469327	1024.55000000
21	.11542609	.18275790	831.70100000
22	.16808850	.21087470	654.41700000
23	.15844310	.17740220	738.43500000
24	.18090110	.18374990	702.04100000
25	.11236883	.13349801	1041.21400000
26	.20963420	.22038460	558.11500000
27	.19083230	.18121050	623.58400000
28	.11988491	.11403686	1025.98400000
29	.17872270	.14808460	783.33600000
30	.14200264	.08520158	1091.52900000
31	.14953520	.12059290	829.23600000
32	.23925280	.21947990	505.74100000
33	.14225290	.15554760	752.18100000
34	.16932390	.15485180	690.98300000
35	.11938770	.16259470	879.48700000
36	.15294970	.17008000	817.26200000
37	.16924440	.20117730	626.31300000
38	.13034090	.13491430	874.62900000

Table 11 (cont.)

SFT NO	RB	RT	SUMT
39	.18596680	.17155080	693.67200000
40	.16316460	.18204320	741.58200000
41	.22216290	.18700040	625.66700000
42	.16976470	.14678900	783.43700000
43	.17520630	.18650990	707.73700000
44	.15603420	.18248070	756.24400000
45	.15801098	.26793160	582.23800000
46	.14800190	.18873630	736.47700000
47	.16941140	.16941140	637.50100000
48	.12674220	.13371890	860.01300000
49	.22402360	.20124160	526.73000000
50	.18539720	.13161786	706.59100000
51	.21051470	.20383170	598.53300000
52	.13754290	.16810810	785.20900000
53	.20392410	.16000200	637.49200000
54	.22753960	.20653590	571.32900000
55	.20490950	.23590420	580.74400000
56	.18238130	.22510120	608.61500000
57	.17511360	.15210600	782.34900000
58	.17245750	.13303860	811.79400000
59	.17930070	.18517940	680.42100000
60	.17708730	.20710210	666.33800000
61	.21499230	.20514530	609.32400000
62	.21355070	.21355070	599.38900000
63	.17144320	.18948990	664.94300000
64	.20055220	.24352770	558.45800000
65	.19473420	.21453770	605.95400000
66	.17229080	.13959330	795.16700000
67	.14466620	.12314560	836.40800000
68	.21476790	.18792190	595.99200000
69	.18971670	.18647360	616.70900000
70	.14801120	.18397660	722.91800000
71	.19706826	.20104940	502.36400000
72	.16156630	.17725230	637.50900000
73	.16260130	.16830670	701.10100000
74	.17690540	.17090860	667.02300000
75	.15796580	.17403010	746.99700000
76	.18569990	.16855840	700.05400000

---

## Logic Diagram for Computer Program No. 2



## FORTRAN Source Program for Computer Program No. 2

```
C PROGRAM FOR DETERMINING THE NUMBER OF TIMES A PARTICLE PASSES
C THE TOP AND BOTTOM LEVEL ANS IN SECONDS
  DIMENSION D(300)
101 FORMAT(I4,I4,F8.3,F8.3,F8.3,F8.3,F8.3,F8.3,F8.3,F8.3)
102 FORMAT(I5)
103 FORMAT(I4,F15.8,F15.8,F15.8,F15.8)
  I=1
200 READ 102,JMAX
  J=1
201 READ 101,M,N,D(J),D(J+1),D(J+2),D(J+3),D(J+4),D(J+5),D(J+6),D(J+7)
  J=J+8
  IF(JM/X-J)202,202,201
202 J=1
  SUMT=0.0
  ZB=0.0
  ZT=0.0
  X=0.0
  1 X=D(J)
  IF(X)203,203,204
203 ZB=1.0+ZB
  X=-X
  GO TO 205
204 ZT=1.0+ZT
205 SUMT=X+SUMT
  J=J+1
  IF(JMAX-J)2,1,1
  2 RT=ZT/SUMT
  RB=ZB/SUMT
  IF(SENSE SWITCH 3)10,11
10 PRINT 103,M,RB,RT,SUMT
  GO TO 12
11 PUNCH 103,M,RB,RT,SUMT
12 I=I+1
  GO TO 200
  END
```

## APPENDIX C

Description and Explanation of the IEM  
1620 Computer FORTRAN Program No. 3 for  
Performing the Fluidization Statistical  
Analysis

This program was written to determine the individual and average times, variances, and skewness of the experimental data obtained from the fluidized bed apparatus.

Figure 93 is an illustration of the different time increments that can be obtained from a set of experimental data.

The average, variance, and skewness of a given time increment are:

$$\bar{t} = \sum_{i=1}^N t_i / N \quad (1C)$$

$$S^2 = \sum_{i=1}^N (t_i - \bar{t})^2 / (N-1) \quad (2C)$$

$$S^3 = \sum_{i=1}^N (t_i - \bar{t})^3 / (N-1) \quad (3C)$$

By utilizing this program, individual values, averages, variances, and skewness of the time increments  $t(\text{BB})$ ,  $t(\text{BT})$ ,  $t(\text{BTL})$ ,  $t(\text{TT})$ ,  $t(\text{TB})$ , and  $t(\text{TBL})$  can be determined from the experimental data. The other time increments shown in Fig. 93 can be determined by combining the output of this code in the following manner:

$$t(\text{TTBB}) = t(\text{TT}) + t(\text{TB}) + t(\text{BB})$$

$$t(\text{BBTT}) = t(\text{BB}) + t(\text{BT}) + t(\text{TT})$$

$$t(\text{TBT}) = t(\text{TB}) + t(\text{BB}) + t(\text{BT})$$

$$t(\text{BTB}) = t(\text{BT}) + t(\text{TT}) + t(\text{TB})$$

$$t(\text{BTT}) = t(\text{BT}) + t(\text{TT})$$

$$t(\text{TBB}) = t(\text{TB}) + t(\text{BB})$$

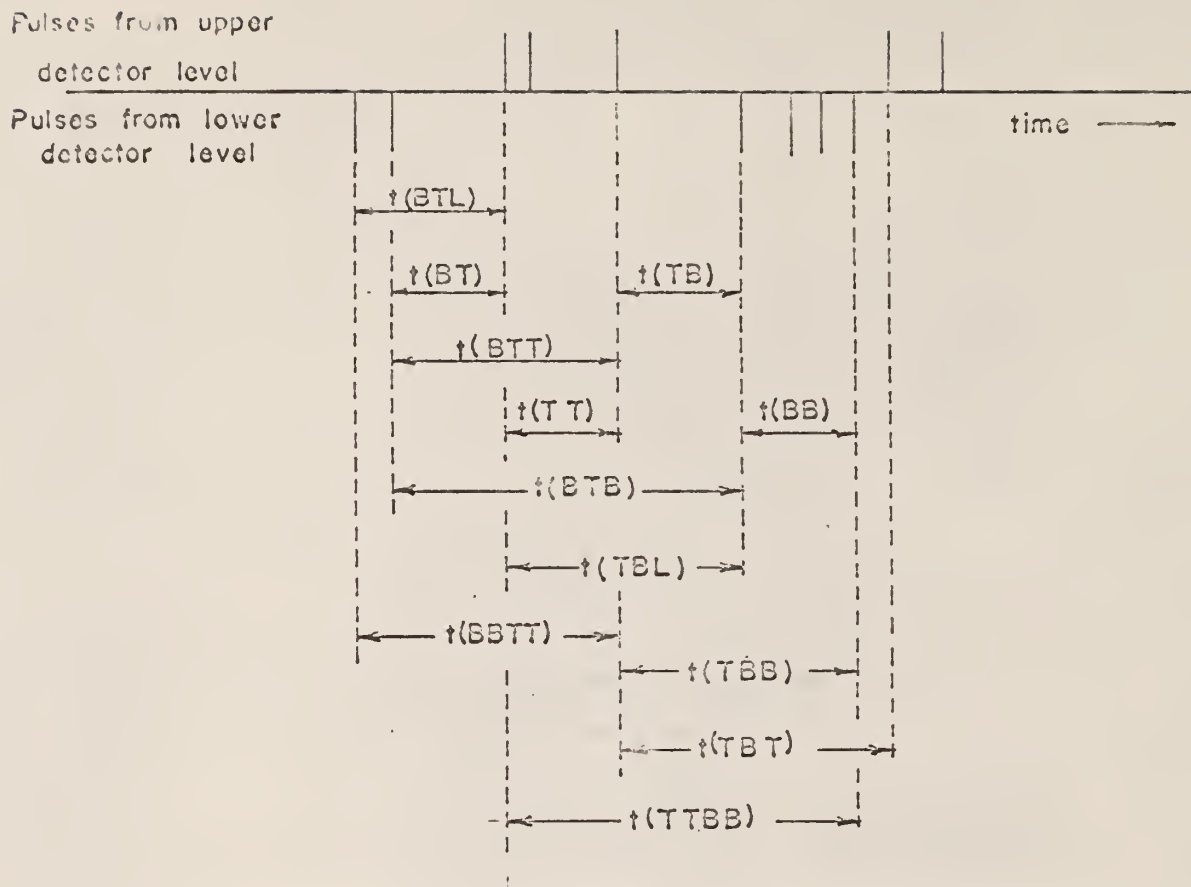


Figure 93. Time Increments Available From a Set of Experimental Data.

Sense switches on the IBM control console route the computer through the program to yield the output desired. Sense Switch 3 ON gives console typewriter output and Sense Switch 3 OFF gives punched card output. Sense Switches 1 and 2 give the following output:

Sense Switch 1	Sense Switch 2	Output
OFF	OFF	Individual values, $t(BB)$ , $t(BT)$ , $t(BTL)$ , $t(TT)$ , $t(TB)$ , and $t(TBL)$
ON	OFF	Individual values, $t(BT)$ and $t(TB)$
ON	ON	Individual values, $t(BB)$ , $t(BT)$ , $t(TT)$ , and $t(TB)$ ; average values, variances, and skewness of $t(BB)$ , $t(BT)$ , $t(BTL)$ , $t(TT)$ , $t(TB)$ , and $t(TBL)$
OFF	ON	Individual values, average values, variances, and skewness of $t(BB)$ , $t(BT)$ , $t(BTL)$ , $t(TT)$ , $t(TB)$ , and $t(TBL)$

Table 12 defines the various symbols utilized in this computer code.

Table 12. Input data and variables required for the IBM 1620 Computer Program No. 3.

SYMBOL	EXPLANATION
JMAX	Number of time increment data for given set
D(J)	Individual time increment data in given set, J = 1 to JMAX, in seconds
I	Data set
N	Number of t(BT or t(TB) in data set
BB, BT, BTL	t(BB), t(BT), t(BTL)
TT, TB, TBL	t(TT), t(TB), t(TBL)
BRA, BTA, BTLA	Average values of t(BB), t(BT), and t(BTL)
TTA, TBA, TBLA	Average values of t(TT), t(TB), and t(TBL)
BBXR, BTXR	Variances of t(BB) and t(BT)
TTXR, TEXR	Variances of t(TT) and t(TB)
BTLXR, TBLXR	Variances of t(BTL) and t(TBL)
BBYR, BTYR	Skewness of t(BB) and t(BT)
TTYR, TBYR	Skewness of t(TT) and t(TB)
BTLYR, TBLYR	Skewness of t(BTL) and t(TBL)

### Input to Computer Program No. 3

The input to Computer Program No. 3 is the output of Computer Program No. 1. The input is read into the computer as FORMAT (I4, I4, 8F8.3).

### Output of Computer Program No. 3

Tables 13 and 14 give the output of Computer Program No. 3. The output given in Table 13 was obtained by setting Sense Switch 1 ON and Sense Switch 2 OFF. The results were the residence times t(BT) and t(TB) of the tagged particle as it passed from one detector level to the other.

Table 14 gives the output of the program when Sense Switch 1 was ON and Sense Switch 2 was ON. The results give the individual time increments of t(BB), t(BT), t(TB), and t(TT) and the average values, variances, and

Table 13. Output of Computer Program No. 3.

52			1	47	.027	2	38	.280
1	1	.219	1	48	.035	2	39	.237
1	2	.223	1	49	.063	2	41	.404
1	3	.071	1	50	.120	2	42	.160
1	4	.096	1	51	.090	2	43	.112
1	5	.123	1	52	.065	2	44	.298
1	6	.255	1	53	.273	2	45	.125
1	8	.072	1	54	.107	2	46	.198
1	9	.067	1	55	.122	2	47	.189
1	10	.061	1	56	.109	2	48	.258
1	11	.084	1	57	.096	2	49	.414
1	12	.132	53			2	50	.179
1	14	.106	2	1	.243	2	51	.220
1	15	.141	2	2	.342	2	52	.112
1	16	.173	2	3	.326	2	53	.162
1	17	.140	2	4	.152	2	54	.149
1	18	.083	2	5	.141	2	55	.193
1	19	.108	2	6	.130	2	56	.229
1	20	.102	2	7	.127	36		
1	21	.226	2	8	.189	3	1	.110
1	22	.097	2	9	.180	3	3	.088
1	23	.114	2	10	.125	3	5	.071
1	26	.114	2	11	.212	3	6	.093
1	27	.109	2	12	.178	3	7	.154
1	28	.109	2	13	.136	3	8	.162
1	29	.119	2	14	.193	3	9	.106
1	30	.113	2	15	.212	3	12	.078
1	31	.265	2	16	.314	3	13	.103
1	32	.256	2	17	.141	3	14	.130
1	34	.035	2	18	.368	3	16	.121
1	35	.124	2	19	.193	3	17	.027
1	36	.027	2	20	.199	3	18	.027
1	37	.119	2	21	.334	3	19	.051
1	38	.217	2	22	.156	3	20	.164
1	39	.191	2	23	.151	3	21	.091
1	40	.078	2	24	.130	3	22	.126
1	41	.152	2	25	.193	3	23	.109
1	42	.173	2	27	.143	3	24	.103
1	43	.027	2	28	.318	3	26	.106
1	44	.237	2	29	.344	3	28	.114
1	45	.069	2	30	.132			
1	46	.227	2	31	.136			
			2	32	.304			
			2	33	.256			
			2	34	.393			
			2	35	.223			
			2	36	.146			

Table 14. Output of Computer Program No. 3.

Data Set	$t(ii)$	$t(ij)$	$t(ijL)$
31	3.28701920	.28257692	3.50498070
31	15.38825900	.10838160	15.04018300
31	135.90179000	.14487333	134.94166000
32	8.05963460	.23053846	8.26719230
32	136.96316000	.07123977	136.49918000
32	3198.29050000	.06782903	3199.70450000
33	2.51266660	2.73101660	3.88613330
33	26.91388100	30.41322800	38.37274400
33	561.69701000	512.40540000	763.84357000
34	3.54749150	1.02400000	4.25988130
34	43.44949600	18.66181200	55.45750800
34	899.12203000	538.81253000	1239.27460000
35	1.72640290	6.31608950	3.35834320
35	8.17724780	146.51537000	33.68341000
35	63.60642500	4793.33400000	807.80359000
36	4.18843930	.31922727	4.33853030
36	83.69991500	.22380333	85.39658300
36	2816.15760000	.63194858	2863.51490000
37	6.20802040	.44144897	6.60061220
37	45.24609100	.07653613	45.49188100
37	555.72408000	.01793786	566.78697000
38	9.46933330	.30862500	9.74420830
38	174.97080000	.02258699	175.37152000
38	3877.21040000	.00257611	3898.11080000
39	4.51019560	.29517391	4.77421730
39	27.86508600	.02092481	28.15774400
39	276.48140000	.00365211	285.51908000
40	8.12597770	.41760000	8.53124440
40	105.52295000	.65326877	106.66721000
40	3312.57840000	3.09779020	3379.24220000
41	5.10441660	.66652777	5.75194440
41	47.04307400	.07792275	47.69543100
41	908.10965000	.03519333	929.79262000
42	8.71800000	.62762162	9.31221620
42	103.18281000	.14275687	104.45862000
42	1583.16050000	.07150366	1599.52760000

---

skewness of  $t(BB)$ ,  $t(BT)$ ,  $t(BTL)$ ,  $t(TT)$ ,  $t(TB)$ , and  $t(TBL)$ .

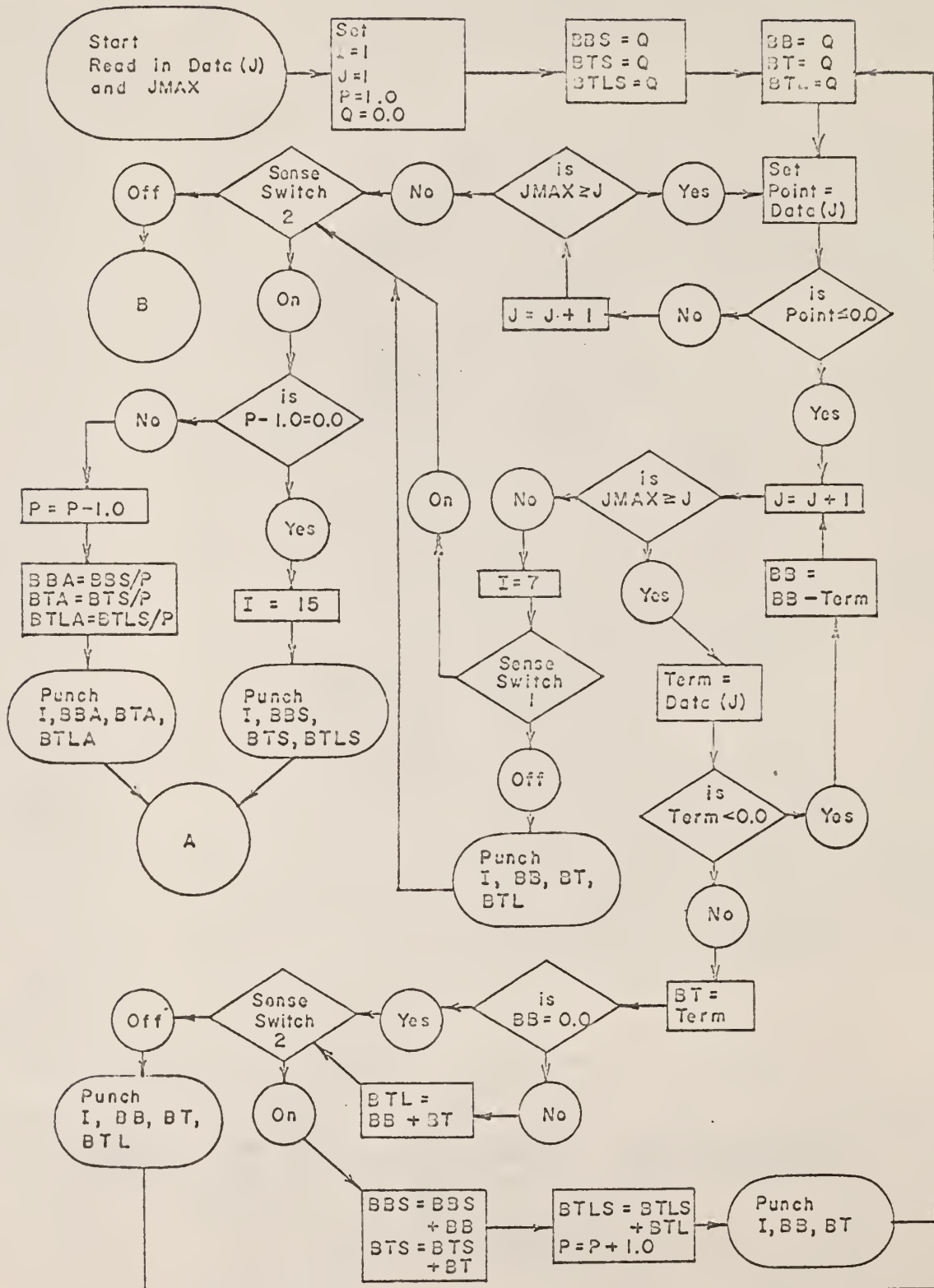
152 residence times sets were obtained from the 76 Data Sets of input.

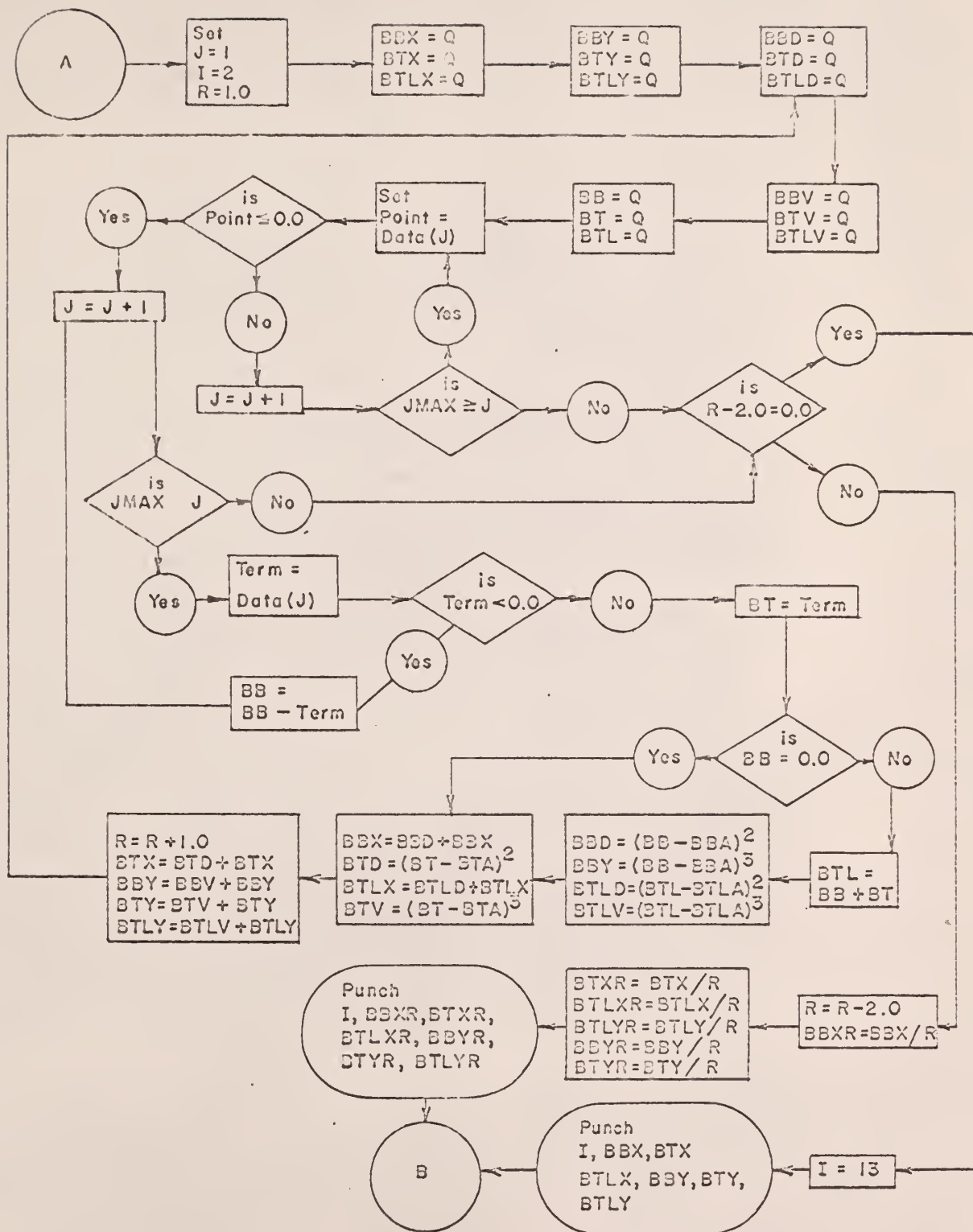
The second column in each set of columns in Table 13 gives the subscript assigned to each individual residence time in each given residence times set. The third column in each set of columns gives, in seconds, each individual residence time in each given residence times set.

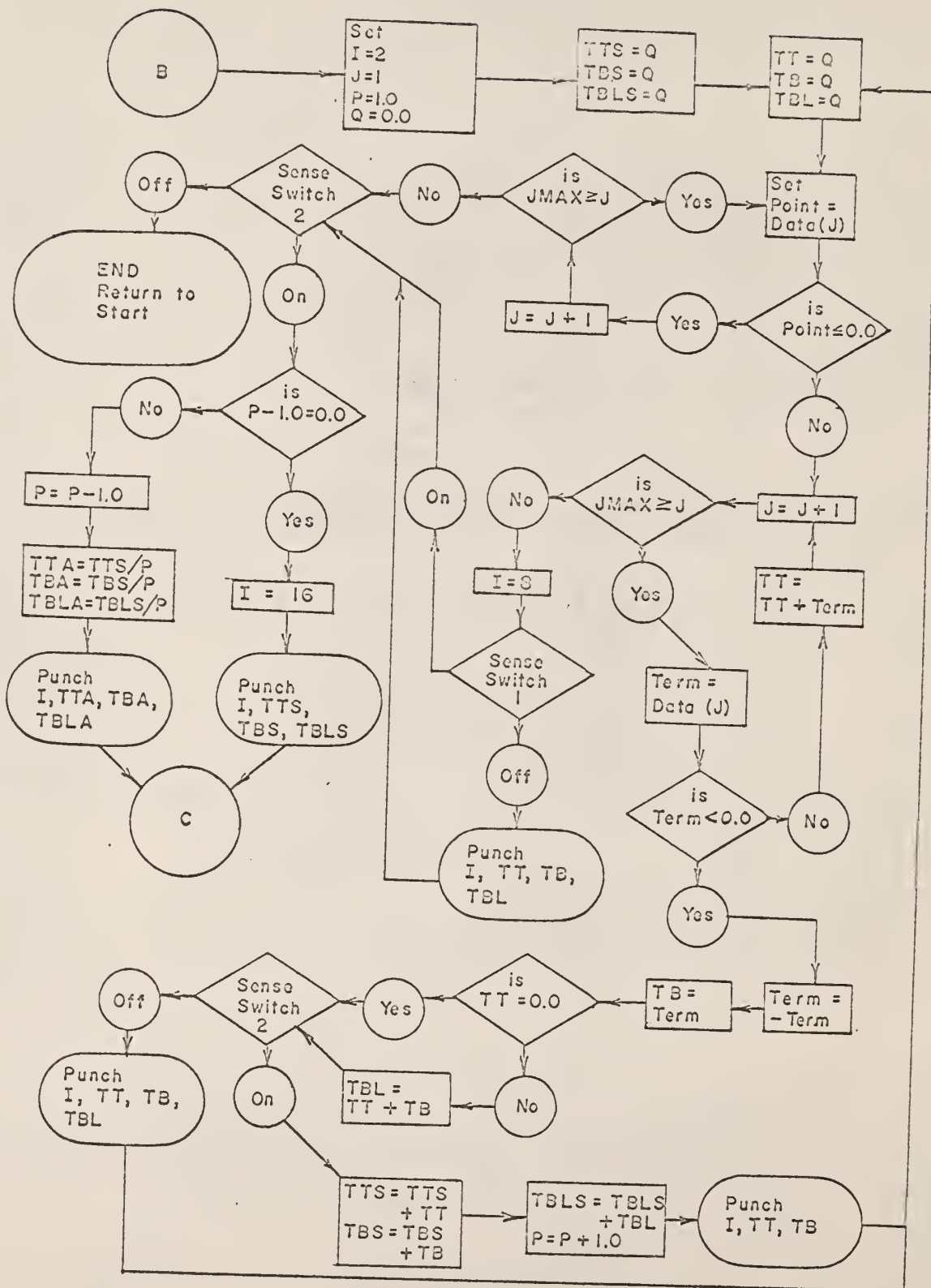
The first row of an even-numbered output set in Table 14 gives, in seconds, the average values of  $t(TT)$ ,  $t(TB)$ , and  $t(TBL)$ , respectively. The second row gives, in  $(\text{seconds})^2$ , the variances of  $t(TT)$ ,  $t(TB)$ , and  $t(TBL)$ , respectively. The third row gives, in  $(\text{seconds})^3$ , the skewness of  $t(TT)$ ,  $t(TB)$ , and  $t(TBL)$ , respectively.

The first row of an odd-numbered output set in Table 14 gives, in seconds, the average values of  $t(BB)$ ,  $t(BT)$ , and  $t(BTL)$ , respectively. The second row gives, in  $(\text{seconds})^2$ , the variances of  $t(BB)$ ,  $t(BT)$ , and  $t(BTL)$ , respectively. The third row gives, in  $(\text{seconds})^3$ , the skewness of  $t(BB)$ ,  $t(BT)$ , and  $t(BTL)$ , respectively.

## Logic Diagram for Computer Program No. 3









## FORTRAN Source Program for Computer Program No. 3

```

        DIMENSION D(300)
101  FORMAT(I4,I4,F8.3,F8.3,F8.3,F8.3,F8.3,F8.3,F8.3,F8.3)
102  FORMAT(I4, F15.8, F15.8, F15.8, F15.8)
103  FORMAT(I5)
104  FORMAT(I4, I4, F7.3)
      I=1
200  READ 103,JMAX
201  J=1
202  READ 101,M,N,D(J),D(J+1),D(J+2),D(J+3),D(J+4),D(J+5),D(J+6),D(J+7)
      J=J+8
      IF(JMAX-J)1,1,202
  1  J=1
  2  N=1
  3  P=1.0
      Q=0.0
  4  BBS=Q
      BTS=Q
      BTLS=Q
  5  BB=Q
      BT=Q
      BTL=Q
  6  PCINT=D(J)
      IF(PCINT)10,10,7
  7  J=J+1
      IF(JMAX-J)19,6,6
 10  J=J+1
      IF(JMAX-J)11,13,13
 11  IF(SENSE SWITCH 1)19,203
203  IF(SENSE SWITCH 3)800,801
800  PRINT 102,I,BB,BT,BTL
      GC TO 19
801  PUNCH 102,I,BB,BT,BTL
      GC TO 19
 13  TERM=D(J)
      IF(TERM)14,15,15
 14  BB=BB-TERM
      GC TO 10
 15  BT=TERM
      IF(BB)16,17,16
 16  BTL=BB+BT
 17  IF(SENSE SWITCH 2)18,204
204  PUNCH 104, I, N, BT
      N=N+1
      GC TO 5

```

```
18 BBS=BBS+BB
   STS=STS+BT
   BTLS=BTLS+BTL
   P=P+1.0
   IF ( SENSE SWITCH 3 ) 205, 217
205 PRINT 102,I,BB,BT
   GC TO 5
217 PUNCH 102, I, BB, BT
   GC TO 5
   19 IF(SENSE SWITCH 2)20,37
   20 IF(P-1.0)22,21,22
   21 IF ( SENSE SWITCH 3 ) 206, 218
206 PRINT 102, I, BBS, BTS, BTLS
   GC TO 24
218 PUNCH 102, I, BBS, BTS, BTLS
   GC TO 24
   22 P=P-1.0
   23 SBA=(BBS/P)
   BTA=(BTS/P)
   BTLA=(BTLS/P)
   IF ( SENSE SWITCH 3 ) 207, 219
207 PRINT 102,I,BBA,BTA,BTLA
   GC TO 24
219 PUNCH 102, I, BBA, BTA, BTLA
24 J=1
   R=1.0
   BBX=Q
   BTX=Q
   BTLX=Q
   BBY=Q
   BTY=Q
   BTLY=Q
25 BBD=Q
   BTD=Q
   BTLD=Q
   BBV=Q
   BTV=Q
   BTLV=Q
   BB=Q
   BT=Q
   BTL=Q
26 PCINT=D(J)
   IF(PCINT)28,28,27
27 J=J+1
   IF(JMAX-J)34,26,26
28 J=J+1
   IF(JMAX-J)34,29,29
29 TERM=D(J)
```

```

      IF (TERM) 30, 31, 31
30  BB=BB-TERM
      GO TO 28
31  BT=TERM
      IF (BB) 32, 33, 32
32  BTL=B3+BT
      BBD=(BB-BBA)**2
      BBV=(BB-BBA)**3
      BTLD=(BTL-BTLA)**2
      BTLV=(BTL-BTLA)**3
33  BBX=BBD+BBX
      BTB=(BT-BTA)**2
      BTLX=BTLD+BTLX
      R=R+1.0
      BTV=(BT-BTA)**3
      BTX=BTB+BTX
      BBY=BBV+BBY
      BTY=BTV+BTY
      BTLY=BTLV+BTLY
      GO TO 25
34  IF (R-2.0) 36, 35, 36
35  IF ( SENSE SWITCH 3 ) 208, 220
208 PRINT 102, I, BBX, BTX, BTLX
      PRINT 102, I, BBY, BTY, BTLY
      GO TO 37
220 PUNCH 102, I, BBX, BTX, BTLX
      PUNCH 102, I, BBY, BTY, BTLY
      GO TO 37
36  R=R-2.0
      BBXR=BBX/R
      BTXR=BTX/R
      BTLXR=BTLX/R
      BBYR=BBY/R
      BTYR=BTY/R
      BTLYR=BTLY/R
      IF ( SENSE SWITCH 3 ) 209, 221
209 PRINT 102, I, BBXR, BTXR, BTLXR
      PRINT 102, I, BBYR, BTYR, BTLYR
      GO TO 45
221 PUNCH 102, I, BBXR, BTXR, BTLXR
      PUNCH 102, I, BBYR, BTYR, BTLYR
37  GO TO 45
45  J=1
      I=I+1
      N=1
      P=1.0
      TTS=Q
      TBS=Q
      TBLS=Q

```

```
46 TT=Q
   TB=Q
   TBL=Q
47 PCINT=D(J)
   IF(PCINT)48,48,49
48 J=J+1
   IF(JMAX-J)58,47,47
49 J=J+1
   IF(JMAX-J)50,52,52
50 IF(SENSE SWITCH 1)51,210
210 PUNCH 102,I,TT,TB,TBL
51 GO TO 58
52 TERM=D(J)
   IF (TERM) 54,53,53
53 TT=TT+TERM
   GO TO 49
54 TERM=-TERM
   TB=TERM
   IF(TT)55,56,55
55 TBL=TT+TB
56 IF(SENSE SWITCH 2)57,211
211 PUNCH 104,I,N,TB
   N=N+1
   GO TO 46
57 TTS=TTS+TT
   TBS=TBS+TB
   TBLS = TBLS + TBL
   P=P+1.0
   IF ( SENSE SWITCH 3 ) 212, 222
212 PRINT 102, I, TT, TB
   GO TO 46
222 PUNCH 102, I, TT, TB
   GO TO 46
58 IF(SENSE SWITCH 2)59,75
59 IF(P-1.0)61,60,61
60 IF ( SENSE SWITCH 3 ) 213, 223
213 PRINT 102, I, TTS, TBS, TBLS
   GO TO 62
223 PUNCH 102, I, TTS, TBS, TBLS
   GO TO 62
61 P=P-1.0
   TTA=TTS/P
   TBA=TBS/P
   TBLA=TBLS/P
   IF ( SENSE SWITCH 3 ) 214, 224
214 PRINT 102,I,TTA,TBA,TBLA
   GO TO 62
224 PUNCH 102, I, TTA, TBA, TBLA
```

```
62 J=1
   R=1.0
   TTX=Q
   TBX=Q
   TBLX=Q
   TTY=Q
   TBY=Q
   TBLY=Q
63 TTD=Q
   TBD=Q
   TBLD=Q
   TTV=Q
   TBV=Q
   TBLV=Q
   TT=Q
   TB=Q
   TBL=Q
64 POINT=D(J)
   IF(POINT)65,65,66
65 J=J+1
   IF(JMAX-J)72,64,64
66 J=J+1
   IF(JMAX-J)72,67,67
67 TERM=D(J)
   IF(TERM)69,68,68
68 TT=TT+TERM
   GC TC 66
69 TERM=-TERM
   TB=TERM
   IF(TT)70,71,70
70 TBL=TT+TB
   TBLD=(TBL-TBLA)**2
   TBLV=(TBL-TBLA)**3
   TTD=(TT-TTA)**2
   TTV=(TT-TTA)**3
71 R=R+1.0
   TBD=(TB-TBA)**2
   TTX=TTD+TTX
   TBX=TBD+TBX
   TBLX=TBLD+TBLX
   TBV=(TB-TBA)**3
   TTY=TTV+TTY
   TBY=TBV+TBY
   TBLY=TBLV+TBLY
   GC TC 63
72 IF(R-2.0)74,73,74
```

```
73 IF ( SENSE SWITCH 3 ) 215, 225
215 PRINT 102,I,TTX,TBX,TBLX
PRINT 102,I,TTY,TBY,TBLY
GO TO 76
225 PUNCH 102, I, TTX, TBX, TBLX
PUNCH 102, I, TTY, TBY, TBLY
GO TO 76
74 R=R-2.0
TTXR=TTX/R
TBXR=TBX/R
TBLXR=TBLX/R
TTYR=TTY/R
TBYR=TBY/R
TBLYR=TBLY/R
IF ( SENSE SWITCH 3 ) 216, 226
216 PRINT 102,I,TTXR,TBXR,TBLXR
PRINT 102,I,TTYR,TBYR,TBLYR
GO TO 76
226 PUNCH 102, I, TTXR, TBXR, TBLXR
PUNCH 102, I, TTYR, TBYR, TBLYR
76 TTA=Q
TBA=Q
TBLA=Q
TTXR=Q
TBXR=Q
TBLXR=Q
TTYR=Q
TBYR=Q
TBLYR=Q
BBA=Q
BTA=Q
BTLA=Q
BBXR=Q
BTXR=Q
BTLXR=Q
BBYR=Q
BTYR=Q
BTLYR=Q
I=I+1
GO TO 200
75 END
```

## APPENDIX D

Description and Explanation of the IEM  
1620 Computer FORTRAN Program No. 4 for  
Determining the Concentration of Tagged  
Particles from Individual Particle Data

This computer program determines the values of IMM, IMP, IPP, and IPM from the experimental data. Figures 82 through 85 illustrate results obtained from this program. Table 15 defines the various symbols utilized in this computer code.

Table 15. Input data and variables required for  
the IEM 1620 Computer Program No. 4.

SYMBOL	EXPLANATION
JMAX	Number of time increments $\Delta t$
T(I)	Ith time increment, in seconds
JMAX	Number of time increment data for given set
D(J)	Individual time increment data in given set, J = 1 to JMAX, in seconds
POINT	Initial data pulse
INI(I)	Number of negative pulses within time increment T(I), starting with an initial negative pulse
IMP(I)	Number of positive pulses within time increment T(I), starting with an initial negative pulse
IPP(I)	Number of positive pulses within time increment T(I), starting with an initial positive pulse
IPM(I)	Number of negative pulses within time increment T(I), starting with an initial positive pulse

Input to Computer Program No. 4

The data input to Computer Program No. 4 is the output of Computer Program No. 1, along with the time increments T(I). The data input is read into the computer as FORMAT (I4, I4, 8F8.3). The time increments T(I) are read into the computer as FORMAT (I4, I4, 5E7.3).

The total number of time increments  $IMAX$  is read into the computer as  $FORMAT (I5)$ . Table 16 gives the time increments  $T(I)$  and the number of time increments  $IMAX$  used in evaluating the data sets for each distance between detector levels  $\Delta Z$ .

The first number in each set of time increments  $T(I)$  for given distances between detector levels  $\Delta Z$  is the total number of time increments  $IMAX$  for the data set. The first column below  $IMAX$  gives the IBM card number, and the second column gives the subscript  $I$  for the first time increment  $T(I)$  on the IBM card. The remaining columns give in seconds,  $T(I)$ ,  $T(I+1)$ ,  $T(I+2)$ ,  $T(I+3)$ , and  $T(I+4)$ , respectively.

Output of Computer Program No. 4

Table 17 gives the output obtained from Computer Program No. 4. The method of tabulating  $IMM$ ,  $IMP$ ,  $IPP$ , and  $IPM$  for  $\Delta Z = 1/2$  inch is indicated in Set 1.

Each row of the tabulated concentrations ( $IMM$ ,  $IMP$ ,  $IPP$ , and  $IPM$ ) gives the number of data pulses counted in the time increments  $T(I)$ ,  $T(I+1)$ ,  $T(I+2)$ ,  $T(I+3)$ , and  $T(I+4)$ , beginning with  $I = 1$ . Blank spaces in the block-tabulations of the output of each data set indicate zeros.

Table 16. Input to Computer Program No. 4.

---

IMAX						
	10					
Card	I	T(I)	T(I+1)	T(I+2)	T(I+3)	T(I+4)
1	1	0.020	0.040	0.060	0.080	0.100
2	6	0.300	0.500	1.000	2.000	3.000

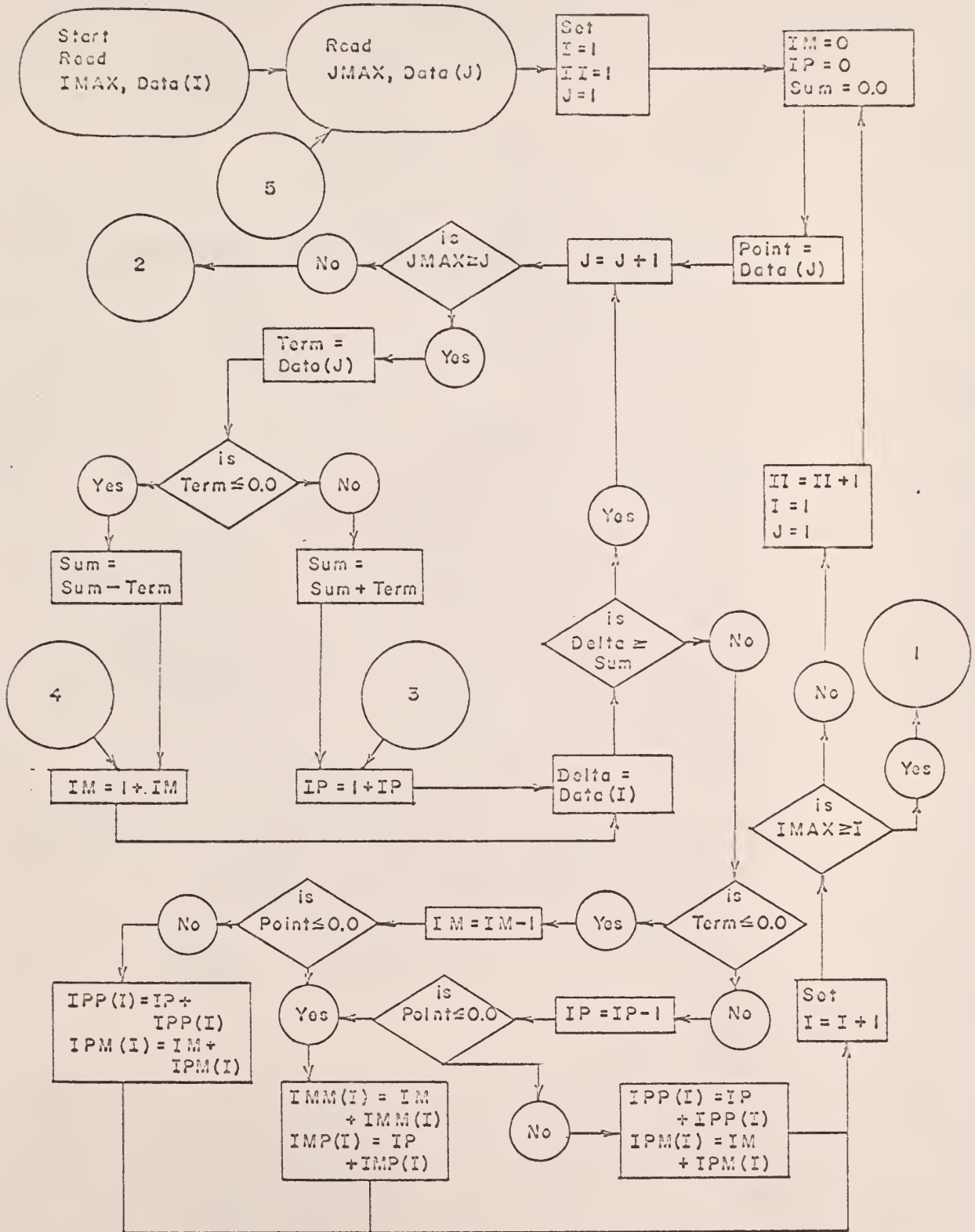
---

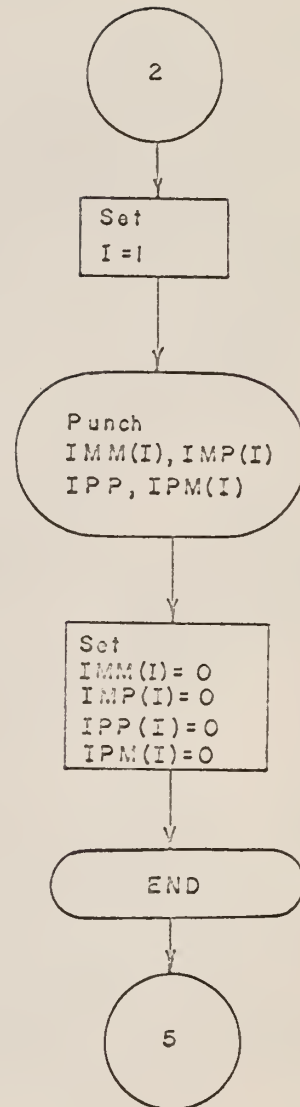
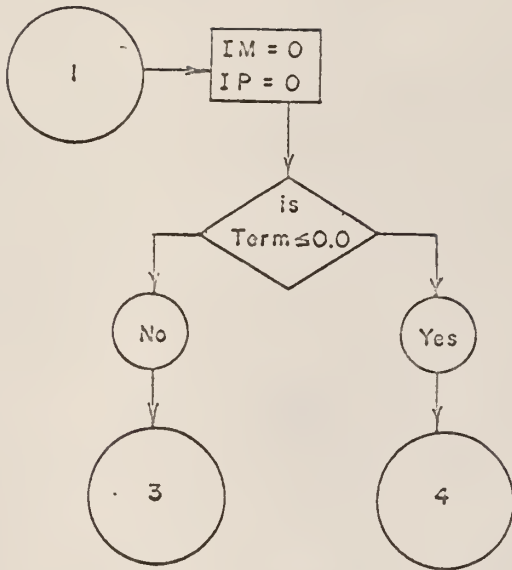
Table 17. Output of Computer Program NO. 4.

$$\Delta Z = \frac{1}{2} \text{ inch}$$

Set 1						Set 32				
	2	2	0	1	IMP	9	4	3	1	1
					IMP					3
	2	1	2	2	IPP	2	3	1	1	0
	5	0	8	5	IPM		2	2	6	10
17	29	61	80	62	IMP	21	14	31	34	36
43	32	52	71	61	IMP	52	24	25	36	30
11	18	49	76	61	IPP	21	16	21	28	42
41	24	47	83	62	IPM	52	18	21	36	42
Set 2						Set 47				
1	1	0	1	0		2	2	4	0	4
				1				4	1	0
	1	1	1	1		3	3	0	1	1
	2	1	5	7			5	3	7	8
18	25	42	55	52		15	11	24	32	18
30	27	39	50	41		42	14	29	25	25
14	21	41	71	50		10	14	27	23	26
33	15	30	77	64		33	19	26	31	20
Set 16						Set 48				
1	0	1	0	0		2	2	0	0	4
				2				5	1	2
1	0	0	0	0		3	4	4	2	1
	1	3	9	14			3	2	2	8
9	13	18	22	19		9	8	19	29	16
54	9	17	18	18		46	18	27	41	29
8	12	16	16	17		25	17	34	37	22
26	17	18	18	17		44	11	36	25	15
Set 17						Set 63				
	1	1	2	0		1	1	0	0	0
			1	5					1	2
	1	0	1	0			1	0	0	1
		1	14	14			8	11	16	9
11	14	27	39	24		10	11	21	43	34
43	14	37	32	22		51	11	21	37	34
11	17	27	33	25		4	8	20	32	31
30	17	29	32	28		13	7	23	41	36
Set 31						Set 64				
3	4	2	4	1					1	0
		3	0	0				1	0	1
4	2	0	2	0						
	3	3	4	6			6	7	12	13
20	13	28	32	26		5	11	22	36	26
38	21	31	25	24		56	13	28	35	30
9	13	21	22	7		11	15	29	43	28
26	12	22	26	11		24	13	23	39	27

Logic Diagram for Computer Program No. 4





## FORTRAN Source Program for Computer Program No. 4

```

C      PROGRAM FOR INCREMENTAL SUMMATION
      DIMENSION T(50),D(600),IMM(50),IMP(50),IPM(50),IPP(50)
101  FORMAT(I4,I4,F8.3,F8.3,F8.3,F8.3,F8.3,F8.3,F8.3,F8.3)
102  FORMAT(I4,I4,I4,I4,I4)
103  FORMAT(I5)
104  FORMAT(I4,I4,E7.3,E7.3,E7.3,E7.3,E7.3,E7.3,E7.3,E7.3)
209  READ 103,IMAX
      I=1
200  READ 104,K,L,T(I),T(I+1),T(I+2),T(I+3),T(I+4)
      I=I+5
      IF(IMAX-I)210,210,200
210  READ 103, JMAX
201  J=1
202  READ101,M,N,D(J),D(J+1),D(J+2),D(J+3),D(J+4),D(J+5),D(J+6),D(J+7)
      J=J+8
      IF(JMAX-J)203,203,202
203  I=1
      II=1
      J=1
20  IM=0
      IP=0
      SUM=0.0
1  POINT=D(J)
2  J=J+1
      IF(JMAX-J)3,3,4
4  TERM=D(J)
      IF(TERM)5,5,7
5  SUM=SUM-TERM
6  IM=1+IM
      GO TO 9
7  SUM=SUM+TERM
8  IP=1+IP
9  DELTA=T(I)
      IF(DELTA-SUM)10,2,2
10 IF(TERM)11,11,12
11 IM=IM-1
      IF(POINT)13,13,14
12 IP=IP-1
      IF(POINT)15,15,16
13 IMM(I)=IM +IMM(I)
      IMP(I)=IP +IMP(I)
      GO TO 17
14 IPM(I)=IM +IPM(I)
      IPP(I)=IP + IPP(I)
      GO TO 17

```

```
15 IMP(I)=IP +IMP(I)
   IMM(I)=IM + IMM(I)
   GO TO 17
16 IPP(I)=IP + IPP(I)
   IPM(I)=IM + IPM(I)
   GO TO 17
17 I=I+1
   IF(IMAX-I)18,19,19
18 II=II+1
   I=1
   J=II
   GO TO 20
19 IM=0
   IP=0
   IF(TERM)6,6,8
   3 I=1
400 IF(SENSE SWITCH 3)206,300
206 PRINT102,IMM(I),IMM(I+1),IMM(I+2),IMM(I+3),IMM(I+4)
   PRINT102,IMP(I),IMP(I+1),IMP(I+2),IMP(I+3),IMP(I+4)
   PRINT102,IPP(I),IPP(I+1),IPP(I+2),IPP(I+3),IPP(I+4)
   PRINT102,IPM(I),IPM(I+1),IPM(I+2),IPM(I+3),IPM(I+4)
   GO TO 500
300 PUNCH102,IMM(I),IMM(I+1),IMM(I+2),IMM(I+3),IMM(I+4)
   PUNCH102,IMP(I),IMP(I+1),IMP(I+2),IMP(I+3),IMP(I+4)
   PUNCH102,IPP(I),IPP(I+1),IPP(I+2),IPP(I+3),IPP(I+4)
   PUNCH102,IPM(I),IPM(I+1),IPM(I+2),IPM(I+3),IPM(I+4)
500 I=I+5
   IF(IMAX-I)205,400,400
205 IF (SENSE SWITCH 1) 207, 211
207 I= 1
208 IMM(I) =0
   IMP(I) =0
   IPP(I) =0
   IPM(I) =0
   I = I+1
   IF(IMAX-I)310,208,208
310 IF(SENSE SWITCH 2)209,210
211 END
```

## APPENDIX E

Description and Explanation of the IBM  
1620 Computer FORTRAN Program No. 5 for  
Calculating the Average Residence Times  
as a Function of the Number of Data Val-  
ues

This computer program determines the average time for a particle to pass from upper-to-lower and lower-to-upper detector level, as a function of the number of data values obtained.

Figures 35 and 36 are illustrations of the results obtained from this computer code. Table 18 defines the various symbols utilized in this code.

Table 18. Input data and variables required for  
the IBM 1620 Computer Program No. 5.

SYMBOL	EXPLANATION
JMAX	Number of time increment data for given set
D(J)	Individual time increment data in given set, J = 1 to JMAX, in seconds
M	Data set
N	Number of data values used to calculate average time
SUMA	Average time increment for given number of data values

After the data in each set is read into the computer, the average time increment is computed for the first five time increments, and this time is punched as output along with the data set N. Then the number of data values N is increased by five, and the process is repeated. N is continuously increased by increments of five until all of the data in the set has been used. The program then continues to the next set of data.

A similar code, Computer Program No. 6, computes, as a function of the number of data values, the variance in the time to pass from one detector level to the other. The input and output of Computer Program No. 6 is included in this appendix.

#### Input to Computer Program No. 5

The input to Computer Program No. 5 is the output of Computer Program No. 3, obtained with Sense Switch 1 ON and Sense Switch 2 OFF. The input is read into the computer as FORMAT (I4, I4, E7.4).

#### Output of Computer Program No. 5

The output of Computer Program No. 5 is given in Table 19. M is the residence times set, where odd-numbered values of M give the residence times between the two detector levels when the tagged particle passed from the lower to the upper detector level, and even-numbered values of M give the residence times between the two detector levels when the tagged particle passed from the upper to the lower detector level. N gives the number of residence time values, in order of appearance in the residence times set, that were used to compute the average residence time SUMA.

#### Input to Computer Program No. 6

The input to Computer Program No. 6 is the output of Computer Program No. 3, obtained with Sense Switch 1 ON and Sense Switch 2 OFF. The input is read into the computer as FORMAT (I4, I4, E7.4).

Table 19. Output of Computer Program No. 5

M	N	AVERAGE	M	N	AVERAGE
1	5	.14640000	6	5	.47620000
1	10	.12710000	6	10	.44430000
1	15	.13086666	6	15	.41813333
1	20	.12895000	6	20	.42895000
1	25	.12576000	6	25	.40332000
1	30	.13123333	6	30	.38133330
1	35	.13054285	6	35	.40297140
1	40	.13067500	6	36	.40300000
1	45	.12664444			
1	50	.12712000	7	5	.14900000
1	52	.12617307	7	10	.18540000
			7	15	.17100000
2	5	.24080000	7	20	.18820000
2	10	.19550000	7	25	.19048000
2	15	.19240000	7	30	.19356666
2	20	.20505000	7	33	.19090909
2	25	.20260000			
2	30	.20460000	8	5	.38880000
2	35	.21314285	8	10	.37430000
2	40	.21632500	8	15	.32866666
2	45	.21602222	8	20	.30215000
2	50	.21616000	8	25	.30568000
2	53	.21469810	8	30	.31150000
			8	34	.32000000
3	5	.10320000			
3	10	.10950000	9	5	.27100000
3	15	.09900000	9	10	.35760000
3	20	.10100000	9	15	.38400000
3	25	.10308000	9	20	.36295000
3	30	.10353333	9	25	.35332000
3	35	.10348571	9	30	.37343330
3	36	.10219444			
			10	5	.61640000
4	5	.26920000	10	10	.60630000
4	10	.25860000	10	15	.65160000
4	15	.23886666	10	20	.71670000
4	20	.24155000	10	25	.70312000
4	25	.23120000	10	30	.70056660
4	30	.22920000	10	33	.69724240
4	35	.23600000			
4	40	.23900000	11	5	.31280000
4	42	.23950000	11	10	.31550000
			11	15	.41646666
5	5	.31620000	11	17	.44470588
5	10	.25930000			
5	15	.26113333			
5	20	.24760000			
5	25	.23996000			
5	30	.24480000			
5	35	.23648571			
5	38	.23676315			

Output of Computer Program No. 6

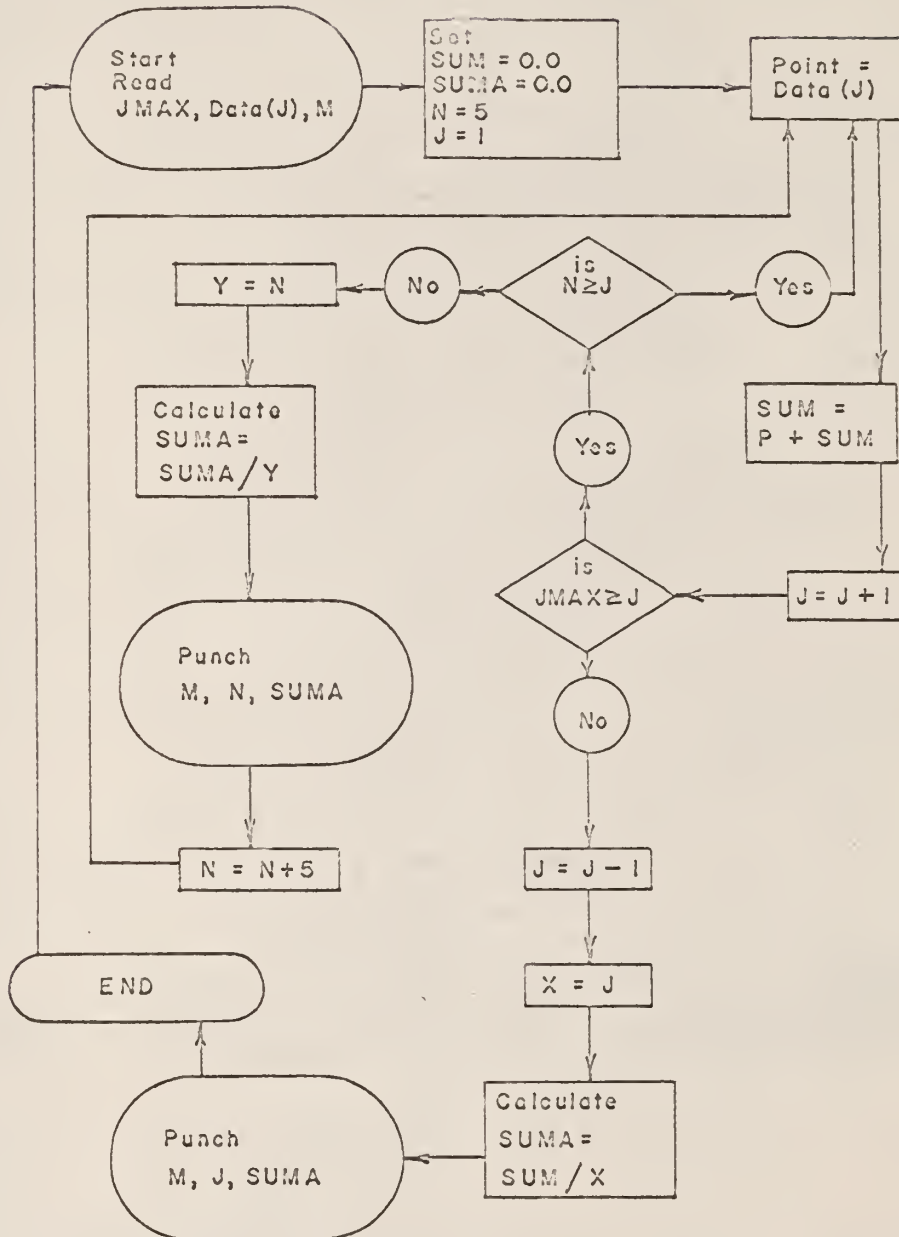
The output of Computer Program No. 6 is given in Table 20, where  $M$  and  $N$  are defined as given in the output of Computer Program No. 5. The variance SIGSQ for the number of residence time values  $N$  is tabulated.

Figures 37 and 38 give illustrations of the variance of the residence times as a function of the number of residence time values  $N$  used to calculate the variance.

Table 20. Output of Computer Program No. 6

M	N	VARIANCE	M	N	VARIANCE
1	5	.00497780	6	5	.02674370
1	10	.00566743	6	10	.02183445
1	15	.00383783	6	15	.02643670
1	20	.00355268	6	20	.02732668
1	25	.00285785	6	25	.02697500
1	30	.00387735	6	30	.02514906
1	35	.00403537	6	35	.02945702
1	40	.00423863	6	36	.02861545
1	45	.00451023	7	5	.00185050
1	50	.00460018	7	10	.00706648
1	52	.00444430	7	15	.00657771
2	5	.00883770	7	20	.00656922
2	10	.00664961	7	25	.00584151
2	15	.00457854	7	30	.00593418
2	20	.00574773	7	33	.00578783
2	25	.00569958	8	5	.01336320
2	30	.00630873	8	10	.01079690
2	35	.00682906	8	15	.01204910
2	40	.00734109	8	20	.01170592
2	45	.00691202	8	25	.01198522
2	50	.00731528	8	30	.01035315
2	53	.00699130	8	34	.00985727
3	5	.00099970	9	5	.01566250
3	10	.00093561	9	10	.02385093
3	15	.00192171	9	15	.02241500
3	20	.00146221	9	20	.02592131
3	25	.00122699	9	25	.02347464
3	30	.00139274	9	30	.02610034
3	35	.00132149	10	5	.03795480
3	36	.00134376	10	10	.05159001
4	5	.01185770	10	15	.09939740
4	10	.00799137	10	20	.11630368
4	15	.00731055	10	25	.10579545
4	20	.00883668	10	30	.10401558
4	25	.00876775	10	33	.09838428
4	30	.00896375	11	5	.01233220
4	35	.00892323	11	10	.01589516
4	40	.00886307	11	15	.03829427
4	42	.00863880	11	17	.04332747
5	5	.03651370	12	5	.03045280
5	10	.02399801	12	10	.08997445
5	15	.01810298	12	15	.20039528
5	20	.01614593	12	18	.21487758
5	25	.01448070	13	5	.06378475
5	30	.01779409	13	10	.08850244
5	35	.01688796	13	15	.09570440
5	38	.01787921	14	5	.05018050
			14	10	.08023684
			14	15	.09274085
			14	17	.14066187

## Logic Diagram for Computer Program No. 5



## FORTRAN Source Program for Computer Program No. 5

```
C PROGRAM FOR COMPUTING THE AVERAGE TIME AS A FUNCTION OF THE
C NUMBER OF DATA POINTS FOR THE BOTTOM TO TOP AND TOP TO BOTTOM DATA
  DIMENSION D(300)
101 FORMAT(I4,I4,E7.4)
102 FORMAT(I5)
103 FORMAT(I5,I5,F15.8)
  I=1
200 READ 102,JMAX
  J=1
201 READ 101,M,N,D(J)
  J=J+1
  IF(JMAX-J)1,201,201
  1 J=1
  SUM=0.0
  SUMA=(.0
  N=5
  2 P=D(J)
  SUM=P+SUM
  J=J+1
  IF(JMAX-J)5,3,3
  3 IF(N-J)4,2,2
  4 Y=N
  SUMA=SUM/Y
  PUNCH 103,M,N,SUMA
  N=N+5
  GO TO 2
  5 J=J-1
  X=J
  SUMA=SUM/X
  PUNCH 103,M,J,SUMA
  I=I+1
  GO TO 200
  END
```

## FORTRAN Source Program for Computer Program No. 6

```
C      PROGRAM FOR COMPUTING THE VARIANCE IN THE
C      AVERAGE TIME AS A FUNCTION OF THE NUMBER
C      OF DATA POINTS FOR THE BOTTOM TO TOP AND
C      TOP TO BOTTOM DATA
      DIMENSION D(300)
101  FORMAT(I4,I4,E7.4)
102  FORMAT(I5)
103  FORMAT(I5,I5,F15.8)
200  READ 102,JMAX
      DO 201 J=1,JMAX
201  READ 101,M,N,D(J)
      1  J=1
          SUM=0.0
          SUMSQ=0.0
          SIGSQ=0.0
          N=5
      2  P=D(J)
          Q=(D(J)**2)
          SUM=P+SUM
          SUMSQ=Q+SUMSQ
          J=J+1
          IF(JMAX-J)5,3,3
      3  IF(N-J)4,2,2
      4  Y=N
          SIGSQ=(SUMSQ-((SUM**2)/Y))/(Y-1.0)
          PUNCH 103,M,N,SIGSQ
          N=N+5
          GO TO 2
      5  J=J-1
          X=J
          SIGSQ=(SUMSQ-((SUM**2)/X))/(X-1.0)
          PUNCH 103,M,J,SIGSQ
          GO TO 200
      END
```

## APPENDIX F

Description and Explanation of the IBM 1620 Computer FORTRAN Program No. 7 for Computing the Average Time, the Most Probable Time, the Variance, and the Gamma Distribution Parameters  $p$  and  $\nu$  of the Residence Times Data

This computer program was written to determine the average time, the most probable time, the variance, and the gamma distribution parameters  $p$  and  $\nu$  for the experimental times obtained when the tagged particle passed from one detector level to the other, moving both upward and downward. Table 21 defines the various symbols utilized in this computer code.

Table 21. Input data and variables required for the IBM 1620 Computer Program No. 7.

SYMBOL	EXPLANATION
JMAX	Number of time increment data for given set
D(J)	Individual time increment data in given set, $J = 1$ to JMAX, in seconds
M, P	Data set, Number of data in set
BA	Average time for data set
PR and V	Gamma distribution parameters $p$ and $\nu$
TP	Most probable time
P	Number of time increment data for given set

A similar code, Computer Program No. 8, computes the average speed, the variance of the average speed, and the gamma distribution parameters  $p$  and  $\nu$ , based upon the Residence Times data. The input and output of Computer Program No. 8 is included in this appendix.

Input to Computer Program No. 7

The input to Computer Program No. 7 is the output of Computer Program No. 3, obtained with Sense Switch 1 ON and Sense Switch 2 OFF. The input is read into the computer as FORMAT (I4, I4, E7.4).

Output of Computer Program No. 7

The output of Computer Program No. 7 is given in Table 22. Input data information tabulated in Table 22 are as follows. The set number M, as explained in the output section of Computer Program No. 5 in Appendix E, is given for each Residence Times set, 1 to 152. The distance between the detector levels (WIDTH) and the water flow rate (INCHES MERCURY) are also given.

Tabulated outputs for each Residence Times set are as follows.

Average residence time (AVERAGE TIME)

Most probable residence time (MOST PROBABLE TIME)

Gamma distribution parameters  $p$  and  $\nu$  (PR & V)

Variance of the residence times (SIGMA SQ)

Speed of the tagged particle based upon the average residence time (VELOCITY BASED ON T AVG)

Speed of the tagged particle based upon the most probable residence time (VELOCITY BASED ON T PROB)

Input to Computer Program No. 8

The input to Computer Program No. 8 is the output of Computer Program No. 3, obtained with Sense Switch 1 ON and Sense Switch 2 OFF. The input is read into the computer as FORMAT (I4, I4, F7.3).

Table 22. Output of Computer Program No. 7

SET NO	1	52. DATA POINTS		
WIDTH=	.50000000		INCHES MERCURY=	2.50000000
SIGMA SQ=	.00444430	V=	.0322383	PR= 3.58203600
AVERAGE TIME=	.12617307		MOST PROBABLE TIME=	.09094922
VELOCITY BASED ON T AVG =			2.96281070	STD DEV= 2.09381510
VELOCITY BASED ON T PROB=			5.49757300	STD DEV= 4.02970900
SET NO	2	53. DATA POINTS		
WIDTH=	.50000000		INCHES MERCURY=	2.50000000
SIGMA SQ=	.00699128	V=	.03256334	PR= 6.59324400
AVERAGE TIME=	.21469810		MOST PROBABLE TIME=	.18213472
VELOCITY BASED ON T AVG =			2.32885150	STD DEV= .90696840
VELOCITY BASED ON T PROB=			2.74522060	STD DEV= 1.26026860
SET NO	3	36. DATA POINTS		
WIDTH=	.50000000		INCHES MERCURY=	2.50000000
SIGMA SQ=	.00134376	V=	.01314905	PR= 7.77199600
AVERAGE TIME=	.10219444		MOST PROBABLE TIME=	.08904536
VELOCITY BASED ON T AVG =			4.89263400	STD DEV= 1.75499710
VELOCITY BASED ON T PROB=			5.61511500	STD DEV= 2.31157600
SET NO	4	42. DATA POINTS		
WIDTH=	.50000000		INCHES MERCURY=	2.50000000
SIGMA SQ=	.00863879	V=	.03607011	PR= 6.63984600
AVERAGE TIME=	.23950000		MOST PROBABLE TIME=	.20342988
VELOCITY BASED ON T AVG =			2.08768260	STD DEV= .81018730
VELOCITY BASED ON T PROB=			2.45784930	STD DEV= 1.12296700
SET NO	5	38. DATA POINTS		
WIDTH=	1.00000000		INCHES MERCURY=	2.50000000
SIGMA SQ=	.01787920	V=	.07551516	PR= 3.13530600
AVERAGE TIME=	.23676315		MOST PROBABLE TIME=	.16124797
VELOCITY BASED ON T AVG =			4.22363000	STD DEV= 2.38531500
VELOCITY BASED ON T PROB=			6.20162800	STD DEV= 5.14263300
SET NO	6	36. DATA POINTS		
WIDTH=	1.00000000		INCHES MERCURY=	2.50000000
SIGMA SQ=	.02861542	V=	.07100600	PR= 5.67557600
AVERAGE TIME=	.40300000		MOST PROBABLE TIME=	.33199395
VELOCITY BASED ON T AVG =			2.48138900	STD DEV= 1.04157350
VELOCITY BASED ON T PROB=			3.01210300	STD DEV= 1.53475730
SET NO	7	33. DATA POINTS		
WIDTH=	1.00000000		INCHES MERCURY=	2.50000000
SIGMA SQ=	.00578783	V=	.03031721	PR= 6.29705200
AVERAGE TIME=	.19090909		MOST PROBABLE TIME=	.16059186
VELOCITY BASED ON T AVG =			5.23809500	STD DEV= 2.08739540
VELOCITY BASED ON T PROB=			6.22696500	STD DEV= 2.94992450

---

Output of Computer Program No. 8

The output of Computer Program No 8 is given in Table 23.

Tabulated outputs for each residence times set are as follows.

Average residence time (AVERAGE TIME)

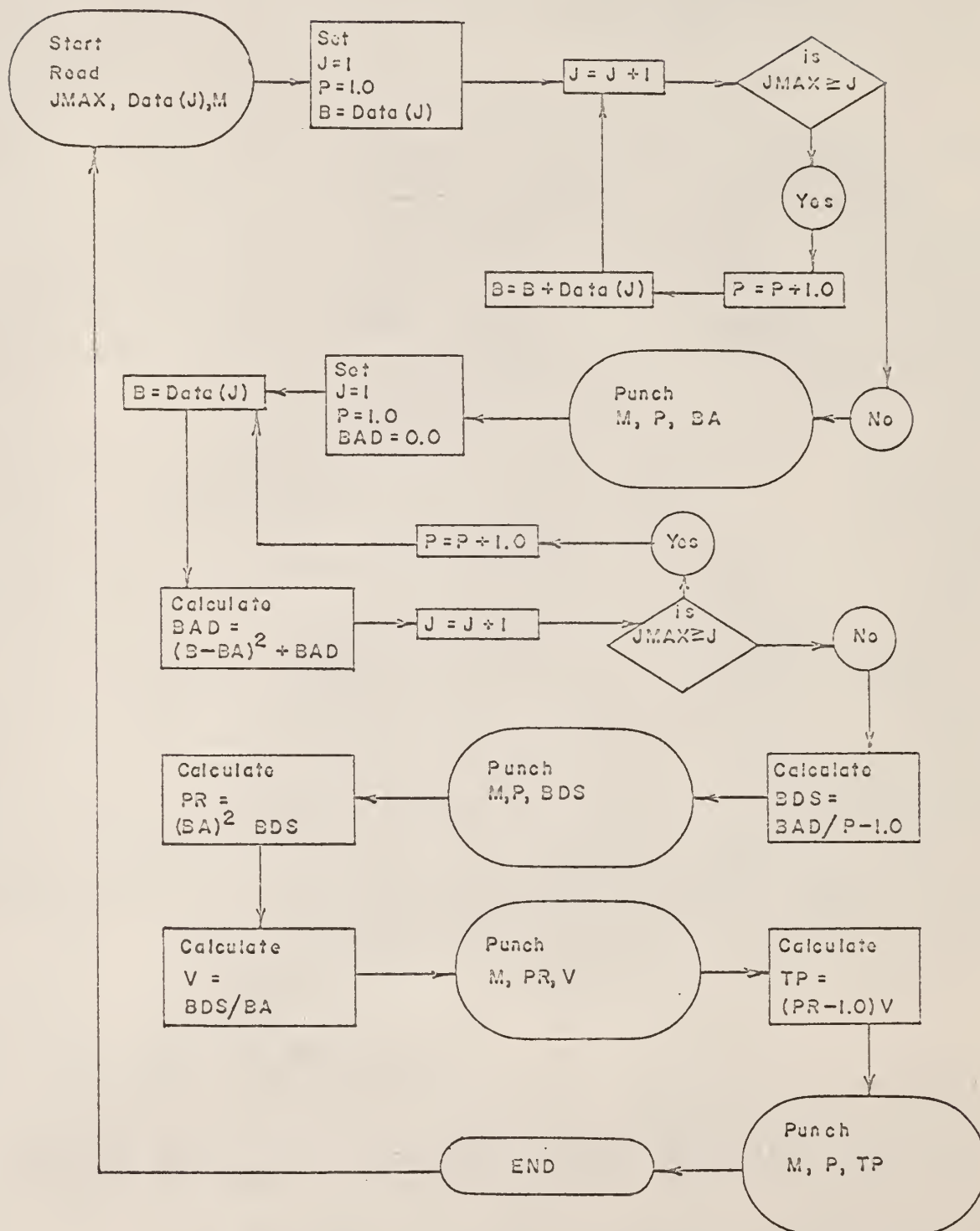
Average particle speed (AVERAGE VEL)

Gamma distribution parameters  $p$  and  $\nu$  (PR & V)

Table 23. Output of Computer Program No. 8

SET NO=	1	52.DATA POINTS		
WIDTH =	.50	INCHES MERCURY=	2.50	
V=	6.08539890	PR=	1.83531000	SGIMA SQ= 67.96605000
AVERAGE TIME=	11.16870900			STD DEV= 8.24415240
AVERAGE VEL=	5.58435450			STD DEV= 6.72964110
SET NO=	2	53.DATA POINTS		
WIDTH =	.50	INCHES MERCURY=	2.50	
V=	.63094580	PR=	8.42853800	SGIMA SQ= 3.35534000
AVERAGE TIME=	5.31795200			STD DEV= 1.83175870
AVERAGE VEL=	2.65897600			STD DEV= .32901816
SET NO=	3	36.DATA POINTS		
WIDTH =	.50	INCHES MERCURY=	2.50	
V=	4.15123330	PR=	2.83539000	SGIMA SQ= 48.86154000
AVERAGE TIME=	11.77036700			STD DEV= 6.99010300
AVERAGE VEL=	5.88518350			STD DEV= 5.84007100
SET NO=	4	42.DATA POINTS		
WIDTH =	.50	INCHES MERCURY=	2.50	
V=	.91904040	PR=	5.34654300	SGIMA SQ= 4.51588000
AVERAGE TIME=	4.91369000			STD DEV= 2.12505990
AVERAGE VEL=	2.45684500			STD DEV= .49869549
SET NO=	5	38.DATA POINTS		
WIDTH =	1.00	INCHES MERCURY=	2.50	
V=	1.32273230	PR=	4.21963300	SGIMA SQ= 7.38275900
AVERAGE TIME=	5.58144600			STD DEV= 2.71712320
AVERAGE VEL=	5.58144600			STD DEV= 1.21371800
SET NO=	6	36.DATA POINTS		
WIDTH =	1.00	INCHES MERCURY=	2.50	
V=	.56442770	PR=	5.24892170	SGIMA SQ= 1.67219450
AVERAGE TIME=	2.96263700			STD DEV= 1.29313350
AVERAGE VEL=	2.96263700			STD DEV= .28265245
SET NO=	7	33.DATA POINTS		
WIDTH =	1.00	INCHES MERCURY=	2.50	
V=	1.29299850	PR=	4.82538400	SGIMA SQ= 8.06729600
AVERAGE TIME=	6.23921500			STD DEV= 2.84029850
AVERAGE VEL=	6.23921500			STD DEV= 1.42610990
SET NO=	8	34.DATA POINTS		
WIDTH =	1.00	INCHES MERCURY=	2.50	
V=	.39266850	PR=	8.79659700	SGIMA SQ= 1.35633480
AVERAGE TIME=	3.45414700			STD DEV= 1.16461730
AVERAGE VEL=	3.45414700			STD DEV= .23610753
SET NO=	9	30.DATA POINTS		
WIDTH =	1.00	INCHES MERCURY=	2.50	
V=	.88564100	PR=	3.76749400	SGIMA SQ= 2.95507240
AVERAGE TIME=	3.33664800			STD DEV= 1.71903240
AVERAGE VEL=	3.33664800			STD DEV= .54874316
SET NO=	10	33.DATA POINTS		
WIDTH =	1.00	INCHES MERCURY=	2.50	
V=	.49079219	PR=	3.65043500	SGIMA SQ= .87930590
AVERAGE TIME=	1.79160530			STD DEV= .93771312
AVERAGE VEL=	1.79160530			STD DEV= .15544078

## Logic Diagram for Computer Program No. 7



## FORTRAN Source Program for Computer Program No. 7

C PROGRAM FOR MU, SIGMA SQUARED, P, NU, AND TP

DIMENSION D(300)

101 FORMAT (I4, I4, E7.4)

102 FORMAT (I5)

103 FORMAT(I4,F15.8,F15.8)

I = 1

200 READ 102, JMAX

J = 1

201 READ 101, M, N, D(J)

J = J + 1

IF (JMAX-J) 202, 201, 201

202 J = 1

P = 1.0

B = D(J)

1 J = J + 1

IF (JMAX-J) 3, 2, 2

2 P = P + 1.0

B=B+D(J)

GO TO 1

3 BA=B/P

IF (SENSE SWITCH 3) 4, 5.

4 PRINT 103, M, P, BA

GO TO 6

5 PUNCH 103, M, P, BA

6 J=1

P=1.0

BAD=0.0

7 B=D(J)

BAD=(B-BA)\*\*2+BAD

J=J+1

IF (JMAX-J) 9, 8, 8

8 P=P+1.0

GO TO 7

9 BDS=BAD/(P-1.0)

IF (SENSE SWITCH 3) 10, 11

10 PRINT 103, M, P, BDS

GO TO 12

11 PUNCH 103, M, P, BDS

12 PR=(BA)\*\*2/(BDS)

V=(BDS)/(BA)

IF (SENSE SWITCH 3) 13, 14

13 PRINT 103, M, PR, V

GO TO 15

14 PUNCH 103, M, PR, V

15 TP=(PR-1.0)\*V

IF (SENSE SWITCH 3) 16, 17

16 PRINT 103, M, P, TP

GO TO 18

17 PUNCH 103, M, P, TP

18 I=I+1

GO TO 200

END

## FORTRAN Source Program for Computer Program No. 8

```
DIMENSION D(150)
101 FORMAT(I4,I4,F7.3)
102 FORMAT(I5)
103 FORMAT(E10.4,E10.4)
  1 FORMAT(7HSET NC=I5,10XF4.0,11HDATA POINTS)
  2 FORMAT(7HWIDTH =F5.2,4X15HINCHES MERCURY=F6.2)
  3 FORMAT(2HV=F15.8,5H PR=F15.8,11H SGIMA SQ=F15.8)
  4 FORMAT(13HAVERAGE TIME=F15.8,14X8HSTD DEV=F15.8)
  5 FORMAT(13HAVERAGE VEL= F15.8,14X8HSTD DEV=F15.8)
  READ 102,K
105 READ 103,CL,VELW
  READ 102,JMAX
  DO 700 J=1,JMAX
700 READ 101,M,N,D(J)
  SUM1=0.0
  SUM=0.0
  DO 800 J=1,JMAX
  D(J)=1.0/D(J)
  SUM=SUM+D(J)
800 SUM1=SUM1+D(J)**2
  CN=JMAX
  SGSQ=(SUM1-(SUM**2)/CN)/(CN-1.0)
  STDD1=SQRT(SGSQ)
  AVG=SUM/CN
  PR=(AVG**2)/SGSQ
  V=SGSQ/AVG
  VEL=CL*AVG
  STDD2=SQRT(CL*(SGSQ**2)/(CN-1.0))
  PUNCH 1,K,CN
  PUNCH 2,CL,VELW
  PUNCH 3,V,PR,SGSQ
  PUNCH 4,AVG,STDD1
  PUNCH 5,VEL,STDD2
  K=K+1
  GO TO 105
END
```

## APPENDIX G

Description and Explanation of the IBM  
1620 Computer FORTRAN Program No. 9 for  
Calculating the T Statistic for Given  
Gamma Distribution Parameters  $p$  and  $\nu$

This program determines  $T$ , the upper limit in the integral

$$\int_0^T f(t) dt = A$$

where  $A$  is the area under the distribution  $f(t)$  integrated from 0 to  $T$ .

Table 24 defines the various symbols utilized in this computer code.

Table 24. Input data and variables required for  
the IBM 1620 Computer Program No. 9.

SYMBOL	EXPLANATION
KMAX	Order of Gaussian quadrature used in the program
A(K)	Christoffel Numbers for the order of Gaussian quadrature used in the program
X(K)	Zeros of the Legendre polynomial of degree KMAX
V	Parameter $\nu$ of the gamma distribution
N	Parameter $p$ of the gamma distribution
T	Upper time limit of the integral
GAMAP	The gamma function $\Gamma(p)$
Y	The value of the integral for given V, N, and T

Input to Computer Program No. 9

The input to Computer Program No. 9 is given in Table 25. The order of Gaussian quadrature KMAX is read into the computer as FORMAT (I5). The Christoffel numbers A(K) are read in as FORMAT (E15.8). The zeros of the Legendre polynomial of degree KMAX is read in as FORMAT (E15.8). The

Table 25. Input to Computer Program No. 9

KMAX

5

A(K)

.47862867  
 .23692688  
 .56888889  
 .23692688  
 .47862867

X(K)

.53846931  
 .90617985  
 .00000000  
 .90617985  
 .53846931

V	N	T	GAMAP
.01	1	0.01	1.0
.01	1	0.02	1.0
.01	1	0.03	1.0
.05	1	0.05	1.0
.05	1	0.10	1.0
.05	1	0.20	1.0
.10	1	0.10	1.0
.10	1	0.20	1.0
.10	1	0.30	1.0
.20	1	0.40	1.0
.20	1	0.50	1.0
.20	1	0.60	1.0
.30	1	0.60	1.0
.30	1	0.70	1.0
.30	1	0.80	1.0
.40	1	0.80	1.0
.40	1	0.90	1.0
.40	1	1.10	1.0
.50	1	1.00	1.0
.50	1	1.10	1.0
.50	1	1.30	1.0

---

parameter  $\nu$  of the gamma distribution (V), the parameter  $p$  of the gamma distribution (N), the T statistic, and the gamma function GAMAP are read into the computer as FORMAT (E10.4, I5, E10.4, E15.8).

Output of Computer Program No. 9

The output of Computer Program No. 9 is given in Table 26, where Y is the value of the integral

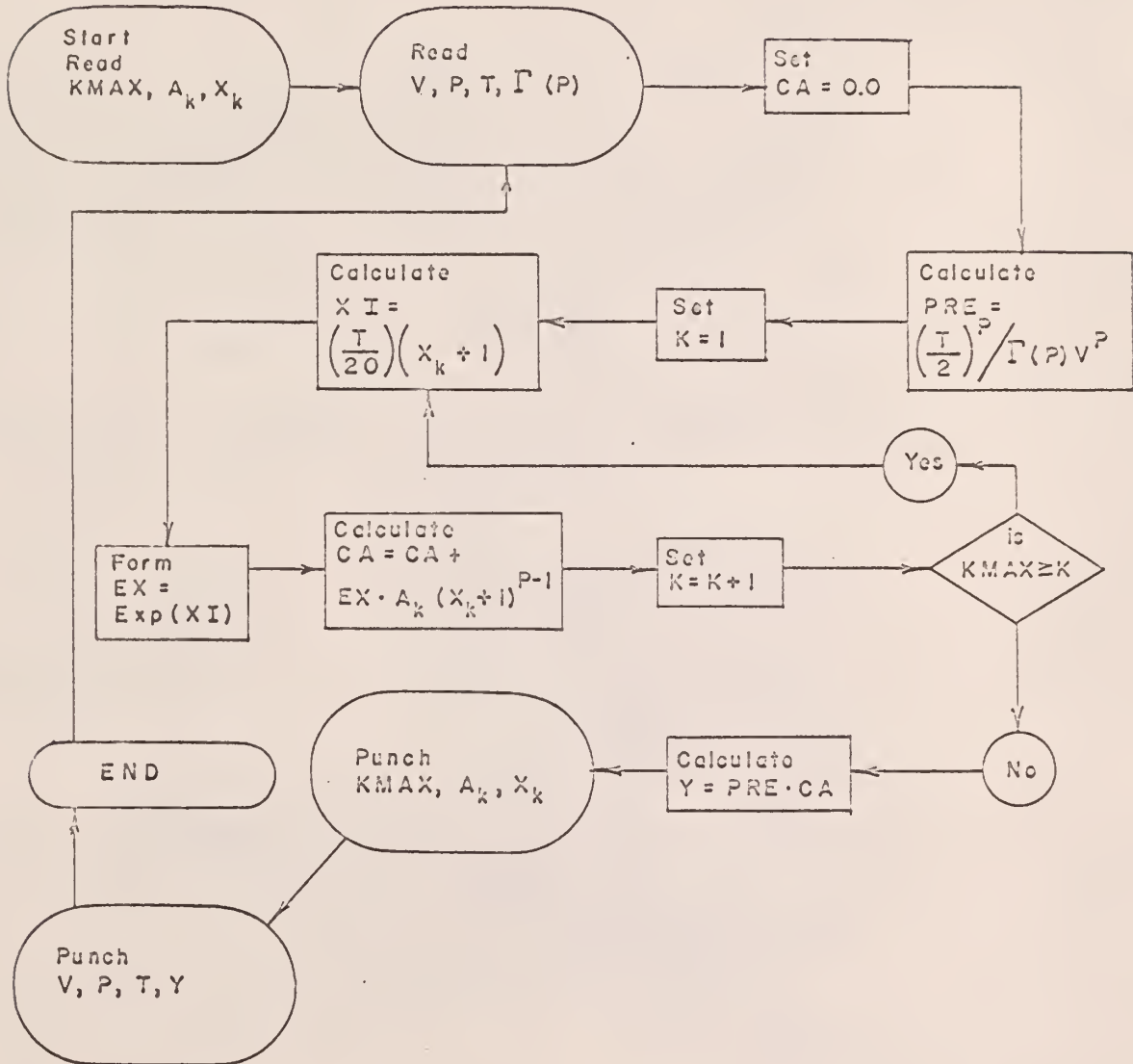
$$\int_0^T f(t) dt = Y$$

for given V, N, and T.

Table 26. Output of Computer Program No. 9

V	N	T	Y
.1000E-01	1	.1000E-01	.63212045E-00
.1000E-01	1	.2000E-01	.86466460E-00
.1000E-01	1	.3000E-01	.95021280E-00
.5000E-01	1	.5000E-01	.63212045E-00
.5000E-01	1	.1000E-00	.86466460E-00
.5000E-01	1	.2000E-00	.98168386E-00
.1000E-00	1	.1000E-00	.63212045E-00
.1000E-00	1	.2000E-00	.86466460E-00
.1000E-00	1	.3000E-00	.95021280E-00
.2000E-00	1	.4000E-00	.86466460E-00
.2000E-00	1	.5000E-00	.91791491E-00
.2000E-00	1	.6000E-00	.95021280E-00
.3000E-00	1	.6000E-00	.86466460E-00
.3000E-00	1	.7000E-00	.90302786E-00
.3000E-00	1	.8000E-00	.93051638E-00
.4000E-00	1	.8000E-00	.86466460E-00
.4000E-00	1	.9000E-00	.89460063E-00
.4000E-00	1	.1100E+01	.93607194E-00
.5000E-00	1	.1000E+01	.86466460E-00
.5000E-00	1	.1100E+01	.88919667E-00
.5000E-00	1	.1300E+01	.92572626E-00
.6000E-00	1	.1200E+01	.86466460E-00
.6000E-00	1	.1300E+01	.88544102E-00
.6000E-00	1	.1800E+01	.95021280E-00
.7000E-00	1	.1400E+01	.86466460E-00
.7000E-00	1	.1500E+01	.88268068E-00
.7000E-00	1	.2000E+01	.94256696E-00
.8000E-00	1	.1600E+01	.86466460E-00
.8000E-00	1	.1700E+01	.88056690E-00
.8000E-00	1	.2500E+01	.95606291E-00
.9000E-00	1	.1800E+01	.86466460E-00
.9000E-00	1	.1900E+01	.87889649E-00
.9000E-00	1	.3000E+01	.96432545E-00
.1000E+01	1	.2000E+01	.86466460E-00
.1000E+01	1	.2500E+01	.91791491E-00
.1000E+01	1	.3000E+01	.95021280E-00
.1000E-01	2	.3000E-01	.80085175E-00
.1000E-01	2	.4000E-01	.90842348E-00
.1000E-01	2	.5000E-01	.95958613E-00
.5000E-01	2	.1000E-00	.59399408E-00
.5000E-01	2	.2000E-00	.90842348E-00
.5000E-01	2	.3000E-00	.98271180E-00
.1000E-00	2	.3000E-00	.80085175E-00
.1000E-00	2	.4000E-00	.90842348E-00
.1000E-00	2	.5000E-00	.95958613E-00
.2000E-00	2	.8000E-00	.90842348E-00

## Logic Diagram for Computer Program No. 9



## FORTRAN Source Program for Computer Program No. 9

```

C   PROGRAM FOR GAUSSIAN QUADRATURE
      DIMENSION A(6),X(6)
101  FORMAT(E15.8)
103  FORMAT(I5)
104  FORMAT(E10.4,I5,E10.4,E15.8)
105  FORMAT(E10.4,E10.4,E10.4,E10.4,E10.4,E10.4)
200  READ 103,KMAX
      PRINT 103,KMAX
      K=1
201  READ 101,A(K)
      PRINT 101,A(K)
      K=K+1
      IF(KMAX-K)202,201,201
202  K=1
203  READ101,X(K)
      PRINT 101,X(K)
      K=K+1
      IF(KMAX-K)204,203,203
204  READ 104,V,N,T,GAMAP
      CA=0.0
      PRE=((T/2.0)**N)/((GAMAP)*(V)**N)
1   K=1
2   XI=-(T/(2.0*V))*(X(K)+1.0)
      EX=EXP(XI)
      CA=(A(K)*((X(K)+1.0)**(N-1))*EX)+CA
      K=K+1
      IF(KMAX-K)3,2,2
3   Y=PRE*CA
      IF(SENSE SWITCH 3)4,5
4   PRINT 104,V,N,T,Y
      GO TO 204
5   PUNCH 104,V,N,T,Y
      GO TO 204
      END

```

## APPENDIX H

Discussion of the Gaussian Quadrature  
Approximation of the Gamma Distribution

Certain required integrations are of such complexity that direct integrations are not feasible. It is, therefore, necessary to fit the data with empirical expressions and solve them by formal analytical methods. Such a technique is commonly known as numerical integration. The general procedure tabulates values of the ordinate  $y$  at  $n$  predetermined values of  $x$ . The integral over the region is then the sum of the products of the ordinate  $y$  multiplied by the difference in the integration limits of  $x$ ,

$$\int_b^a f(x) dx = a_1 y(x_1) + a_2 y(x_2) + \dots + a_n y(x_n) + E(x) \quad (1H)$$

where  $E(x)$  is the error resulting from the replacement of  $x$  with a polynomial approximation.

Gauss utilized unequal spacings of specific values of  $x_i$  to use in equation (1H). The technique developed is simple to use, is more accurate than the well-known equal-interval numerical integration formulas, and is well-suited for digital computation. The method is generally known as Gaussian quadrature.(1,2).

Lapidus (6) presents an excellent discussion of the derivation of the technique of Gaussian quadrature numerical integration. Highlights of his discussion are as follows:

Certain properties of orthogonal functions should first be presented. A pair of real functions is said to be orthogonal over a region with respect

to a weighting function  $w(x)$  if

$$\int_a^b w(x) g_n(x) g_m(x) dx = 0, \quad n \neq m; \quad (2H)$$

$$= C_n, \quad n = m.$$

By proper choice of constants involved in  $g_n(x)$  and  $w(x)$ ,

$$C_n = 1.0. \quad (3H)$$

Functions of the first kind and degree  $n$  which are solutions of Legendre's equation

$$(1-x^2)y'' - 2xy' + n(n+1)y = 0 \quad (4H)$$

are known as the Legendre polynomials, indicated symbolically as  $P_n(x)$ .

The Legendre polynomials are orthogonal in the interval  $(-1, 1)$  when  $w(x) = 1.0$ .

$$\int_{-1}^1 P_n(x) P_m(x) dx = 0, \quad n \neq m; \quad (5H)$$

$$= 2/(2n+1), \quad n = m; \quad n, m = 0, 1, 2, \dots$$

$P_n(x)$  is orthogonal to any polynomial of degree less than  $n$ , since  $P_n(x)$  is a polynomial.

$$\int_{-1}^1 P_n(x) x^m dx = 0, \quad m = 0, 1, 2, \dots, n-1. \quad (6H)$$

Going back to Equation 1H,  $\int_a^b f(x) dx$  will be exact if  $f(x)$  is a degree of  $2n-1$  or less. This is because there are  $2n$  coefficients,  $a_k$  and  $x_k$ , to be determined.

Choosing  $f(x)$  to have the form

$$f(x) = x^r P_N(x), \quad r = 0, 1, \dots, N-1, \quad (7H)$$

$P_N(x)$  is the Legendre polynomial of degree  $N$ .

If  $P_N(x_k) = 0$  for  $k = 1, 2, \dots, N$ ;  $x_k$  must be the roots of the Legendre polynomial of degree  $N$ .

Choose the polynomial  $f(x)$  to be 0 at  $x = x_1, x_2, \dots, x_N$ ; except at  $x_k$  where it has the value 1.0.

One polynomial of degree  $N-1$  which fits the  $N$  points is

$$f(x) = \sum_{k=1}^N \frac{P_N(x)y(x_k)}{(x-x_k)P_N'(x_k)} \quad (8H)$$

If, however,  $f(x)$  is a polynomial of degree  $2N-1$  or less, it is possible to write

$$f(x) = \sum_{k=1}^N \frac{P_N(x)y(x_k)}{(x-x_k)P_N'(x_k)} + P_N(x)x^m \quad (9H)$$

Integrating both sides between  $a$  and  $b$ ,

$$\int_a^b f(x) dx = \sum_{k=1}^N a_k y(x_k) + E(x) \quad (10H)$$

Thus;

$$a_k = \int_a^b \frac{P_N(x) dx}{(x-x_k)P_N'(x_k)} \quad (11H)$$

$$E(x) = \int_a^b P_N(x)x^m dx \quad (12H)$$

If  $E(x) = 0$ , then this representation will be exact for  $f(x)$  being a polynomial of degree  $2N-1$  or less. Recalling that if  $(a, b) = (-1, 1)$ ,

$$E(x) = \int_{-1}^1 P_N(x)x^m dx = 0, \quad m = 1, 2, 3, \dots, N-1.$$

Therefore

$$\int_{-1}^1 f(x) dx = \sum_{k=1}^N a_k y(x_k) . \quad (13H)$$

This also implies that the  $x_k$ 's in Equation 10 H are the roots of the Legendre polynomial of degree N. Choice of a value N automatically determines  $x_1, x_2, \dots, x_N$ , and the  $a_k$ 's are given uniquely by Equation 11H. While only N ordinate values are used, the representation behaves as if 2N ordinate values are used as long as the  $x_k$ 's are the roots of the Legendre polynomial.

Any finite interval of integration ( a, b ) may be changed to ( -1, 1 ) by means of the transformation

$$x = \frac{2u - (a+b)}{b-a} \quad (14H)$$

$$\int_a^b f(u) du = \frac{b-a}{2} \int_{-1}^1 f(x) dx \quad (15H)$$

Table 27 gives  $x_k$  and  $a_k$  values for values of n up through n = 6 ( 2 ).

Since  $x_k = -x_{n-k+1}$  and  $a_k = a_{n-k+1}$ , only half of the values are tabulated.

Table 27. Parameters utilized in Gauss' mechanical quadrature formula ( 2 ).

n	k	$x_k$	$a_k$
2	1	0.577350269189626	1.00000000000000
	2	0.577350269189626	1.00000000000000
3	1	0.774596669241483	0.555555555555556
	2	0.000000000000000	0.888888888888889
4	1	0.339981043584856	0.65214515486255
	2	0.861136311594053	0.34785484513745
5	1	0.538469310105683	0.47862867049937
	2	0.906179845938664	0.23692688505619
	3	0.000000000000000	0.568888888888889
6	1	0.238619186083197	0.46791393457269
	2	0.360761573048139	0.36076157304814
	3	0.932469514203152	0.17132449237917

AN INVESTIGATION OF THE MOVEMENT OF PARTICLES  
IN  
FLUIDIZED BEDS .

by

JERRY LEE RATHBUN

B. S., Kansas State University, 1962

---

AN ABSTRACT OF  
A MASTER'S THESIS

submitted in partial fulfillment of the  
requirements for the degree

MASTER OF SCIENCE

Department of Nuclear Engineering

KANSAS STATE UNIVERSITY

Manhattan, Kansas

1965

## ABSTRACT

The movement of a single particle in a liquid fluidized bed was followed using a radioactive tracer technique. The fluidized bed was made up of precision ground stainless steel balls fluidized with water. A single ball bearing was made radioactive by irradiation in the Kansas State University TRIGA Mark II Nuclear Reactor, and introduced into the bed. The axial motion of this particle was followed by measuring the passage of the particle past two horizontal planes in the bed.

The construction of the fluidized bed and the detection system that was developed are described in detail.

Preliminary data consisting of over 20,000 data values were obtained for a single sized particle and single packed bed height. The data were analyzed to give several parameters that can be used to characterize a fluidized bed. These parameters include the average particle velocity, particle velocity distribution, reflection coefficient, particle traffic, residence time distribution, dispersion coefficient, reflectivity and transmissivity. The mathematical analyses necessary to describe these parameters are presented. IBM-1620 computer programs in FORTRAN used to reduce the data to obtain these parameters are given.

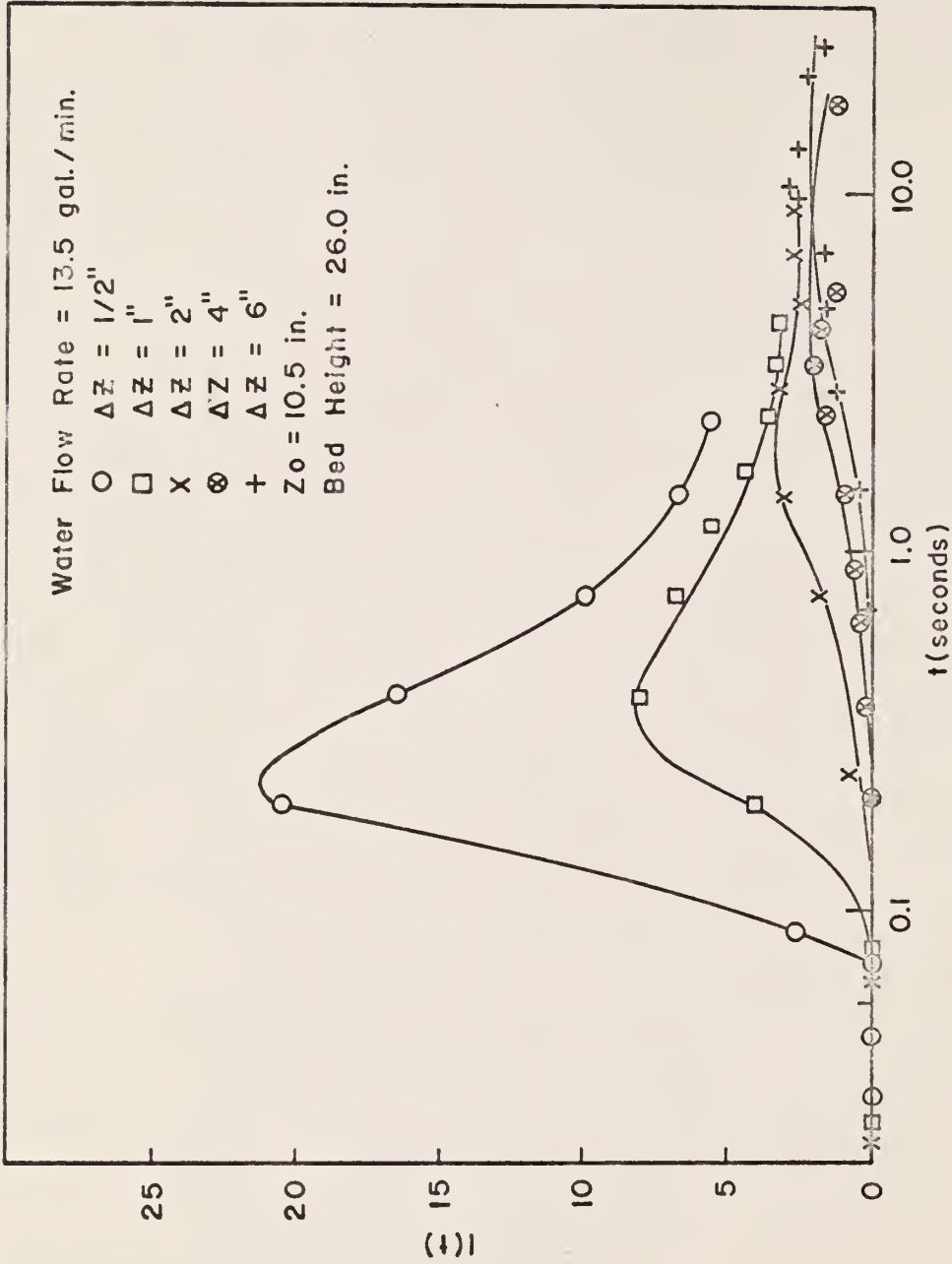


Figure 86. Experimental Particle Concentration Data, at Flow Rate  $B_1$ .

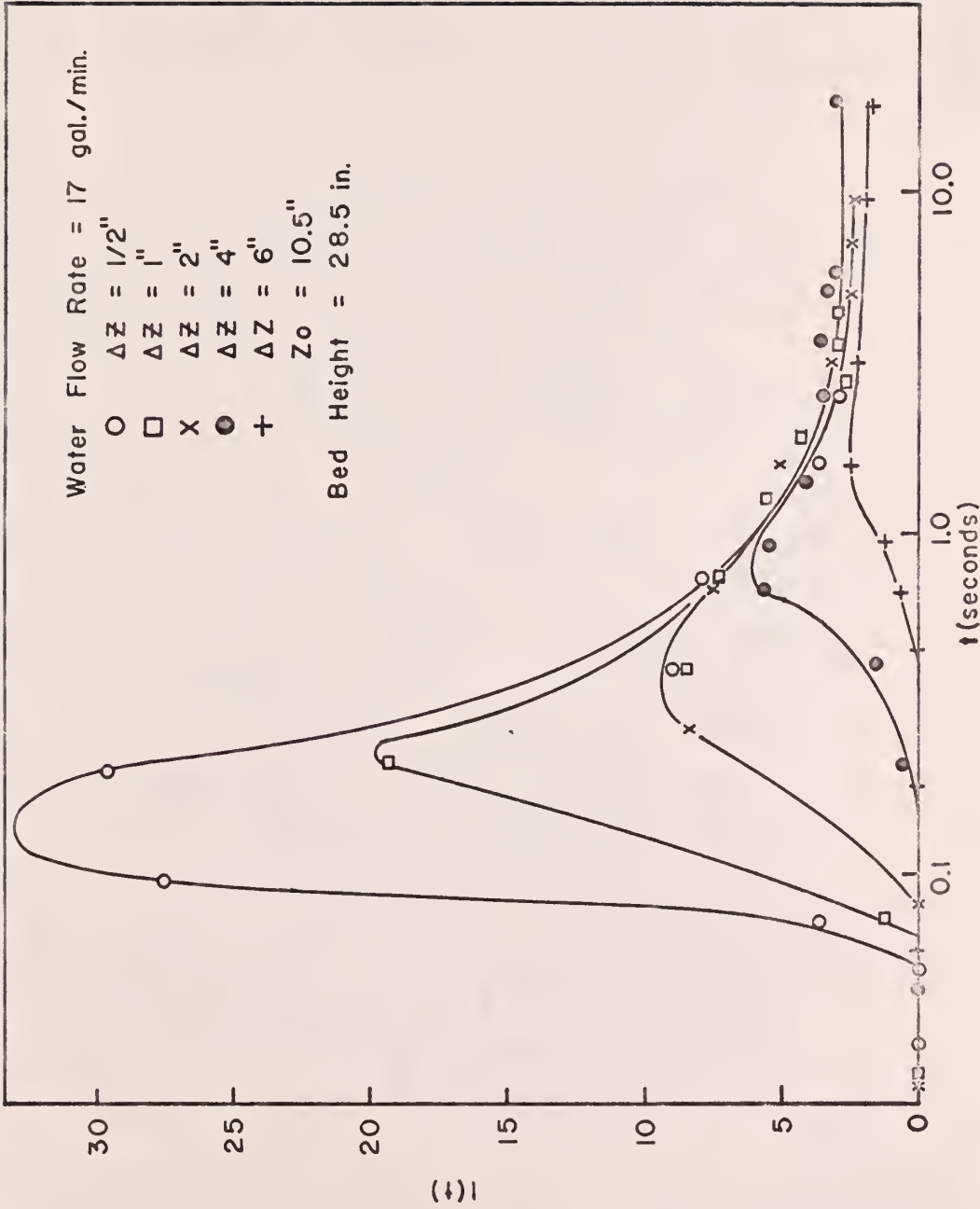


Figure 87. Experimental Particle Concentration Data, at Flow Rate B2.

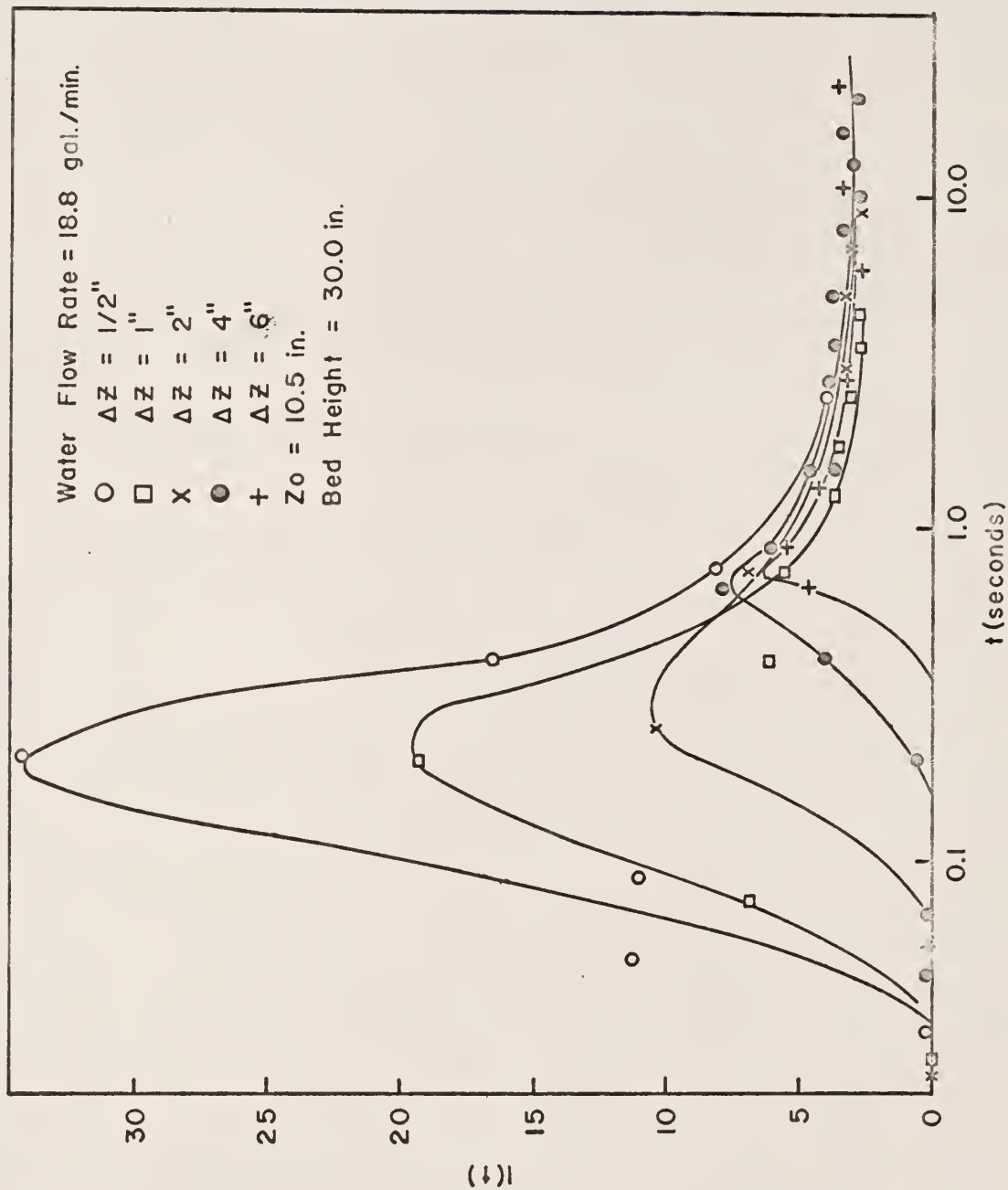


Figure 88. Experimental Particle Concentration Data, at Flow Rate B3.

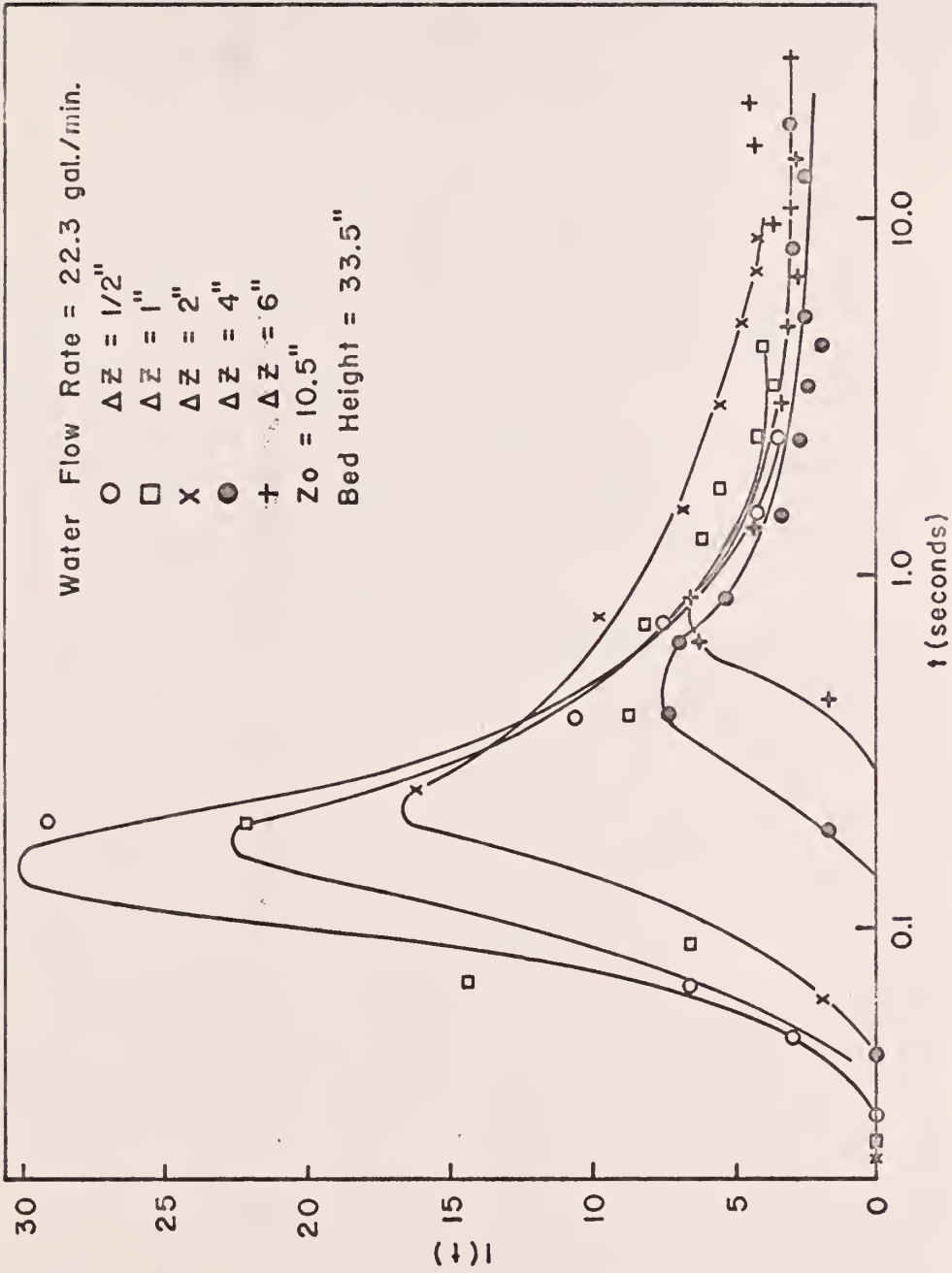


Figure 89. Experimental Particle Concentration Data, at Flow Rate B<sub>4</sub>.

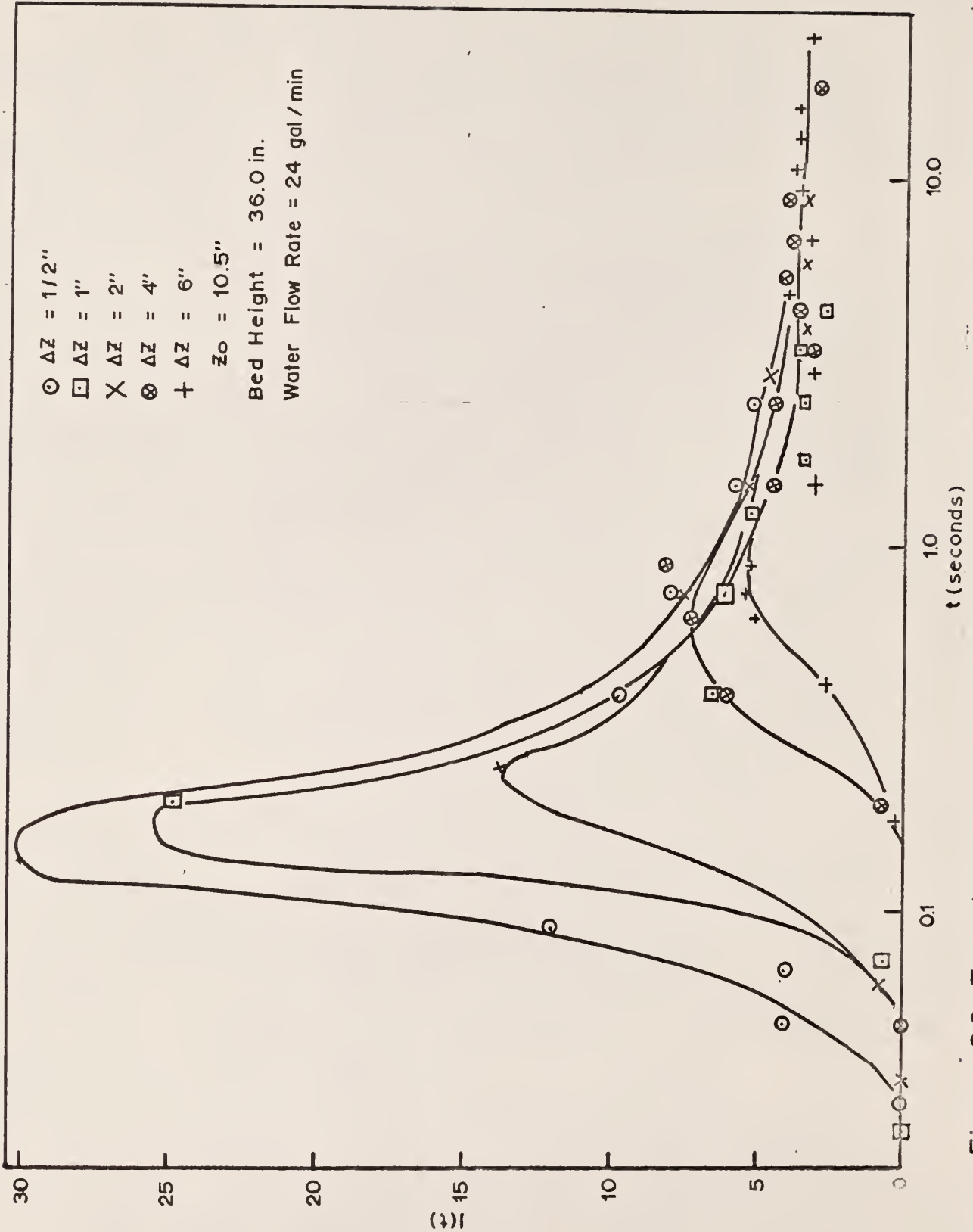


Figure 90. Experimental Particle Concentration Data, at Flow Rate B<sub>5</sub>.

and

$$\frac{\partial \tau_m}{\partial E_z} = \frac{t_m}{L^2} \cdot \quad (97)$$

An iterative procedure used to solve for  $E_z$  was as follows:

The quantities  $(t_{\text{exp}})_m$ ,  $L$ , and  $(x-x_0)_m$  were extracted from the data first. A value of  $E_z$  was then assumed. The quantities  $\tau_m$  and  $t_m$  were calculated, where

$$\tau_m = \frac{(t_{\text{exp}})_m E_z}{L^2} \cdot ,$$

and

$$t_m = \text{time corresponding to } (C/C_\infty)_{\text{max}} \cdot$$

The left-hand side of Equation 94 was calculated after inserting the quantities into Equations 95, 96, and 97. The value of the left-hand side of Equation 94 was plotted versus  $E_z$ , and the  $E_z$  corresponding to the value of the left-hand side of Equation 94 being equal to zero was the least squares analysis solution for the dispersion coefficient for the given water flow rate, based upon minimizing the sum of the squares of the deviations of the times corresponding to the correlated  $(C/C_\infty)_{\text{max}}$  and the experimental  $(I/I_\infty)_{\text{max}}$  with respect to  $E_z$ .

Method 2. The second method minimized the sum of the squares of the errors of the experimental values of  $I/I_\infty$  for five distances between detector levels with respect to  $E_z$  for each water flow rate studied. The least squares analysis equation used for the second method was

$$\sum_{m=1}^5 \sum_{j=1}^5 \frac{\partial \tau_{jm}}{\partial E_z} \frac{\partial}{\partial \tau_{jm}} \left[ (C/C_\infty)_{jm} - (I/I_\infty)_{jm} \right]^2 = 0, \quad (98)$$

where  $m$  is the subscript for the distance between detector levels,  $\Delta Z$ , and  $j$  is the subscript for the correlated,  $C/C_\infty$ , and experimental,  $I/I_\infty$ , particle concentrations as functions of time for each distance between detector levels. The values of  $I/I_\infty$  were obtained from Figs. 86 through 90. From Equation 97,

$$\frac{\partial \tau_{jm}}{\partial E_z} = \frac{t_{jm}}{L^2} .$$

Differentiating  $\left[ (C/C_\infty)_{jm} - (I/I_\infty)_{jm} \right]^2$  with respect to  $\tau_{jm}$  gives

$$\frac{\partial}{\partial \tau_{jm}} \left[ (C/C_\infty)_{jm} - (I/I_\infty)_{jm} \right]^2 = 2 \left[ (C/C_\infty)_{jm} - (I/I_\infty)_{jm} \right] \frac{\partial (C/C_\infty)_{jm}}{\partial \tau_{jm}} , \quad (99)$$

where  $\frac{\partial (C/C_\infty)_{jm}}{\partial \tau_{jm}}$  is obtained by differentiating Equation 85 with respect to  $\tau_{jm}$ . Thus,

$$\begin{aligned} \frac{\partial (C/C_\infty)_{jm}}{\partial \tau_{jm}} = & 2 \sum_{n=1}^{\infty} (-n^2 \pi^2) e^{-n^2 \pi^2 \tau_{jm}} \cos(n\pi x_m) \cos(n\pi x_0) \\ & + \frac{e^{-(x-x_0)_m^2 / 4\tau_{jm}}}{4\pi^{1/2} \tau_{jm}^{3/2}} \left[ \frac{(x-x_0)_m^2}{2\tau_{jm}} - 1 \right] . \end{aligned} \quad (100)$$

An iterative procedure was used to attempt to obtain a solution for  $E_z$ . The procedure was as follows:

The quantities  $(I/I_\infty)_{jm}$ ,  $L$ ,  $t_{jm}$ ,  $x_m$ , and  $x_0$  were extracted from the data first. A value of  $E_z$  was then assumed. The quantities  $\tau_{jm}$  and  $(C/C_\infty)_{jm}$  were then calculated from Equations 83 and 85. The numerical value of the

left-hand side of Equation 98 was calculated, utilizing Equations 97, 99, and 100. The value of the left-hand side of Equation 98 was then plotted versus  $E_z$ , and the  $E_z$  corresponding to the value of the left-hand side of Equation 98 being equal to zero was to be the dispersion coefficient based upon minimizing the sum of the squares of the deviations of  $(C/C_\infty)-(I/I_\infty)$  with respect to  $E_z$ . However, a plot of  $E_z$  versus the left-hand side of Equation 98 gave curves asymptotically approaching zero with increasing  $E_z$  for all water flow rates studied.

## 5.0 DISCUSSION OF RESULTS

This section has been divided into four parts. Each part contains a discussion of one of the four quantities extracted from the experimental data.

Almost 20,000 individual data values were obtained in this investigation, and these are recorded on IBM cards. Since it is impractical to present all of the data and results, only representative samples have been shown in Section 4.0 and in the appendices. A complete listing of the data and results, in the form of computer input and output, is available in Project 2324, Supplement Number One, which may be obtained from the Kansas State University Engineering Experiment Station.

### 5.1 Residence Times

Figures 35 through 38 illustrate that about 50 individual data values per data set were sufficient to study the characteristics of the residence time distribution, with adequate assurance that the samples taken represented the population distribution.

Figures 39 through 46 show that the residence time data can be represented by a gamma distribution in practically all of the data sets obtained.

Figures 47 through 56 give, as functions of the distance between detector levels, the trends of the gamma distribution parameters  $p$  and  $\nu$  for each water flow rate studied. Knowledge of their trends enables prediction of the characteristics of the fluidized bed, as discussed in Section 4.3.

The residence time results were corrected for instrument characteristics error. Experimental residence times of less than 0.2 second were subject to a major correction, and, therefore, the data, in cases where very short residence times were obtained, were least reliable. The major source of this



